

Liquid Chromatography-Mass Spectrometry Platforms Hyphenated  
With Coulometric Array and Microscale Nuclear Magnetic  
Resonance Detection

A dissertation presented

by

Susan Schiavo

to

The Department of Chemistry and Chemical Biology

In partial fulfillment of the requirements for the degree of  
Doctor of Philosophy

in the field of

Chemistry

Northeastern University  
Boston, Massachusetts  
February 2009



Liquid Chromatography-Mass Spectrometry Platforms Hyphenated  
With Coulometric Array and Microscale Nuclear Magnetic  
Resonance Detection

by

Susan Schiavo

ABSTRACT OF DISSERTATION

Submitted in partial fulfillment of the requirements  
for the degree of Doctor of Philosophy in Chemistry  
in the Graduate School of Arts and Sciences of  
Northeastern University, February 2009

## ABSTRACT

This manuscript centers on the hyphenation of analytical detection technologies, specifically, the coupling of liquid chromatography-mass spectrometry (LC-MS) to the complementary analytical methods of electrochemical array (EC-array) detection and nuclear magnetic resonance (NMR). Chapter 1 provides a detailed overview of the specific detection methods used throughout this dissertation.

Chapter 2 focuses on the combination, in parallel, of LC-MS and EC-array detection methods into a streamlined platform and its application to drug metabolism studies. The platform's performance was evaluated by demonstrating retention of chromatographic integrity between the two detectors where retention times and peak widths at half height between the EC-array and MS were reproducible with relative standard deviations (RSD) < 10 %. Additionally, through a comparison of EC-array and MS relative limits of detection the system's compatibility for parallel metabolite analysis is clearly established, detecting down to 600 pg injected on column with merely femtogram levels being delivered to the MS. An investigation of an eight compound mixture, representative of the diversity typically encountered in physiological systems, both in neat solution and a serum matrix with limited sample cleanup demonstrates the system's ability to handle biological samples without concern for biological matrix effects. Finally, by using the nanoelectrospray LC-EC-array-MS system, its unique abilities in preliminary metabolomics analyses were highlighted through successful identification of unknown

sodium phenyl butyrate (SPB) drug metabolites in Huntington's disease (HD) patient plasma.

Chapter 3 applies the LC-EC-array-MS platform to a more detailed metabolic assessment of the oral drug SPB as a histone deacetylation (HDAC) inhibitor in a safety and tolerability study of SPB in HD patients. Using a method employing gradient LC with EC-array, UV and Fluorescence (F) (LCECA/UV/F), treated patient plasma and urine gave individual-specific patterns of *ca.* 20 SPB metabolites which may relate to the selection of subjects for extended trials of SPB. The structural identification of these metabolites was of critical importance, since characterization will aid in the understanding of mechanisms of drug action and possible side effects. An iterative process was developed with LC-EC-array and parallel LC-EC-array-MS detection for characterizing these metabolites. 10 metabolites were identified in treated subjects including indole species in urine that are not directly related to structural modifications of SPB, but were only found in SPB treated HD patients. The application of the process was directed at understanding metabolic pathways that differ among HD individuals when being treated with SPB and when not treated. These previously unreported metabolites resulting from SPB therapy may have both implications both on the disease processes in HD and a secondary effect of the therapeutic intervention in combination with HDAC processes. Both of these aspects will all be discussed.

In Chapter 4, two innovations in microscale analysis, nanoSplitter LC-MS (Chapter 2) and microdroplet NMR were combined for the identification of unknown compounds

found at low concentrations in complex sample matrices as frequently encountered in metabolomics or natural products discovery. Microdroplet NMR is a droplet microfluidic NMR loading method providing several-fold higher sample efficiency than conventional flow-injection methods. Performing NMR offline from LC-UV-MS accommodated the disparity between MS and NMR in their sample mass and time requirements, as well as allowing NMR spectra to be requested retrospectively, after review of the LC-MS data. Interpretable 1D NMR spectra were obtained from analytes at the 200 ng level, in 1-hour-per-well automated NMR data acquisitions. The system also showed excellent intra- and inter-detector reproducibility with retention time RSD values less than 2%, and sample recovery on the order of 93%. When applied to a cyanobacterial extract showing antibacterial activity, the platform recognized several previously-known metabolites, down to the 1% level, in a single 30  $\mu\text{g}$  injection, and prioritized one unknown for further study.

In Chapter 5, the synthesis, isolation and analytical characterization of DNA-adducts, using the microscale LC-MS-NMR platform, is described. These adducts include both N-(deoxyguanosin-8-yl)-aminobiphenyl (C8-dG-ABP) and N-(deoxyguanosin-8-yl)-aminobiphenyl-*d*<sub>9</sub> (C8-dG-ABP-*d*<sub>9</sub>), as well as the identification of various isomeric compounds associated with the two adducts. This characterization was achieved using the LC-MS-NMR platform described in Chapter 4 of this thesis, but, with manual microdroplet injections into the microcoil NMR as opposed to using the automated sample handler. This change was made in order to more effectively recover the analytes for post-NMR use and allow interactive NMR acquisition, as well as provide more

efficient sample injections for trace analysis compounds. Both the LC-MS fraction collection and manual injection microdroplet NMR analyses were evaluated for sample recovery and injection efficiency, using a dG standard, prior to adduct analysis. Each adduct was analyzed using LC-MS-microcoilNMR and subsequently recovered for future use in *in vitro* and *in vivo* studies correlating DNA adduct isomer persistence to biological endpoints such as apoptosis, gene transcription, mutagenesis and cancer.

Chapter 6 offers recommendations for future research based on the studies presented in this dissertation.

## ACKNOWLEDGEMENTS

The overall theme of this thesis is hyphenated technologies which when put together make an analysis stronger and more complete. This theme is also more than appropriate to be applied to my graduate school career in general. Throughout my time in Boston and at Northeastern, I have had the pleasure to meet and work with many people who have irrevocably changed me personally and professionally to be stronger and more complete. Before any work can be discussed, I must thank these people.

First I must thank my undergraduate advisor, Dr. R. Daniel Libby. He not only gave me excellent research opportunities but also pushed me to pursue graduate school in the first place. He saw my potential well before I ever did and for that I am very grateful.

Next I would like to sincerely thank my advisor, Dr. Paul Vouros, who has given me incredible guidance and support. He has provided me with more than just a well respected scientific laboratory from which to learn. He has, in addition, grown a large, loud and well respected scientific family that I feel privileged to be a part of. Thank you, Dr. Vouros, for taking possibly the largest role in shaping my graduate career. You will undoubtedly, and possibly unknowingly, continue to shape my career that has yet to come.

I have also had the opportunity to work with a few collaborators from which I have learned an immeasurable amount. Dr. Wayne Matson's laboratory at the Bedford VA



Hospital in Bedford, MA was always very welcoming and inspirational. I am a much more confident and knowledgeable person from working with Wayne and his group. This includes, his daughter Samantha Matson, as well as other colleagues; Misha Bogdanov, Lei Wang, Swati Sharma and Erika Ebbel. The entire group was complimentary as well as very fun and I am so glad to have met with and worked with them all.

In addition I've also had the pleasure of collaborating with Dr. Bruce Kristal, currently at the Department of Neurosurgery, Brigham and Women's Hospital, Boston, MA. Bruce and I do not always speak the same scientific language and our different styles have only helped me grow professionally more than I ever expected. I've learned a great deal from Bruce and I must thank him for his guidance and help. I look forward to continuing to work with him in the future.

Lastly, and most recently, I've begun working with Dr. Roger Kautz of the Barnett Institute at Northeastern University. Roger is an inspiration to me in many ways, but mostly it's his excitement and passion for whatever he does that has left a large impression on me. Thank you Roger, you have taught me so much in such a limited time.

I can not forget to thank the wonderful members of the Vouros group, both past and present. Those who came before me that I've had the pleasure to meet; Tom Trainor, Roland Annan, Jack Cuniff, Tim Baker, Liza Marzilli, Lynn Gennarro and Yuri

Dunayevskiy, you are all inspirations for what can come after graduate school and you must be thanked for that as well as all the laughs you have provided.

To the Vouros group members that I have had the pleasure of working with, I will genuinely say thank you. I've learned a great deal from you all and at the same time had a lot of fun. These past years would have felt a lot longer if not for each of you. Thank you, Dayana Argoti, John Williams, Daren Levin, Jimmy Flarakos, Wennan Xiong, Adam Hall, Terrence Black, Josh Klaene and Dennis Szymanski. I'd like to especially thank the group members and Northeastern graduate students who have had a profound effect on my development by helping me even when I thought I didn't need it, motivating me when I thought I had nothing left and building my confidence with all their well wishes. Thank you, Jim Glick, Caroline Ceailles Flarakos, Rose Gathungu, Stefano Gulla, Kevin Millea, Kristen Randall, Elaine Ricicki, Heather Brodtkin and Christine Andrews. I must especially thank Christine, who I will always consider a best friend first and a colleague last.

In addition, I have relied on many individuals throughout my time in the Chemistry and Chemical Biology Department. I would like to thank all my professors, especially Dr. Mabrouk, Dr. Forsyth and Dr. Hancock for their help in finishing up my dissertation as well as members of the staff, in particular Rich Pumphrey, Shari Khalil, Nancy Weston and Jean Harris.

To my friends living outside of Boston, Sheli McHugh, Kelly Wroblewski, Kelly Gaidula, Heidi Peoples, Rachel Kane, Michelle Clewell, Melissa Schraeder, Summer Morris and Mike Lukens, thank you for all the fun times and immense amounts of support you've given. I've known you all for such a long time you are more like family to me in addition to being very good friends. You've all been such motivations, and I hope you know how much you mean to me.

A very humble and sincere thank you must be said to my mother Barbara, my father Jim and my brothers, Jimmy, Matthew, Billy and David for always supporting me with everything I've ever done or wanted to do. You may not have always understood my endeavors, but you were always there as my loudest cheering section and my biggest fans. You make me crazy and you make me laugh, for both of these things I couldn't be more thankful. I'm sure you're glad this part of my journey is over as much as I am.

Last to thank but certainly not least is my partner in everything and my true favorite person, Benjamin Bird. I tell you often that I am lucky to have met you and I sincerely mean it. You always and without question, stand beside me, hold my hand and smile while guiding me through things I never think I can accomplish. You believe in me so strongly, it's impossible not to believe in myself. Thank you always and for everything.

*To my family  
both those chosen for me and those I have chosen*

**TABLE OF CONTENTS**

	<b>Page</b>
Abstract	3
Acknowledgements	8
Dedication	12
Table of Contents	13
List of Figures	18
List of Tables	22
List of Abbreviations	23
<b>Chapter 1. Introduction to Liquid Chromatography and Mass Spectrometry</b>	<b>27</b>
<b>    and their Hyphenation with Electrochemical Array detection</b>	
<b>    And Nuclear Magnetic Resonance</b>	
Section 1.1 Introduction	28
1.2 Introduction to Liquid Chromatography	29
1.2a Introduction to Reverse Phase Chromatography	30
1.3 UV Detection	33
1.4 Electrochemical Array Detection	34
1.5 Mass Spectrometry	38
1.5a Components of a Mass Spectrometer	38

	14
	<b>Page</b>
1.5b Ionization Sources	39
1.5c Types of Mass Analyzers	43
1.5d Types of Detectors	59
1.5e The Mass Spectrum	61
1.6 Nuclear Magnetic Resonance	62
1.7 Liquid Chromatography-Mass Spectrometry Hyphenation	65
1.8 LC-MS and LC-EC-array Hyphenation	66
1.9 LC-MS and flow based-NMR Hyphenation	70
1.10 Conclusions	74
1.11 References	75
<b>Chapter 2. Establishment of a Liquid Chromatography-Electrochemical Array-Mass Spectrometry Integrated System for Metabolite Identification</b>	<b>81</b>
Section 2.1 Introduction to Metabolomic Analyses	82
2.2 HPLC-EC-array Metabolomics	83
2.3 HPLC-EC-array-MS Hyphenation	84
2.4 Project Goals	86
2.5 Materials and Methods	86
2.6 Results and Discussion	91

	15
	<b>Page</b>
2.7 Conclusions	113
2.8 References	115
<b>Chapter 3. Identification of Unknown Phenyl Butyrate Metabolites in Huntington's Disease Patients using Parallel LC-EC-array-MS Detection</b>	<b>118</b>
Section 3.1 Introduction to Huntington's Disease	119
3.2 Introduction to Sodium Phenyl Butyrate Treatment	120
3.3 LC-EC-array-MS Platform for Metabolite Identification	121
3.4 Project Goals	123
3.5 Materials and Methods	123
3.6 Results and Discussion of Analysis Method	129
3.7 Discussion of Disease and Individual Metabolism of SPB	139
3.8 Conclusions	140
3.9 References	141
<b>Chapter 4. A Microscale LC-MS-NMR Platform Applied to the Identification of Active Cyanobacterial Metabolites</b>	<b>144</b>
Section 4.1 Introduction	145
4.2 Introduction to Microcoil NMR Probes	145
4.3 Droplet Microfluidics for flow-NMR	147

	16
	<b>Page</b>
4.4 Hyphenation of Microdroplet NMR and nanoSplitter MS	150
4.5 Project Goals	151
4.6 Materials and Methods	152
4.7 Results and Discussion	160
4.8 Conclusions	176
4.9 References	178
<b>Chapter 5. Identification of Minor DNA Adduct Isomers using a</b>	<b>181</b>
<b>Microscale LC-MS-NMR Platform</b>	
Section 5.1 Introduction to DNA Adduct Metabolism	182
5.2 DNA Adduct Synthesis <i>in vitro</i> and Isomer Persistence	185
5.3 Low Abundance Isomer Characterization	187
5.4 Project Goals	189
5.5 Materials and Methods	190
5.6 Results and Discussion	197
5.7 Conclusions	223
5.8 References	224
<b>Chapter 6. Future Directions</b>	<b>228</b>
Section 6.1 LC-EC-array Platform	229
6.2 Microscale LC-MS-NMR Platform	230



**Page**

6.3 References

231

**Biographical Data****232**

## LIST OF FIGURES

<u>Chapter 1</u>	<b>Page</b>
Figure 1.1    Example of RPC Separation	32
Figure 1.2    UV Detector	34
Figure 1.3    2 Electrode Coulometric Cell Array	36
Figure 1.4    Cutaway of the ESA 6010 Cell	37
Figure 1.5    Components of the Mass Spectrometer	39
Figure 1.6    Schematic of ESI	41
Figure 1.7    Quadrupole Mass Analyzer	45
Figure 1.8    Mathieu Stability Diagram	45
Figure 1.9    Schematic and Picture of the ThermoFischer Quantum Triple Quadrupole Mass Spectrometer	47
Figure 1.10   Triple Quadrupole MS/MS Scan Modes	48
Figure 1.11   Cross Section of a QIT	51
Figure 1.12   Mathieu Stability Diagram for Ion Trap MS	52
Figure 1.13   ToF Mass Analyzer and Reflectron ToF Mass Analyzer	55
Figure 1.14   Qq-ToF Mass Analyzer	56
Figure 1.15   Cutaway of Orbitrap Mass Analyzer	58
Figure 1.16   Schematic of an Electron multiplier	60
Figure 1.17   Mass Spectrum Example	61
Figure 1.18   TMS NMR Reference Spectrum and Functional Group Frequencies	64

<u>Chapter 2</u>		<b>Page</b>
Figure 2.1	LC-EC-array-MS Schematic	92
Figure 2.2	Chromatography Comparison of MS and EC-array for DA and 3-MT	94
Figure 2.3	8 Compound Standard Mixture MS and EC-array Chromatograms	101
Figure 2.4	Plasma Spiked 8 Compound Standard Mixture MS and EC-array Chromatograms	102
Figure 2.5	Bar Graphs for MS Data of 8 Compound Mixture	104
Figure 2.6	Bar Graphs for EC-array Data of 8 Compound Mixture	105
Figure 2.7	EC-array and MS Chromatograms for Plasma Blank	106
Figure 2.8	LC-EC-array Chromatograms for Baseline and SPB Treated HD Patient Plasma	108
Figure 2.9	MS and EC-array Chromatograms for HD Patient Sample	109
Figure 2.10	Unknown Metabolite MS and MS/MS Spectra	110
Figure 2.11	SPB LC-MS Chromatogram and MS and MS/MS Spectra	112
 <u>Chapter 3</u>		
Figure 3.1	Overall LC-EC-array-MS Method Flow Chart	131
Figure 3.2	LC-EC-array Chromatograms for Baseline and SPB Treated HD Patient	132
Figure 3.3	LC-EC-array Chromatogram for HD Patient Sample	133

**Page**

Figure 3.4	LC-MS Chromatogram and XIC Chromatograms for HD Patient Sample	134
Figure 3.5	High Resolution MS and MS/MS Spectra for Unknown SPB Metabolite	135
Figure 3.6	SPB Metabolite Structures and MS/MS Fragmentations	138
 <u>Chapter 4</u>		
Figure 4.1	Comparison of Saddle and Microcoil NMR Probes	147
Figure 4.2	Comparison of FIA, SFA and Zero Dispersion SFA Methods for Flow NMR	149
Figure 4.3	LC-MS- $\mu$ NMR Platform Flow Chart	161
Figure 4.4	LC-MS-NRM Data with UV, MS and NMR Correlation	163
Figure 4.5	Quantitative NMR Recovery Study	166
Figure 4.6	System Limit of Detection Based on NMR Data	168
Figure 4.7	UV Chromatogram of Bioactive Cyanobacteria Extract	172
Figure 4.8	MS and NMR Comparison of Hapalindole H and Unknown Compound	173
Figure 4.9	LOD of Active Cyanobacteria Fraction Based on NMR of Taxol	175
 <u>Chapter 5</u>		
Figure 5.1	Metabolic Pathway of PhIP	183

**Page**

Figure 5.2	2-Aminonaphthalene Nitrenium Ion and Charge Delocalization	184
Figure 5.3	1 D Proton NMR Spectrum of dG	202
Figure 5.4	LC-UV and MS Chromatograms for dG-ABP Reaction Mixture	205
Figure 5.5	NMR Spectra for dG-ABP Reaction Mixture	206
Figure 5.6	Possible dG-ABP isomer Structure	208
Figure 5.7	Pre and Post NMR Comparison of dG-ABP isomer RT 9.04 MS Spectra	209
Figure 5.8	LC-UV and MS Chromatograms for dG-ABP- <i>d</i> <sub>9</sub> Reaction Mixture	211
Figure 5.9	NMR and MS Chromatogram and Spectra of C-8 isomers for dG-ABP and dG-ABP- <i>d</i> <sub>9</sub> Co-elution	212
Figure 5.10	LC-UV Chromatogram and NMR Spectra for dG-ABP- <i>d</i> <sub>9</sub> Reaction Mixture	214
Figure 5.11	dG-ABP- <i>d</i> <sub>9</sub> Isomer 4 MS Spectrum and Possible Structure	216
Figure 5.12	dG-ABP- <i>d</i> <sub>9</sub> Isomer 3 MS Spectrum and Possible Structure	217
Figure 5.13	dG-ABP- <i>d</i> <sub>9</sub> Isomer 1 MS and MS/MS Spectra and Possible Structure	219
Figure 5.14	dG-ABP- <i>d</i> <sub>9</sub> Isomer 2 MS and MS/MS Spectra	220
Figure 5.15	dG-ABP- <i>d</i> <sub>9</sub> Isomer 6 MS and MS/MS Spectra	222
Figure 5.16	Post NMR MS Spectra of dG-ABP- <i>d</i> <sub>9</sub> Isomer 6	223

**LIST OF TABLES**

		<b>Page</b>
<u>Chapter 2</u>		
Table 2.1	Comparison of MS and EC-array Data for Dopamine and Methoxytyramine	95
Table 2.2	8 Analyte Standard Mixture SRM Detection Parameters	100
Table 2.3	Comparison of MS and EC-array Areas for 8 Analyte Standards over Two Concentrations	103
<u>Chapter 3</u>		
Table 3.1	SPB Metabolites Found in Patient Plasma	137
Table 3.2	SPB Metabolites Found in Patient Urine	137
<u>Chapter 4</u>		
Table 4.1	Ambiguine Compounds	173
<u>Chapter 5</u>		
Table 5.1	LC and LC/MS Fraction Collector Recovery	199
Table 5.2	LC-MS-NMR Fraction Collector Recovery	200
Table 5.3	NMR Assessment of Recovery and NMR Loading Efficiency	203

**LIST OF ABBREVIATIONS**

3-MT	3-Methoxytyramine
AA	Aromatic Amine
ACN	Acetonitrile
AN	Aminonaphthalene
ABP	Aminobiphenyl
ac	Alternating current
CA	Coulometric Array
CE	Capillary Electrophoresis
CID	Collisionally induced dissociation
CNL	Constant neutral loss
DA	Dopamine
Da	Dalton
dA	Deoxyadenosine
dC	Deoxycytosine
dG	Deoxyguanosine
dc	Direct current
DNA	Deoxyribonucleic acid
ECD	Electrochemical Detection
EC-array	Electrochemical Array Detection
ESI	Electrospray ionization

F	Fluorescence
FFT	Fast Fourier Transform
FIA	Flow Injection Analysis
FID	Free Induction Decay
FTICR	Fourier Transform Ion Cyclotron Resonance
GC	Gas Chromatography
HAA	Heterocyclic Aromatic Amines
HD	Huntington's Disease
HDAC	Histone Deacetylase
HLM	Human Liver Microsomes
HPLC	High performance liquid chromatography
Hz	Hertz
IDA	Independent Data Acquisition
IQ	2-amino-3-methylimidazo[4,5-f]quinoline
IR	Infrared spectroscopy
LC	Liquid chromatography
LC-MS	Liquid Chromatography - mass spectrometry
MRM	Multiple Reaction Monitoring
MS	Mass spectrometry
MS/MS	Tandem mass spectrometry (two stages)
MS <sup>n</sup>	Tandem mass spectrometry (n stages)
<i>m/z</i>	Mass-to-charge ratio



mV	Mili-Volt
MW	Molecular Weight
nC	Nano-Coulombs
nESI	Nanoelectrospray Ionization
NMR	Nuclear magnetic resonance spectroscopy
PA	Phenyl Acetate
PAH	Polycyclic aromatic hydrocarbon
ppm	Parts per million
PDA	Photodiode Array
PSDVB	Polystyrene divinylbenzene
QQQ	Triple quadrupole
QIT	Quadrupole Ion Trap
Qq-ToF	Quadrupole-Time of Flight
rf	Radio frequency
RPC	Reversed phase chromatography
RT	Retention Time
SIM	Single ion monitoring
S/N	Signal-to-noise
SFA	Segmented Flow Analysis
SPB	Sodium Phenyl Butyrate
SPE	Solid Phase Extraction
SRM	Selected reaction monitoring

TIC	Total Ion Current
TMS	Tetramethylsilane
TDC	Time to Digital Converter
TLC	Thin Layer Chromatography
ToF	Time-of-flight
UV	Ultraviolet Detection
V	Voltage
XIC	Extracted Ion Chromatogram

Chapter 1:

Introduction to Liquid Chromatography and Mass Spectrometry and Their Hyphenation

with Electrochemical Array and Nuclear Magnetic Resonance Detection

## 1.1 Introduction

Hyphenated technologies have great importance in analytical chemistry. To extract the most information from complex mixtures, complementary instrumentation can be put together for both complex sample profiling and targeted analyses, including quantitation studies. These configurations are usually comprised of a separation technique such as liquid chromatography (LC) or Solid Phase Extraction (SPE) followed by analytical detection methods, either in series or parallel. The analytical detection methodologies used in this dissertation were electrochemical array detection (EC-array), Mass Spectrometry (MS), ultraviolet detection (UV) and Nuclear Magnetic Resonance (NMR). It is possible to arrange the instrumentation together in series or parallel as either on-line or off-line technologies, depending on the complementarities of each method. In any hyphenated analyses using the detectors just defined, the information gathered should paint a comprehensive picture of the analyte(s) through individual molecular weight (MW), structure, polarity and electrochemical (EC) response in addition to chromophore presence.

The combination of these detection techniques with LC and MS is not trivial in its design and will be discussed, with great detail, in each research chapter dedicated to the specific platform developed. Outlined below is an introduction to both LC and MS separately as well as the hyphenated technique, LC-MS. Also the other detection methods utilized, UV detection, EC-array detection and NMR will be introduced. Finally, LC/MS coupled to

both EC-array and NMR will be discussed. This background will serve as a primer for the specific experiments and applications outlined in the remainder of this manuscript.

## 1.2 Introduction to Liquid Chromatography<sup>1</sup>

Liquid Chromatography (LC) or high pressure liquid chromatography (HPLC) as it is sometimes referred, is a flow based separation technique where the sample, dissolved in a liquid mobile phase, is pumped through a chromatography column filled with one of many possible stationary phases all directed toward separating the analyte mixture prior to detection. This entire process is done at a relatively high pressure (approximately 20-120 bar) through the use of a mechanical pump.

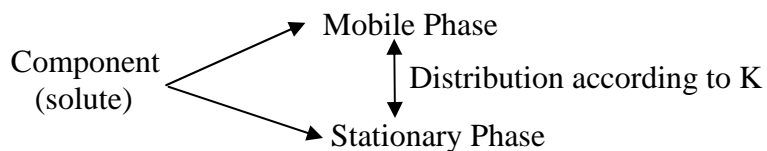
The basic components of a liquid chromatograph include: a means of introducing the sample into the system (i.e., a switching valve with sample loop controlled manually or by an autosampler), a mechanical pump, typically with at least two solvent reservoirs, an analytical column which is packed with the stationary phase, and a detector. The components are connected through the use of stainless steel or PEEK tubing. The chromatographic columns used in HPLC can be packed with many different stationary phases based on individual separation needs. For example, possibilities include linear alkane phases such as C4, C8, or C18, polymer based matrices like polystyrene divinyl benzene, or more polar functional groups, such as diol compounds, attached to a hydrocarbon residue, such as hexane or benzene. Chromatographic conditions can be

changed by altering the column packing materials as well as the mobile phases and buffers being used in the analysis.

### 1.2a Introduction to Reversed Phase Chromatography<sup>1</sup>

Reversed phase chromatography (RPC), is often the first choice utilized in the laboratory due to its convenience and efficiency as well as its amenability to various types of LC detectors, such as UV and MS. Also, it is the only means of chromatographic separation used throughout this dissertation and will be the only type discussed.

RPC is separation based on hydrophobic binding interactions between an analyte in the mobile phase and an immobilized hydrophobic stationary phase, like those discussed previously. In effect, the analyte is partitioned between the mobile phase and the stationary phase, creating equilibrium, described by the distribution ratio,  $K$ . The distribution of the analyte between the phases depends on the binding properties of the stationary phase, the hydrophobicity of the analyte molecule, and the composition of the mobile phase.



Mobile phase composition in RPC is one main reason the technique is easily amenable to LC detection. Since, like discussed, separation is based on hydrophobicity with the most

polar molecules eluting first and the more hydrophobic to follow, mobile phases are based on a mixture of aqueous and organic solvents. At the beginning of the analysis, mobile phase conditions are set so that the analyte will be adsorbed onto the stationary phase, by maintaining highly aqueous conditions at the start. These, and other conditions can then be adapted to favor the selective desorption of the analyte or analytes from the stationary phase back into the mobile phase in order to ultimately be eluted from the column and detected.

Since the stationary phase is usually immobilized in a column that the mobile phase flows through, it would be difficult to change its characteristics simply between experiments. The simplest parameters to change during an analysis are mobile phase composition, pH, and temperature. Buffer salts and / or acids may be added to the mobile phase to change the adsorption / desorption characteristics as well, but selective desorption is most often accomplished by ramping the organic composition of the mobile phase higher as the run proceeds. The ramp can be gradual (gradient HPLC), or can be accomplished through steep changes (step gradient HPLC). Once the analytes have eluted from the column, the stationary phase must be re-equilibrated to return to its original state.

As mentioned above, separation in RPC is based on adsorption and desorption from the stationary phase, and the hydrophobic properties of individual analytes determine when they desorb. When analyzing complex mixtures, like the biological samples blood and urine, the diversity of compound hydrophobicity can be quite great. There can be

molecules that bind strongly to the stationary phase under aqueous conditions to those that desorb in a narrow range of organic modifier concentration. Gradient elution gradually increases the hydrophobicity of the mobile phase and continually and systematically draws diverse analytes out of the stationary phase for detection.

In gradient elution, the column must first be equilibrated at its initial starting conditions, usually highly aqueous, to ensure the analyte will be adsorbed onto the non-polar stationary phase, but the hydrophobic analyte must also be soluble in the highly aqueous conditions. It is usually desirable to have 1-5% organic (methanol or acetonitrile) in water as the starting conditions, and to make certain that the analytes of interest are soluble in these conditions.

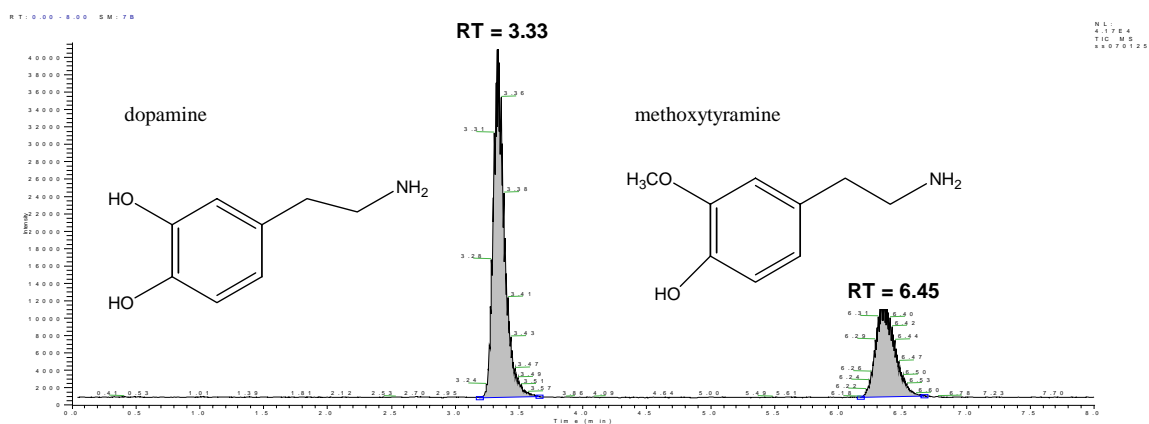


**Figure 1.1** RPC separation and MS detection of dopamine and methoxytyramine. The x axis shows analyte retention time and the y axis shows ion intensity.

Figure 1.1 shows a simple example of RPC, once the sample is applied to the column, the conditions are altered so that the analytes will be selectively desorbed from the stationary phase and flow through the column with the mobile phase and into the detector. In RPC compounds elute in order of polarity. The most polar molecules elute first with the less



polar compounds to follow, as indicated. In this example, mass spectrometry was used to detect the molecules. There are many types of detectors available for LC analyses and several of them are used in this dissertation. The different types of LC detection methods used here will be described next.

### 1.3 UV Detection<sup>1</sup>

The detector most associated with LC analysis is simply UV detection. UV is a non-destructive detection method consisting of a UV-transmitting flow cell through which the post column eluent flows, a deuterium or tungsten lamp and photodiode arrays (PDA) or phototube detectors. A deuterium lamp is used to provide light between 190 and 400 nm through the flow cell which then is directed on a diode, used to measure the light intensity ( $I$ ). The original light intensity ( $I_0$ ) is also measured by directing the light to a reference diode and the two signals are converted into absorbance by taking the log of the  $I_0$  to  $I$  ratio. The technique is very easily amendable to most LC configurations as well as for most analytes of interest, providing the analyte is of sufficient concentration, contains a UV radiation-absorbing chromophore, and no structural information is required from the analysis. A schematic of the detector with a PDA detector can be seen in Figure 1.2.

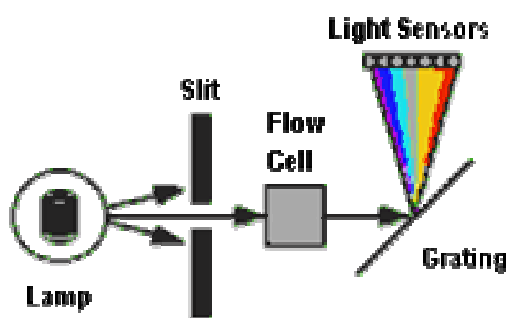


**Figure 1.2 Schematic of a UV flow cell with PDA detection. HPLC flow is perpendicular to the flow of light indicated with black arrows.**

Since the technique is non-destructive, UV detectors are ideal to be placed in series with other instruments such as MS detection or fraction collection. In this case the analytes of interest could be simultaneously separated and detected as well as collected for additional analyses such as offline-MS or NMR studies. UV-guided fraction collection is utilized in both Chapters 4 and 5 of this dissertation. In this context the techniques were done in parallel with MS detection and will be described later in this chapter of the dissertation. Next electrochemical array detection (EC-array), which is another LC detection technique, will be discussed.

#### 1.4 Electrochemical Array Detection<sup>2</sup>

Electrochemical array detection (EC-array) is a technique developed by Dr. Wayne Matson et al.<sup>3</sup> based on coulometric electrochemical detection (ECD) with the hopes of making the electrochemical equivalent of the PDA. The EC-array is a serial array made of up to 16 coulometric electrodes, with each individual electrode consisting of a flow-through porous graphite working electrode yielding close to 100% analyte conversion

efficiency. This efficiency, in combination with electrodes in series, provides detection advantages such as selectivity allowing for co-eluting species to be resolved and sensitivity with limits of detection down to the low femtomole (pg/mL) range.

Figure 1.3 shows a schematic of a two coulometric electrode cell array, highlighting how compounds with differing oxidation potentials can be detected. In the example compound A readily oxidizes to compound P at 200 mV with compound B passing through unchanged until reaching the second electrode where it oxidizes to compound Q and compound P flows through unchanged. Just like in UV detection, the sample is dissolved in the LC mobile phases and is chromatographically separated in the column before being delivered via the mobile phase to the EC-array detector. The EC-array maintains a constant potential across each individual electrochemical cell in the array, controlled by a potentiostat. When an EC active compound enters the electrode, it can be oxidized or reduced depending on the compound and the potential being applied. When a compound is oxidized it loses electrons and responds with a positive change in current. This current change is detected by the potentiostat and plotted in the EC chromatogram. In the example given in Figure 1.3<sup>2</sup>, the two compounds are separated chromatographically as well as electrochemically. If the compounds were to co-elute, as is sometimes the case with complex mixtures, the compounds could still be able to be discerned by their different electrochemical responses.

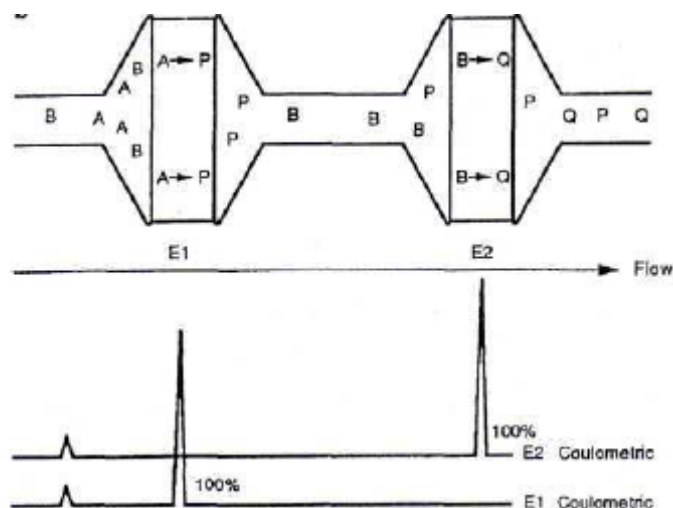


**Figure 1.3** The top panel shows a two coulometric electrode array where E1 is held at 200 mV oxidizing compound A to P, allowing B to flow through unchanged and E2 is held at 600 mV oxidizing compound B to Q allowing P to flow through unchanged. The bottom panel shows two chromatograms representing the compounds eluting from the detectors and being detected.

In addition to its specificity, coulometric detection offers a major advantage for quantitative studies. Since, as discussed, 100% of the analyte is either oxidized or reduced when passing through the electrode with its response recorded as the change in current, one can then directly correlate peak area, or total amount of charge transferred, to moles of analyte by using Faraday's law. This aspect of EC-array detection is utilized in Chapter 2 of this manuscript and will be described in greater detail in that section.

In the commercially available EC-array instruments distributed by ESA inc. Bedford, MA, each electrochemical "cell" contains 4 coulometric array electrodes in series. Since the instrument can handle up to 16 electrodes, the instrument can control up to 4 "cells" via the potentiostat. Figure 1.4 shows a cross-sectional cut out of the ESA 6010 cell, which was used throughout Chapters 2 and 3 of this dissertation, labeling the porous graphite working electrodes as well as the palladium counter and reference electrodes.

Finally, the flow channel which allows the LC mobile phase to be pumped between them is shown.

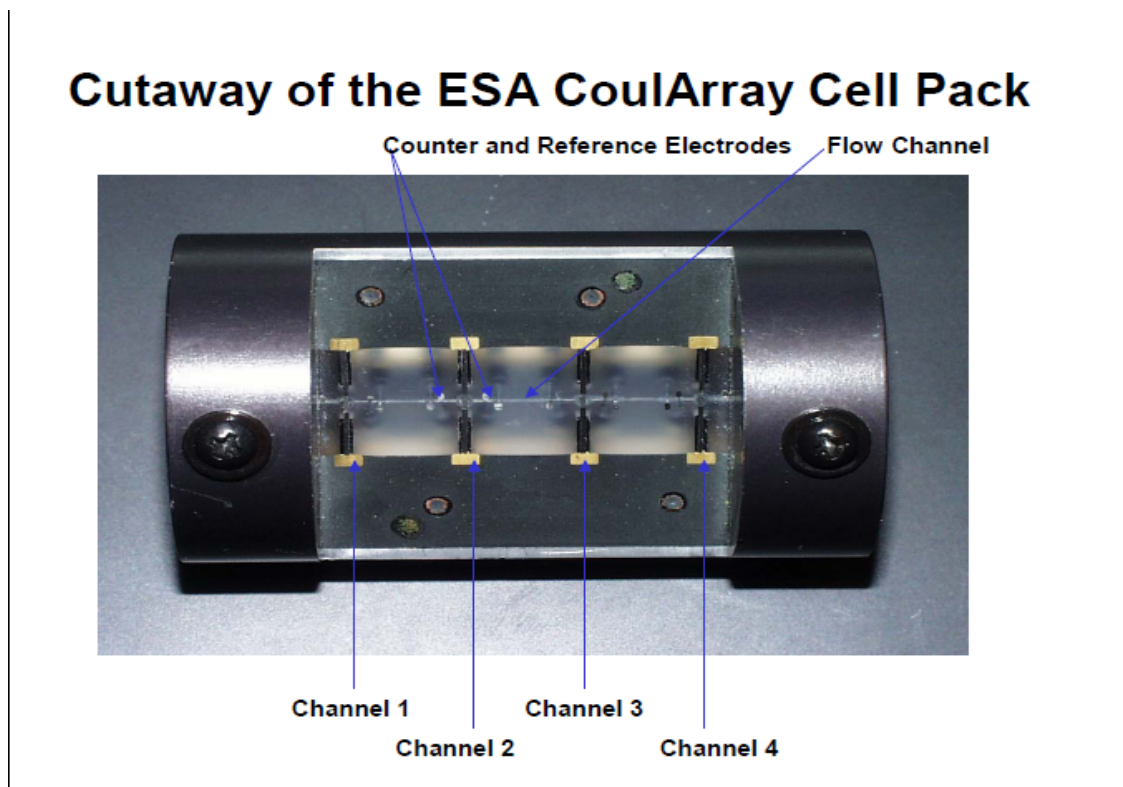


**Figure 1.4** A cross-section cut out of the ESA 6010 cell Pack indicating the 4 porous graphite flow through electrodes as well as the reference and counter electrodes. LC flows from left to right in the Figure.

Unlike UV detection, EC-array detection is a destructive technique in that once the compound passes through the electrochemical cell it is either oxidized or reduced and therefore altered from its original state. This aspect of the detection technique becomes important when trying to combine it with additional LC detection techniques, such as MS which has the further ability to characterize unknown compounds, and will be discussed further at the end of this chapter. Theory and basics of MS analysis and detection will be discussed next.

## 1.5 Mass Spectrometry<sup>4</sup>

Mass Spectrometry (MS) is a technique based on the separation and detection of gas-phase ions via their individual mass-to-charge ratios ( $m/z$ ). MS is unique among instrumental methods of analysis in that there are different physical principles used to separate ions. Mass-to-charge can be based on kinetic energy, or momentum of the ion as well as path stability, frequency of oscillation and velocity, depending on the instrument being used. These measurements can be used to facilitate unknown compound identification through individual mass determinations in addition to unique molecular fragmentations that are also important in MS detection. Before delving into the specifics of the technique, it is important to understand the basic components of a mass spectrometer prior to discussing each in detail.

### 1.5a Components of a Mass Spectrometer

A mass spectrometer consists of four basic parts: the source, where analytes may be transferred into the gas-phase and undergo ionization; the mass analyzer, typically held under vacuum, where the ions are separated from each other based on their  $m/z$  ratios; the detector, where the abundance of each ion is determined, and the data system, where the results are organized and reported<sup>5</sup>. Figure 1.5 provides a schematic of these basic components. There are many combinations of sources and analyzers, producing many variations of mass spectrometers. A certain combination of source and analyzer can be

more suitable to examine particular types of analytes, or to provide specific information, such as exact molecular mass, isotope content, structural information, or analyte quantitation. Each chapter of this dissertation contains MS data; however, different instruments containing different ionization sources as well as analyzers and data systems were utilized. Throughout this section, each component of the MS will be discussed in relation to the specific techniques used in the remainder of this manuscript.

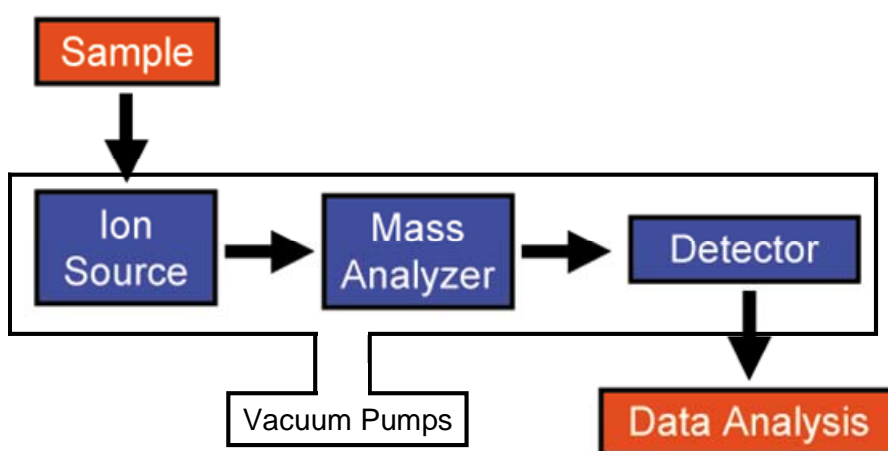


**Figure 1.5** A schematic representation of the 4 parts of the MS detection system.

### 1.5b Ionization Sources

In order for a substance to be analyzed by MS, it must become a gas-phase charged entity called an ion. Ions can be positively or negatively charged, depending on the manner in which the charge is gained. For positively charged ions, the most common charging method is protonation (addition of a hydrogen atom), which results in the formation of a  $[M+H]^+$  ion. For negatively charged ions, deprotonation is the most prevalent scheme, producing a  $[M-H]^-$  ion. There are many methods by which charge is gained, called

ionization, however, only one specific technique, electrospray ionization, and a variation of this technique, were used in this dissertation and will therefore be the only methods discussed.

### *i* Electrospray Ionization<sup>6,7</sup>

Conventional electrospray was first introduced in 1984 by John Fenn at Yale University<sup>8</sup>, and was instrumental in allowing biomolecules to be successfully transferred to the gas-phase and ionized without significant fragmentation, permitting their MWs to be accurately determined.

Electrospray ionization (ESI) operates on the basic principles of an electrochemical cell, and is represented in Figure 1.6<sup>9</sup>. A liquid flow, like that from an HPLC or other pumping system, is introduced into a stainless steel needle. A potential of between 2 and 5 kV, depending on the liquid composition and flow rate, is applied between the needle and a counter electrode, and ions in the solution migrate accordingly. If a positive potential is applied, the positive ions flow toward the outlet of the needle, attracted to the counter electrode, held at ground. The negative ions in the solution migrate back in to the bulk solution, creating a charge separation in the liquid. As the positive ions are pulled toward the counter electrode, the stream of ions is pulled out of the needle in the form of a spray.



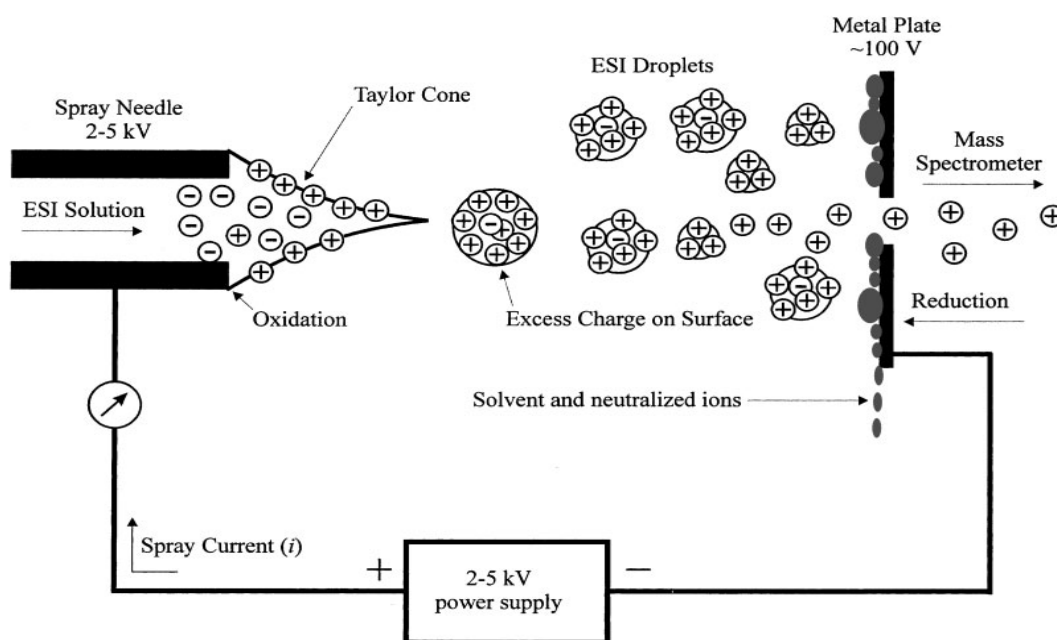


**Figure 1.6** Picture representation of ESI showing the bulk liquid flow exiting the spray needle as positively charged ions due to the 2-5 kV potential applied. The sprayed droplets then travel toward the inlet of the MS, desolvating as they travel and prior to entering the mass analyzer.

As the stream is pulled from the needle, a cone is formed, called the Taylor cone<sup>10</sup>. The ions in the cone are dispersed into finer and finer droplets. As the droplets become smaller, the charge-to-surface-area ratio increases, forcing the drops to become increasingly unstable. At a point that the charge-to-surface-area ratio approaches the Rayleigh limit, the drop undergoes coulombic fission and the ions are released into the gas phase, as illustrated in Figure 1.6<sup>11</sup>. The gas-phase ions continue on their path toward the counter electrode, and enter the mass spectrometer through the orifice. A sheath gas or heat is sometimes used to aid in the desolvation.

## *ii* Nanoelectrospray Ionization

Nanoelectrospray ionization (nESI), which can be viewed as a miniaturization of ESI, was first introduced by Wilm and Mann in 1996<sup>12</sup>. Nanoelectrospray utilizes a much narrower needle or fused silica capillary than conventional electrospray<sup>13</sup>, and usually does not require a sheath gas for desolvation due to its lower flow rates providing a lesser volume into the MS. Nanoelectrospray ionization operates at flow rates ~300 nL/min or less and has been implemented both statically without mechanical pumping<sup>12</sup>, and dynamically.

There are inherent advantages to utilizing nESI over conventional ESI<sup>9, 12</sup>. The lower flow rates yield smaller droplets out of the capillary tip which desolvate easier, eliminating the need for a nebulizing gas. The drops contain a lower number of molecules, which decreases analyte clustering and increases ionization efficiency. Nanospray ionization droplets have a higher surface-area-to-volume ratio and a 20-25x higher charge-to-volume ratio, allowing more analyte molecules to reside on the droplet surface, and thus increasing the desolvation of these analytes. Also, nanospray ionization allows the spray tip to be placed in close proximity to the orifice, further increasing ion transmission efficiency without concern for arcing. Additionally, the technique tolerates higher salt concentrations, which allows for minimal sample clean up. Chapters 2, 4 and 5 all deal with nESI, and its implications to those experiments will be discussed in greater detail in the introduction to those sections.

### 1.5c Types of Mass Analyzers

There are many different types of mass analyzers, and each one has different characteristics that make it the optimum analyzer for a particular analysis. These characteristics are often described by a set of mass spectrometric figures of merit<sup>14</sup>. Several of the figures will be helpful to define as they will be useful in describing the specific mass analyzers used in this dissertation. A key figure is mass resolution, which is defined as the mass associated with the apex of the peak divided by the width at a specified height (x). Mass accuracy is the ratio of the mass-to-charge measurement error (i.e., the difference between the measured M and the true M) divided by the true mass-to-charge ratio and is usually stated in parts per million (ppm). The mass range of an instrument is the range of mass-to-charge ratios amenable to the analysis by a given analyzer. The linear dynamic range is the range over which ion signal is linear with analyte concentration. An instrument's efficiency is determined by the product of the transmission of the analyzer and its duty cycle. The duty cycle is defined as the fraction or percentage of the ions of interest (formed in the ionization step) that enter the mass analyzer and are actually detected. The last figure of merit to be noted is the speed of analysis of a given instrument that is the time frame of the experiment; ultimately used to determine the number of spectra per unit time that can be generated described in Hertz. As done with ionization methods, only the analyzers that pertain to the work described in this manuscript will be discussed in detail.

*i* Quadrupole Analyzers<sup>4,15</sup>

Quadrupole mass analyzers achieve mass separation based directly on the mass-to-charge ratio of the ions. Ions move within a dynamic (radio frequency (rf)) electric field, and mass separation is a function of the rf voltages and the direct current (dc) applied to the four cylindrical rods, or “quadrupoles.” A schematic of a quadrupole is shown in Figure 1.7. A series of focusing optics filter the ions produced in the source into the mass analyzer and as ions pass between the quadrupoles, traveling along their axis, the applied voltages cause certain ions to become unstable and crash into the rods instead of passing through in a stable trajectory. The detector is positioned at the exit of the quadrupole, and only ions passing through in a stable trajectory are detected. The equations of motion in a quadrupole analyzer are based on second order differential equations, and are graphically represented by the Mathieu stability diagram (Figure 1.8). The Mathieu diagram is a plot of a parameter  $q$ , which relates to the rf voltage, versus a parameter  $a$ , which relates to the dc voltage. Ions with different  $m/z$  values are separated by increasing the magnitude of the rf and dc voltages, while keeping their ratio constant.

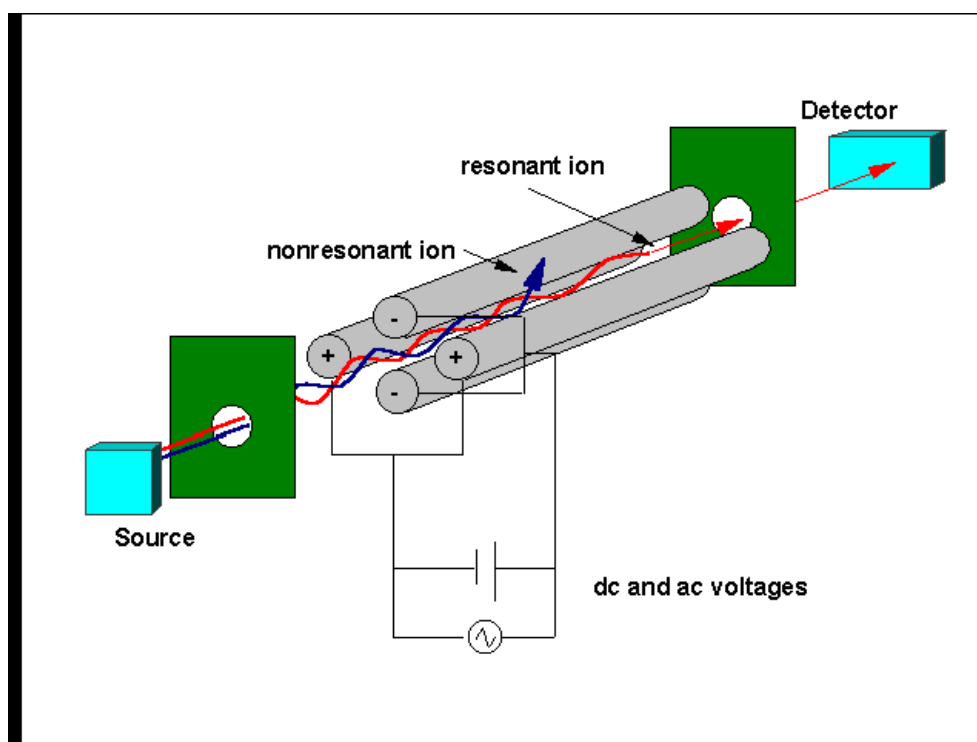


Figure 1.7 Schematic of a quadrupole mass analyzer showing the separation of the red and blue ions due to changing the magnitude of the dc/ac ratio.

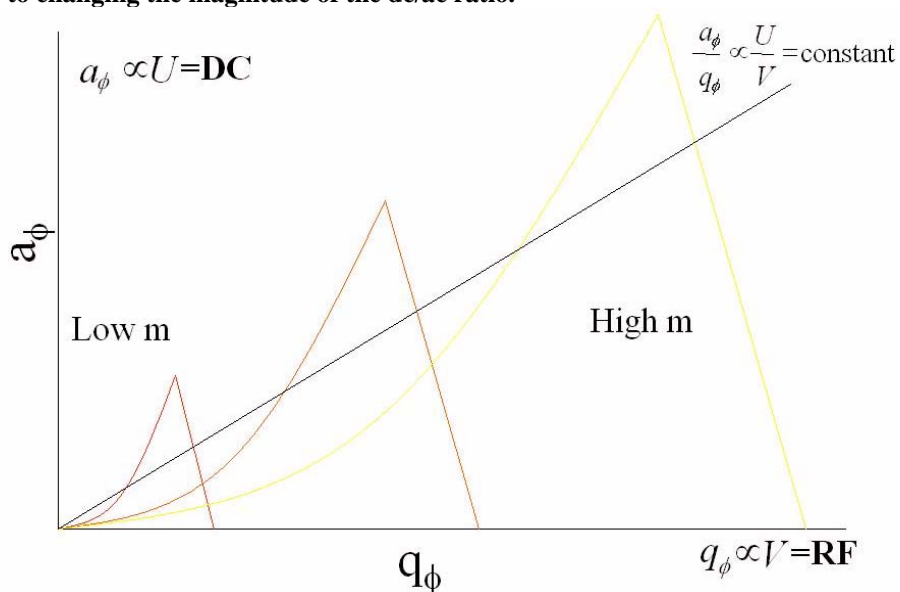


Figure 1.8 Mathieu stability diagram for a quadrupole mass analyzer

Quadrupoles have the ability to perform different types of ion scanning methods. The first type of single quadrupole analysis is the full scan experiment. During this

experiment, the rf and dc voltages are scanned sequentially to allow all ions to pass through the quadrupole at a certain point. The detector then constructs a mass spectrum that provides  $m/z$  values for all the ions detected. In addition to the full scan mode, selected ion monitoring (SIM) can also be accomplished. In this mode a single  $m/z$  value or a very small range around a single value are constantly monitored and no other  $m/z$  values are seen. This mode provides a high degree of sensitivity, since a single value of interest is being examined at all times (100% duty cycle).

Quadrupoles are probably the least expensive mass spectrometers, which is why they are often used as detectors for LC experiments. They are small, bench-top instruments, with unit mass resolving power across their mass range (usually 100-4000 Daltons)<sup>14</sup>. Most of the MS experiments described in this manuscript were conducted on instruments that are based on the quadrupole analyzer, but that are more sophisticated, and capable of more intricate techniques. The two main variations of quadrupole instruments used herein are the triple quadrupole and the quadrupole ion trap mass spectrometers and each will next be described in more detail.

#### *ii Triple Quadrupoles and their Scan Modes*<sup>4, 16, 17</sup>

A triple quadrupole mass spectrometer consists of three quadrupole analyzers placed in series. Figure 1.9 provides a schematic drawing and a picture of a commercially available triple quadrupole mass spectrometer (QQQ)<sup>18</sup>. This particular mass spectrometer has a bent design which allows it to be much smaller than many other QQQ MS. Also shown in

the design are two preliminary pumping regions (Q00 and Q0) which may help to focus the ions and transfer them efficiently from the atmospheric pressure ionization region, e.g., ESI, to the first quadrupole (Q1) which is under high vacuum. The middle quadrupole, or Q2, acts a collision cell which allows ions to be excited and fragmented. The third quadrupole (Q3) operates in the same manner as Q1, usually separating the ions just prior to detection. The three quadrupoles can be operated in a particular manner to select an ion or ions, fragment it (them), and then detect the products of the fragmentation. This is called an MS/MS or tandem MS experiment. There are many forms of MS/MS experiments, some which allow for a great deal of structural information, some which provide a high level of selectivity in the analysis. All forms of MS/MS experiments are variations on having each quadrupole either parked on a particular mass, or scanning through a range. Figure 1.10 illustrates the forms of MS/MS studies<sup>18</sup> regularly utilized with a QQQ analyzer. These scan modes are based on the quadrupole scanning methods described previously.

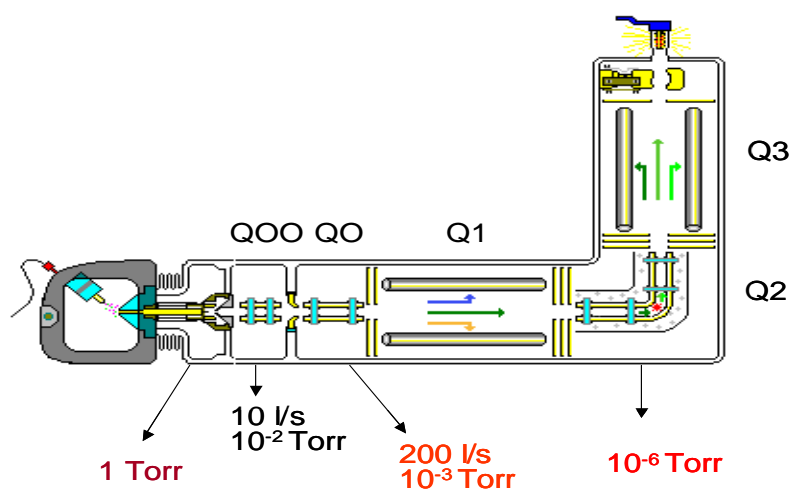


**Figure 1.9** Top view of a commercially available triple quadrupole mass analyzer showing different pumping regions and the pressure maintained.

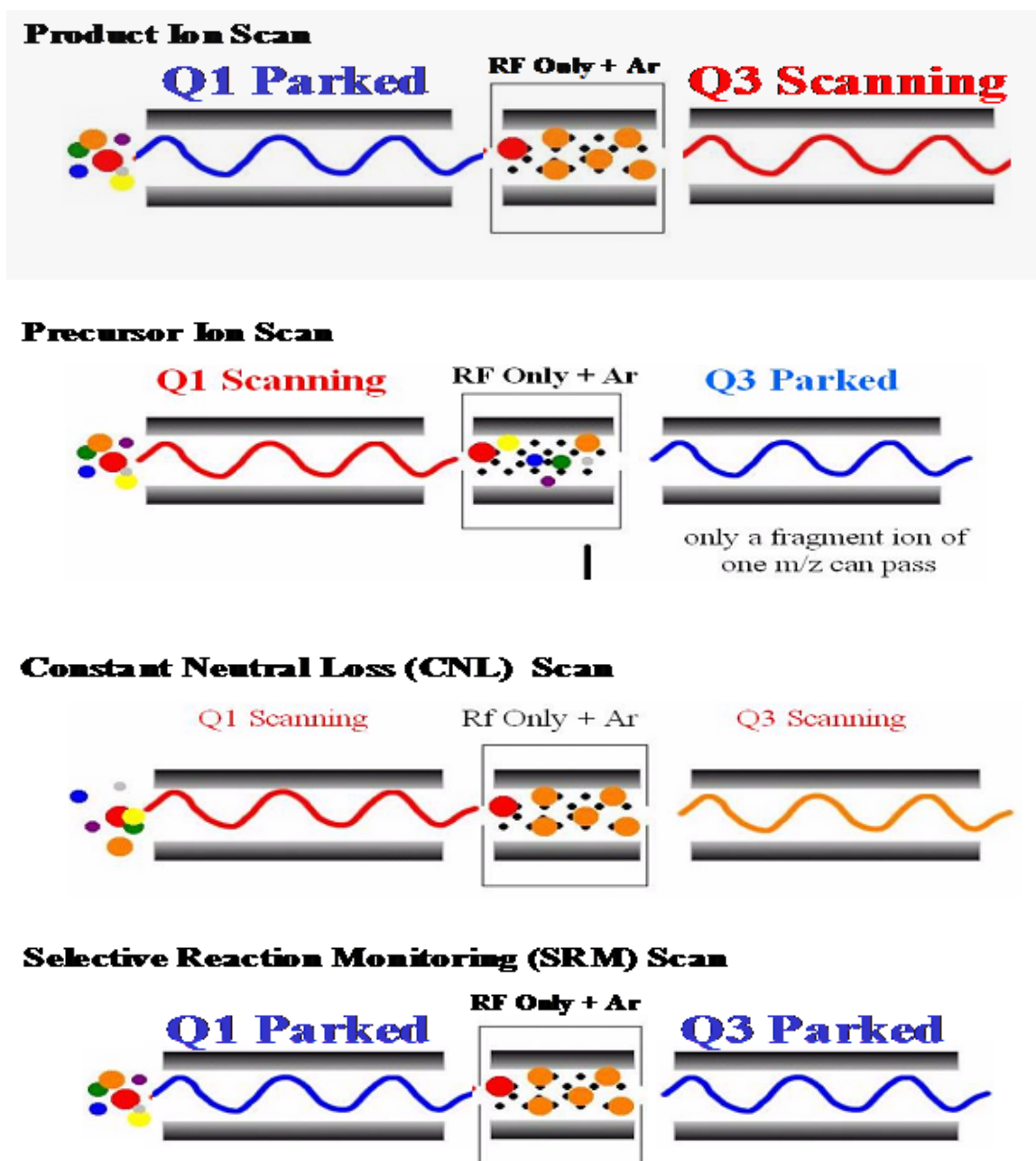


Figure 1.10 Representation of the 4 scanning modes of a triple quadrupole mass analyzer.

The first MS/MS mode to be discussed is product ion monitoring. In this mode, a single ion is selected in the first quadrupole (Q1), fragmented in the second quadrupole (Q2) by applying an rf voltage only and increasing the pressure of the cell with an inert gas



(usually Argon), and then all ions produced by the fragmentation are analyzed by the third quadrupole (Q3). The third quadrupole is scanned through a range of masses in the same manner as a full scan experiment in MS. The mechanism of fragmentation is often referred to as collisionally induced dissociation (CID). It provides structural information by elucidating features such as functional groups and providing information on their position within the molecule. This scan mode was utilized in Chapter 2 of this dissertation.

The next scan mode is the precursor ion scan which can be considered the reverse of the product ion scan. It allows isolation of a particular product ion, and determination of all the  $m/z$  ratios that fragmented to produce that specific product ion. To accomplish this, Q1 is scanned, and Q3 is “parked” on the  $m/z$  value of the specific product ion.

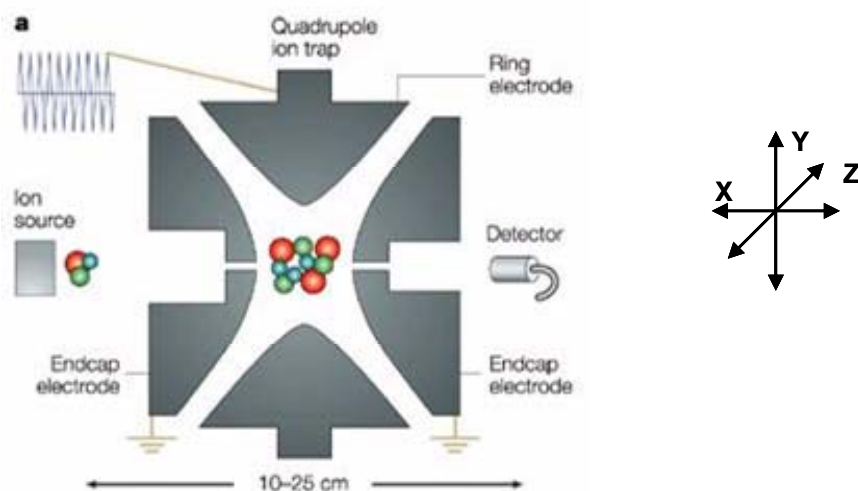
The third type of MS/MS mode is constant neutral loss (CNL). CNL is similar to precursor ion scanning, but the transition that is examined involves loss of a common neutral fragment, which is not detectable in a mass spectrometer since it does not carry charge. In this mode, both Q1 and Q3 are scanning, but they are offset by a certain mass value that corresponds to the loss of the neutral fragment, which occurs during collisions in Q2. This scan allows for monitoring of ions that lose the same uncharged segment. For example, many DNA adduct experiments monitor the loss of sugar from a nucleoside monomer, thus detecting the aglycon ion of the adducted unit. This allows for detection of new adducts without prior knowledge of their structure<sup>19</sup>.

The final MS/MS scan to be defined is selected reaction monitoring (SRM). In this mode, both Q1 and Q3 are parked at a selected mass, and a specific fragmentation is monitored by detecting the transition between the  $m/z$  ratio of a precursor ion and the  $m/z$  ratio of a specific product ion. In some studies where the precursor ion yields multiple fragments, more than one product ion can be monitored for a single precursor ion, increasing the selectivity of the analysis. Also, multiple transitions in general can be monitored, often referred to as multiple reaction monitoring (MRM), thus providing a method to monitor an analyte and an internal standard in quantification experiments. This scan provides the most selectivity and a high degree of sensitivity, since only a single value or very small ranges of  $m/z$  values are scanned. In addition to increases in sensitivity and selectivity, all MS/MS experiments increase the signal-to-noise ratio of the analyte by removing chemical noise from other ions that would also be detected in full scan modes of operation. This scan mode was also used in Chapter 2 and the specifics of its design are further defined there.

### *iii* Quadrupole Ion Traps and Scan Modes <sup>4, 14, 20-22</sup>

Another type of quadrupole analyzer is the quadrupole ion trap MS (QIT). The QIT is similar to the quadrupole analyzer in that it uses rf voltages in the x and y direction of the x, y, z plane to manipulate analyte ions in the quadrupole, but in addition has a third voltage applied in the z plane, which allows ions to become trapped in the electric field, rather than altering their paths as they pass through the field. This is accomplished through the ion trap design, consisting of three hyperbolic electrodes, one ring shaped

and two endcaps, as illustrated in Figure 1.11<sup>4</sup>. When ions become trapped in the electric field, they oscillate around the center axis of the ion trap. Instead of detecting ions moving in a stable trajectory through the quadrupole analyzers, in a QIT, ions need to become unstable and leave their stable oscillation in the trap to be detected.



## Cross section of ion trap

**Figure 1.11** Cross section view of the quadrupole ion trap MS showing the flow of ion from the ion source into the trap and out to the detector.

In 1983, George Stafford at Finnigan MAT (now ThermoFischer) developed the mass-selective instability mode, allowing packets of ions with the same  $m/z$  value to be sequentially ejected over a given time period<sup>23,24</sup>. Prior to this, the ion trap needed to be emptied before the next packet of ions was introduced. Stability of an ion is described by the Mathieu equation, just as in a quadrupole analyzer with the following substitutions:

The stability of an ion is dependent on the mass and charge of an ion ( $m$ ), the size of the ion trap ( $r_0$ ), the oscillating frequency of the fundamental rf ( $\omega$ ), and the amplitude of the applied dc ( $U$ ) and rf ( $V$ ) voltages, as shown diagram in Figure 1.12. Ions “travel” along

the differing regions of the diagram, and are ejected when they “travel” outside the stable region, that is, they become unstable.

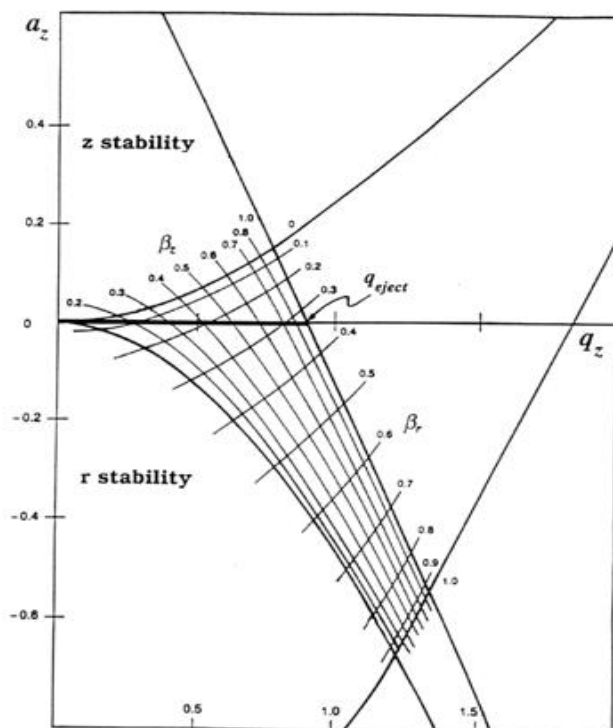


**Figure 1.12 Mathieu stability diagram for the quadrupole mass analyzer.**

Ion traps can perform full scan and selected ion monitoring analyses, as were described for single quadrupole analyzers. Additionally, QITs can perform product ion scans just as a triple quadrupole instrument, but the experiments are accomplished as tandem-in-time as opposed to tandem-in-space as with the QQQ. Triple quadrupole instruments are described as tandem-in-space instruments, since different stages of MS analysis occur in different regions of the mass spectrometer. Since all MS events occur inside the trap, QITs are tandem in time, and MS/MS experiments can often be accomplished much faster than in a tandem-in-space instrument, since there is no delay for ions to be

transferred to another part of the mass spectrometer. Usually an ion of interest is isolated, and ions of other  $m/z$  values are ejected from the trap. This allows ion traps to perform product ion scans, but not constant neutral loss or precursor scans.

The product ion scan in a QIT is quite unique and is often termed,  $MS^n$  scanning, which allows for multiple stages of product ion scans. These stages are accomplished in a sequential manner, as an ion is isolated, collided, and then a product ion is isolated and collided, and so on until the sample is consumed, or the desired information is obtained.

Ion trap mass spectrometers today are relatively inexpensive, high utility laboratory instruments. They have high duty cycles, and are excellent mass spectrometers for LC/MS experiments. The mass accuracy of an ion trap is fairly low (50 – 100 ppm), and the resolution is typically unit resolution across its entire mass range<sup>14</sup>. This instrument was utilized in Chapters 2, 4 and 5 of this dissertation.

#### *iv* Time of Flight Analyzer<sup>4</sup>

Time of flight (ToF) mass analyzers separate ions based on their velocity, which is related to their  $m/z$  value. The equations that govern the motion of ions in a time of flight analyzer are listed below:

$$\text{K.E.} = qV \qquad qV = \frac{1}{2} mv^2 \qquad V = \left(\frac{2qV}{m}\right)^{1/2}$$

$$t = L / \left(\frac{2qV}{m}\right)^{1/2}$$

Where KE is the kinetic energy,  $q$  is the ion charge and  $V$  is the applied voltage,  $m$  is the mass of the ion,  $v$  is the velocity of the ion, and  $t$  is the length of time an ion takes to travel through a flight tube of length  $L$  measured in microseconds<sup>4</sup>.

It is easy to visualize the ion separation and detection in a ToF if one thinks of the entire process as an ion race. All ions are formed at the same place, or the “starting line”, and are accelerated through a fixed potential (typically 1-20 kV) into a field-free region, and then are allowed to drift at their own pace to the detector, which in this analogy would be the “finish line”. Ions with the same charge acquire the same kinetic energy after they are accelerated through the potential, and the velocity of the ion is inversely proportional to the square root of its  $m/z$  value. Since there is no field acting on the ions, and they are all traveling the same distance to the detector (0.5 – 2 meters), it is possible to determine their mass to charge ratio by measuring the time they take to reach the detector. This design is shown in Figure 1.13a<sup>4</sup>.

In addition to the linear ToF design which was just described, there is another variation called the reflectron ToF, as illustrated in Figure 1.13b. In reflectron ToF, ions travel the length of a flight tube and then enter an electrostatic mirror. Heavier ions penetrate the mirror’s field deeper than lighter ones, and all ions are reflected into a second flight tube. The electrostatic mirror serves to focus ions with the same  $m/z$  value but with slight velocity variations, thus increasing the resolution of the mass analyzer<sup>25, 26</sup>.

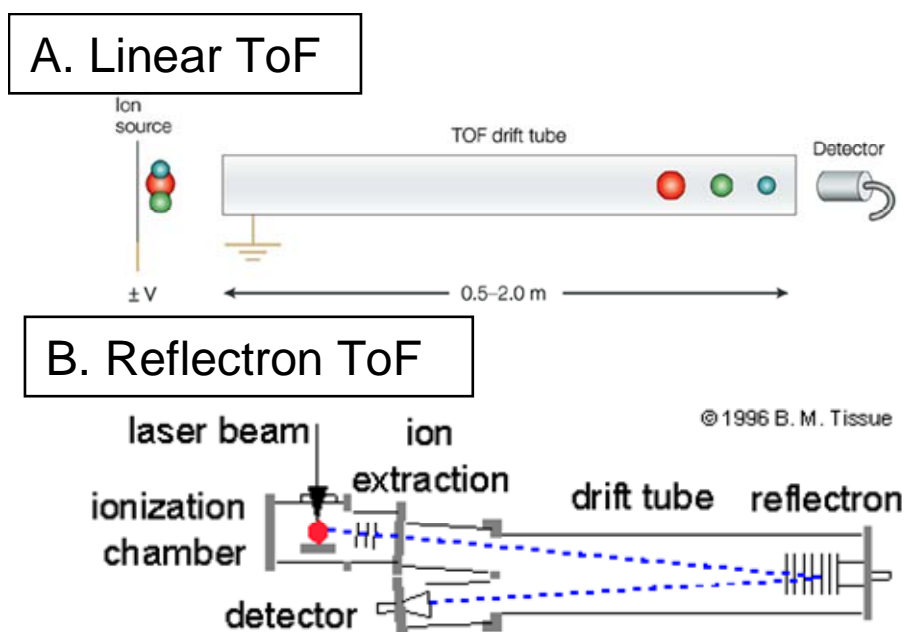


**Figure 1.13 A.** is a linear ToF analyzer showing the injection and separation of three ions whose masses are represented by spherical size with the largest ion arriving at the detector last. **B.** is a reflectron ToF mass analyzer showing the path of a single ion into the ion mirror and reflected toward the detector.

Time of flight analyzers have high mass accuracy (usually (5-50 ppm)), an extremely large dynamic range ( $>10^5$  Daltons) and the fastest speed of analysis among the mass spectrometers commonly used today ( $10\text{-}10^4$  Hertz)<sup>14</sup>. They are also readily hyphenated with quadrupole analyzers to yield a quadrupole – time of flight MS design (q-ToF). This mass analyzer will be described next.

#### $\nu$ Quadrupole-Time of Flight<sup>27-29</sup>

The simplest way to describe this MS configuration is to think of it as a triple quadrupole MS with the last quadrupole replaced by a time of flight mass analyzer. A schematic of this quadrupole-time of flight (Qq-ToF) hyphenation is seen in Figure 1.14<sup>27</sup>. In this configuration an additional r.f. quadrupole labeled Q0 is added to provide collisional cooling and focusing of ions entering the instrument, similar to the QQQ instrument

described previously. Overall the instrument consists of three quadrupoles followed by a reflecting ToF mass analyzer with orthogonal injection of ions<sup>29</sup>, and principles of this technique are defined in the following publication<sup>30</sup>.

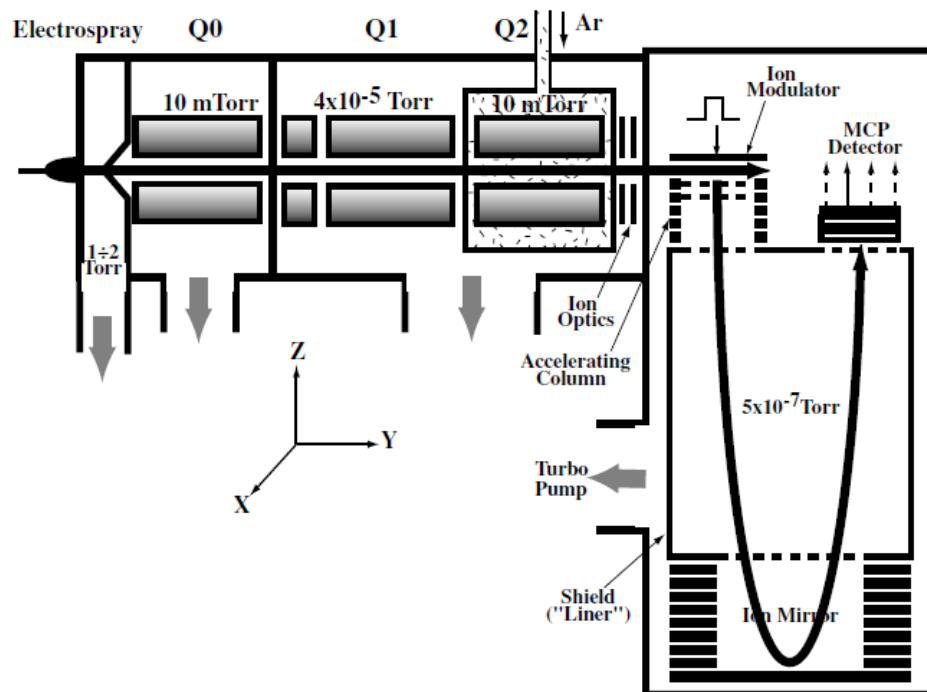


**Figure 1.14** Quadrupole-time of Flight MS schematic indicating the pumping regions, ion optics, ToF mass analyzer and detector.

In continuing with the QQQ comparison, the Qq-ToF can also provide several different mass analysis modes providing benefits such as mass resolution, mass accuracy and high sensitivity simply by replacing the Q3 with a ToF mass analyzer. In full scan MS experiments Q1 is operated only in r.f. transmitting mode while the ToF analyzer is used to record the spectra, resulting in highly resolved and accurate mass determination from the ability of the ToF analyzer to record all ions in parallel without scanning.



For MS/MS experiments, such as product ion spectra, Q1 is operated in ion filter mode which allows the selection of ions of interest. The collision cell, Q2, is operated in the same manner as the previously discussed QQQ MS, where the ions under CID with argon or nitrogen. After leaving Q2, ions are re-accelerated to the required energy and focused into parallel beam that continuously enters the ion modulator ToF analyzer, which is labeled in Figure 1.14. A pulsed electric field is applied across the modulator gap, pushing ions in a direction orthogonal to their original trajectory into the accelerating column where they acquire their final energy of several keV per charge, arriving in the field-free drift region where ToF separation occurs. Ions are detected by two multichannel plates in a chevron configuration and mass spectra are reordered with a time-to-digital converter (TDC). A Qq-ToF mass analyzer was briefly used in Chapter 3 in this dissertation. The MS analysis modes used in the experiments performed are explained and defined in greater detail in that specific section.

#### *vi Orbitrap*<sup>31-34</sup>

The orbitrap is a relatively new type of mass analyzer invented by Alexander Makarov in 2000, employing ion trapping in an electrostatic field around two axial electrodes, an outer barrel-like electrode and a central spindle-like one<sup>31</sup>. Orbiting ions also perform harmonic oscillations along the electrode with ion frequency proportional to  $(m/z)^{-1/2}$ . The ion frequencies are measured non-destructively by acquisition of time-domain image current transients, with fast Fourier transforms (FFTs) used to obtain the mass spectra. Figure 1.15<sup>33</sup>, shows a cutaway view of the mass analyzer, where ions are injected at the

point indicated by the red arrow. Ion injection has been described as being analogous to pulling back a pendulum and releasing it to oscillate. Equations defining the specially shaped electrodes and the cylindrical coordinates  $r$  and  $z$  as well as the harmonic ion motion are described by Makarov in great detail elsewhere<sup>31</sup>.

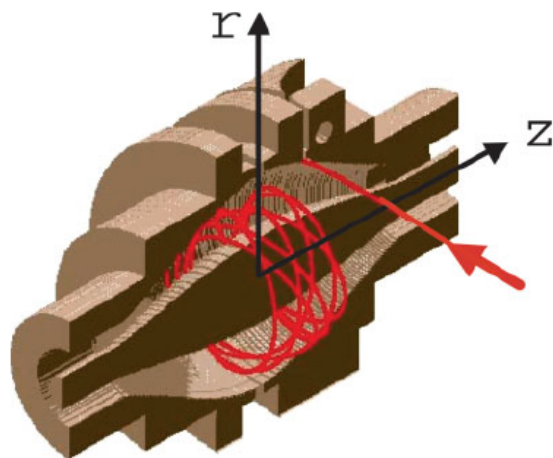


**Figure 1.15** Cutaway view of the orbitrap mass analyzer showing the injection of an ion in the direction of the red arrow, perpendicular to the  $z$  coordinate and its subsequent oscillation around the axial electrode.

Commercial orbitrap mass analyzers have been developed by ThermoFischer Corporation (San Jose, CA) and equipped with an ESI source for ion injection into the MS<sup>33</sup>. In this configuration, a series of quadrupole analyzers guide ions produced by the ESI source through several stages of pumping regions from the atmospheric ion source. The ions then proceed into a linear quadrupole<sup>35</sup> or ‘storage quadrupole’ similar to the QIT described previously in order to couple the continuous ESI source with the pulsed function of the orbitrap. Ions are then accelerated through an ion optical deflection lens system into the mass analyzer where they are then detected as previously described in this section.

Important features of the orbitrap include high mass resolution (up to 150,000), large space charge capacity, high mass accuracy (2-5ppm), mass range of at least 6000 Daltons and a dynamic range greater than  $10^3$ . In addition the analyzer has been described to be less complex with similarly high performance while also being less expensive than the Fourier transform Ion Cyclotron<sup>36</sup> (FT ICR) MS which similarly detects ions. This mass analyzer was used briefly in Chapter 3 to obtain high resolution accurate mass MS data. Accurate mass measurements make it possible to restrict the enormous number of possible molecular formulas that might represent a particular molecular mass. This aspect will be discussed further in Chapter 3 of this dissertation.

#### 1.5d Types of MS Detectors

Although the many different types of mass spectrometers offer unique versions of mass analysis, they all utilize similar methods of detection. The most common types of detectors used today are multi-channel plates, photomultiplier tubes, faraday cups, conversion dynodes and electron multipliers. Multi-channel plates are often used in ToF instruments because they have favorable aspects for high mass detection. In this detection method, each ion that strikes the MCP creates a pulse of electrons at the anode which is amplified and sent to the TDC. The TDC registers the time of arrival of each pulse in reference to the start of the ToF extraction pulse, occurring at the rate of a few kHz resulting in a spectrum of arrival times which form a mass spectrum<sup>27</sup>.

The QIT and QQQ mass spectrometers used in this dissertation use a conversion dynode and an electron multiplier. The conversion dynode generates an electrical signal, which is then amplified  $10^3 - 10^8$  times by the electron multiplier. When the electrons of the signal strike the conversion dynode, it emits several secondary electrons, which then generate a cascade of electrons, thus magnifying the original electron signal by several orders of magnitude (Figure 1.16).

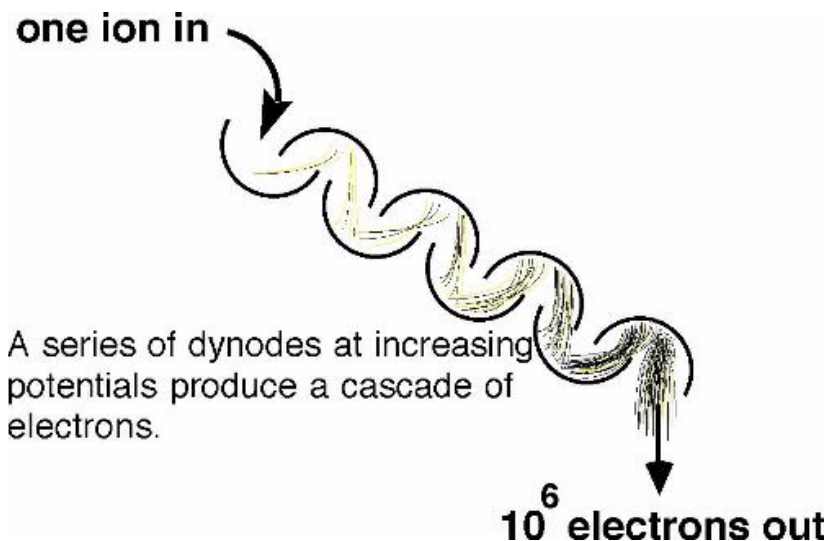


**Figure 1.16** Picture representation of an electron multiplier showing how one ion produces a cascade of electrons amplifying the signal. (Reproduced from [masspec.scripps.edu/](http://masspec.scripps.edu/) (accessed January 2009)).

Also important in a mass spectrometry system is the data system which converts the electrical signal from the instrument into the mass spectrum. These data systems are typically high-speed computers responsible for instrument control, data acquisition and data processing. The mass spectrum will be discussed next and will be the final aspect of MS detection described.

## 1.5e The Mass Spectrum

Mass spectrometry results are often reported as a mass spectrum, a graphical representation that plots ion abundance as a percentage of the most abundant ion versus mass-to-charge ratio, as seen in Figure 1.17. The information gained from the spectrum is the total ion abundances of the analytes being detected, the mass-to-charge ratios of those ions, as well as ion isotope ratios. The example given is a positive ESI full scan mass spectrum of epinephrine obtained on a triple quadrupole mass spectrometer, scanning the mass range between 100 and 500 Daltons. As is clear from the spectrum, we have the  $[M+H]^+$  ion of epinephrine at  $m/z$  183.8, in addition to an ion at  $m/z$  165.8. This fragmentation involves the loss of water upon protonation of one of the hydroxyl groups attached to the molecule. This is an excellent and clean example to show the information yielded by a simple MS mass spectrum.

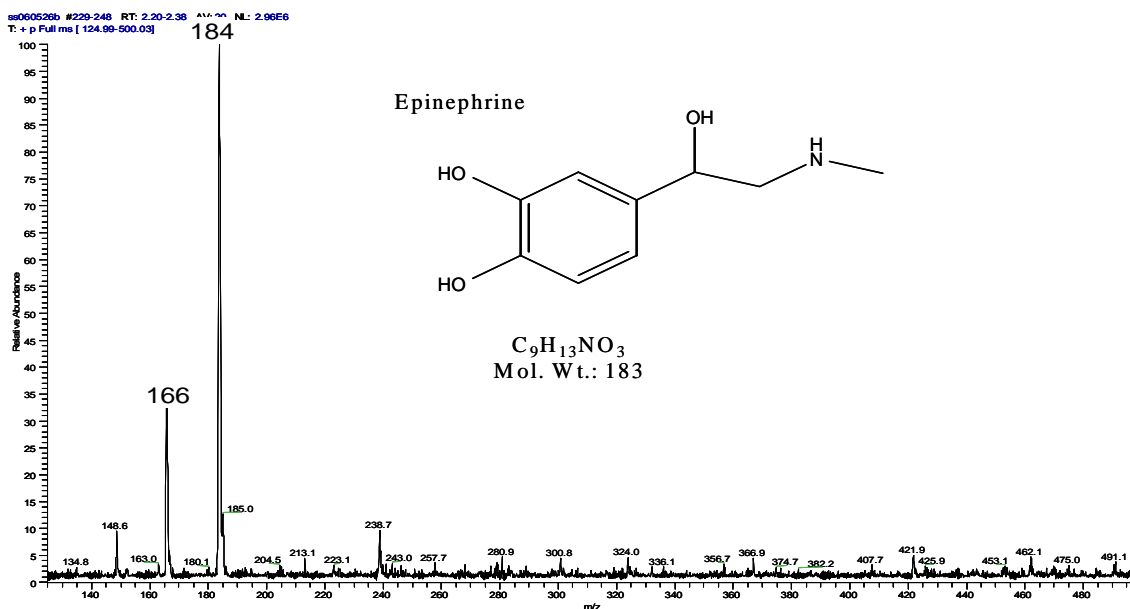


Figure 1.17 Full Scan mass spectrum of Epinephrine obtained on a triple quadrupole MS scanning between 100 and 500 Daltons. The  $[M+H]^+$  ion is represented at  $m/z$  183.8.

## 1.6 Nuclear Magnetic Resonance<sup>37,38</sup>

Nuclear Magnetic Resonance (NMR) is a well-established and powerful analytical spectroscopic technique for elucidating molecular structure. NMR can be applied as long as the molecule analyzed contains NMR-active nuclei, commonly  $^1\text{H}$  and  $^{13}\text{C}$ . NMR active nuclei have odd numbers of protons and/or neutrons yielding an intrinsic magnetic moment and angular momentum, commonly referred to as spin. Because these are both vector quantities, when the molecule is placed in an external static magnetic field, the moments align themselves relative to the field in a number of orientations based on the quantum number  $I$ . The total number of spin orientations is determined in accordance to the formula  $2I+1$ . For example, hydrogen, which has a spin of  $1/2$ , yields two spin states in the presence of an external magnetic field,  $B_0$ . The lower energy state is referred to as having a spin of  $+1/2$  and the higher energy state is spin  $-1/2$ . The static magnetic field imposes a torque on the moment which therefore traces a circular path around the applied field, known as its Larmor precession. Hydrogen, the most commonly studied nucleus, will continue to be the example used throughout the remainder of this section.

To achieve a detectable nuclear magnetic resonance signal, the proton nucleus must change its spin state. This is driven by the absorption of electromagnetic radiation, applied at a frequency that matches the Larmor precession frequency. This r.f. radiation is transmitted via an antenna, or coil, surrounding the sample, which generates r.f. perpendicular to the static magnetic field. The presence and frequency of active nuclei can be detected in the sample in two ways, (i) by scanning through multiple wavelengths

(continuous wave NMR) or (ii) as a short burst of high power that excites a broad range of transitions (pulsed NMR) to re-emit. Only pulsed NMR experiments were used in this dissertation. After the short burst of rf frequency, the nucleus then returns to its original state producing a weak oscillating voltage in the coil surrounding the sample: NMR provides non-destructive analyte detection. This signal decays as the nucleus returns to equilibrium producing what is called the free induction decay (FID). The signals collected represent the sum of the Larmor frequency of each proton and are recorded as the difference from the applied field. The FID is then Fourier transformed into a conventional NMR spectrum, with the lowest frequencies to the right on the x axis and the higher frequencies to the left. The difference increases with magnetic field strength, however, those differences are still very small, typically 10 kHz on a 500 MHz spectrometer. Because the energy difference of spin up and spin down is so small, at room temperature the populations are nearly equal (only 1 in 10,000 analyte molecules produce a signal) explaining why NMR is so insensitive in comparison to other spectroscopic techniques, such as UV detection.

Protons in different locations on a molecule can be “shielded” to varying extents dependent upon their surrounding electron cloud density which changes as a result of the chemical environment. These varying chemical environments affect the Larmor frequencies and in relation to a reference proton ultimately yield the different peaks in the representative NMR spectrum. This is how molecular structure can eventually be assigned.

For example, a generally used reference compound is tetramethylsilane (TMS) because it's chemically inert, symmetrical and soluble in most organic solvents. In addition, all of its protons are chemically equivalent, as seen in Figure 1.18, yielding one sharp absorption peak in the NMR. Also, its protons are strongly shielded by the high electron density surrounding Si. This means that most hydrogen atoms bonded to carbon, nitrogen or oxygen will be less shielded than those in TMS. Thus, TMS occurs at the far right of an NMR spectrum, and any protons less shielded than those in TMS will occur at higher frequencies and therefore will yield signals to the left of the reference peak. The chemical shifts can also be expressed as dimensionless units that are independent of the applied frequency by dividing the resonance frequency (in Hz) by the applied frequency (in Hz) and multiplying by  $10^6$ . The chemical shifts are then expressed as parts per million (ppm). This is customary nomenclature and will be used in Chapters 4 and 5.

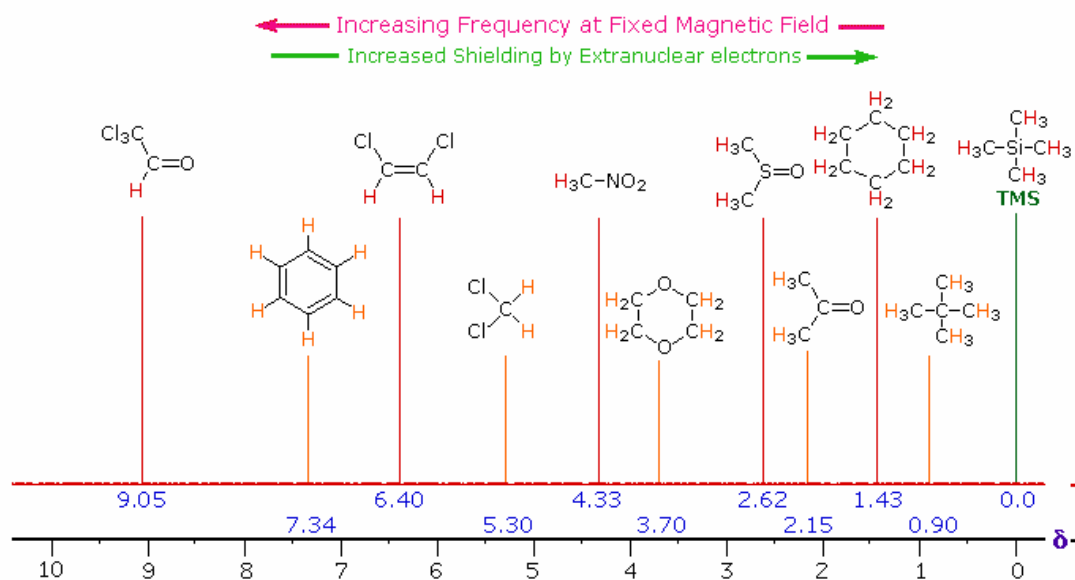


Figure 1.18. NMR spectrum of TMS showing one singlet peak at 0 ppm. (reproduced from <http://www.cem.msu.edu/~reusch/VirtualText/Spectrpy/nmr/nmr1.htm>, accessed January 2009)



Different molecular functional groups yield specific chemical shifts relative to TMS, as seen in Figure 1.18, and these chemical shifts can be used to assign structure when seeing representative peaks in a given NMR experiment. The simple NMR experiments explained are defined as 1 dimensional (1D) proton NMR experiments and are utilized in Chapters 4 and 5 of this dissertation as a means to facilitate compound structural identification that could not be determined by the other detection techniques used in the analysis. This section was meant to be a simple introduction to the theory behind NMR detection and the methods by which the NMR spectra are obtained throughout this dissertation are described in great detail in those chapters.

### 1.7. Liquid Chromatography-Mass Spectrometry Hyphenation

HPLC is routinely coupled to mass spectrometry and used in many industries and research fields, including forensics<sup>39</sup>, pharmaceutical<sup>40-47</sup>, and biotechnology<sup>48-51</sup> as well as for metabolomics<sup>52, 53</sup> and proteomics<sup>54, 55</sup>. This separation technique offers the ability to resolve individual compounds in complex samples which if left as a mixture can often adversely affect the MS detection process. Additionally, RPC is easily coupled to MS detection, especially through ESI methodologies.

Important considerations in this hyphenation are the volatility of the LC mobile phase and its additives as well as the LC flow rate into the MS. Since ESI involves a change from liquid to gas phase, it is important that all constituents are transferred efficiently

into the gas phase. This excludes the use of buffers such as phosphate. Also, efficient desolvation of gas phase ions can affect ion transfer and the process is governed by the LC flow into the ESI source, as described in the ionization section of this chapter. Finally, the incorporation of high concentrations of salt to the LC mobile phase, which may improve the chromatography i.e., efficiency or, in the case of EC-array facilitate electrochemical detection, can additionally suppress analyte ionization.

Some of the trends in HPLC that have made its coupling to mass spectrometry so successful are the use of capillary columns and trends toward miniaturization<sup>56</sup>. This is advantageous on both sides of the interface, as capillary LC leads to higher numbers of theoretical plates, and nESI leads to more sensitive MS detection. Chapters 2 and 4 of this manuscript deal with an alternative interface design that allows coupling of nESI with normal bore liquid chromatography columns<sup>57-60</sup>. This allows an analyst to benefit from the high mass loading, low cost, and the ruggedness of a larger bore column without sacrificing the sensitivity of MS detection and will be described in more detail in those chapters.

### 1.8 LC-MS and LC-EC-array Hyphenation

Two research chapters of this dissertation, Chapters 2 and 3, are dedicated to the coupling of LC-MS and LC-EC-array detection technologies into an online detection platform. There are pros and cons associated with both techniques, but pros such as MS's ability to structurally characterize compounds in combination with the ability of EC-array to

directly quantify analytes without reference compounds, have the potential to yield a very powerful hyphenated analytical technology. The practical considerations for hyphenating these two methods are discussed in detail in Chapter 2 and the remainder of this section will provide an understanding behind why these techniques were initially combined as well as what kind of research opportunities their hyphenation has had a role in aiding.

Once different MS ionization methods were developed that could interface HPLC with MS it seemed a natural progression to couple the technologies together with other HPLC detectors such as UV and ECD. Techniques such as thermospray-MS<sup>61-64</sup> and Fast atom bombardment-MS<sup>65, 66</sup> have been coupled to EC detection to study redox reactions and nonvolatile neutral analyte species with limited follow through apart from those few examples just cited. It was the implementation of ESI that yielded the most promise for hyphenating the two technologies.

In 1995, Zhou and Van Berkel published work based on coupling, in series, an ECD and a QIT MS equipped with an ESI source<sup>67</sup>. In this work, the authors' evaluated the use of this system to aid in the electrochemical ionization of neutral compounds<sup>68, 69</sup>, to study electrode reactions,<sup>70-72</sup> and to provide anodic stripping voltammetry for enhanced trace element determination. From these experiments it became obvious that the online system, in series, provided a clean and efficient means to examine oxidation reactions. In this configuration, MS provides molecular weight information as well as fragmentations which can help elucidate oxidation product structure. The researchers went on to develop an ECD that is placed in the source of the ESI emitter tip to further facilitate the

combination of the two techniques by removing any unnecessary dead volume between the detectors, increasing efficiency<sup>69, 72</sup>.

More recently the potential of the ECD-ESI/MS system to mimic oxidations catalyzed by cytochrome P450 enzymes as a means to study drug metabolism and reaction mechanisms was studied. Bruins et al.<sup>73</sup> in 2000 used an online in series EC-ESI/MS to evaluate the dopamine agonist 2-(N-propyl-N-2-thienylethylamino)-5-hydroxytetralin. The group successfully mimicked previously reported N-dealkylation, however the oxidation of the phenol function was not fully observed since the compounds formed were immediately oxidized to the corresponding quinones. These results suggested the method to be an extremely valuable tool in the early phases of drug discovery since it can provide a rapid and easy way to research the metabolic stability of possible drug candidates.

Jurva and colleagues<sup>74</sup> utilized a unique power of the EC-ESI/MS system by carrying out EC reactions on a semi-preparative scale as a means to produce oxidation products that are too reactive to survive *in vivo*, and then characterize these species by MS/MS, IR and NMR. Because the metabolites are created without the presence of biological nucleophiles, these very reactive metabolites remain un-conjugated and the addition of selected nucleophiles such as cysteine and glutathione can be done under a controlled environment to assess the conjugates formed. The results obtained from these studies were then successfully used to search for the conjugates in human liver microsomal (HLM) incubations, comparing the two different methods. The researchers provided a

unique and more streamlined opportunity to study reactive metabolites for risk assessment studies of new compound classes.

Lohmann and Karst<sup>75</sup> then went on to compare HLM incubations of model compounds amodiaquine, amsacrine, and mitoxantrone to an ECD-ESI/MS system and a system that contained online coupling of horseradish peroxidase immobilized on magnetic microparticles with LC/ESI/MS. In the same manner as when the electrochemical cell was placed in line with the MS, the immobilized enzyme was used to mimic biological oxidation of the model compounds. The two LC/MS techniques proved to be valuable complementary methods since reactive quinine, quinine imine, and quinine diimine species could be detected directly instead of only after trapping with glutathione following HLM experiments. This example showed the ability of the in series EC-array-MS system to identify both reactive and stable metabolites in drug development.

Until now, we have been discussing the hyphenation of LC/MS and LC/ECD in series where the MS detects the EC altered compounds. It is also possible to place the two detectors in parallel, as a dual detection system placed post the LC chromatographic column. In this method, it is possible to exploit the profiling power of EC-array detection with the structural elucidating power of MS detection.

Gamache et al.<sup>76</sup> were the first to describe the parallel coupling of these two detectors with a post column split ratio of 4:1 from 1 mL/min LC flow rate to the EC-array and MS detectors respectively. The concurrent detection showed several advantages in EC-array

multivariate profiling, including covering a more diverse chemical range due to the incorporation of the MS in addition to increasing the concentration range of endogenous metabolites. Furthermore, EC-Array facilitated more targeted interrogation of corresponding MS data. When combined, the qualitative information from both techniques was useful for data normalization, peak purity, and structural elucidation studies in rat urinary metabolite profiles associated with xenobiotic toxin exposure of the compounds maleic acid and chloroethanamine. The results obtained were in agreement with NMR based metabolomic studies.

Apart from this study, the research conducted in Chapters 2<sup>59</sup> and 3 of this dissertation are the only other examples of parallel EC-array and LC/MS detection. The parallel configuration in those chapters is similar to the one described by Gamache in that a post LC column split was utilized in order to couple the two detectors. However, our execution of this was quite different and will be explained in great detail in those sections.

### 1.9 LC-MS and flow-based NMR Hyphenation<sup>77</sup>

The final two research chapters of this dissertation, Chapters 4 and 5, involve coupling an LC-MS system with a flow-based NMR system. There are many advantages, disadvantages and practical considerations that were factored into actually achieving the final platform that was used. These aspects of our specific LC-MS-NMR workflow are

discussed throughout Chapter 4. In this section a brief and basic introduction to LC-NMR and LC-MS online hyphenation will be discussed.

When establishing an LC-NMR system, several parameters need to be taken into account. The first is the necessity of using NMR compatible solvents. In conventional tube-based NMR analyses, the sample is diluted in a deuterated solvent, meaning that in an HPLC version the mobile phases should be made of deuterated solvents, creating a highly expensive analysis. One way to address this issue is by miniaturizing the HPLC system to a capillary system, requiring far less solvent to be used than your typical analysis. This miniaturization has additional benefits since lower flow rates mean smaller chromatography columns and since the column diameter dictates the peak volume of the eluting analyte, smaller columns produce more concentrated peaks<sup>78</sup>. Also, the size of the NMR detection probe is scaled to a smaller volume, thereby increasing its overall mass sensitivity as well. Chapter 4 discusses the concept of NMR probe miniaturization in more detail, since the concept is utilized in those experiments. Also, normal HPLC solvents can be used, but not without complicated solvent suppression techniques which can often affect NMR detection at frequencies near those solvent peaks.

Another parameter to consider is LC gradient analysis, which is commonly implemented to create more efficient separations or yield shorter separation times. This LC method causes problems when hyphenated with NMR, due to the changes in solvent composition over the gradient. This results in changing chemical shifts and degrading the magnetic field homogeneity across the NMR coil<sup>78</sup> as the solvent flows through. In order to

eliminate this problem, stop-flow NMR acquisition can be utilized. In this practice, the HPLC pump is turned off when the analyte is positioned inside the NMR probe, instead of acquiring NMR as the sample passes through (on-flow). Another advantage to this method is that, because the flow is stopped, a lesser amount of sample is generally required than when using on-flow techniques since more time can be spent acquiring the spectrum. Stop flow techniques are usually hyphenated with another non-destructive detection technique, like UV, to trigger the NMR to stop based on peak detection and a calibrated time delay between the two detectors<sup>79</sup>. This analysis mode causes problems with chromatographic resolution due to sample diffusion when analytes are queued in the capillary tubing post chromatographic separation. The means to eliminate this problem are discussed in the introduction of Chapter 4.

When hyphenating LC-NMR with MS in an online platform the same parameters, as just discussed, must be considered again to best suit both detectors. Typically this dual detection mode is established by using a flow splitter to deliver the post-column LC eluent to both detectors. The majority of the flow is sent to the NMR because of its inherent lack of sensitivity in comparison to MS. Additionally, a time delay between the two detectors is calibrated. This is so that when a peak of interest is seen in the MS it could be programmed to stop the HPLC pump in order to acquire the corresponding NMR spectrum.

The problematic consideration for this hyphenation is the need for deuterated solvents in the NMR. As introduced in the LC-MS hyphenation section of this chapter, capillary LC



techniques, which require lower flow rates and less solvent consumption, are beneficial in ESI-MS studies allowing for the advantages of nESI to be utilized, as well as being advantageous to stop-flow NMR analyses. However, analytes with exchangeable protons can equilibrate with the deuterium in the mobile phase causing the generation of a complex molecular ion profile in their mass spectra, due to the random H/D exchange process. If non-deuterated solvents were to be used, then in the NMR signal the solvent peaks would be much larger than those due to the analyte and need to be suppressed. Again, the disadvantage of solvent suppression is the possible effect it can have on nearby analyte signals, causing a loss of structural information. Both of these solvent systems have been used successfully in drug metabolite identification studies<sup>80-82</sup>.

For unknown compound structural elucidation, it can be extremely beneficial to obtain both MS and NMR data. The direct online coupling of these methods has proved to be relevant for many fields of academic and industrial research, including the identification of pharmaceutical degradation products<sup>83</sup>, and drug metabolite identification<sup>80-82</sup>. In addition to coupling the techniques together in an online system, researchers have also been using the two techniques off-line. This was done as a means to better optimize each detector. Sample concentration techniques such as solid phase extraction<sup>84</sup> which is utilized in the commercially available Bruker BioSpin Metabolic Profiler as well as semi-preparative LC-MS<sup>85</sup> or pre-concentration column trapping<sup>83</sup> has been studied for off-line LC-MS-NMR detection platforms. In Chapters 4 and 5 of this dissertation, the benefit of this design will be discussed in detail and exploited in the areas of natural products research<sup>86</sup> and DNA-adduct isomer characterization.

## 1.10 Conclusions

Several analytical techniques have been defined and described, in this introductory chapter, with focus in the context of their use and applicability in the remainder of the dissertation. These techniques have the ability to obtain information such as compound molecular structure, molecular weight, polarity, chromophore presence, and electrochemical response. When used together as hyphenated technologies, these techniques paint a more complete picture of the analytes being assayed.

It has been stated throughout the previous sections which methods will be utilized and described further in each research chapter. Chapters 2 and 3 include LC-MS and LC-EC-array detection methodologies. Chapter 2 involves the development of a novel parallel LC-MS-EC-array detection platform for metabolite identification studies, while Chapter 3 shows how online parallel hyphenation of LC-MS and LC-EC-array detection can aid in identifying unknown Sodium Phenyl Butyrate metabolites from Huntington's disease patients being treated in a phase II clinical trial. Chapters 4 and 5 include LC-UV, LC-MS and microcoil NMR detection methodologies. Chapter 4 shows the development of a novel LC-MS microcoil-NMR detection platform and utilizes this platform to develop a streamlined approach to natural products research. Chapter 5 goes on to exploit the platform's ability to analyze microgram to nanogram quantities of material in low abundance DNA-adduct isomer characterization studies.

## 1.11 References

\* Reference numbers that appear next to section headings served as general references for the entire section.

- (1) Snyder, L. R. *Practical HPLC Method Development*, Second ed.; John Wiley & Sons, Inc.: New York, NY, 1997.
- (2) Acworth, I. N.; Gamache, P. H. *American Laboratory (Shelton, Connecticut)* **1996**, 28, 33-38.
- (3) Matson, W. R.; Langlais, P.; Volicer, L.; Gamache, P. H.; Bird, E.; Mark, K. A. *Clin Chem* **1984**, 30, 1477-1488.
- (4) Glish, G. L.; Vachet, R. W. *Nat Rev Drug Discov* **2003**, 2, 140-150.
- (5) Chiu, C. M.; Muddiman, D. C.; American Society of Mass Spectrometry, 2001.
- (6) Blades, A. T.; Ikononou, M. G.; Kebarle, P. *Anal Chem* **1991**, 63, 2109-2114.
- (7) Van Berkel, G. J. In *Electrospray Ionization Mass Spectrometry: Fundamentals Instrumentation & Applications*; Cole, R. B., Ed.; John Wiley & Sons, Inc.: New York, NY, 1997, pp 65-105.
- (8) Yamashita, M.; Fenn, J. B. *J Phys Chem* **1984**, 88, 4451-4459.
- (9) Cech, N. B.; Enke, C. G. *Mass Spectrom Rev* **2001**, 20, 362-387.
- (10) Kebarle, P.; Ho, Y. In *Electrospray Ionization Mass Spectrometry: Fundamentals Instrumentation & Applications*; Cole, R. B., Ed.; John Wiley & Sons, Inc.: New York, NY, 1997, pp 3-61.
- (11) Kebarle, P.; Tang, L. *Anal Chem* **1993**, 65, 972A-986A.
- (12) Wilm, M.; Mann, M. *Anal Chem* **1996**, 68, 1-8.
- (13) Juraschek, R.; Dulcks, T.; Karas, M. *J Am Soc Mass Spectrom* **1999**, 10, 300-308.
- (14) McLuckey, S. A.; Wells, J. M. *Chem Rev* **2001**, 101, 571-606.
- (15) Siuzdak, G.; Scripps Center from Mass Spectrometry, 2001.
- (16) Lee, M. S.; Yost, R. A. *Biomed Environ Mass Spectrom* **1988**, 15, 193-204.
- (17) Yost, R. A.; Perchalski, R. J.; Brotherton, H. O.; Johnson, J. V.; Budd, M. B. *Talanta* **1984**, 31, 929-935.

- (18) Paul, G.: Chicago, IL, 2001.
- (19) Bessette, E. E.; Goodenough, A. K.; Langouet, S.; Yasa, I.; Kozekov, I. D.; Spivack, S. D.; Turesky, R. J. *Anal. Chem. (Washington, DC, U. S.) FIELD Full Journal Title: Analytical Chemistry (Washington, DC, United States)* **2009**, *81*, 809-819.
- (20) March, R. E. *Journal of Mass Spectrometry* **1997**, *32*, 351-369.
- (21) Jonsher, K. R.; Yates, J. R. *Anal Biochem* **1997**, *244*, 1-15.
- (22) Stafford, G., Jr. *J Am Soc Mass Spectrom* **2002**, *13*, 589-596.
- (23) Schwartz, J. C.; Jardine, I. *Methods Enzymol* **1996**, *270*, 552-586.
- (24) McLuckey, S. A.; Van Berkel, G. J.; Goeringer, D. E.; Glish, G. L. *Anal Chem* **1994**, *66*, 737A-743A.
- (25) Kaufmann, R.; Spengler, B.; Lutzenkirchen, F. *Rapid Commun Mass Spectrom* **1993**, *7*, 902-910.
- (26) Noble, D. *Anal Chem* **1995**, *67*, 497A-501A.
- (27) Chernushevich, I. V.; Loboda, A. V.; Thomson, B. A. *J Mass Spectrom* **2001**, *36*, 849-865.
- (28) Morris, H. R.; Paxton, T.; Dell, A.; Langhorne, J.; Berg, M.; Bordoli, R. S.; Hoyes, J.; Bateman, R. H. *Rapid Commun Mass Spectrom* **1996**, *10*, 889-896.
- (29) Shevchenko, A.; Chernushevich, I.; Ens, W.; Standing, K. G.; Thomson, B.; Wilm, M.; Mann, M. *Rapid Commun Mass Spectrom* **1997**, *11*, 1015-1024.
- (30) Chernushevich, I. V.; Ens, W.; Standing, K. G. In *Electrospray Ionization Mass Spectrometry: Fundamentals, Instrumentation & Applications* Cole, R., Ed.; John Wiley & Sons: New York, NY, 1997, pp 203.
- (31) Makarov, A. *Anal Chem* **2000**, *72*, 1156-1162.
- (32) Hardman, M.; Makarov, A. A. *Anal Chem* **2003**, *75*, 1699-1705.
- (33) Hu, Q.; Noll, R. J.; Li, H.; Makarov, A.; Hardman, M.; Graham Cooks, R. *J Mass Spectrom* **2005**, *40*, 430-443.
- (34) Perry, R. H.; Cooks, R. G.; Noll, R. J. *Mass Spectrom Rev* **2008**, *27*, 661-699.
- (35) Schwartz, J. C.; Senko, M. W.; Syka, J. E. *J Am Soc Mass Spectrom* **2002**, *13*, 659-669.

- (36) Hendrickson, C. L.; Emmett, M. R. *Annu Rev Phys Chem* **1999**, *50*, 517-536.
- (37) Silverstein, R. M.; Webster, F. X. *Spectroscopic Identification of Organic Compounds*, Sixth ed.; John Wiley & Sons: Hoboken, NJ, 1998.
- (38) Claridge, T. D. W. *High-Resolution NMR Techniques in Organic Chemistry*; Elsevier: Oxford, UK, 1999.
- (39) Chernushevich, I. V.; Loboda, A. V.; Thomson, B. A. *J Mass Spectrom* **2001**, *36*, 849-865.
- (40) Erni, F. *J Chromatogr* **1982**, *251*, 141-151.
- (41) Qin, X. Z.; Ip, D. P.; Chang, K. H.; Dradransky, P. M.; Brooks, M. A.; Sakuma, T. *J Pharm Biomed Anal* **1994**, *12*, 221-233.
- (42) Hoja, H.; Marquet, P.; Verneuil, B.; Lotfi, H.; Penicaut, B.; Lachatre, G. *J Anal Toxicol* **1997**, *21*, 116-126.
- (43) Zheng, M.; McErlane, K. M.; Ong, M. C. *J Pharm Biomed Anal* **1998**, *16*, 971-980.
- (44) Yu, L. L.; Chao, C. K.; Liao, W. J.; Twu, T. Y.; Liu, C. M.; Yang, T. H.; Lin, E. T. *J Chromatogr B Biomed Sci Appl* **1999**, *724*, 287-294.
- (45) Lee, M. S.; Kerns, E. H. *Mass Spectrom Rev* **1999**, *18*, 187-279.
- (46) Oliveira, E. J.; Watson, D. G. *Biomed Chromatogr* **2000**, *14*, 351-372.
- (47) Ermer, J.; Vogel, M. *Biomed Chromatogr* **2000**, *14*, 373-383.
- (48) Battersby, J. E.; Guzzetta, A. W.; Hancock, W. S. *J Chromatogr B Biomed Appl* **1994**, *662*, 335-342.
- (49) Headley, J. V.; Peru, K. M.; Friesen, D. A.; Neu, T. *J Chromatogr A* **2001**, *917*, 159-165.
- (50) Vinzant, T. B.; Adney, W. S.; Decker, S. R.; Baker, J. O.; Kinter, M. T.; Sherman, N. E.; Fox, J. W.; Himmel, M. E. *Appl Biochem Biotechnol* **2001**, *91-93*, 99-107.
- (51) Buchholz, A.; Hurlebaus, J.; Wandrey, C.; Takors, R. *Biomol Eng* **2002**, *19*, 5-15.
- (52) Theodoridis, G.; Gika, H. G.; Wilson, I. D. *TrAC, Trends Anal. Chem. FIELD Full Journal Title:TrAC, Trends in Analytical Chemistry* **2008**, *27*, 251-260.
- (53) Chen, C.; Gonzalez, F. J.; Idle, J. R. *Drug Metab. Rev. FIELD Full Journal Title:Drug Metabolism Reviews* **2007**, *39*, 581-597.

- (54) Ishihama, Y. *Chromatography FIELD Full Journal Title:Chromatography* **2008**, 29, 25-31.
- (55) Froehlich, T.; Arnold, G. J. *J. Neural Transm. FIELD Full Journal Title:Journal of Neural Transmission* **2006**, 113, 973-994.
- (56) Raida, M. *Mass Spectrom. Hyphenated Tech. Neuropept. Res. FIELD Full Journal Title:Mass Spectrometry and Hyphenated Techniques in Neuropeptide Research* **2002**, 109-134.
- (57) Andrews, C. L.; Yu, C. P.; Yang, E.; Vouros, P. *J Chromatogr A* **2004**, 1053, 151-159.
- (58) Gangl, E. T.; Annan, M. M.; Spooner, N.; Vouros, P. *Anal Chem* **2001**, 73, 5635-5644.
- (59) Schiavo, S.; Ebbel, E.; Sharma, S.; Matson, W.; Kristal, B. S.; Hersch, S.; Vouros, P. *Anal Chem* **2008**, 80, 5912-5923.
- (60) Gangl, E. T.; Vouros, P.: US, 2004.
- (61) Hambitzer, G.; Heitbaum, H. *Anal Chem* **1986**, 58, 1067-1070.
- (62) Volk, K. J.; Lee, M. S.; Yost, R. A.; Brajter-Toth, A. *Analytical Chemistry* **1988**, 60, 720-722.
- (63) Volk, K. J.; Yost, R. A.; Brajter-Toth, A. *Analytical Chemistry* **1989**, 61, 1709-1717.
- (64) Volk, K. J.; Yost, R. A.; Brajter-Toth, A. *J. Chromatogr. FIELD Full Journal Title:Journal of Chromatography* **1989**, 474, 231-243.
- (65) Bartmess, J. E.; Phillips, L. R. *Anal. Chem. FIELD Full Journal Title:Analytical Chemistry* **1987**, 59, 2012-2014.
- (66) Phillips, L. R.; Bartmess, J. E.; (United States Dept. of Health and Human Services, USA). Application: US  
US, 1987, pp 20 pp Avail NTIS Order No PAT-APPL-26-867 013.
- (67) Zhou, F.; Van Berkel, G. J. *Analytical Chemistry* **1995**, 67, 3643-3649.
- (68) Van Berkel, G. J.; Zhou, F. *Analytical Chemistry* **1995**, 67, 3958-3964.
- (69) Van Berkel, G. J.; Zhou, F. *Analytical Chemistry* **1995**, 67, 2916-2923.
- (70) Deng, H.; Van Berkel, G. J. *Anal. Chem. FIELD Full Journal Title:Analytical Chemistry* **1999**, 71, 4284-4293.

- (71) Deng, H.; Van Berkel, G. J. *Electroanalysis FIELD Full Journal Title:Electroanalysis* **1999**, *11*, 857-865.
- (72) Van Berkel, G. J.; Kertesz, V.; Ford, M. J.; Granger, M. C. *Journal of the American Society for Mass Spectrometry* **2004**, *15*, 1755-1766.
- (73) Jurva, U.; Wikstrom, H. V.; Bruins, A. P. *Rapid Communications in Mass Spectrometry* **2000**, *14*, 529-533.
- (74) Jurva, U.; Holmen, A.; Groenberg, G.; Masimirembwa, C.; Weidolf, L. *Chem. Res. Toxicol. FIELD Full Journal Title:Chemical Research in Toxicology* **2008**, *21*, 928-935.
- (75) Lohmann, W.; Karst, U. *Analytical Chemistry (Washington, DC, United States)* **2007**, *79*, 6831-6839.
- (76) Gamache, P. H.; Meyer, D. F.; Granger, M. C.; Acworth, I. N. *Journal of the American Society for Mass Spectrometry* **2004**, *15*, 1717-1726.
- (77) Silva Elipe, M. V. *Analytica Chimica Acta* **2003**, *497*, 1-25.
- (78) Jayawickrama, D. A.; Sweedler, J. V. *J Chromatogr A* **2003**, *1000*, 819-840.
- (79) Silva, M. V.; Huskey, S.-E. W.; Zhu, B. J. *Pharm. Biomed. Anal* **2003**, *30*.
- (80) Dear, G. J.; Plumb, R. S.; Sweatman, B. C.; Ayrton, J.; Lindon, J. C.; Nicholson, J. K.; Ismail, I. M. *J. Chromatogr., B: Biomed. Sci. Appl. FIELD Full Journal Title:Journal of Chromatography, B: Biomedical Sciences and Applications* **2000**, *748*, 281-293.
- (81) Shockcor, J. P.; Unger, S. E.; Savina, P.; Nicholson, J. K.; Lindon, J. C. *J. Chromatogr., B: Biomed. Sci. Appl. FIELD Full Journal Title:Journal of Chromatography, B: Biomedical Sciences and Applications* **2000**, *748*, 269-279.
- (82) Dear, G. J.; Ayrton, J.; Plumb, R.; Sweatman, B. C.; Ismail, I. M.; Fraser, I. J.; Mutch, P. J. *Rapid Commun. Mass Spectrom. FIELD Full Journal Title:Rapid Communications in Mass Spectrometry* **1998**, *12*, 2023-2030.
- (83) Murakami, T.; Fukutsu, N.; Kondo, J.; Kawasaki, T.; Kusu, F. *Journal of Chromatography, A* **2008**, *1181*, 67-76.
- (84) Lambert, M.; Wolfender, J.-L.; Staerk, D.; Christensen, S. B.; Hostettmann, K.; Jaroszewski Jerzy, W. *Anal Chem FIELD Full Journal Title:Analytical chemistry* **2007**, *79*, 727-735.

- (85) Glauser, G.; Guillarme, D.; Grata, E.; Boccard, J.; Thiocone, A.; Carrupt, P.-A.; Veuthey, J.-L.; Rudaz, S.; Wolfender, J.-L. *J. Chromatogr., A FIELD Full Journal Title:Journal of Chromatography, A* **2008**, *1180*, 90-98.
- (86) Lin, Y.; Schiavo, S.; Orjala, J.; Vouros, P.; Kautz, R. *Anal Chem* **2008**, *80*, 8045-8054.



Chapter 2:

Establishment of a Liquid Chromatography-Electrochemical Array-Mass Spectrometry  
Integrated System for Metabolite Identification

Published in Analytical Chemistry:

Schiavo, S; Ebbel, E; Sharma, S; Matson, WR; Kristal, B.S.; Hersch, S.; Vouros, P.;  
Metabolite Identification Using a Nanoelectrospray LC-EC-array-MS Integrated System  
*Analytical Chemistry* **2008**, 80, 5912-5923.

## 2.1 Introduction to Metabolomic Analyses

Metabolomics is considered a comprehensive study of metabolites, typically of molecular weight (MW) less than 1000 grams per mole, found in biological systems<sup>1</sup>. This basic definition spans quite a broad range of possible aims that can be pursued in any metabolomics project, where researchers are trying to globally and comprehensively identify, characterize and determine the function of all molecules in a system. For example, in metabolomic profiling experiments, an entire biological system is generally compared to a control environment in order to assess small molecule changes and these system differences can be based on instances such as disease, disease state, medication, diet or numerous other environmental stresses. Additionally, any changes can be assessed by any number of molecular criteria such as polarity, via Liquid Chromatography (LC) analyses, to molecular structure via Nuclear Magnetic Resonance (NMR) experiments. Through these inclusive analyses, metabolomics researchers seek to aid comprehension of the important processes of an organism, organ system, cell type, cell, subcellular system and so on<sup>2,3</sup>. It is therefore understandable that the complexity of a given metabolite sample can be quite great, requiring the ability to analyze a large spectrum of compound class types over an ever greater dynamic range in concentration.

It is imperative to have analytical techniques available that can analyze a great range of classes and concentrations while present in biological matrices such as blood, plasma and urine. One can encounter a gamut of molecular species, from very polar to very hydrophobic, within the same sample. The most common means to cover large types of

compounds and eliminate any assay interferences from such complex matrices is by using hyphenated techniques and complementary instrumentation in parallel. Generally, a separation technique such as Solid Phase Extraction (SPE), LC, Gas Chromatography (GC), Thin Layer Chromatography (TLC) and Capillary Electrophoresis (CE) is used before the employment of a sensitive detection technique such as mass spectrometry (MS), electrochemical or coulometric array detection (EC-array), NMR, Fourier transform infrared (FT-IR) or Raman spectroscopies<sup>4, 5</sup>. In this research chapter, the techniques of LC-EC-array detection and LC-MS detection are combined in a novel parallel manner for the application to metabolomics type experiments. First, the aspects of combining the techniques will be discussed as a background for the experimental design.

## 2.2 HPLC-EC-array Metabolomics

HPLC coupled with electrochemical detection (EC) has proven to be a very sensitive technique for analyzing, profiling<sup>6</sup> and quantifying redox -active compounds down to pM concentrations<sup>7, 8</sup> while also having the ability to analyze more than 1000 metabolites in a given HPLC chromatographic run<sup>9, 10</sup>. In addition to being sensitive and highly precise<sup>11-13</sup>, use of EC cells in an array (EC-array)<sup>14</sup> allows differences in oxidation potentials to resolve co-eluting species, adding an element of specificity to the analysis. However, despite this high specificity, the inability to elucidate the structures of such species is a major limitation of the EC-array detection.

EC-array metabolomics profiling studies have been used to uniquely separate categories of lower motor neuron disease from controls<sup>15</sup> and diagnosed Parkinson's disease from control<sup>6</sup> by using sophisticated statistical analysis methods such as principle component analyses. However, the strongest discriminating compounds, creating the important statistical difference between the groups, are often structurally unknown. One way to overcome this limitation is via the parallel coupling of EC-array with MS detection<sup>16-19</sup>.

### 2.3 HPLC-EC-array-MS Hyphenation

The effective coupling of these two complementary detectors requires the consideration of several analysis parameters. For example, the redox activity of a compound is not only dependent on its chemical class and structure but also the conditions under which it is being assayed. Solvent properties such as pH and supporting electrolyte (ideally > 20 mM Buffer) as well as LC flow rate need to be optimized for simultaneous EC-array and MS detection without compromising their respective sensitivities<sup>20</sup>. The high concentration salt buffers typically employed in EC-array analysis are detrimental to ESI-MS analysis, creating analyte adducts and causing ion suppression often rendering analytes of interest undetectable<sup>21</sup>. Nanospray-ESI-MS (flow rates <200-300 nL/min) has been proposed as an alternative method to overcome many of the MS problems discussed as it has been proven to increase ionization, desolvation, and ion-transfer efficiency over ESI conducted at higher flow rates<sup>20</sup> while also decreasing ion suppression due to matrix effects<sup>21</sup>.

The low flow rate of nanoESI experiments, although beneficial to MS analysis, is in sharp contrast to HPLC-EC-array which is normally operated in combination with normal bore (4.6 mm i.d.) columns and in a flow regime of the order of 1mL/min<sup>22, 23</sup>. As a result, although coupling nanospray ESI-MS with EC-array detection appears to be a logical approach for global metabolomics analyses, several obstacles have to be overcome. In particular, appropriate adjustment of mobile phase composition and flow conditions need to be considered so as to maintain the chromatographic integrity of the dual detection system while also maintaining optimal performance of each detector.

In view of the aforementioned mismatch in the detection requirements of MS and EC-array, it is advantageous to design a flow splitting interface that would accommodate the integration of the two detectors into a common HPLC system. The nanoSplitter interface, developed previously in our laboratory and which delivers a very small fraction (< 0.1%) of the HPLC effluent into the MS via a concentric split design, has demonstrated significant improvements in MS sensitivity when compared to a conventional LC-ESI-MS system for both *in vitro* and *in vivo* metabolism studies<sup>24</sup>. These improvements ranged from 1.8- to 40-fold increases in analyte peak area, dependent on analyte and gradient elution profile. The most significant improvements were demonstrated by polar analytes, eluting under high aqueous conditions<sup>25</sup>. Also, and most important for incorporating EC-array with nanospray-ESI-MS, the nanoSplitter allows for the use of large bore HPLC columns and high flow rates, while also having the ability to take advantage of the sensitivity of nanospray-ESI-MS.

## 2.4 Project Goals

In the following chapter, a novel approach to the parallel coupling of normal bore HPLC with EC-array and nanospray ESI-MS based on the use of a nanoSplitting interface is presented. Through the experiments performed, it is shown that both detectors are utilized at their optimal detection mode for this parallel configuration while also maintaining the full chromatographic integrity of the system. Additionally, the system's ability to identify unknown metabolites in biological samples is shown and discussed.

## 2.5 Materials and Methods

### **LC-EC-array-MS instrumentation**

Gradient LC-MS analyses were performed using an Agilent 1100 binary HPLC pump (Wilmington, DE) and an ESA model 6210 CoulArray detector (Bedford, MA) equipped with 4 electrochemical cells coupled on-line to either a ThermoFinnigan TSQ700 triple quadrupole mass spectrometer or LCQ classic ion trap MS (San Jose, CA). Metabolite mixtures, for system establishment, were separated on a 4.6 mm x 150 mm LC column (Agilent Zorbax C<sub>18</sub> SB<sub>aq</sub>, 3.5 μm, Wilmington, DE), Huntington's Disease (HD) patient samples were separated on a 4.6 x 250 mm Atlantis<sup>®</sup> T3 5 μm HPLC column (Waters, Milford, MA). In order to achieve nanoflow conditions into the mass spectrometer, an in-house concentric nanoSplitting device was used and has been described elsewhere in detail<sup>21, 24</sup>. The flow rate through the LC column was held at 1.0 mL/min and then split post-column, using a conventional T split providing 0.8 mL/min to the CoulArray, and 0.2 mL/min to the nanoSplitter where the MS flow was split again and 300 nL/min

entered the mass spectrometer. Flow rates into the MS were determined at 50% of the gradient flow with the voltage disconnected from the nanoSplitter. A stopwatch and a glass microcapillary scored in 1  $\mu$ L increments were used to determine the amount of LC flow out of the tip at a given time period.

**Plasma extracts preparation:**

A 9 mL plasma sample was precipitated with 9 mL Acetonitrile (ACN)/0.4% Glacial Acetic Acid at  $-80^{\circ}\text{C}$ , vortexed for 20 sec, and centrifuged for 30 min/12000 g at  $-2^{\circ}\text{C}$ . The supernatant was transferred and aspirated to dryness under vacuum in a CentriVap & Concentrator (Labconco). The dry precipitate was dissolved in 200 $\mu$ L of mobile phase A (2% ACN 25 mM ammonium formate (pH 3.1)). An aliquot (24.5  $\mu$ L) of each sample was injected manually into the HPLC system.

**Mass spectrometry and HPLC conditions on extracts:**

Solvent A was 2% ACN 25 mM ammonium formate (pH 3.1), and solvent B was 80 % ACN 25 mM ammonium formate 0.3 % formic acid with gradient conditions as shown below.

%B	Time
0%	5 minutes
0-85%	25 minutes
0%	25.01 minutes

The mass spectrometric conditions on the triple quadrupole MS were as follows: Full scan mass spectra acquired in the positive mode with Q1 scanning the range from  $m/z$  125 to 500, a total scan time of 0.5 second and the electron multiplier set to 1080 volts. SRM transitions of standard metabolite solutions of, dopamine, tyramine, kynuerine, methoxytyramine, guanosine, tryptophan, tryptophol and melatonin, were determined by infusion of 1  $\mu\text{g/ml}$  concentration of analyte into the nanosplitter at 15  $\mu\text{l/min}$  using a syringe pump and further split to 300 nL/min being delivered to the MS. The MS was then operated in product ion scanning mode, where Q1 was used to isolate the ion of interest, Q2 was used as a collision cell and Q3 scanned between  $m/z$  100 and 300. Multiple reaction monitoring (MRM) analyses were done using an ICL program written to adjust the SRM transition monitored based on the scan time of the instrument and the elution time of each analyte so each SRM was monitored individually during a given scan window. All SRMs used a total scan time of 0.4 seconds with varied collision voltages depending on analyte chemical composition and the electron multiplier set to 1300 volts. For all MS analyses, the capillary temperature was set to 190°C and the capillary voltage was held at 2.5 kilovolts. No sheath gas was used due to the low flow rate.

### **Collaborations for LC-EC-array profiling and HD patient samples**

The next two sections were done in collaboration with Dr. Wayne Matson's laboratory in the Department of Systems Biochemistry, Bedford VA Medical Center, Bedford, MA. The patient samples were acquired from Dr. Steven Hersch from the Department of Neurology, Massachusetts General Hospital, Harvard Medical School, Charlestown, MA, who has been conducting the phase II SPB patient trial.



**Phenyl Butyrate Patient sample preparation and LC-EC-array profiling conditions:**

250  $\mu$ L of plasma from stage II Huntington's disease patients administered the drug phenyl butyrate was precipitated with 1 mL ACN/0.4% Glacial Acetic Acid, vortexed for 20 sec, and centrifuged for 30 min/12000 g at  $-2^{\circ}\text{C}$ . The supernatant was transferred and evaporated to dryness under vacuum in CentriVap & Concentrator (Labconco). The dry precipitate was dissolved in 100  $\mu$ L of mobile phase A. An ESA model 5240 system equipped with 12 EC-array cells, a UV cell and a fluorescence cell was used to screen the samples. Each analysis proceeded from 0-55% ACN with 100 mM lithium phosphate in a linear 35 minute gradient.

**Preparation of plasma fractions for LC-EC-array-MS metabolite identification:**

4 mL of plasma from patients receiving the therapeutic drug Sodium Phenyl Butyrate was precipitated with 16 mL ACN/0.4% Glacial Acetic Acid, vortexed for 20 sec, and centrifuged for 30 min/12000 g at  $-2^{\circ}\text{C}$ . The supernatant was transferred and evaporated to dryness under vacuum in CentriVap & Concentrator (Labconco). The dry precipitate was dissolved in 300  $\mu$ L of deionized water and SPE was performed using a 500 mg  $\text{C}_{18}$  SPE column (Diazan). The SPE column was eluted with 1 mL of deionized water, 10, 20, 30, 40 and 100 % ACN. 1 mL fractions were collected and subsequently evaporated to 100  $\mu$ L of sample. Fractions were diluted in a 1:1 ratio with HPLC grade water prior to nano-electrospray LC-EC-array-MS analysis.

**Sodium Phenyl Butyrate Plasma Sample LC-EC-array-MS Instrumentation:**

Analyses were conducted using a Waters 717 plus autosampler (Milford, MA), an Agilent 1100 binary HPLC pump (Wilmington, DE) and an ESA model 5240 CoulArray detector (Bedford, MA) equipped with 4 electrochemical cells all coupled on-line to a ThermoFinnigan LCQ classic Ion Trap mass spectrometer (San Jose, CA). Separations were conducted on a 4.6 x 250 mm Atlantis<sup>®</sup> T3 5  $\mu$ m HPLC column (Waters, Milford, MA). HPLC flow was split between the two detectors and calibrated into the MS in the same manner as described in the previous section.

**Sodium Phenyl Butyrate Plasma Sample Mass Spectrometry and HPLC Conditions:**

Solvent A was 2% ACN 25 mM ammonium formate (pH 3.1), and solvent B was 80 % ACN 25 mM ammonium formate 0.3 % formic acid.

%B	Time
0%	0 minutes
0-100%	35 minutes
0%	35.01 minutes

The mass spectrometric conditions on the quadrupole ion trap were as follows: Full scan mass spectra were acquired using data dependent fragmentation in the negative ion mode. The mass spectrometer was tuned and optimized in negative ion mode using a solution of 2-hydroxyphenyl acetic acid. Ions were sampled into the mass spectrometer at a maximum injection time of 300 ms. The first scan event was operated in full scan mode

ranging from 100 to 500 Da. The second scan event was set as an MS/MS dependent scan on ions with an intensity minimum of  $1 \times 10^4$ , using relative collision energy set to 40% and isolation width of 4 Da. The capillary temperature was set to 190°C and the voltage was held at 2.0 kilovolts. No sheath gas was used due to the low flow rate.

## 2.6 Results and Discussion

Figure 2.1 shows a schematic of the integrated nanoelectrospray LC-EC-array-MS detection system. The system consists of a binary HPLC pump connected to a large bore, 4.6 mm ID, column followed by a zero dead volume T union used to split the flow 80:20 to the EC-array and nanoSplitter respectively. The nanoSplitter expanded view in Figure 2.1 illustrates how the remaining 200  $\mu\text{L}/\text{min}$  of liquid is split concentrically down to 285 nL/min of eluent delivered to the mass spectrometer. As noted earlier, it is important that there is a reproducible agreement of retention times between the EC-array and MS in order to confidently identify analytes between both instruments. In addition, chromatographic integrity must be retained for the most favorable evaluation of metabolites in solution and optimization of both detection techniques. Although, it has been demonstrated previously that on-line incorporation of an LC-EC-array with MS is possible<sup>16</sup>, the high flow rates necessary for the EC-array analysis compromise the MS detection and performing aggressive splits on a 1 mL/min solution to submicroliter flow rates will irrevocably destroy the chromatography leading to diffusion of analytes, shifts in retention and poor nanoelectrospray-ESI-MS analysis.

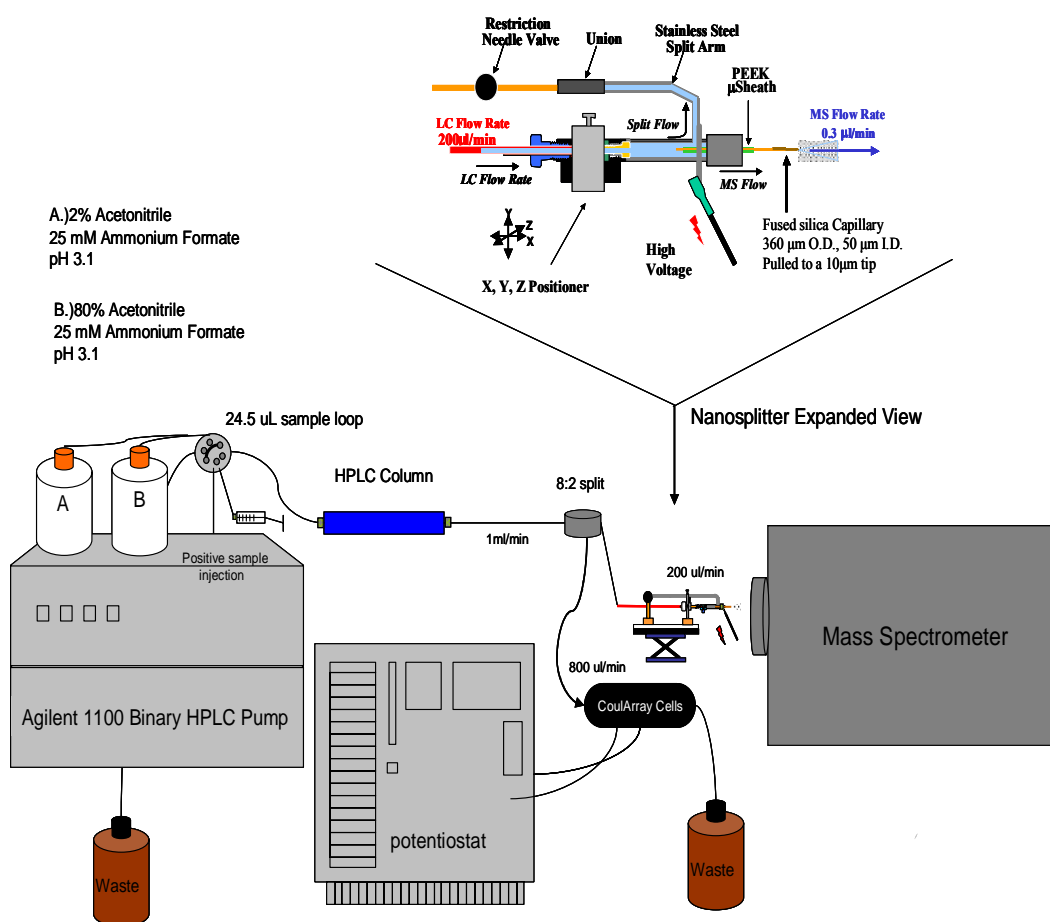


**Figure 2.1** Experimental setup of nanoelectrospray LC-EC-array-MS system as it would be configured to any mass spectrometer, including nanosplitter interface. The expanded view shows the nanosplitter in detail and the means by which it achieves concentric split ratios of up to 5000:1, with a stainless steel split arm allowing bulk flow not sampled by the capillary tip emitter to be taken to waste and a restriction needle valve controlling the eluent flow into the mass spectrometer.

## Evaluation of System Performance

### *i. Chromatography*

In order to establish the utility of the integrated nanoelectrospray LC-EC-array -MS detection system several parameters concerning chromatographic integrity, such as retention time and peak width at half height were compared and contrasted. A solution of the neurotransmitter dopamine (DA), MW = 153, and its metabolite 3-methoxytyramine (3MT), MW = 167, were assayed using MRM scanning as described in the materials and methods section. The spectra of both molecules showed an abundance ion of  $[M+H-17]^+$ , therefore, the transitions  $m/z$  154  $\rightarrow$  137 and  $m/z$  168  $\rightarrow$  151 were monitored for DA and 3-MT, respectively. These two molecules were chosen for analysis because of their different chromatographic retentions, their relation to each other in terms of metabolism and their strong EC-array as well as MS responses.

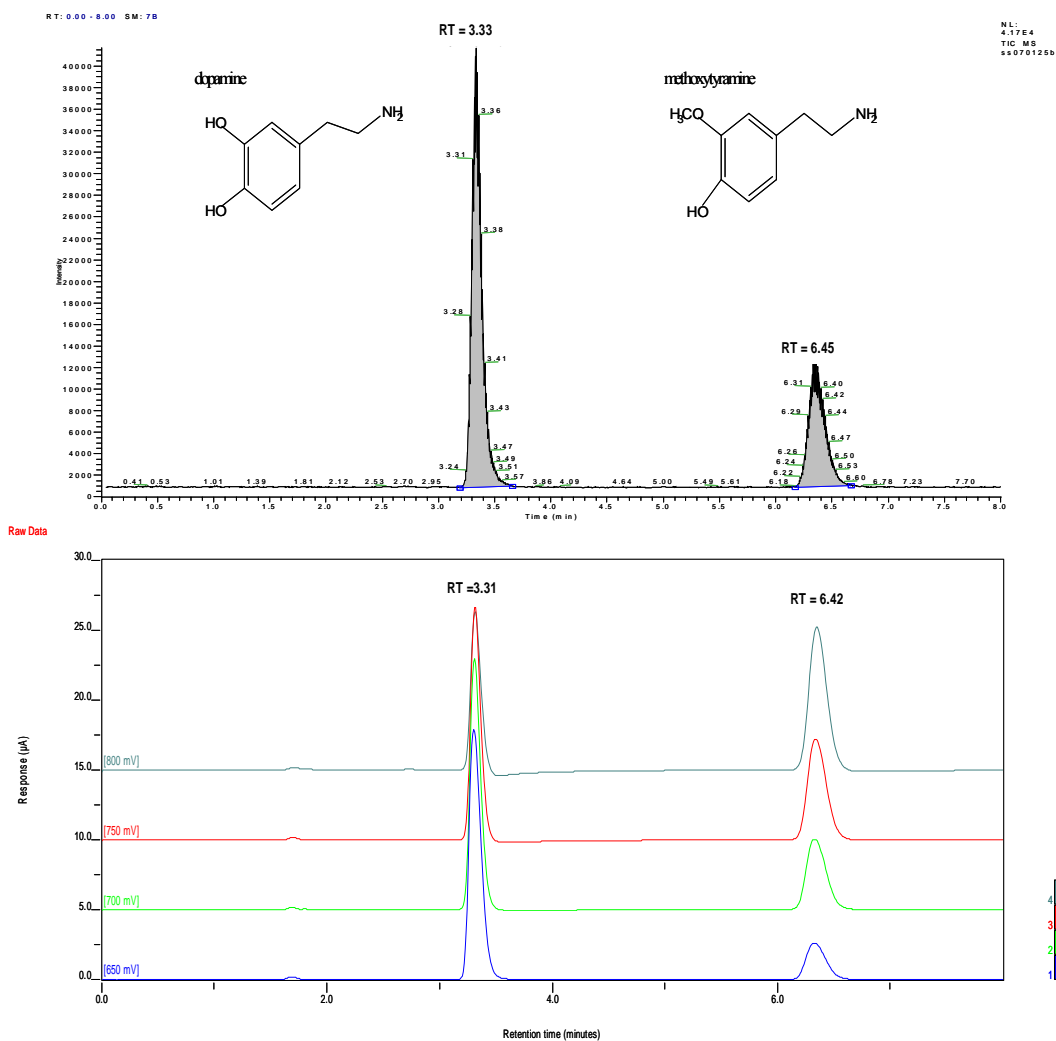


**Figure 2.2** The top panel shows an MRM TIC and the bottom an EC-array chromatogram for the analysis of a 20 ug/ml mixture of dopamine and its metabolite methoxytyramine.

Table 2.1 details the three chromatographic properties evaluated, showing comparisons between EC-array and MS for both analytes. Both detectors showed reproducible run to run retention times with RSDs less than 2% and those RSDs remained less than 2% when the retention times were compared between the detectors. Assurance of identical analyte retention times allows for accurate identification of compounds between both detectors which is especially useful in the analysis of unknown peaks. Additionally, as seen through the comparison of peak width at half height the chromatographic efficiency is

maintained through the entire system. This is also illustrated in Figure 2.2 which compares the EC-array and MS (MRM) chromatograms of DA and 3-MT. Comparisons of these chromatographic values verify that through two aggressive splits there is limited sample diffusion and well maintained separation efficiency essential for accurate analysis. These results prove the efficiency of the dual detection system for analyte comparison between detectors.

Conc (ng/mL)	Amt Inj (ng)	Dopamine							
		MS				EC-array			
		pg to MS	RT	Peak width	Signal to Noise	ng to CA	RT	Peak width	Signal to Noise
400	10	2.00	3.33	0.10	12	8	3.32	0.11	16
200	5	1.00	3.44	0.09	9	4	3.32	0.11	13
100	2.5	0.50	3.42	0.09	7	2	3.35	0.1	8
50	1.25	0.25	3.41	0.11	4	1	3.32	0.1	5
25	0.625	0.13	3.41	0.11	3	0.5	3.32	0.1	3
		<b>Average</b>	3.40	0.10		<b>Average</b>	3.33	0.10	
		<b>%RSD</b>	1.24	10.00		<b>%RSD</b>	0.40	5.27	

Conc (ng/mL)	Amt Inj (ng)	Methoxytyramine							
		MS				EC-array			
		pg to MS	RT	Peak width	Signal to Noise	ng to CA	RT	Peak width	Signal to Noise
400	10	2.00	6.45	0.2	5	8	6.45	0.17	6
200	5	1.00	6.54	0.17	4	4	6.43	0.17	4
100	2.5	0.50	6.46	0.15	3	2	6.38	0.16	3
50	1.25	**	**	**	**	**	**	**	**
25	0.625	**	**	**	**	**	**	**	**
		<b>Average</b>	6.48	0.17		<b>Average</b>	6.42	0.17	
		<b>%RSD</b>	0.76	14.52		<b>%RSD</b>	0.56	3.46	

**Table 2.1** The top block compares the chromatographic parameters of retention time, peak width at half height as well as signal to noise values for both the MS and EC-array detector over 5 concentrations of dopamine. The bottom block does the same for the dopamine metabolite methoxytyramine.

### *ii. EC-array and MS Detector Comparison*

The general utility of the integrated nanoelectrospray LC-EC-array-MS detection system is also dependent on identifying the relative responses of the two detectors under the flow split conditions used. Due to the variety of compounds and concentrations commonly found in a given metabolomics sample, it is often difficult to match limits of detection throughout chemical classes of compounds. However, if the two detectors are to be used

in a complementary fashion, it is important to identify their respective sensitivities under the system's flow split conditions in order to use the data in a comprehensive manner.

The model compounds DA and 3-MT were used again in order to compare the limits of detection of the integrated nanoelectrospray LC-EC-array-MS system. As indicated in Table 2.1, the assay is more sensitive for the neurotransmitter DA, detecting reproducibly down to 25 ng/ml which translates to 0.625 ng of material on column of which 0.13 pg and 500 pg are delivered to the MS and EC-array respectively. These mass delivery numbers reflect the initial 80% of the sample diverted to the EC-array after the first split and the eventual mass transferred to the MS via the nanoSplitter. Although, it is commonly found that the EC-array is more sensitive than the MS, in this instance, when splitting the HPLC flow in the manner done here it is found that both detectors reproducibly detect down to a concentration of 25 ng/ml with a signal-to-noise ratio (S/N) of 3. In this case the MS, while analyzing the same concentration of sample, actually detected 3 orders of magnitude less sample mass than the EC-array.

As can be seen in Table 2.1, for both DA and 3-MT the relative limit of detection observed between both the EC-array and MS detectors was for the same sample concentration injected, although differing amounts of material were delivered to both detectors. It is important that the same sample concentration was observed for each detector in order to ensure their compatibility while working in parallel mode. It is understandable that the MS detected a lesser amount of material than the EC-array in this study due to the samples being analyzed by MRM, the most sensitive and selective triple



quadrupole scanning mode. Also, the mobile phase composition such as pH and ionic strength has a great effect on performance of the EC-array. The mobile phase make-up is a compromise of salt concentrations that would allow the EC-array to work efficiently without completely destroying the MS signal.

It has been reported by Alvarez et al., that both DA and 3-MT could be detected down to the low pg level using EC-array<sup>26</sup>. However, these detection limits were achieved by using a mobile phase consisting of 25 mM potassium dihydrogen phosphate, 0.4 mM heptane sulphonic acid and 50 mM EDTA and adjusted to pH 2.5 with 85% phosphoric acid. Under those conditions, the MS would not be able to detect any analytes of interest, even while operating under nanospray conditions. Thus, we are recognizing that the optimal conditions for each individual detector may be different; the LC-EC-array-MS platform described here provides optimal performance conditions when used in parallel. It is important to remember that although lower level detection are reported for DA and 3-MT from using EC-array or MS alone, these are using only one detection source where the conditions can be optimized based on those specific analytes and experimental environments.

### *iii. Quantification using EC-array*

A definitive advantage of EC-array detection is its ability to use Faraday's law to directly quantify the amount of material being oxidized or reduced without the need of internal standards or response factors<sup>14</sup>. In EC-array detection, a porous graphite working

electrode is used where 100% of the LC effluent is passed through and subsequently, 100% of each analyte is oxidized when monitored at its optimal oxidation potential. Faraday's Law,  $Q = nFN$ , can then be applied.

Where  $Q$  is the amount of charge transferred in the reaction equal to the integrated area under a chromatographic peak,  $n$  is the number electrons transferred in the reaction and is unique to each analyte,  $F$  is faraday's constant of 96,500 C and  $N$  is the number of moles of analyte oxidized.

Faraday's law was applied to calculate the amount of DA and 3-MT oxidized by the EC-array in the integrated system and compared to the amount of DA and 3-MT that was actually delivered to the EC-array for analysis. At the concentration of 25 ng/ml, 625 pg of each was injected on column and 80% or 500 pg were directed to the EC-array. The EC-array was set to potentials 650, 700, 750 and 800 mV for cells 1 through 4 respectively. The highest oxidation potential for DA was observed at 650 mV and for 3-MT was at 800 mV. The oxidation of DA is a two electron transfer process, therefore  $n = 2$ , and at 25 ng/ml and 650 mV it was found through integration of the DA peak that 540 nC of charge was transferred. Applying Faraday's law, 430 pg of DA was calculated as being oxidized. For 3-MT at the same concentration, 285 nC of charge was transferred in the one electron oxidation process, equating to 496 pg.

The values calculated were within 15% of the theoretical amount delivered to the detector without the need for an internal standard or calibration plot. This aspect is very useful, especially in comparison to mass spectrometry where stable labeled internal standards are

needed for quantitative analyses. Direct quantification can then be done using the EC-array free of internal standards and without compromising the identification and characterization properties of nanoelectrospray MS.

*iv. Analysis in a Biological Matrix*

As discussed in the introduction, detection systems in metabolomic analysis should be able to cover different classes of chemical compounds encountered in blood, plasma, urine etc. over a range of concentrations. Thus, in order to determine the general applicability of the dual EC-array-MS detection system, an eight compound mixture representative of the diversity typically encountered in such physiological systems was analyzed both in neat solution and a plasma matrix. These specific analytes were selected due to their differences in chromatographic retention, their strong EC-array and MS responses, as well as their penchant for being found in urine and plasma samples.

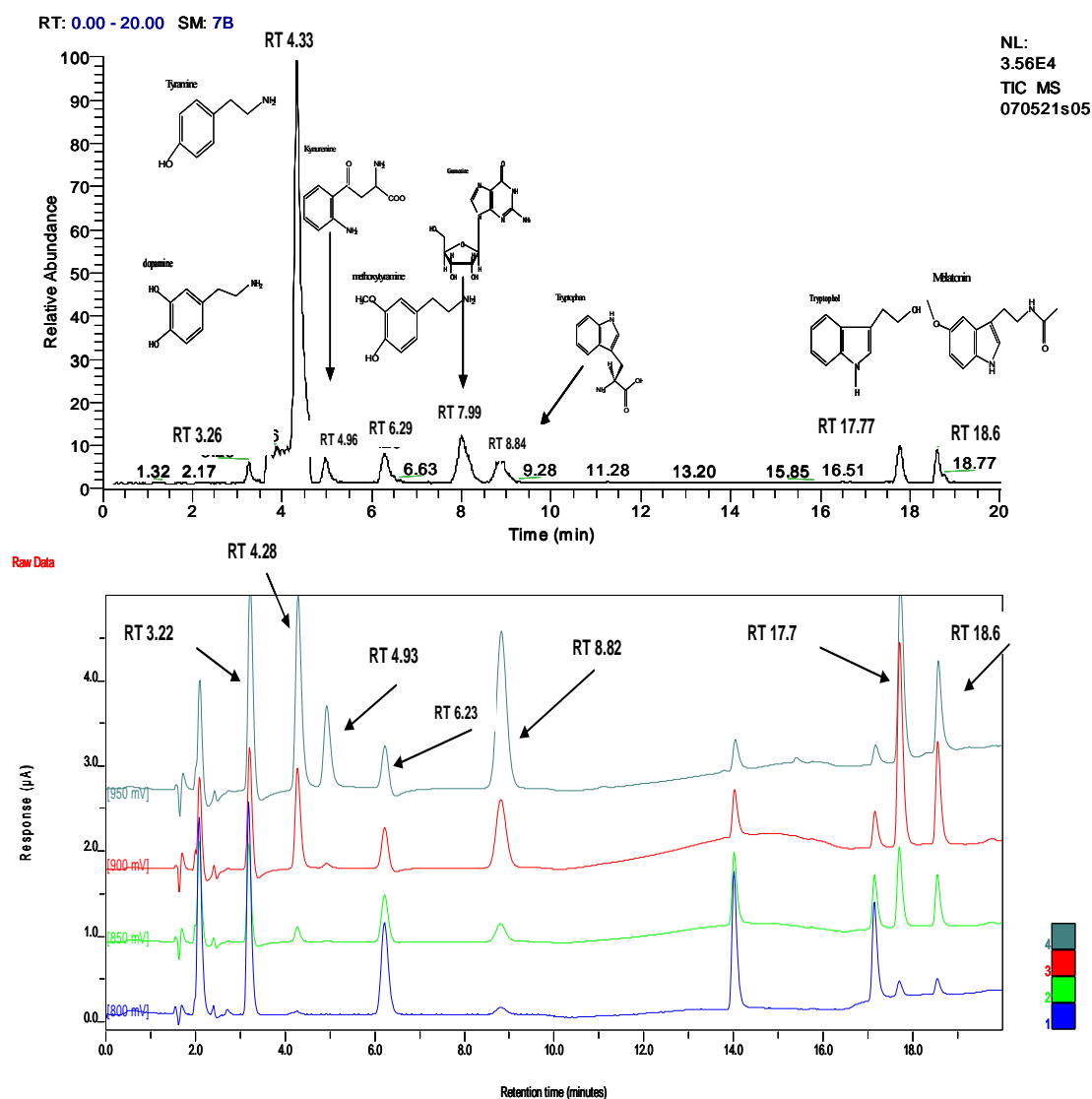
After obtaining the product ion spectra for each of the eight compounds, eight SRM transitions were identified for selective monitoring of the analytes. Next, by comparing retention times from our preliminary nanoelectrospray LC-EC-array-MS analysis where the MS was run in full scan in parallel with the EC-array, the elution times of the compounds were determined. This information was then used to write a UNIX system based ICL program that allowed the MS to monitor a specific SRM transition with collision energies optimized for each analyte over a given time period measured in MS scan events.

<u>Metabolite</u>	<u>Molecular Weight (amu)</u>	<u>MS/MS Transition (amu)</u>	<u>Retention Time (CA)</u>	<u>Retention Time (MS)</u>
Dopamine	153	154 → 137	3.22 min	3.26 min
Tyramine	137	138 → 103	4.28 min	4.33 min
Kynurenine	208	209 → 120	4.93 min	4.96 min
Methoxytyramine	167	168 → 151	6.23 min	6.29 min
Guanosine	283	284 → 152	NO SIGNAL	7.99 min
Tryptophan	204	205 → 118	8.82 min	8.84 min
Tryptophol	161	162 → 144	17.7 min	17.7 min
Melatonin	231	232 → 174	18.6 min	18.57 min

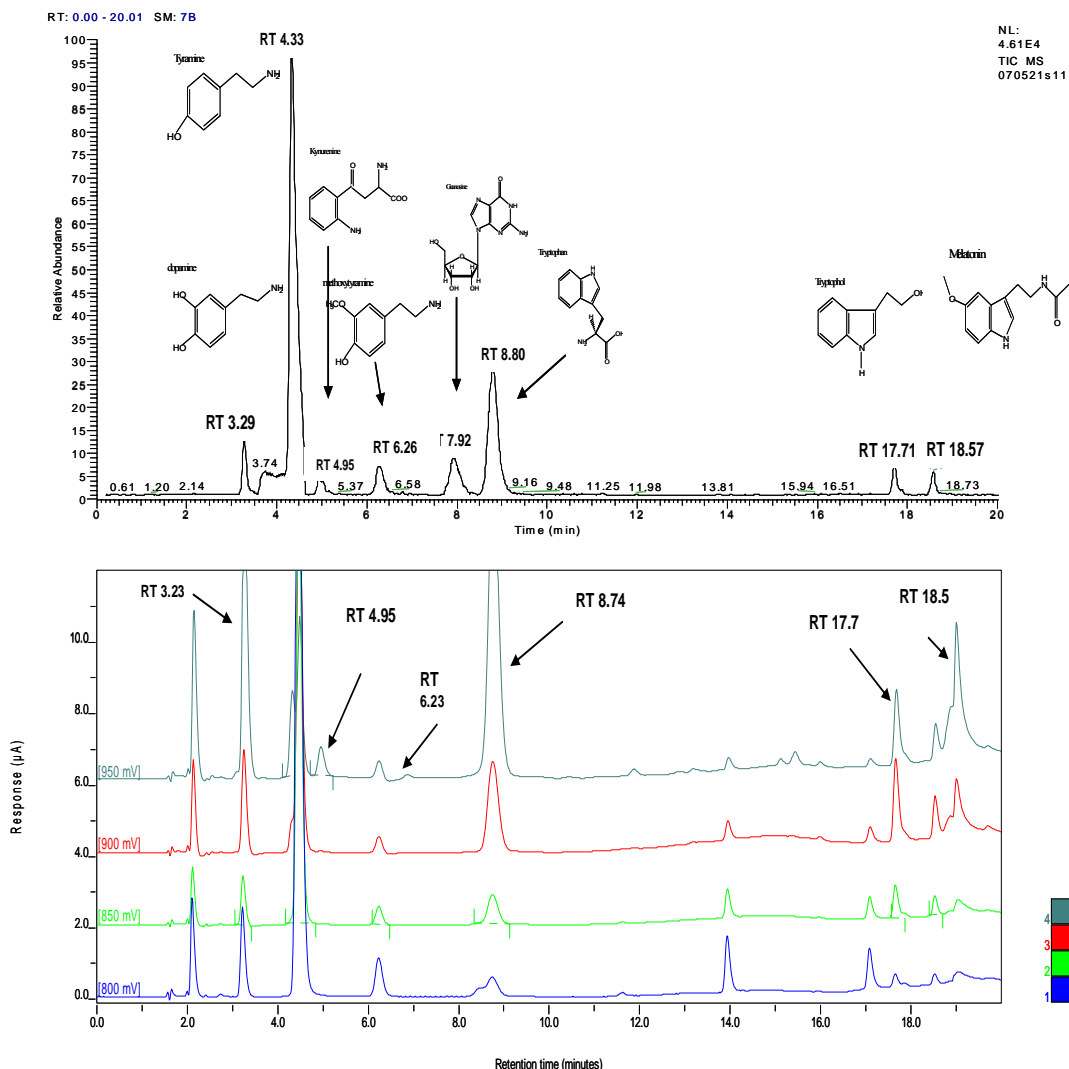
**Table 2.2 Description of all 8 analytes simultaneously assayed both in neat solution and plasma matrix. Their molecular weight, individual MS/MS transition determined via product ion scan, and retention times for the EC-array and MS respectively.**

Table 2.2 summarizes some key parameters for the analysis of the 8 metabolites including molecular weights, SRM transition monitored, and retention times as detected by EC-array and MS. Actual LC-EC-array-MS chromatograms of the mixture at a concentration of 250 ng/ml both neat solution and spiked into plasma matrix following protein precipitation are shown in Figures 2.3 and 2.4. As with the previous two-component mixture of DA and 3-MT, it is significant to note the excellent reproducibility in MS and EC-array retention times of all compounds both in the neat solution and the plasma sample. Through a comparison of analyte retention times and signals observed, it is evident that, in the spiked plasma sample EC-array chromatogram (Figure 2.4) several new and, often, co-eluting peaks can be monitored. At a retention time of 4.45 minutes and potential of 800 mV a large peak, not present in the neat solution is observed. This peak, only evident in the matrix sample, distorts the Tyramine (RT 4.3 min) EC-array

signal while its MS signal remains essentially constant. Presumably, the use of nanospray ESI and the selectivity associated with the SRM scanning mode of the MS, results in minimal matrix effects on the analyte signals when monitored by MS as opposed to by EC-array.



**Figure 2.3** The top panel shows an MRM TIC chromatogram and the bottom panel an EC-array chromatogram, for the analysis of 250 ng/ml mixture (6.25 ng injected on column) of 8 metabolites in neat solution. The MS MRM chromatogram shows detection of all 8 metabolites, where the EC-array chromatogram only shows 7, due to guanosine (MS Retention time 7.99 minutes) requiring a much larger potential in order to yield an oxidation response.



**Figure 2.4** The top panel shows an MRM TIC chromatogram and the bottom panel an EC-array chromatogram, for the analysis of 250 ng/ml (6.25 ng injected on column) mixture of 8 metabolites in plasma matrix. The matrix minimally affects the MS MRM transition peak intensities while having a greater effect on the detection of EC-array peaks due to matrix signals overlapping with analyte signals. Metabolite tyramine, at RT 4.33 minutes, is clearly detected in the MS chromatogram; however its signal is suppressed in the EC-array due to a matrix peak at 4.5 minutes.

The eight-metabolite mixture was analyzed both neat and in plasma over four concentrations (250, 125, 62 and 31 ng/mL), the lowest of which is close to the MS limit of detection ( $S/N = 3$ ) determined for DA (RT 3.22 min) in neat solution of 25 ng/mL. The effects of the plasma matrix on both the EC-array and MS detectors were examined

by comparing the absolute signal area observed for the 8 analytes in neat and plasma solution and are summarized in Table 2.3. It should be noted that limited sample preparation was done concerning the plasma samples. Merely a protein precipitation was performed before spiking the analytes and conducting the analysis.

	Conc (ng/mL)	Amt Inj (ng)	Neat Solution				Plasma Sample			
			MS		CA (nA)		MS		CA (nA)	
			Area	%RSD	Area	%RSD	Area	%RSD	Area	%RSD
Dopamine	31	0.78	2462	27.55	235	7.51	3953	8.77	3413	12.12
	62	1.55	2528	5.55	647	5.98	7859	4.64	3633	15.16
	125	3.13	5577	*	1350	*	12652	*	5130	*
	250	6.25	11087	*	2690	*	37745	*	8920	*
Tyramine	31	0.78	60526	28.26	178	15.1	85213	11.04	155	8.7
	62	1.55	123486	11.88	588	2.87	144834	11.04	NS	*
	125	3.13	14500	*	1160	*	227334	*	2200	*
	250	6.25	321510	*	2290	*	471092	*	2390	*
Kynurenine	31	0.78	1970	27.11	33	7.92	4524	22.53	29	4.69
	62	1.55	4345	5.98	221	8.14	6640	35.79	87	6.72
	125	3.13	8673	*	474	*	13703	*	435	*
	250	6.25	23372	*	948	*	18326	*	811	*
Methoxytyramine	31	0.78	5504	19.51	107	4.65	5326	11.96	114	2.03
	62	1.55	9508	13.78	269	5.68	9723	20.26	191	8.92
	125	3.13	14310	*	548	*	19721	*	543	*
	250	6.25	28196	*	1080	*	36575	*	1090	*
Guanosine	31	0.78	9672	18.77	NS	*	11003	22.53	NS	*
	62	1.55	19856	5.98	NS	*	23906	35.79	NS	*
	125	3.13	37243	*	NS	*	32980	*	NS	*
	250	6.25	63202	*	NS	*	60909	*	NS	*
Tryptophan	31	0.78	4321	17.49	208	1.36	199073	4.67	4617	5.9
	62	1.55	9797	9.48	472	3.87	198004	9.32	4597	11.6
	125	3.13	19590	*	938	*	185457	*	5830	*
	250	6.25	38227	*	1840	*	201128	*	8510	*
Tryptophol	31	0.78	3373	17.9	262	1.62	2673	19.3	260	4.95
	62	1.55	3626	13.8	635	6.05	5153	35.09	482	8.02
	125	3.13	12500	*	1270	*	11241	*	1230	*
	250	6.25	27706	*	2420	*	22681	*	2300	*
Melatonin	31	0.78	3407	13.93	115	6.79	2446	21.67	118	2.45
	62	1.55	7647	23.39	295	5.08	4453	36.32	225	5.64
	125	3.13	12385	*	610	*	15563	*	567	*
	250	6.25	25684	*	1210	*	15939	*	1110	*

**Table 2.3 Comparison of 4 concentrations of the 8 metabolites simultaneously analyzed via MRM and EC-array both in neat solution and a plasma matrix. MS and EC-array area values are from manual integration of each analyte peak.**

The results in Table 2.3 show good reproducibility in MS response at all concentrations for both the neat and plasma samples with % RSD values generally below 30% and, as expected, lower variance in the analysis of the neat solutions. Moreover, as indicated in the bar graphs of Figure 2.5, with the sole exception of tryptophan which is a major constituent of plasma as indicated in the plasma blank (Figure 2.7), the MS response for

all analytes at a given concentration remained constant between the neat solutions and the plasma samples. A similar trend was also observed with the EC-array detection (Figure 2.6) except that, in addition to tryptophan a significant signal increase was observed for DA (RT 3.27 minutes) when spiked into plasma.

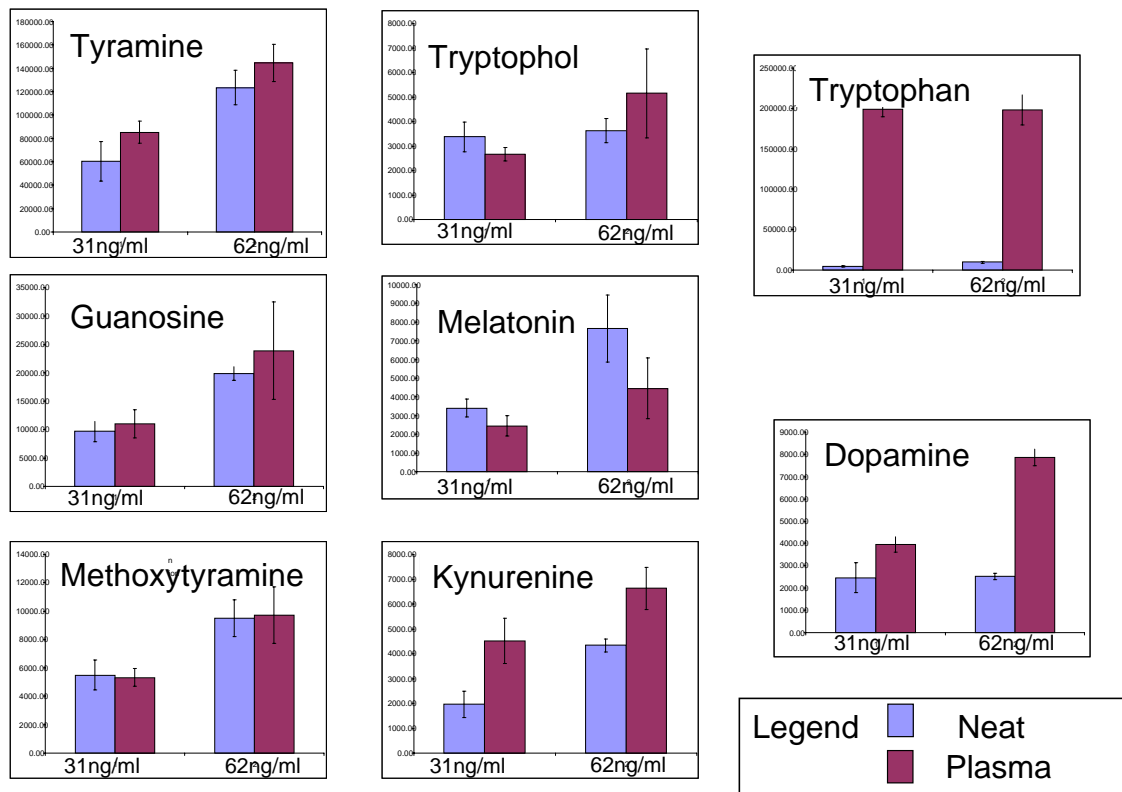


**Figure 2.5** Bar graphs represent a comparison of analyte MS signals in both neat and plasma solution for the concentrations 31 ng/ml and 62 ng/ml. Y error bars are for 3 replicates of each concentration. Tryptophan shows a statistically significant difference between the signals observed in neat and plasma solutions.



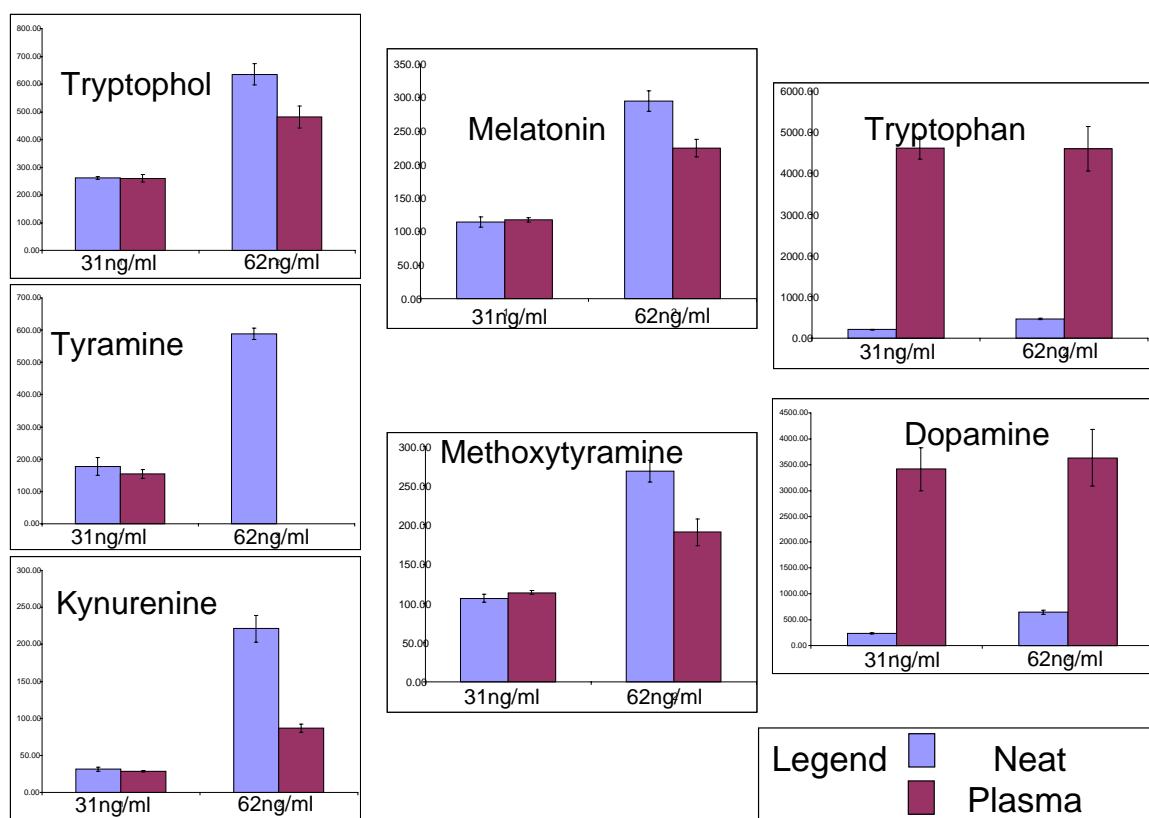


**Figure 2.6** Bar graphs represent a comparison of analyte EC-array signals in both neat and plasma solution for the concentrations 31 ng/ml and 62 ng/ml. Y error bars are for 3 replicates of each concentration. Both Dopamine and Tryptophan show a statistically significant difference between the signals observed in neat and plasma solutions.

A peak of interest eluting in the EC-array chromatogram of the plasma blank (Figure 2.7) at 3.27 minutes, shows a maximum oxidation peak at 950 mV as opposed to in Figure 2.3 where the maximum oxidation for DA in neat solution was observed at 800 mV. This oxidation profile difference suggests DA is not being observed in the plasma sample but a co-eluting species may be contributing to the increased EC-array signal for DA when spiked into the plasma matrix.

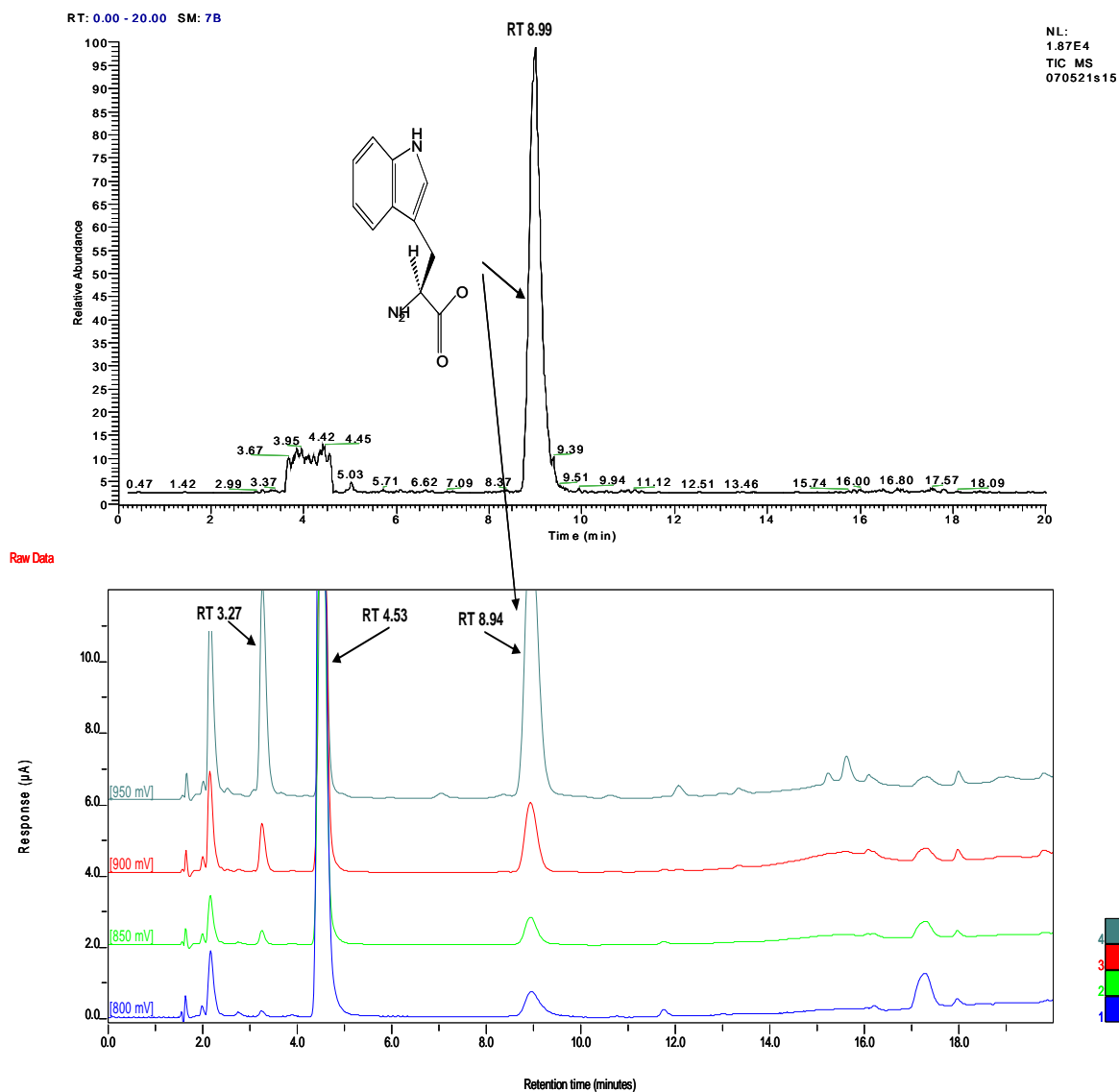


**Figure 2.7** The top panel shows an MRM TIC chromatogram and the bottom panel an EC-array chromatogram, for the analysis of a plasma blank. An intense peak at 8.99 minutes is observed in each chromatogram indicating tryptophan is present in the blank. The peak at 3.27 minutes elutes at the same time as dopamine, although with a different oxidation profile. These matrix peaks in the EC-array interfere with the signals from spiked analytes, making accurate identifications complicated without MS.

From this experiment, it is obvious that a biological sample with limited cleanup can be accurately assayed using the nanoelectrospray LC-EC-array-MS system without concern for biological matrix effects. The retention times, chromatography and absolute analyte area signals for each metabolite either remained constant throughout the analysis between

neat solutions and plasma or any variations observed (e.g., tryptophan or dopamine) can be fully accounted for by having two detected in parallel.

#### Identification of Unknown Sodium Phenylbutyrate Metabolites

Following confirmation of the efficiency of the nanoelectrospray LC-EC-array-MS platform, we examined next its practical utility toward the the identification of unknown metabolites of the pro-drug sodium phenylbutyrate (SPB) in patient plasma. SPB is known to be highly effective for the treatment of patients with hyperammonemia<sup>27-29</sup>, as well as showing promise in the treatment of cystic fibrosis<sup>30, 31</sup>, sickle-cell anemia<sup>32</sup> and thalassemia. Its clinical effectiveness, however, is limited by known occasions of toxicity from bodily metabolism of the drug<sup>33, 34</sup>. It is currently being investigated for treatment of Huntington's disease (HD) patients and undergoing patient tolerability and efficacy trials.

An initial patient plasma screening, where possible metabolites were identified, was performed and optimized using a 12 channel HPLC-EC-array system. Baseline patient plasma, prior to SPB treatment, and plasma taken post SPB treatment were compared to detect profile changes between the patient time points. These analysis conditions were not directly compatible with the nanoelectrospray LC-EC-array-MS system. Consequently, fraction collection and analysis conditions for evaluation of compounds identified as sodium phenyl butyrate metabolites had to be transferred to an MS compatible formate buffer system. Patient plasma underwent the same protein

precipitation for LC-EC-array-MS analysis, but, then was subjected to SPE fraction collection using the MS compatible elution solvents of water and ACN. The metabolite peaks, indicated in Figure 2.8, were collected in the 30% ACN SPE elution fraction isolated from patient plasma and were then analyzed using the integrated nano-electrospray LC-EC-array-MS system. The EC-array was held at potentials of 700, 800, 900 and 1000 mV respectively and the LCQ ion trap MS was operated in negative ion detection mode using data dependent full scans.

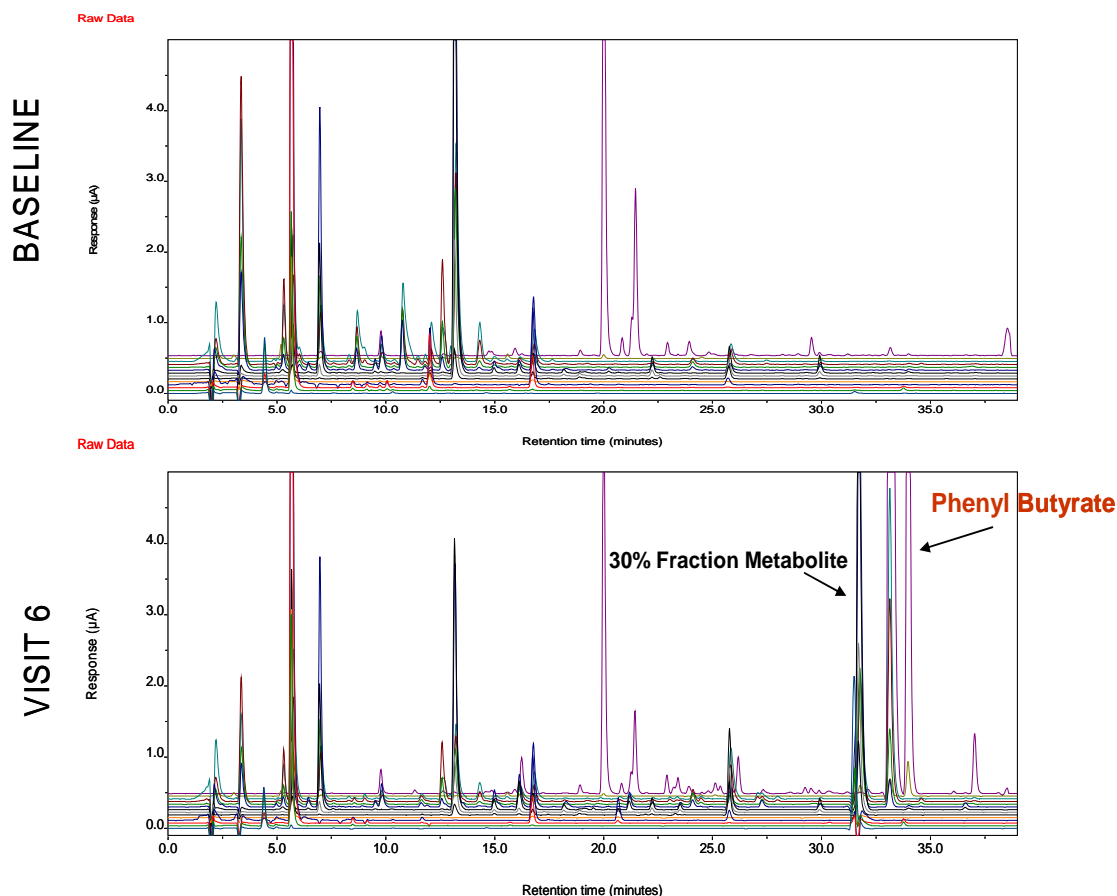


**Figure 2.8** The top panel represents HD patient plasma prior to SPB administration. The bottom panel is HD patient serum at the patient's 6th visit to be administered SPB. Several changes in the chromatograms are evident; however, indicated is the metabolite area collected in the 30% SPE fractionation and the SPB parent drug peak. Both chromatograms were acquired on a 12 channel EC-array system equipped with UV and fluorescence detection.

Figure 2.9 is an LC-EC-array-MS chromatogram where the bottom panel shows that at 800mV the LC-EC-array detected three distinct peaks occurring at retention times of 17.0, 18.3 and 19.3 minutes. These retention times coincide with the extracted ion chromatograms (XIC) of three molecular species of  $m/z$  179, presumably isomeric  $[M-H]^-$  ions, shown in the top panel of Figure 2.9. The matching retention times confirm that the peaks monitored in the MS are indeed the metabolites detected by the LC-EC-array detector. In addition to the aforementioned three isomers, the XIC of a fourth compound with molecular mass of  $m/z$  339 ( $[M-H]^-$ ) not detected by EC-array was observed by the MS detector at 18.4 minutes. The MS/MS spectra of the major isomeric metabolite of  $m/z$  179 and that of the  $m/z$  339 ion are presented in Figures 2.10A and B respectively.

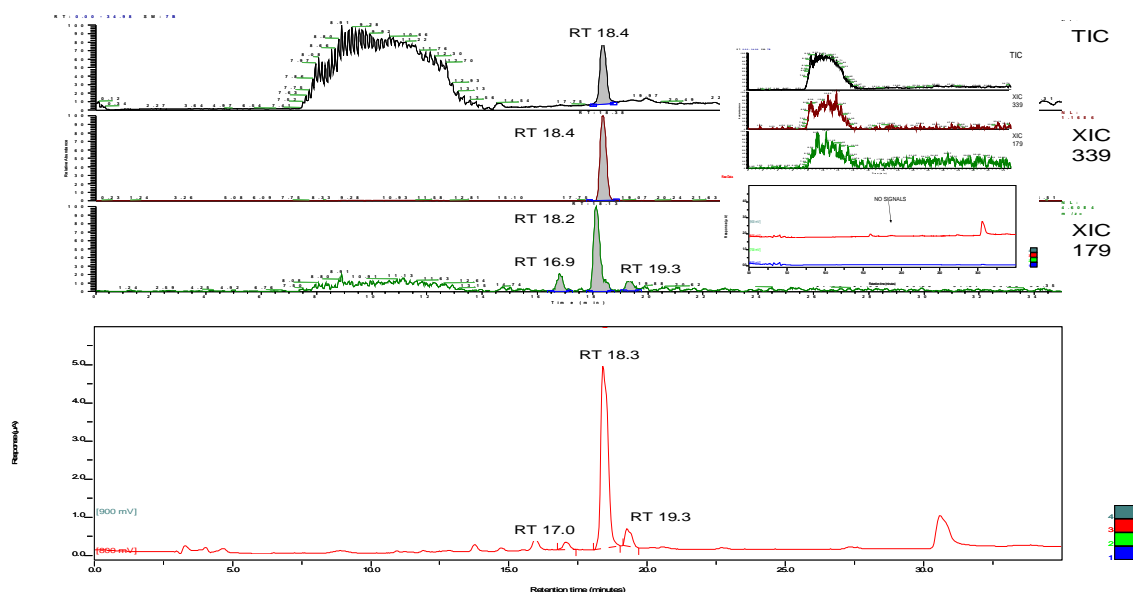


**Figure 2.9** The top panel shows a full scan MS chromatogram, as well as two extracted ion chromatograms (XIC) for  $m/z$  339 and  $m/z$  179 corresponding to the metabolite masses observed in the 30% fraction. The bottom panel shows the EC-array chromatogram from the analysis with a large peak at 800 mV and 18.4 minutes. Two smaller EC-array peaks, representing isomers of the  $m/z$  179 ion are also observed. The inset shows a water blank analysis with the same TIC and XIC chromatograms.

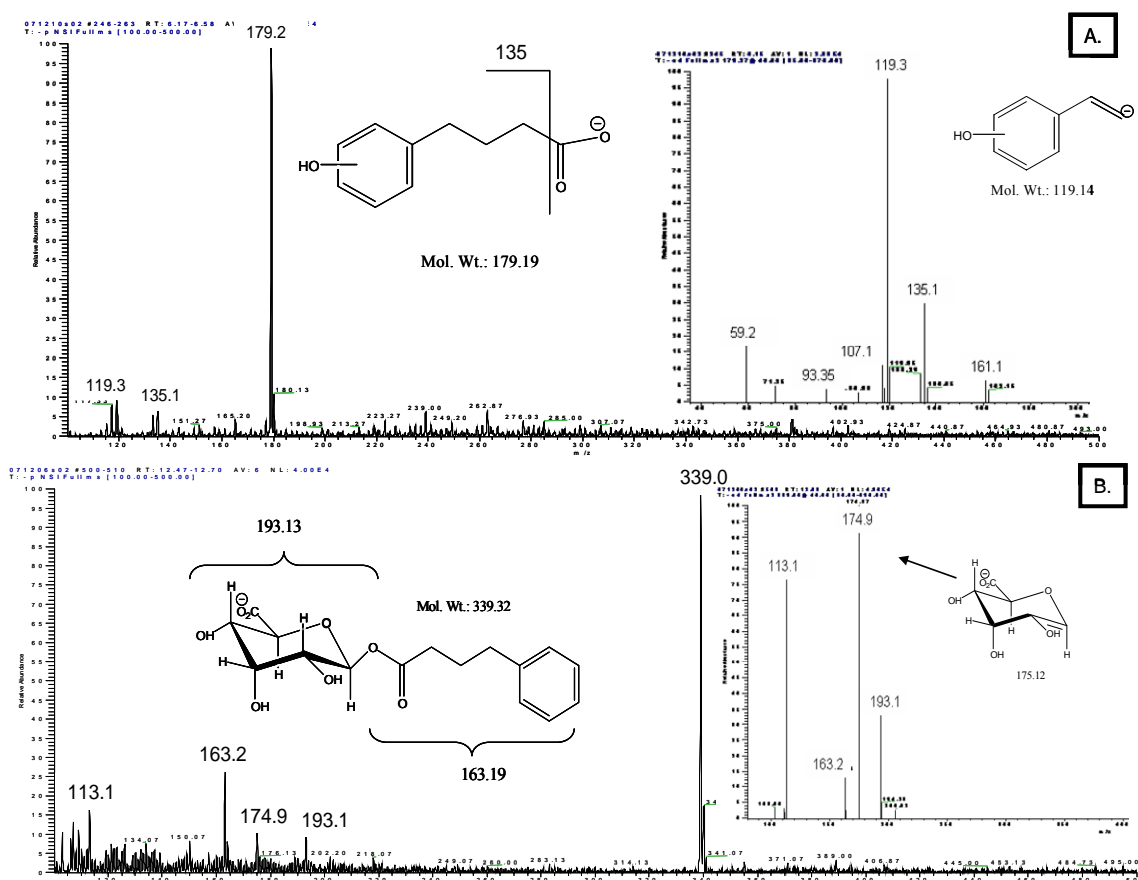


**Figure 2.10** Panel A shows the mass spectrum between  $m/z$  100 and 500 for the peak at 18.2 minutes. The inset is its data dependent MS/MS scan giving fragments of  $m/z$  135 and 119 indicating fragments of the proposed hydroxyphenylbutyric acid metabolite shown. Panel B shows the mass spectrum between  $m/z$  100 and 500 observed under the peak at 18.4 minutes observed in figure 2.9. The inset is the data dependent MS/MS scan of the same peak, giving fragment ions of  $m/z$  193, 175 and 163 corresponding to the indicated portions of the proposed phenylbutyryl- $\beta$ -glucuronate metabolite shown.

The 179 Da mass of the  $[M-H]^-$  ion of the three isomeric metabolites, shown in Figure 2.10A, represents a 16 Da increment over that of the parent drug and is consistent with a hydroxylation, presumably at the aromatic ring of the compound. This ring hydroxylation is further supported by the EC-array signal since the group is more readily oxidized when connected to an aromatic moiety. The MS/MS spectra also confirm this assignment although in the absence of reference compounds it is difficult to distinguish among the different isomers through MS fragmentations alone. Analysis of hydroxyphenylacetic

acid isomers, using the LC-EC-array-MS integrated system, proved the isomer elution order to be para-, ortho-, and meta-hydroxy substituted phenylacetic acid compounds respectively when using the same method as the HD patient samples (data not shown). This finding allows more insight to be gained from the hydroxyphenylbutyric acid metabolites identified, since the EC-array data compiled shows a considerable amount of the 2-hydroxyphenylbutyric acid metabolite in comparison to the other two isomers.

In Figure 2.10B the MS/MS spectrum of the compound eluting at 18.4 minutes ( $m/z$  339 [M-H<sup>-</sup>]), shows an abundant fragment ion of  $m/z$  163, strongly suggesting the presence of a SPB moiety in the molecule. The inset in the figure shows the MS/MS spectrum of the  $m/z$  339 ion and its subsequent fragments of  $m/z$  193, 175, 163 and 113. This fragmentation pattern may be explained by the presence of a glucuronide metabolite as shown. This assignment is further supported by the data of Bruengraber et al., who recently reported on the formation of a phenylbutyryl- $\beta$ -glucuronate metabolite indirectly by incubating SPB patient urine with  $\beta$ -glucuronidase and monitoring the increase in SPB concentration<sup>35</sup>. Their experiment indicated the probable formation of the phenylbutyryl- $\beta$ -glucuronate metabolite of SPB along with several other secondary SPB metabolites in both humans and rats. The proposed glucuronide metabolite structure also explains the absence of any distinguishable EC-array signal at 18.4 minutes since its functional groups are not expected to be oxidized at the voltages employed.

It should also be pointed out that the elution range of *ca.* 16-20 minutes for the four metabolites in Figure 2.9 is earlier than that of the parent drug, which was observed at

20.74 minutes when translated to the formate buffer system, as shown in Figure 2.11. This behavior is consistent with the more polar character of these metabolites compared to the SPB pro-drug and further supports the structural assignments. The ability to confidently compare signals between detectors for unknown peaks greatly facilitated the possible structural identification of unknown SPB metabolites. Additionally, MS can be utilized to find metabolites that are not EC active, adding an additional dimension to the analysis. This experiment clearly demonstrates the utility of the nanoelectrospray LC-EC-array-MS system for metabolite identification in biological matrices.

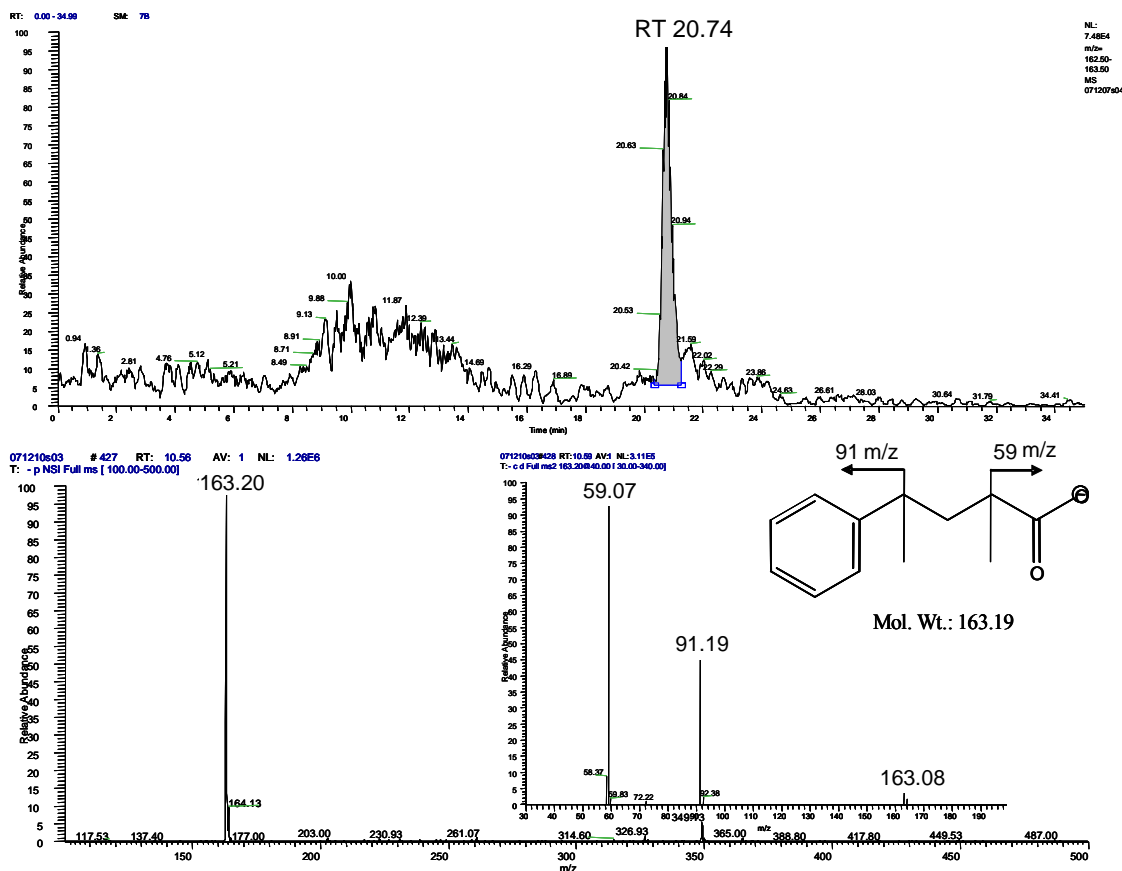


Figure 2.11 LC-MS-EC-array analysis of SPB drug standard with the bottom panel showing the full MS spectrum for the peak at RT 20.74minutes. The inset in the bottom panel shows the MS/MS fragmentation of standard.



## 2.7 Conclusions

An objective in any ‘omics inspired research is to identify and characterize any change in biological make-up as a result of disease, xenobiotic exposure that can cause disease<sup>36</sup> or drug metabolism. Once these changes are identified and characterized they can potentially be used as biomarkers to track disease or drug efficacy and progression. HPLC in combination with EC-array detection has been shown to be highly effective in metabolite profiling and screening of urine<sup>37</sup> and plasma<sup>6, 38</sup> matrices requiring minimal or even no sample cleanup<sup>39</sup>. Sophisticated pattern recognition software can then be used to identify significant variations in the profiles and locate potential biomarkers for both the diagnosis of disease as well as monitoring disease progression<sup>6</sup>. Additionally, the sensitivity of EC-array is often times unrivaled in low level analyte detection<sup>11-13</sup>. Despite these significant features, a fundamental drawback of the technique is the inability to generate definitive structural information on these markers, especially when dealing with unknown compounds. The parallel use of mass spectrometry with EC-array detection can address this problem.

A previous HPLC-EC-array-MS parallel combination has been shown to compromise the performance of the MS detector with high flow rates and biological matrix effects<sup>16</sup>. The platform discussed here permits operation of the MS under optimal nanoelectrospray conditions while also maintaining full chromatographic integrity and, essentially perfect correspondence of band retention times between the two detectors. The nanoSplitter’s ability to use a large bore high flow rate HPLC in a nanoelectrospray-MS analysis also

allows the direct coupling of this technique to the sensitive EC-array technology. The novel approach to the utilization of these two techniques allows us to capitalize on the sensitivities of both detectors for metabolomics studies for both targeted analysis and unknown metabolite identification and characterization. The results presented clearly show the utility of the combined detection system to simultaneously monitor several metabolites both in and out of a biological matrix reproducibly and down to levels commonly found in biological samples. Also, the system's ability to detect and structurally identify unknown compounds in a real biological sample has been clearly demonstrated. This proof of concept was established using a basic 4 cell EC-array system with limited ability to discern between varying oxidation potentials. Significant improvement in the overall nanoelectrospray LC-EC-array system would be possible by incorporation of a complete 16 cell EC-array system where the full advantage of EC-array's powerful selectivity could be realized.

## 2.8 References

- (1) Daviss, B. *The Scientist* **2005**, *19*, 25-28.
- (2) Nobeli, I.; Ponstingl, H.; Krissinel, E. B.; Thornton, J. M. *J Mol Biol* **2003**, *334*, 697-719.
- (3) Castrillo, J. I.; Oliver, S. G. *J Biochem Mol Biol* **2004**, *37*, 93-106.
- (4) Harrigan, G. G.; Goodacre, R.; Editors *Metabolic profiling: Its role in biomarker discovery and gene function analysis*, 2003.
- (5) Vaidyanathan, S.; Harrigan, G. G.; Goodacre, R. *Metabolome Analyses* **2005**, 1-7.
- (6) Bogdanov, M.; Matson Wayne, R.; Wang, L.; Matson, T.; Saunders-Pullman, R.; Bressman Susan, S.; Flint Beal, M. *Brain FIELD Full Journal Title:Brain : a journal of neurology* **2008**, *131*, 389-396.
- (7) Gamache, P. H.; McCabe, D. R.; Parvez, H.; Parvez, S.; Acworth, I. N. *Progress in HPLC-HPCE* **1997**, *6*, 99-126.
- (8) Milbury, P. E. *Progress in HPLC-HPCE* **1997**, *6*, 127-144.
- (9) Kristal, B. S.; Vigneau-Callahan, K. E.; Matson, W. R. *Anal Biochem* **1998**, *263*, 18-25.
- (10) Kristal, B. S.; Vigneau-Callahan, K.; Matson, W. R. *Methods Mol Biol* **2002**, *186*, 185-194.
- (11) Shurubor, Y. I.; Matson, W. R.; Willett, W. C.; Hankinson, S. E.; Kristal, B. S. *BMC Clin Pathol* **2007**, *7*, 9.
- (12) Shurubor, Y. I.; Matson, W. R.; Martin, R. J.; Kristal, B. S. *Metabolomics* **2005**, *1*, 159-168.
- (13) Shurubor, Y. I.; Paolucci, U.; Krasnikov, B. F.; Matson, W. R.; Kristal, B. S. *Metabolomics* **2005**, *1*, 75-85.
- (14) Matson, W. R.; Langlais, P.; Volicer, L.; Gamache, P. H.; Bird, E.; Mark, K. A. *Clin Chem* **1984**, *30*, 1477-1488.
- (15) Rozen, S.; Cudkowicz, M. E.; Bogdanov, M.; Matson, W. R.; Kristal, B. S.; Beecher, C.; Harrison, S.; Vouros, P.; Flarakos, J.; Vigneau-Callahan, K.; Matson, T. D.; Newhall, K. M.; Beal, M. F.; Brown, R. H., Jr.; Kaddurah-Daouk, R. *Metabolomics* **2005**, *1*, 101-108.

- (16) Gamache, P. H.; Meyer, D. F.; Granger, M. C.; Acworth, I. N. *J Am Soc Mass Spectrom* **2004**, *15*, 1717-1726.
- (17) Meyer, D. F.; Gamache, P. H.; Acworth, I. N. *Metabolome Analyses* **2005**, 119-135.
- (18) Zhou, F.; Van Berkel, G. J. *Analytical Chemistry* **1995**, *67*, 3643-3649.
- (19) Jurva, U.; Wikstrom, H. V.; Weidolf, L.; Bruins, A. P. *Rapid Commun Mass Spectrom* **2003**, *17*, 800-810.
- (20) Karst, H. H. a. U. *Analytical Chemistry* **2003**, *75*, 4833-4840.
- (21) Gangl, E. T.; Annan, M. M.; Spooner, N.; Vouros, P. *Anal Chem* **2001**, *73*, 5635-5644.
- (22) Wilm, M.; Mann, M. *Anal Chem* **1996**, *68*, 1-8.
- (23) Juraschek, R.; Dulcks, T.; Karas, M. *J Am Soc Mass Spectrom* **1999**, *10*, 300-308.
- (24) Gangl, E. T.; Vouros, P.: US, 2004.
- (25) Andrews, C. L.; Li, F.; Yang, E.; Yu, C.-P.; Vouros, P. *J Mass Spectrom* **2006**, *41*, 43-49.
- (26) Alvarez, J. C.; Bothua, D.; Collignon, I.; Advenier, C.; Spreux-Varoquaux, O. *Biomed Chromatogr* **1999**, *13*, 293-298.
- (27) Batshaw, M. L.; Thomas, G. H.; Brusilow, S. W. *Pediatrics* **1981**, *68*, 290-297.
- (28) Batshaw, M. L.; MacArthur, R. B.; Tuchman, M. *J Pediatr* **2001**, *138*, S46-54; discussion S54-45.
- (29) Brusilow, S. W. *Pediatr Res* **1991**, *29*, 147-150.
- (30) Rubenstein, R. C.; Zeitlin, P. L. *Am J Physiol Cell Physiol* **2000**, *278*, C259-267.
- (31) Zeitlin, P. L.; Diener-West, M.; Rubenstein, R. C.; Boyle, M. P.; Lee, C. K. K.; Brass-Ernst, L. *Mol Ther* **2002**, *6*, 119-126.
- (32) Dover, G. J.; Brusilow, S.; Charache, S. *Blood* **1994**, *84*, 339-343.
- (33) Carducci, M. A.; Gilbert, J.; Bowling, M. K.; Noe, D.; Eisenberger, M. A.; Sinibaldi, V.; Zabelina, Y.; Chen, T. L.; Grochow, L. B.; Donehower, R. C. *Clin Cancer Res* **2001**, *7*, 3047-3055.

- (34) Gore, S. D.; Weng, L.-J.; Figg, W. D.; Zhai, S.; Donehower, R. C.; Dover, G.; Grever, M. R.; Griffin, C.; Grochow, L. B.; Hawkins, A.; Burks, K.; Zabelena, Y.; Miller, C. B. *Clin Cancer Res* **2002**, *8*, 963-970.
- (35) Kasumov, T.; Brunengraber, L. L.; Comte, B.; Puchowicz, M. A.; Jobbins, K.; Thomas, K.; David, F.; Kinman, R.; Wehrli, S.; Dahms, W.; Kerr, D.; Nissim, I.; Brunengraber, H. *Drug Metab Dispos* **2004**, *32*, 10-19.
- (36) Castrillo, J. I.; Oliver, S. G. *Metabolome Analyses* **2005**, 9-29.
- (37) Mullersman, G.; Toufflin, S.; Derendorf, H. *J Pharm Biomed Anal* **1987**, *5*, 303-308.
- (38) Luo, H.; Cox, S. B.; Gao, W.; Yu, J.; Tang, L.; Wang, J.-S. *Metabolomics* **2006**, *2*, 235-241.
- (39) Rima Kaddurah-Daouk, B. S. K., Mikhail Bogdanov, Wyne R. Matson, M. Flint Beal In *Metabolome Analyses: Strategies For Systems Biology*; Seetharaman Vaidyanathan, G. G. H. a. R. G., Ed.; Springer Science+Business Media, Inc.: New York, NY, 2005, pp 45-61.

### Chapter 3

#### Identification of Unknown Phenyl Butyrate Metabolites in Huntington's Disease Patients using Parallel LC-EC-array-MS Detection

Submitted to Analytical Biochemistry:

Ebbel, E; Schiavo, S; Sharma; Gevorkain, S.; Hersch, S.; Bogdanov, M.; Wang, L.; Costello, C.E. and Matson, W.R.; Identification of Unknown Phenyl Butyrate-Generated Metabolites in Huntington 's Disease Patients using Parallel LC-EC-array-MS Detection (*Submitted*).

### 3.1 Introduction to Huntington's Disease (HD)

Huntington's disease (HD) is an inherited neurodegenerative disorder characterized by motor and psychiatric dysfunction such as choreic movements and dementia, with symptomatic onset occurring typically between 30 and 50 years of age<sup>1</sup>. HD is caused by the expansion of an unstable CAG trinucleotide repeat located in the Huntington gene of affected individuals. This repeat transcribes a polyglutamine chain near the N-terminus of the huntingtin protein, and puts HD in the broader category of polyglutamine diseases. Polyglutamine chains longer than 36 glutamines result in a toxic, mutant form of the huntingtin protein and cause those individuals to invariably develop HD. Mutant huntingtin has been shown to disrupt activator-dependent transcription in the early stages of HD pathogenesis<sup>2</sup>. Additionally, transcriptional deregulation and functional loss of transcriptional co-activator proteins have been implicated in pathogenesis of HD<sup>3, 4</sup> and lead to neuronal loss and gliosis, particularly in the cortex and striatum regions of the HD patient brain<sup>5</sup>.

Although there is no cure for HD, progress has been made in slowing the rate of neurodegeneration as well as reducing or alleviating disease symptoms in genetic animal models. Studies done in cell culture, yeast, and *Drosophila* models of polyglutamine disease have shown that histone deacetylase (HDAC) inhibitors might provide a useful class of therapeutic agents for HD due to histone acetylation being associated with gene transcription<sup>6-10</sup>. Steffan and colleagues have shown that fragments of the mutant huntingtin protein interact with CREB-binding protein, decreasing the acetylation of

histone 4<sup>7</sup>, and when a transgenic drosophila model containing this protein-protein interaction was treated with a HDAC inhibitor, showing a decrease in degeneration and early adult death<sup>7</sup>. These results suggest that reduced acetylase transferase activity may be an important component to polyglutamine disease pathogenesis. Thus, HDAC inhibitors may possibly be used to lessen the transcriptional changes in HD<sup>11</sup>.

### 3.2 Introduction to Sodium Phenylbutyrate Treatment and Metabolic Analyses

Sodium phenylbutyrate (SPB) has been explored as a HDAC inhibitor in clinical trials for cytostatic antineoplastic agents and showed the ability to potentiate the effect of cytotoxic agents on tumors<sup>12, 13</sup>. SPB treatment has been promising due to its limited side effects in both phase I and phase II clinical trials, as well as its use in treating patients for urea cycle disorders, sickle cell anemia, thalassemia minor, as well as cystic fibrosis<sup>14-16</sup>. This evidence, in addition to recent findings suggesting that the global reduction of HDAC activity slows the rate of neurodegeneration in *in vivo* models of HD,<sup>7, 9, 10, 17</sup> advocated SPB as a therapeutic agent for HD.

To understand of mechanisms of SPB drug action and possible individual specific side effects in HD it is essential to identify the structures of metabolites present in both HD patient urine and plasma samples. Using both direct and indirect methods, studies have been performed identifying the metabolites of SPB in both human plasma and urine<sup>18, 19</sup>. Also research has been conducted exploring the possible biochemical pathways SPB could take in the body<sup>18</sup>. Literature data suggests that different disorders may have



different patterns of SPB metabolites. Recent studies using SPB as a therapeutic agent in for Amyotrophic Lateral Sclerosis (ALS) with the same LCECA/UV/F analytical protocol employed in this work also suggest different patterns of metabolites between ALS and HD<sup>20</sup>. Therefore, although certain SPB metabolites have been identified in patients after SPB administration, it does not necessarily predict the path of SPB metabolism in HD patient therapy.

Previous techniques used to characterize SPB metabolites in urine included Nuclear Magnetic Resonance (NMR) in addition to Gas Chromatography Mass Spectrometry (GC/MS) analyses to further confirm several suspected metabolites<sup>18, 19</sup>. Although these techniques have been able to identify unknown metabolites, they require either large amounts of analyte –  $\mu\text{g}$  to  $\text{mg}$  of material as in the case of NMR– or volatile analytes and complicated derivatization as with GC/MS. Additionally, in the studies cited it is clear that greater than 38% of metabolites in humans have yet to be identified and characterized.

### 3.3 LC-EC-array-MS Platform for SPB Metabolite Identification

In the previous chapter we demonstrated the use of parallel liquid chromatography electrochemical array with nanoelectrospray mass spectrometry (LC-EC-array-MS) to identify several SPB metabolites in plasma of SPB treated HD subjects<sup>21</sup>. This was preliminary work used to show the ability of the integrated system to detect and characterize those metabolites previously identified and characteristic of SPB in HD patients using HPLC-ECarray. HPLC coupled with electrochemical array detection (EC-

Array) is a very sensitive technique used for profiling<sup>22</sup> and quantifying redox active species, such as metabolites, down to picomolar concentrations<sup>23, 24</sup>. In addition to its sensitivity, this technique also has the ability to analyze over 1000 metabolites in one HPLC run<sup>25, 26</sup>, while also being able to differentiate between co-eluting species based on their oxidation potentials, adding specificity to the analysis. Use of multivariate data analysis has also been shown to be able to completely separate groups based on both disease and medication<sup>22, 27</sup>. Series coupling of ECA with UV and fluorescence provides a further modality of detection to the analysis, which is especially important in studies where certain drugs or drug candidates, such as SPB, are not EC active.

The major limitation of the EC-Array is its inability to provide structural information of the compounds it is profiling. This limitation has been overcome in our prior work by parallel coupling of EC-array with MS detection<sup>21</sup>, and more specifically nano-electrospray (nanoESI) MS, which is important when considering the ion suppression effects of biological fluids. Although initial coupling requires the consideration of a number of parameters including redox activity of a compound, solvent properties such as pH and the supporting electrolyte, and LC flow rate, creating a method that effectively satisfies the requirements of both the EC array and the mass spectrometer has been possible.

### 3.4 Project Goals

In this chapter, we present an approach utilizing the powers of offline LC-EC-array analysis to identify additional unique SPB metabolites present in plasma and urine, compared to controls, and going on to perform further structural elucidation of these compounds using both a parallel coupling of LC-EC-array and nanoESI-MS and offline MS and MS/MS for full characterization. Plasma and urine samples were obtained from patients undergoing SPB treatment during a 4 month long double blind placebo controlled multicenter phase II study of SPB in individuals with early symptomatic HD (PHEND-HD). Using the new total methodology outlined in Figure 3.1, several new and previously known SPB metabolites have been isolated and the structures identified. This scheme provides a more comprehensive approach to more complete understanding of the biochemical effects of SPB as a therapeutic agent for HD and to classifying individual responses to the drug.

### 3.5 Materials and Methods

The work conducted in this research chapter was in collaboration with Dr. Wayne Matson's laboratory in the Department of Systems Biochemistry at the Bedford VA Medical Center, Bedford, MA, as well as Dr. Steven Hersch in the Department of Neurology, Massachusetts General Hospital, Harvard Medical School, Charlestown, MA. Dr. Hersch performed the phase II patient studies and Dr. Matson and colleagues in his lab performed all sample preparations and LC-ECarray-UV-FL studies.

### **Plasma and urine Samples**

Two hundred sixty-eight serial plasma and urine samples were obtained from 60 HD subjects in the PHEND-HD phase II study. Baseline samples were obtained before treatment and additional samples were collected at five subsequent visits. SPB dose levels were up to 15 g/day. Half the subjects were on placebo through visit 2 and afterwards all subjects were on active medication until washout.

### **Initial Data base creation and analysis**

For pharmacokinetic and compliance studies all samples were analyzed using gradient LC with serial ECA/UV/F optimized for ECA to resolve SPB and PA from *ca.* 600 plasma or urine metabolites at ng/mL levels. Gradient LC-EC analyses were performed using ESA model 582 Pumps (ESA Biosciences Inc., Chelmsford, MA) and a 14 channel ESA model 5600 CoulArray detector. Channels 1-12 used series coulometric electrodes set in equal increments from 0-840 mV. Channel 13 measured UV absorbance at  $\lambda$  210 nm. Channel 14 recorded fluorescence with excitation  $\lambda$  220 nm/ emission  $\lambda$  320 nm (ESA Biosciences Inc., Chelmsford, MA). A 4.6 mm x 250 mm Shiseido C18 5  $\mu$ m column (ESA Biosciences Inc, Chelmsford, MA) was used. The gradient employed was linear from 0% Phase A: (0.1 M LiPO<sub>4</sub> pH 3); to 100% Phase B: (0.1 M LiPO<sub>4</sub> pH 3, 55% acetonitrile) over 45 min.

Plasma samples were prepared by a standard method, as follows. Plasma (125  $\mu$ L) was precipitated with 500  $\mu$ L of acetonitrile/0.4% acetic acid, vortexed for 30 sec., centrifuged at 21,000 x *g* for 25 min at 4 °C. The supernatant (500  $\mu$ L) was centrifugally

evaporated, reconstituted to 100  $\mu$ L in mobile phase A and a 50- $\mu$ L aliquot was injected onto the system. Urine samples were diluted 1/5 with mobile phase A and 50  $\mu$ L was directly injected onto the system. All urine assays in the original data set were normalized to creatinine.

**Procedure for selecting peaks for identification:**

From the created database, identification of components related to SPB, phenyl acetate (PA), creatine and creatinine were selected for identification as follows. Patterns of all analytes were exported as peak tables and as digital maps, following protocols developed in a study of Parkinson's Disease<sup>22</sup>. These captured the entirety of the response of the platform<sup>22</sup>. Maps and peak tables were compared for baseline *vs.* dosed subjects to determine levels of direct or induced metabolites. The criteria for selection of peaks as candidates for structural identification were that the peaks: A) had levels 50 times greater in dosed subjects *vs.* baseline, B) showed correlation with either SPB or PA; and C) demonstrated consistency within an individual subject. Twenty peaks met these criteria.

**Preparation of plasma fractions for offline LC-EC-array metabolite identification:**

Pools of plasma from baseline and SPB treated subjects were prepared from 200  $\mu$ L sub aliquots. 6mL of plasma pools from baseline and treated HD subjects were precipitated with 24 mL of acetonitrile (ACN)/0.4% glacial acetic acid at 20° C. Samples were vortexed for 30 seconds and centrifuged for 30 min at 8000 x g at 4° C. The supernatant was centrifugally vacuum evaporated and concentrated to 300  $\mu$ L.

**Fractionation of Plasma Samples:**

Concentrated plasma was fractionated using solid phase extraction (500 mg Diazom C-18 SPE). Columns were equilibrated with 2 mL DIW, 2 mL acetonitrile and 2 mL 2% acetic acid. 300  $\mu$ L of concentrated supernatant from the plasma preparation was loaded onto the SPE column. A single 300  $\mu$ L collection was then made of a void fraction and then 2 mL of each of the following elutions: 0%, 10%, 20%, 30%, 40%, and 100% ACN. Each of the fractions was centrifugally evaporated and reconstituted in 200  $\mu$ L of 0.02M ammonium acetate at pH 4.2.

**Fractionation of Urine samples:**

Pools of urines were created from 15 subjects showing the highest levels of SPB at visit 5 and the same subjects at baseline. These were concentrated by centrifugal evaporation by a factor of four. 300  $\mu$ L aliquots were separated on the SPE columns as above and the fractions centrifugally evaporated and reconstituted as described previously.

**Offline LC-EC-array Run of Fractions in MS Buffer:**

10  $\mu$ L of each fraction was diluted to 100  $\mu$ L. First, 20  $\mu$ L were analyzed using the primary analytical method described above to confirm the position and intensity of the peaks selected for structural identification from the initial data analysis. Next, the LCECA/UV/F platform was configured for an MS compatible buffer systems (Phase A: 0.02 M ammonium formate/formic acid pH 3.1; Phase B: 0.02 M ammonium formate/formic acid pH 3, 55% ACN; gradient 0% A-100% B over 45 min and Phase A: 0.02 M ammonium acetate/acetic Acid pH 4.2; Phase B: 0.1 M ammonium acetate/acetic

acid pH 4.2, 55% ACN; gradient 0% A-100% B over 45 min). Using 20  $\mu$ L injections the selected peak locations and intensities confirmed in these system.

Due to the presence of numerous compounds of interest in urine fractions 0%, 10% and 30% ACN, these were re-extracted with smaller increments of ACN (0%-20% in 2% increments). These fractions were once again run on the offline LC-EC-array to verify the positions of metabolites of interest.

#### **Parallel LC-EC-array-MS instrumentation:**

LC-MS analyses were performed using ESA model 582 Pumps (ESA Biosciences Inc., Chelmsford, MA) and an ESA model 5600 CoulArray detector; channels 1-12, 0-840 mV in 70 mV increments (ESA Biosciences Inc., Chelmsford, MA) coupled on-line to a Sciex (Applied Biosystems, Foster City, CA) QStar quadrupole time of flight (q-tof) mass spectrometer equipped with ESI ion source used in both positive and negative ion scan mode ( $m/z$  100-2000, ionspray voltage 4.5-5.5 kV). Metabolite mixtures were separated on a 4.6 mm x 250 mm (5 micron Shiseido C18) column at a flow rate between 0.8-1.0 mL/min. The HPLC eluent was then split at a ratio of 9:1 with 90% being directed to the EC-array and 10 % being delivered to the MS.

#### **LC-EC-array-MS method:**

The 20% and 30% plasma fractions were diluted between 1:10 and 1:100 times in 60:40 mobile phase A:B and assayed using a 20 minute isocratic method of 0.500 mL/min

mobile phase A (0.1 M Ammonium Acetate) 0.300 mL/min mobile phase B (60% ACN 0.1 M Ammonium Acetate). An Information Dependent Acquisition (IDA) MS method was designed to monitor the two most intense ion peaks between  $m/z$  100-500 and subsequently fragment those with the collision energy set to 20 eV and quad resolution set to low. This made it possible to monitor the retention times of the metabolites of interest as they passed through the mass spectrometer and compare those times to the EC-array simultaneously, while also obtaining MS/MS fragmentation. The above method was also used on the 0 and 10% urine fractions as well as the 20% ACN re-extracted portion from the 0% urine fraction and the 15% ACN re-extracted portion from the 10% urine fraction.

Additionally, the 40% plasma fraction was diluted as above and assayed using a 60 minute isocratic method of 0.900  $\mu$ L/min A (0.1 M Ammonium Acetate) and 0.100  $\mu$ L/min B (75% ACN 0.1 M Ammonium Acetate). A similar IDA MS method was used as above, with the collision energy changed to 50 eV.

### **Fragmentation Confirmation by MS and MS/MS**

#### **Plasma Samples:**

Additional MS and MS/MS data was obtained by infusion using an LTQ-Orbitrap (Thermo-Fisher, San Jose, CA) with NanoMate (Advion, Ithaca, NY). Samples from the 20%, 30%, and 40% fractions were diluted 1:10 in 50/50 methanol/water and run using nanoelectrospray in negative ion mode.



**Urine Samples:**

Additional MS and MS/MS data was obtained by infusion using an LCQ Classic Quadrupole Ion Trap (Thermo-Fisher, San Jose, CA). Samples re-extracted from the 0% and 10% urine fractions were diluted 1:10 in 70/30 methanol/water and run by nanoelectrospray in negative ion mode.

The initial LC-EC-array screening of the sample fractions allowed for only those fractions containing metabolites of interest to be prioritized and analyzed via parallel LC-EC-array-MS. The compounds found in plasma samples were confirmed by high resolution MS and fragmentation on an LTQ Orbitrap, while compounds from urine fractions were subjected to MS/MS fragmentation using an LCQ classic quadrupole ion trap MS.

### 3.6 Results and Discussion of Analysis Methodology

The analysis method developed here provides a comprehensive evaluation of SPB treated HD patient plasma and urine using EC-array and MS detection both separately and in parallel. The system used to analyze samples obtained from SPB treated HD patients taking part in the PHEND-HD tolerability trial study consisted of a parallel LC-EC-array-MS detection system. The MS used in the parallel experiments performed within this chapter was a Sciex (Applied Biosystems, Foster City, CA) QStar quadrupole time of flight (q-tof) mass spectrometer equipped with turbo-spray ESI ion source, capable of handling flow rates between 5 and 1000  $\mu\text{L}/\text{min}$  with excellent ionization efficiency.

Overall, the platform consisted of a binary HPLC pump connected to a normal bore C-18 column followed by a 9:1 passive flow splitter used to divert the eluent between the EC-array and MS detectors. The established 9:1 split ratio allows a larger volume of the HPLC flow to enter the EC-array detector and a much lesser volume to be delivered to the MS. The MS flow rate was maintained  $<100 \mu\text{L}/\text{min}$  in order to minimize possible ion suppression effects from both the biological samples and the high salt containing EC-array buffers and facilitate efficient ion transfer. Additionally, the flow split was important in preserving agreement of the retention times between the EC-array and the MS chromatograms in order to confidently compare and identify SPB metabolites between both instruments<sup>21</sup>. Those compounds identified between the two detectors could then go on to be further characterized through both high resolution MS and MS/MS fragmentation.

A detailed account of the entire metabolite characterization method scheme from sample processing and initial offline LC-EC-array profiling to parallel LC-EC-array-MS analyses and final high resolution MS and MS/MS characterization can be seen in Figure 3.1. As shown in this figure, the first step after preparing the samples with a simple protein precipitation and concentration is to efficiently separate all electrochemically active compounds present and discern the possible SPB metabolites by comparing baseline, or pre-treatment patient samples with treated patient samples. In addition to profiling the EC active metabolites, the system used for this offline LC-EC-array analysis also monitored the samples with UV and fluorescence (F) due to SPB's lack of

electrochemical activity, but strong UV and F signals.

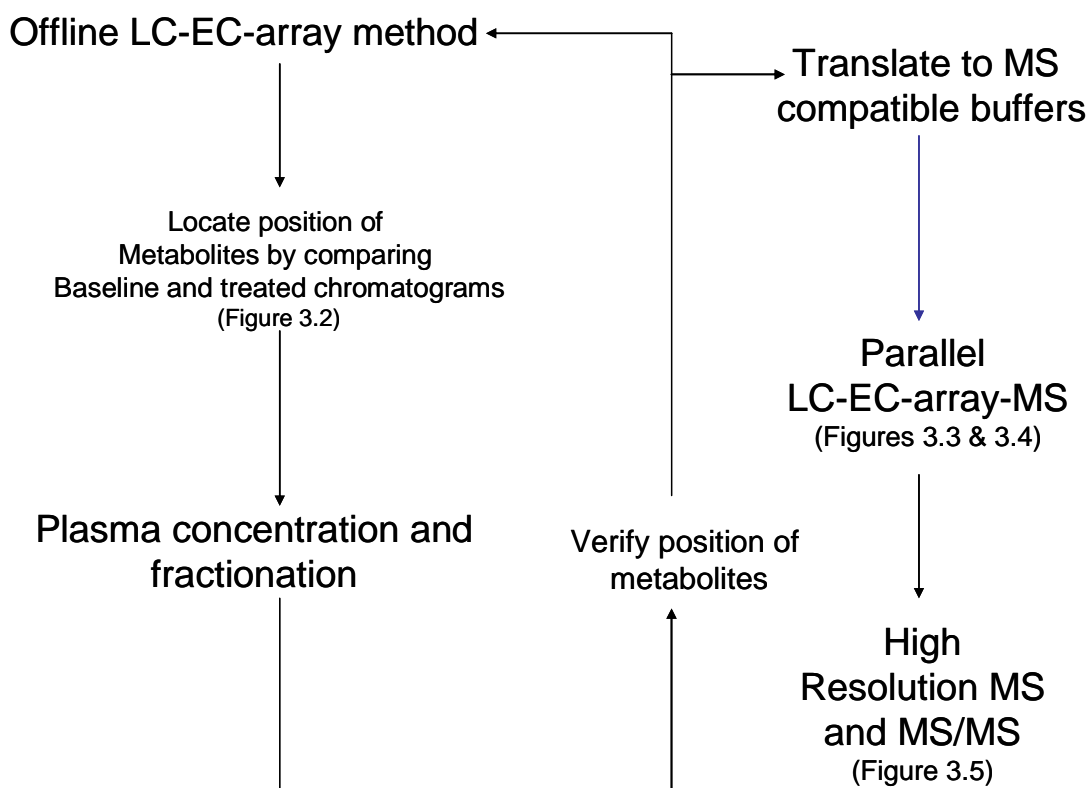


**Figure 3.1** Method flow chart describing the course of samples from initial offline LC-EC-array screening through sample fractionation, parallel LC-EC-array-MS analysis and high resolution and MS/MS characterization.

Figure 3.2 shows a comparison of two typical offline LC-EC-array chromatograms used to determine SPB metabolites from HD patients. The upper panel of the figure, indicated as baseline, shows the LC-EC-array chromatogram of pooled plasma from HD patients prior to SPB administration. The bottom trace, marked as Visit 6, shows the LC-EC array chromatogram of pooled plasma after the patient's sixth visit for SPB administration. There are distinct changes in the chromatograms, marked with the letter "M" in Figure 3.2, representing new metabolites formed as a result of the SPB drug treatment. In order to structurally characterize these metabolites it was necessary to simplify the number of compounds being studied at one time. Thus, in accordance with

the next portion of our methodology, the concentrated and pooled HD patient samples were fractionated using SPE. 10%, 20%, 30%, 40% and 100% ACN fractions were collected off of a Diazam SPE C-18 column and were subsequently run on both the offline LC-EC-array and parallel LC-EC-array-MS systems. The fractions were re-run on the offline LC-EC-array system in order to verify the position of those metabolites in comparison to the un-fractionated sample chromatogram as will be shown in the example outlined.

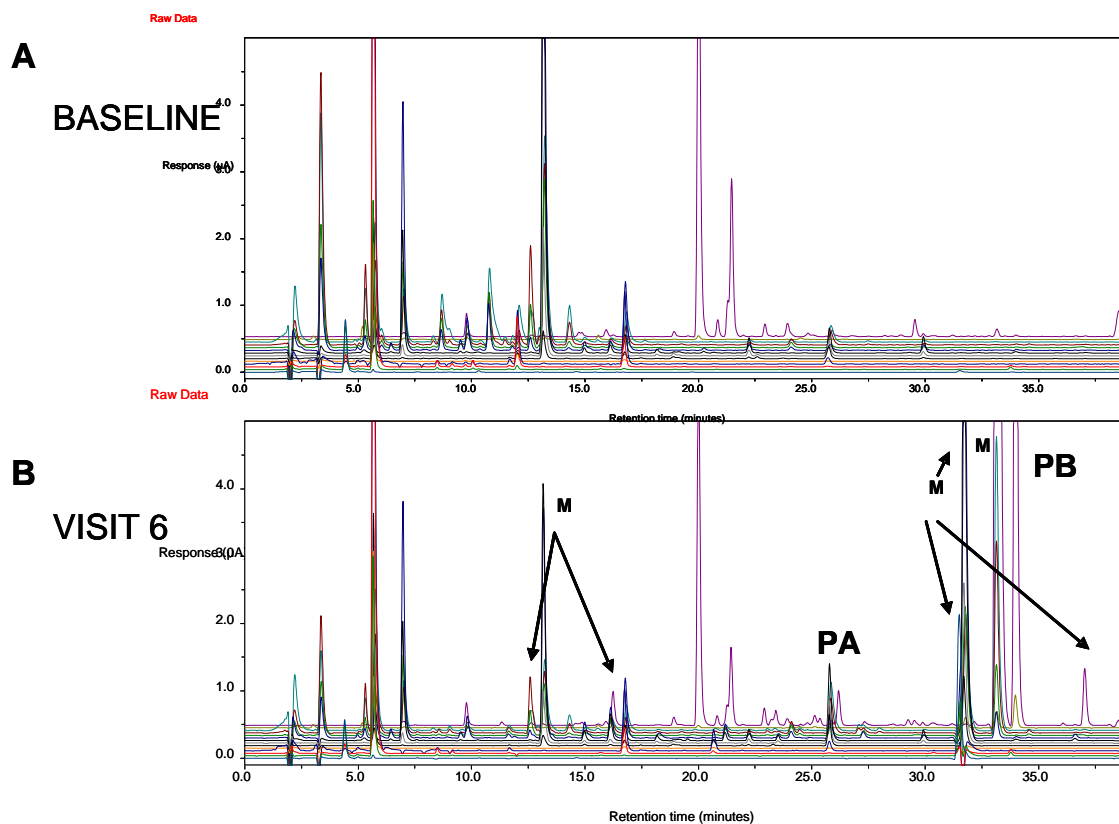
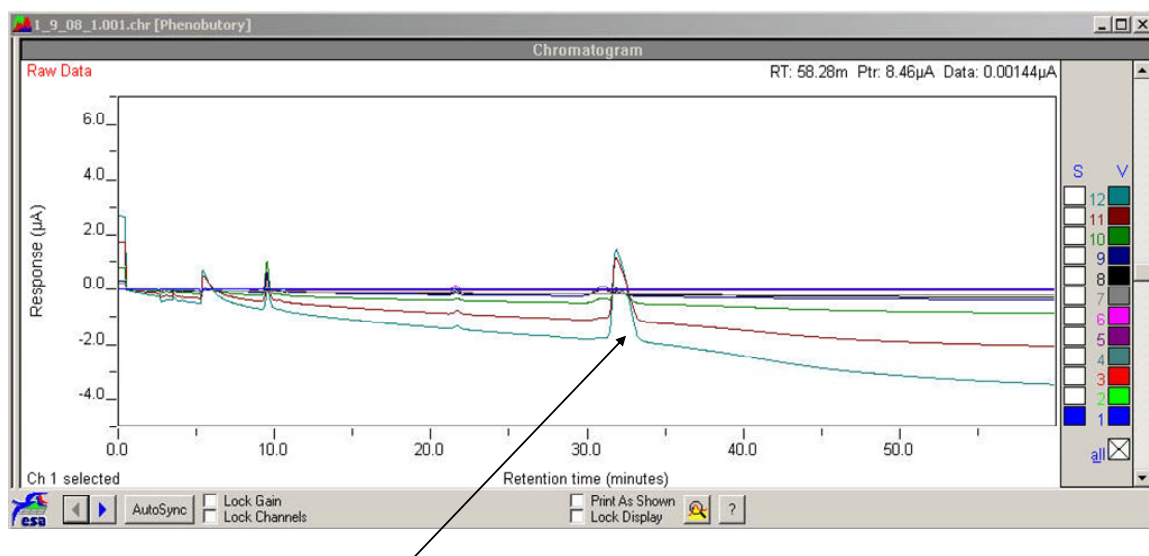


**Figure 3.2 Standard LC-EC-array/UV/F method showing full 14-channel LC-EC-array/UV/Fluorescence- detected chromatograms of plasmas from baseline (A) and SPB-treated (B) patients. Metabolites of interest are labeled in B. Also, phenylacetate (PA) and phenylbutyrate (PB) are labeled in B.**

After initial LC-EC-array screening of the plasma fractions, it was found that the 40% ACN sample isolated a metabolite previously observed in the un-fractionated sample.

This compound can be seen eluting at 32 minutes in Figure 3.2B. A parallel LC-EC-array-MS analysis was then done on the 40% fraction in order to characterize the possible SPB metabolite. Figure 3.3 shows the LC-EC-array chromatogram from the 40% ACN fraction obtained from the parallel LC-EC-array-MS system. The LC-EC-array retention time of the 40% peak was again 32 minutes, which corresponded identically to a MS observed peak of the same retention time (Panel A of Figure 3.4). IDA MS data (Figure 3.4) indicated that the  $m/z$  of the compound(s) present at 32



#### Unknown Metabolite of Interest

**Figure 3.3 LC-EC-array spectra of the 40% ACN plasma fraction collected from the Diazam C-18 column. Eluted metabolite of interest is indicated above at retention time of 32 minutes. SPB is not EC active.**

minutes was 161.07 and 117.08. The extracted ion chromatograms (XIC) of each mass (Panels C and D Figure 3.4), and the spectrum under the 32 minute peak indicated that the parent mass of the compound was  $m/z$  161.07 and that the  $m/z$  117.08 was a fragment of the parent mass. Also, as indicated previously, SPB itself is not electrochemically active and thus was not present on the LC-EC-array chromatogram, but was visible as  $m/z$  163.10 in the MS chromatogram at approximately 35 minutes (Panel B Figure 3.4).

The ability to monitor both EC active and inactive compounds via parallel EC-array and MS detection proves the metabolite detection methodology developed here to be a powerful tool in unknown metabolite identification.

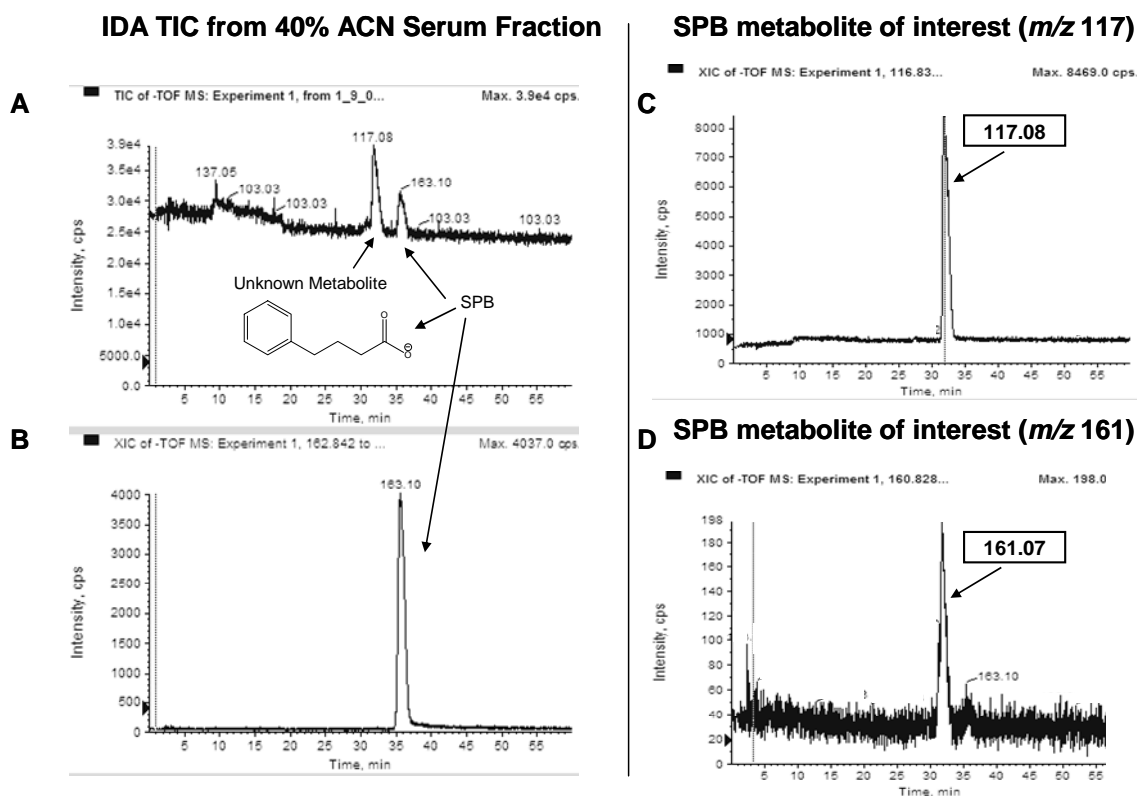


**Figure 3.4** A) TIC from IDA of QStar MS spectra of sodium phenylbutyrate (SPB) and unknown SPB metabolite. B) XIC of SPB. C and D) Two  $m/z$  values ( $m/z$  117 and  $m/z$  161) showed maxima at the retention time (32 min) of the unknown metabolite.

To obtain high resolution MS data and verify the structure of the  $m/z$  161.07 metabolite by MS/MS fragmentation, the 40% fraction was run via infusion using nano-electrospray on an LTQ orbitrap MS. Figure 3.5 shows the full mass spectrum of the 40% fraction between 100 and 200 Daltons. Visible is the  $m/z$  163.10 ion, indicated as the parent drug SPB. Also, both  $m/z$  161.06 and 117.07 ions are present and marked in Figure 3.4 as unknown metabolite peaks. Subsequent fragmentation of  $m/z$  161.07, shown in the inset of Figure 3.5, shows the various product ions formed. Present, is the  $m/z$  117.08 ion,

indicating a loss of CO<sub>2</sub> from the parent molecule and proving further that the compound observed in the parallel LC-EC-array-MS experiment was a single metabolite of SPB. Additionally, several other unique fragmentations were observed, allowing the structure of the metabolite to be proposed. The right hand side of the inset in Figure 3.5 shows the proposed structures of these abundant fragments, such as the loss of a CO group, giving  $m/z$  133.0659 and additionally,  $m/z$  91.0556, which is the benzene ring with a single CH<sub>2</sub> side chain. The proposed unknown SPB metabolite structure, 4-phenyl-trans-crotonate, was found in previous SPB studies done on the mechanism of 3-hydroxy-4-phenylbutyrate formation in SPB perfused rat livers<sup>18</sup>. However, this compound has not been observed in any human studies directly, and gives further insight into HD patient metabolism of SPB.

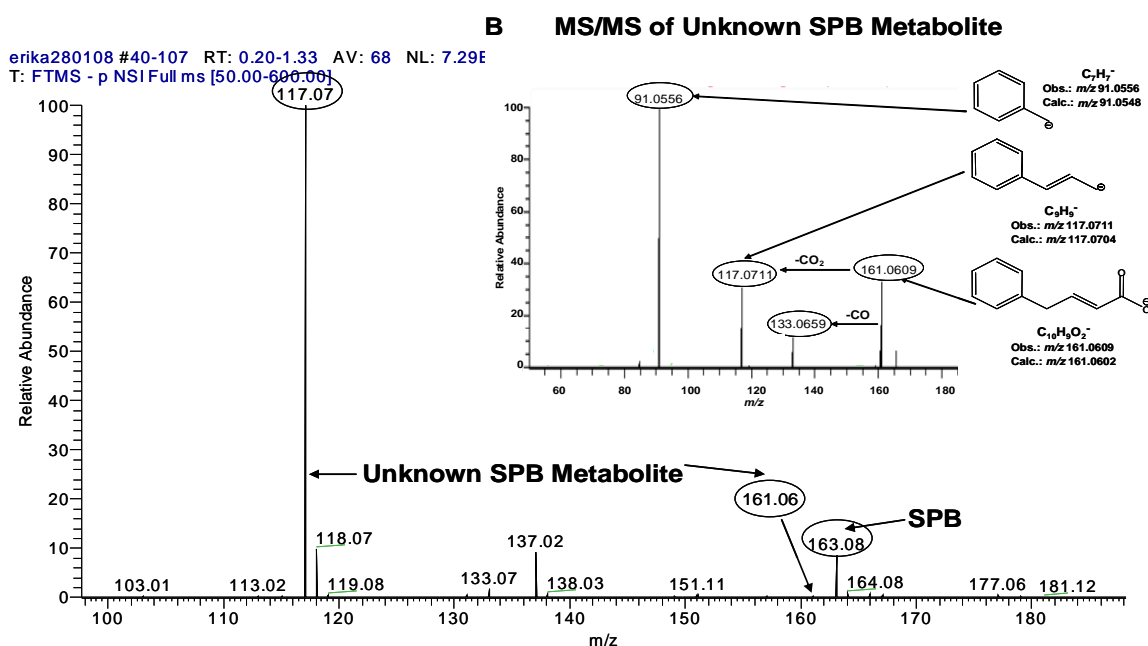


**Figure 3.5 A)** Orbitrap full MS spectrum of 40% ACN fraction collected from Diazam C-18 column at 32 min. Unknown SPB Metabolite ions ( $m/z$  161.06, 117.07) are circled. Parent drug SPB ( $m/z$  163.08) from adjacent LC peak is also labeled. **6B (inset).** Orbitrap MS/MS spectrum of SPB unknown metabolite,  $m/z$  161.06. At right, the structures of the abundant metabolite fragments are indicated.

Once it was clear that the complete analysis method outlined in Figure 3.1 could accurately and efficiently be used to identify and characterize unknown SPB metabolites, it was then applied to the remaining fractions of interest, both plasma and urine. As described above for the 40% ACN plasma fraction, these samples were injected on the parallel LC-EC-array-MS system, with the MS operating in negative ion mode. It was only necessary, however, to run these fractions for 20 minutes because they were more polar compared to both the identified 4-phenyl-trans-crotonate metabolite and the parent SPB drug. Each subsequent fraction was analyzed in the same manner as the 40% fraction; with each parallel LC-EC-array-IDA-MS examined for compounds showing identical EC-array and MS retention times. The  $m/z$  values of the  $[M-H]^-$  signals corresponding to those compounds were then determined from the MS spectrum recorded at this retention time. Each such unknown compound was further characterized using high resolution MS analysis and/or CID MS/MS fragmentation.

Tables 3.1 and 3.2 list the metabolites found in both the plasma and urine samples from the various ACN fractions of interest collected from the SPE of the total collected HD patient sample. Using the approach in this study we identified seven metabolites that have been previously reported in the literature<sup>18,21</sup> and three possibly novel metabolites (H, I, J in Figure 3.6). The identification of these metabolites and their molecular weight allows the location time and response to be determined in the screening method. In the absence of authentic standard reference materials the estimation of their concentrations can be made from the response in the LCECA<sup>21</sup>.



Serum Metabolite, Instrument data was acquired on	[M-H] <sup>-</sup> Obs. m/z, Exact. m/z, error (ppm)	Plasma Fraction	Major Fragments
Phenylbutyryl-β-glucuronate (A) LTQ Orbitrap (full MS and fragmentation)	339.1083, 339.1085, -0.5	20% ACN	193.0348 [C <sub>8</sub> H <sub>9</sub> O <sub>7</sub> ] <sup>-</sup> 175.0243 [C <sub>6</sub> H <sub>7</sub> O <sub>6</sub> ] <sup>-</sup> 163.0764 [C <sub>10</sub> H <sub>11</sub> O <sub>2</sub> ] <sup>-</sup> 113.0243 [C <sub>5</sub> H <sub>5</sub> O <sub>3</sub> ] <sup>-</sup>
Phenylacetylglutamine (B) LTQ Orbitrap (full MS and fragmentation)	263.1031, 263.1037, -2.3	20% ACN	245.0928 [C <sub>13</sub> H <sub>13</sub> N <sub>2</sub> O] <sup>-</sup> 145.0617 [C <sub>5</sub> H <sub>9</sub> N <sub>2</sub> O <sub>3</sub> ] <sup>-</sup>
Phenylacetate (C) LTQ Orbitrap (full MS and fragmentation)	135.0455, 135.0452, 2.2	20% ACN	(solvent interference prevented MS/MS)
Phenylacetyl-β-glucuronate (D) LTQ Orbitrap (full MS and fragmentation)	311.0771, 311.0772, -0.3	20% ACN	193.0350 [C <sub>6</sub> H <sub>9</sub> O <sub>7</sub> ] <sup>-</sup> 175.0245 [C <sub>6</sub> H <sub>7</sub> O <sub>6</sub> ] <sup>-</sup> 135.0449 [C <sub>8</sub> H <sub>7</sub> O <sub>2</sub> ] <sup>-</sup> 113.0244 [C <sub>5</sub> H <sub>5</sub> O <sub>3</sub> ] <sup>-</sup>
3-hydroxy-4-phenylbutyrate (E) LTQ Orbitrap (full MS and fragmentation)	179.0717, 179.0714, 1.7	20% ACN	161.0605 [C <sub>10</sub> H <sub>9</sub> O <sub>2</sub> ] <sup>-</sup> 135.0814 [C <sub>9</sub> H <sub>11</sub> O] <sup>-</sup> 133.0658 [C <sub>9</sub> H <sub>9</sub> O] <sup>-</sup> 119.0502 [C <sub>8</sub> H <sub>7</sub> O] <sup>-</sup> 117.0717 [C <sub>9</sub> H <sub>9</sub> ] <sup>-</sup>
Hydroxyphenylbutyric acid(s) (F) 3 isomers LCQ Classic (full MS and fragmentation)	179.071,	30% ACN	135.08 C <sub>9</sub> H <sub>11</sub> O 119.14 C <sub>8</sub> H <sub>7</sub> O 93.10 C <sub>6</sub> H <sub>5</sub> O 59.04 C <sub>2</sub> H <sub>3</sub> O <sub>2</sub>
4-phenyl- <i>trans</i> -crotonate (G) LTQ Orbitrap (full MS and fragmentation)	161.0609, 161.0608, -0.6	40% ACN	117.0711 [C <sub>9</sub> H <sub>9</sub> ] <sup>-</sup> 91.0556 [C <sub>7</sub> H <sub>7</sub> ] <sup>-</sup>

Table 3.1 Metabolites found in SPB treated HD patient plasma.

Urine Metabolite Instrument data was acquired on	[M-H] <sup>-</sup> Obs. m/z	Urine Fraction	Major Fragments
Phenylacetylglutamine (B) LTQ Orbitrap (full MS) QStar (fragmentation)	263.1036 263.1037 -0.4	0% ACN (20% re-extracted)	m/z 145.05 [C <sub>5</sub> H <sub>9</sub> N <sub>2</sub> O <sub>3</sub> ] <sup>-</sup> m/z 127.04 [C <sub>5</sub> H <sub>7</sub> N <sub>2</sub> ] <sup>-</sup>
3-hydroxy-4-phenylbutyrate (E) LTQ Orbitrap (full MS and fragmentation)	179.0715 179.0714 0.6	10% ACN	m/z 161.0605 [C <sub>10</sub> H <sub>9</sub> O <sub>2</sub> ] <sup>-</sup> m/z 135.0814 [C <sub>9</sub> H <sub>11</sub> O] <sup>-</sup> m/z 133.0658 [C <sub>9</sub> H <sub>9</sub> O] <sup>-</sup> m/z 119.0502 [C <sub>8</sub> H <sub>7</sub> O] <sup>-</sup> m/z 117.0717 [C <sub>9</sub> H <sub>9</sub> ] <sup>-</sup>
3-carboxy sulfate indoline (H) LTQ Orbitrap (full MS) LCQ (fragmentation)	242.0125 242.0129 -1.6	10% ACN (15% re-extracted)	m/z 162.04 [C <sub>9</sub> H <sub>8</sub> NO <sub>2</sub> ] <sup>-</sup> m/z 123.99 [CO <sub>5</sub> S] <sup>-</sup> m/z 79.95 [SO <sub>3</sub> ] <sup>-</sup>
3-Indoxyl sulfate (I) LTQ Orbitrap (full MS) LCQ (fragmentation)	212.0023 212.0023 0	10% ACN (15% re-extracted)	m/z 132.03 [C <sub>8</sub> H <sub>6</sub> NO] <sup>-</sup> m/z 79.95 [SO <sub>3</sub> ] <sup>-</sup>
Benzyloxyl sulfate (J) LTQ Orbitrap (full MS) LCQ (fragmentation)	187.0071 187.0071 0	10% ACN (15% re-extracted)	m/z 107.04 [C <sub>7</sub> H <sub>7</sub> O] <sup>-</sup> m/z 79.95 [SO <sub>3</sub> ] <sup>-</sup>

Table 3.2 Metabolites found in SPB treated HD patient urine.

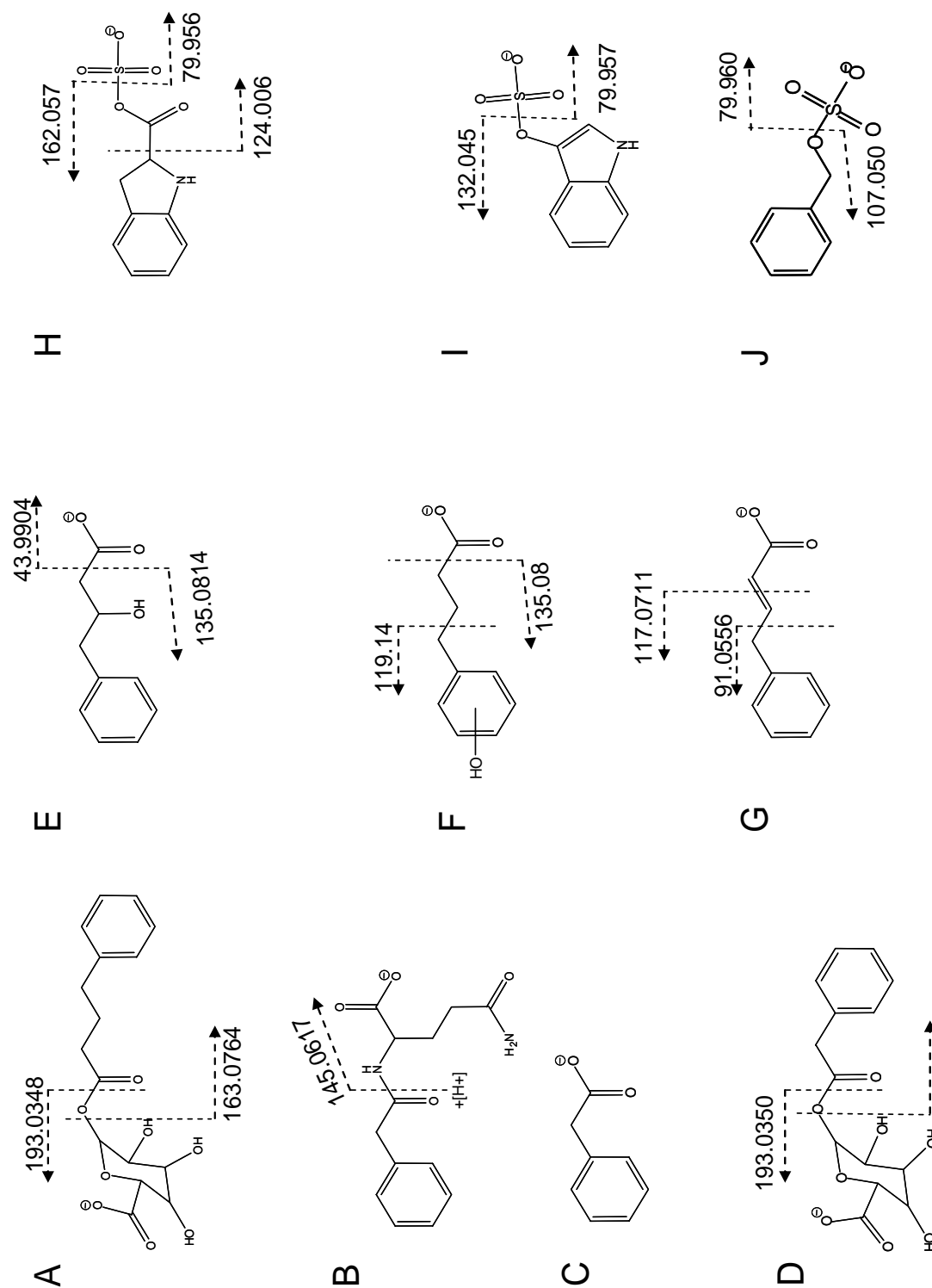


**Figure 3.6 Structures of Metabolites found in SPB Treated HD Patient Plasma and Urine. Structures and fragmentations correspond to those listed in Tables 3.1 and 3.2.**

### 3.7 Discussion of Disease and individual metabolism of SPB

The metabolites presented in Tables 3.1 and 3.2 reflect various types of SPB metabolism. These include the enzymatic conversion pathways to PA, non enzymatic pathways related to oxidative stress, kidney and liver function that result in sulfonation and glucuronidation and suggest a possible effect on indole metabolism. Each of these processes can be postulated to be different among disorders and within individuals. Compounds E and G (Figure 3.6), 3-hydroxy-4-phenylbutyrate and 4-phenyl-trans-crotonate, are side products of CoA-mediated metabolism to PA. The hydroxyphenyl butyrates (F in Figure 3.6) can be enzymatically derived or can alternatively reflect direct hydroxylation that occurs as a result of the high level of free radical production and oxidative stress in HD <sup>28</sup>. The glucuronide (A and D in Figure 3.6) and sulfated compounds (H, I, J in Figure 3.6) reflect modified patterns of kidney and liver function.

Identifying these metabolites becomes important especially on a patient to patient basis when assessing SPB as HD treatment. By understanding either positive or adverse patient reaction to SPB treatment and correlating this reaction to the patient's individual metabolite patterns, biomarkers of drug response may be defined. Once defined, these biomarkers may assist in identifying how patients will react to SPB treatment based on the presence and concentration of metabolites shown to uniquely elicit a positive response to the drug. These biomarkers can be identified as either metabolites of SPB itself, such as a glucuronide conjugate, or molecules from other metabolic pathways that are being affected by SPB treatment.

For example, the indole sulfates (H and I in Figure 3.6) found only in the urine of HD subjects treated with SPB reflects a possible role of SPB in modulating indole pathways. The formation of oxidized indoles has been shown to lead to toxicity in neurodegenerative diseases<sup>29-31</sup> such as in HD where aberrations in the tryptophan pathway are well known to occur<sup>32, 33</sup>. Ultimately, this neurotoxicity is caused by aggregates formed from proteins crosslinked by oxidized indoles<sup>34-38</sup>. In particular, the intermediate free radical indole species formed by hydroxyl radical attack have been implicated in protein aggregation<sup>31, 39</sup>, and may be involved in cross linking mechanisms similar to those of polyglutamines which are elevated in HD<sup>40</sup>. While mechanistic studies were not the primary focus of this work, the excretion of indoles from SPB treated HD patients, may indicate a secondary mechanism of SPB which modulates the potentially neurotoxic effect of indolic species.

### 3.8 Conclusions

We have demonstrated a systematic process for unknown metabolite identification using EC-array and MS detection both separately and in parallel. The process was applied to studying SPB metabolism in HD patients. By applying this process we have expanded the capability of a method for simply evaluating SPB and primary PA metabolite levels to include compounds reflecting multiple modes of SPB metabolism reflecting both disease and individual specific processes. Most importantly applying the process to this sample set yielded the unexpected result of finding increased excretion of indole species as a

result of therapy. These previously unreported metabolites resulting from SPB therapy may have implications both on the disease processes in HD and a secondary effect of the therapeutic intervention in combination with HDAC processes.

### 3.9 References

- (1) Imarisio, S.; Carmichael, J.; Korolchuk, V.; Chen, C. W.; Saiki, S.; Rose, C.; Krishna, G.; Davies, J. E.; Ttofi, E.; Underwood, B. R.; Rubinsztein, D. C. *Biochem J* **2008**, *412*, 191-209.
- (2) Dunah, A. W.; Jeong, H.; Griffin, A.; Kim, Y. M.; Standaert, D. G.; Hersch, S. M.; Mouradian, M. M.; Young, A. B.; Tanese, N.; Krainc, D. *Science* **2002**, *296*, 2238-2243.
- (3) Harjes, P.; Wanker, E. E. *Trends Biochem Sci* **2003**, *28*, 425-433.
- (4) Sugars, K. L.; Rubinsztein, D. C. *Trends Genet* **2003**, *19*, 233-238.
- (5) Vonsattel, J. P.; DiFiglia, M. *J Neuropathol Exp Neurol* **1998**, *57*, 369-384.
- (6) McCampbell, A.; Taye, A. A.; Whitty, L.; Penney, E.; Steffan, J. S.; Fischbeck, K. H. *Proc Natl Acad Sci U S A* **2001**, *98*, 15179-15184.
- (7) Steffan, J. S.; Bodai, L.; Pallos, J.; Poelman, M.; McCampbell, A.; Apostol, B. L.; Kazantsev, A.; Schmidt, E.; Zhu, Y. Z.; Greenwald, M.; Kurokawa, R.; Housman, D. E.; Jackson, G. R.; Marsh, J. L.; Thompson, L. M. *Nature* **2001**, *413*, 739-743.
- (8) Hughes, R. E.; Lo, R. S.; Davis, C.; Strand, A. D.; Neal, C. L.; Olson, J. M.; Fields, S. *Proc Natl Acad Sci U S A* **2001**, *98*, 13201-13206.
- (9) Hockly, E.; Richon, V. M.; Woodman, B.; Smith, D. L.; Zhou, X.; Rosa, E.; Sathasivam, K.; Ghazi-Noori, S.; Mahal, A.; Lowden, P. A.; Steffan, J. S.; Marsh, J. L.; Thompson, L. M.; Lewis, C. M.; Marks, P. A.; Bates, G. P. *Proc Natl Acad Sci U S A* **2003**, *100*, 2041-2046.
- (10) Ferrante, R. J.; Kubilus, J. K.; Lee, J.; Ryu, H.; Beesen, A.; Zucker, B.; Smith, K.; Kowall, N. W.; Ratan, R. R.; Luthi-Carter, R.; Hersch, S. M. *J Neurosci* **2003**, *23*, 9418-9427.
- (11) Thomas, E. A.; Coppola, G.; Desplats, P. A.; Tang, B.; Soragni, E.; Burnett, R.; Gao, F.; Fitzgerald, K. M.; Borok, J. F.; Herman, D.; Geschwind, D. H.; Gottesfeld, J. M. *Proc Natl Acad Sci U S A* **2008**, *105*, 15564-15569.

- (12) Samid, D.; Hudgins, W. R.; Shack, S.; Liu, L.; Prasanna, P.; Myers, C. E. *Adv Exp Med Biol* **1997**, 400A, 501-505.
- (13) Gilbert, J.; Baker, S. D.; Bowling, M. K.; Grochow, L.; Figg, W. D.; Zabelina, Y.; Donehower, R. C.; Carducci, M. A. *Clin Cancer Res* **2001**, 7, 2292-2300.
- (14) Shin, H. J.; Baek, K. H.; Jeon, A. H.; Kim, S. J.; Jang, K. L.; Sung, Y. C.; Kim, C. M.; Lee, C. W. *Oncogene* **2003**, 22, 3853-3858.
- (15) Dover, G. J.; Brusilow, S.; Charache, S. *Blood* **1994**, 84, 339-343.
- (16) Rubenstein, R. C.; Zeitlin, P. L. *Am J Respir Crit Care Med* **1998**, 157, 484-490.
- (17) Sadri-Vakili, G.; Cha, J. H. *Curr Alzheimer Res* **2006**, 3, 403-408.
- (18) Kasumov, T.; Brunengraber, L. L.; Comte, B.; Puchowicz, M. A.; Jobbins, K.; Thomas, K.; David, F.; Kinman, R.; Wehrli, S.; Dahms, W.; Kerr, D.; Nissim, I.; Brunengraber, H. *Drug Metab Dispos* **2004**, 32, 10-19.
- (19) Comte, B.; Kasumov, T.; Pierce, B. A.; Puchowicz, M. A.; Scott, M. E.; Dahms, W.; Kerr, D.; Nissim, I.; Brunengraber, H. *J Mass Spectrom* **2002**, 37, 581-590.
- (20) Cudkowicz, M. E.; Andres, P. L.; Macdonald, S. A.; Bedlack, R. S.; Choudry, R.; Brown, R. H., Jr.; Zhang, H.; Schoenfeld, D. A.; Shefner, J.; Matson, S.; Matson, W. R.; Ferrante, R. J. *Amyotroph Lateral Scler* **2008**, 1-8.
- (21) Schiavo, S.; Ebbel, E.; Sharma, S.; Matson, W.; Kristal, B. S.; Hersch, S.; Vouros, P. *Anal Chem* **2008**, 80, 5912-5923.
- (22) Bogdanov, M.; Matson Wayne, R.; Wang, L.; Matson, T.; Saunders-Pullman, R.; Bressman Susan, S.; Flint Beal, M. *Brain FIELD Full Journal Title:Brain : a journal of neurology* **2008**, 131, 389-396.
- (23) Gamache, P. H.; McCabe, D. R.; Parvez, H.; Parvez, S.; Acworth, I. N. *Progress in HPLC-HPCE* **1997**, 6, 99-126.
- (24) Milbury, P. E. *Progress in HPLC-HPCE* **1997**, 6, 127-144.
- (25) Kristal, B. S.; Vigneau-Callahan, K.; Matson, W. R. *Methods Mol Biol* **2002**, 186, 185-194.
- (26) Kristal, B. S.; Vigneau-Callahan, K. E.; Matson, W. R. *Anal Biochem* **1998**, 263, 18-25.
- (27) Rozen, S.; Cudkowicz, M. E.; Bogdanov, M.; Matson, W. R.; Kristal, B. S.; Beecher, C.; Harrison, S.; Vouros, P.; Flarakos, J.; Vigneau-Callahan, K.; Matson,

- T. D.; Newhall, K. M.; Beal, M. F.; Brown, R. H., Jr.; Kaddurah-Daouk, R. *Metabolomics* **2005**, *1*, 101-108.
- (28) Hersch, S. M.; Gevorkian, S.; Marder, K.; Moskowitz, C.; Feigin, A.; Cox, M.; Como, P.; Zimmerman, C.; Lin, M.; Zhang, L.; Ulug, A. M.; Beal, M. F.; Matson, W.; Bogdanov, M.; Ebbel, E.; Zaleta, A.; Kaneko, Y.; Jenkins, B.; Hevelone, N.; Zhang, H.; Yu, H.; Schoenfeld, D.; Ferrante, R.; Rosas, H. D. *Neurology* **2006**, *66*, 250-252.
- (29) Volicer, L.; Chen, J. C.; Crino, P. B.; Vogt, B. A.; Fishman, J.; Rubins, J.; Schenepfer, P. W.; Wolfe, N. *Prog Clin Biol Res* **1989**, *317*, 453-465.
- (30) Crino, P. B.; Vogt, B. A.; Chen, J. C.; Volicer, L. *Brain Res* **1989**, *504*, 247-257.
- (31) Volicer, L.; Langlais, P. J.; Matson, W. R.; Mark, K. A.; Gamache, P. H. *Arch Neurol* **1985**, *42*, 1158-1161.
- (32) Beal, M. F.; Matson, W. R.; Swartz, K. J.; Gamache, P. H.; Bird, E. D. *J Neurochem* **1990**, *55*, 1327-1339.
- (33) Beal, M. F.; Matson, W. R.; Storey, E.; Milbury, P.; Ryan, E. A.; Ogawa, T.; Bird, E. D. *J Neurol Sci* **1992**, *108*, 80-87.
- (34) Tamir, H.; Liu, K. P. *J Neurochem* **1982**, *38*, 135-141.
- (35) Korlimbinis, A.; Hains, P. G.; Truscott, R. J.; Aquilina, J. A. *Biochemistry* **2006**, *45*, 1852-1860.
- (36) Korlimbinis, A.; Truscott, R. J. *Biochemistry* **2006**, *45*, 1950-1960.
- (37) Parker, N. R.; Jamie, J. F.; Davies, M. J.; Truscott, R. J. *Free Radic Biol Med* **2004**, *37*, 1479-1489.
- (38) Fishman, J. B.; Rubins, J. B.; Chen, J. C.; Dickey, B. F.; Volicer, L. *J Neurochem* **1991**, *56*, 1851-1854.
- (39) Broderick, P. A. R., D.N; Kolodny, E.H, Ed. *Bioimaging in Neurodegeneration*; Humana Press, 2005.
- (40) Jeitner, T. M.; Matson, W. R.; Folk, J. E.; Blass, J. P.; Cooper, A. J. *J Neurochem* **2008**, *106*, 37-44.

## Chapter 4

### A Microscale LC-MS-NMR Platform Applied to the Identification of Active Cyanobacterial Metabolites

Published in Analytical Chemistry:

Lin, Y., Schiavo, S; Orjala, J.; Vouros, P., Kautz, R.A.; A Microscale LC-MS-NMR Platform Applied to the Identification of Active Cyanobacterial Metabolites *Analytical Chemistry* **2008**, 80, 8045-8054.



#### 4.1 Introduction

As discussed in the introduction chapter of this thesis, over the past two decades, considerable efforts have been dedicated to the hyphenation of high-performance liquid chromatography (HPLC), mass spectrometry (MS), and nuclear magnetic resonance spectroscopy (NMR)<sup>1-4</sup>. This combination of technologies has emerged as an extremely powerful tool for the detection, identification, and quantitation of known, and more importantly unknown, compounds in complex clinical and pharmaceutical matrices as well as in natural product extracts<sup>5</sup>.

Definitive identification of unknowns is essential in the discovery of new biomarkers or drug candidates, and in the characterization of drug metabolites. However, compounds in complex matrices generally require extensive separation and consequently often are only available in small quantities, from the microgram to nanogram level. Such low analyte amounts are problematic in even recognizing known compounds, let alone *de novo* structure determination. In order to effectively couple both NMR and MS to HPLC for low microgram to nanogram analyte characterization, a number of challenges need to be overcome.

#### 4.2 Introduction to microcoil NMR probes

The primary challenge is the intrinsically low sensitivity of NMR relative to MS and HPLC-UV. Where MS and MS/MS analyses are completed in less than 1 sec with nanograms of analyte, 5 mm probe NMR analysis at the microgram level requires acquisition times of hours for simple 1D spectra to days for many 2D spectra. Therefore

it is important to address this sensitivity disparity by moving toward utilizing more sensitive NMR probes.

Marked improvements in NMR mass sensitivity have been achieved in recent years with the development of microcoil probes which use very small, highly-sensitive radio frequency (RF) detectors. It has been shown that reduction in the RF coil diameter proportionally decreases noise in the NMR probe, improving signal-to-noise (S/N) if the same amount of analyte is soluble in the smaller volume, which is typically the case with LC-purified analytes<sup>6,7</sup>. This improvement in S/N can also be defined by mass sensitivity ( $S_m$ ), the minimum amount of material detected, when comparing the performance of different probes.  $S_m$  may be defined as:

$$S_m = \frac{S/N}{mol * t^{1/2}}$$

Where  $mol$  is the number of moles inside the probe observed volume ( $V_{obs}$ ) and  $t$  is the acquisition time.

In addition to decreasing the size of the coil, using a solenoidal shaped coil provides 3-fold higher signal than a comparably-sized saddle coil<sup>8-10</sup> (both seen in Figure 4.1). In a comparison with other NMR techniques being developed to boost NMR sensitivity, such as cryogenically cooled coils which also reduce receiver coil noise, microcoil probes have shown better  $S_m$  at similar field strengths. It should also be noted that a 1 mm superconducting probe currently holds the  $S_m$  record<sup>11</sup>, however, microcoil probes have

major advantages in being affordable, priced similar to conventional tube probes, and they can be quickly exchanged with other probes on shared NMR instruments, and thus are more readily available.

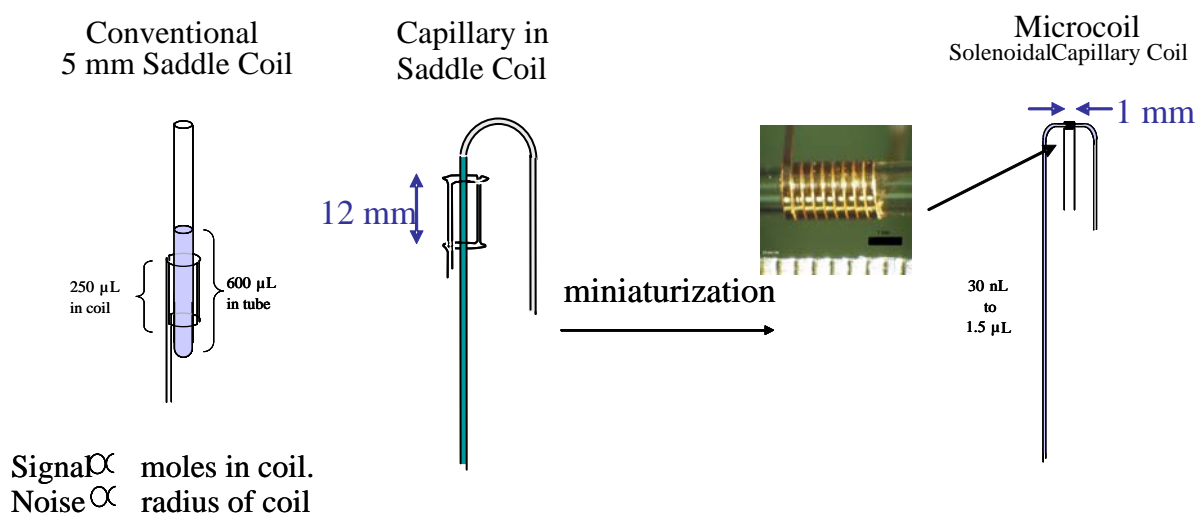


**Figure 4.1** Side by side comparison of a saddle coil NMR probe and a microcoil NMR probe.

#### 4.3 Droplet microfluidics for flow NMR

Achieving high sensitivity in flow NMR requires attention to sample preparation and loading, in addition to utilizing microcoil NMR probes. The commercially-available microcoil probe used in this platform, for example, requires filling a 1.5  $\mu\text{L}$  NMR observed volume through a significant dead volume – 6  $\mu\text{L}$  from the probe inlet and 25  $\mu\text{L}$  or more from a sample handler. The resulting NMR sample efficiency, meaning the ratio of the final volume of injected sample to the observed volume, can be low due to sample diffusion in most flow based methods. Addressing issues of sample efficiency and dilution, several flow NMR methods have been developed<sup>12, 13</sup> including direct

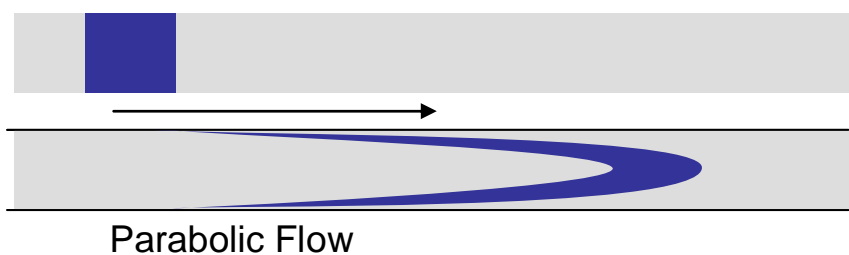
injection NMR (DI-NMR)<sup>14</sup>, flow injection analysis NMR (FIA-NMR)<sup>9, 13</sup>, and recently segmented flow analysis NMR (SFA-NMR)<sup>15, 16</sup>, which includes the technique used here, microdroplet NMR.

Segmented flow analysis (SFA) has been demonstrated to be a particularly mass-sensitive, sample-efficient approach for high-throughput microcoil NMR<sup>15</sup>. In SFA, samples are moved as a “plug” in an immiscible carrier fluid; “droplet microfluidics” is a rapidly emerging field<sup>17</sup>. Because segmented sample plugs do not disperse into the immiscible carrier, as sample zones do in FIA, smaller sample volumes can be loaded without dilution or dispersion, providing an exponential reduction in NMR acquisition times as well as reducing consumption of both analyte and deuterated solvent. Successful implementation of SFA-NMR requires that sample plugs be moved through several meters of transfer capillary between the sample loader and the NMR probe without the sample plugs becoming fragmented or the sample adsorbing onto capillary surfaces.

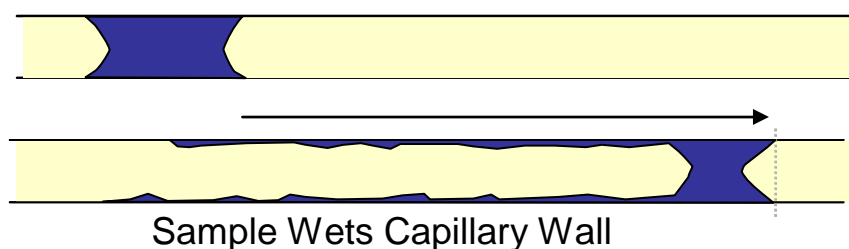
The microdroplet system, used in this chapter, utilizes “zero dispersion” segmented flow, based on the principle that if the carrier fluid has a favorable contact energy with the tubing wall, relative to the sample, a layer of carrier is maintained between the wall and the sample as the plugs are transported<sup>18-20</sup>; this phenomenon is described in Figure 4.2. Perfluorocarbons, which have a Teflon-like immiscibility with all common NMR solvents, may be used as carrier fluids in Teflon tubing to achieve zero-dispersion sample transfer<sup>19, 20</sup>. Based on this principle, an automated system for loading samples into a microcoil NMR probe from 96-well plates was developed and has been applied to high-throughput NMR analysis of compound libraries<sup>15</sup>. Although the published system was

optimized for rapid analysis of compound libraries in a custom-built microcoil probe, its sample loading efficiency was quite high relative to other flow-NMR methods and even NMR tubes. It has been further developed here for trace analysis applications and adapted to commercially available microcoil probes.

### FIA (miscible carrier)



### SFA (immiscible carrier)



### Zero-Dispersion SFA

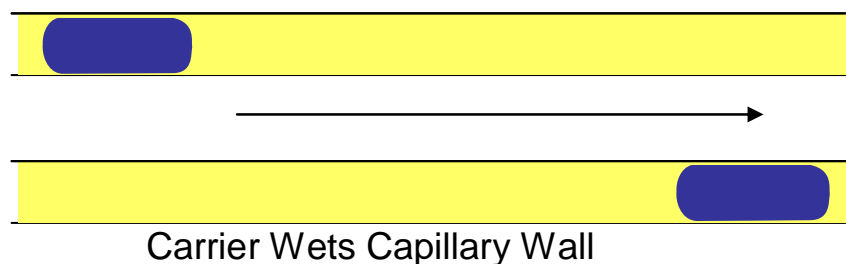


**Figure 4.2 Comparison of FIA and SFA flow methods.** In the top capillary, FIA analysis in a miscible carrier illustrates the mechanism of sample dispersion and dilution. In the second capillary SFA method the sample wets the carrier wall, and in the bottom capillary SFA method the carrier fluid remains in contact with the capillary wall, providing more plug like flow and makes sample losses negligible.

#### 4.4 Hyphenation of microdroplet NMR with nanoSplitter MS

A second challenge in the development of an LC-MS-NMR system is the establishment of an LC-MS interface which provides fast, sensitive and routine MS analysis, while collecting as much material as possible for NMR. When LC is coupled to MS for the analysis of samples in complex matrices, such as biofluids or crude natural product extracts, nanoelectrospray ionization is overwhelmingly preferred. Nanoelectrospray provides better MS sensitivity by lowering ion suppression, increasing ionization efficiency and minimizing sample consumption<sup>21</sup>. Nanoelectrospray is generally limited to low-capacity narrow-bore columns (75  $\mu\text{m}$  I.D.) which feed the entire eluent flow to the MS at a flow rate of < 300 nL/minute. To provide as much material as possible for NMR analysis, a normal bore (> 2 mm I.D.) as opposed to a narrow bore column is required. Traditional packed 4.6 mm columns have loading capacities of as much as 200  $\mu\text{g}$  per injection, or even as much as 1 mg of material for new 4 mm monolithic columns. Moreover, normal-bore columns are justifiably considered easier to use, have more reproducible retention times, and can tolerate injection of larger volumes of relatively less clean samples, such as reaction mixtures or biological fluids.

An LC-MS-NMR platform would thus ideally couple normal-bore HPLC with nanoelectrospray ionization, in order to provide enough material for the NMR while maximizing the sensitivity of MS. With these considerations in mind, our laboratory has recently developed an interface, termed the nanoSplitter, that accomplishes this goal by delivering a small fraction of the HPLC effluent (< 0.1%) to the MS through a novel

concentric split design while maintaining the chromatographic integrity of the LC/MS system<sup>22, 23</sup>. When compared to conventional LC electrospray ionization MS, the nanoSplitter interface showed an average improvement of 10-fold in concentration sensitivity and 1000-fold in mass sensitivity<sup>24</sup>.

In order to effectively couple the two detectors, LC-MS and microdroplet-NMR, post LC column fraction collection was used. With a 4.6 mm column, the LC flow was 1 mL/min. The configuration implemented here splits the bulk flow using a conventional T splitter to direct > 90% of the eluent to a UV-guided fraction collector. The remaining liquid is directed toward the nanoSplitter to be further split down to nanoelectrospray conditions. Thus injecting 200 µg on column, at minimum 180 µg should be collected for NMR analyses.

#### 4.5 Project Goals

In the approach described here, 98% of the large-bore column HPLC effluent is directed to a fraction collector for subsequent NMR and bioassay studies while the remaining 2% is directed to the nanoSplitter for nanospray LC-MS analysis. To evaluate this system, a series of experiments testing separation, fraction collection, preconcentration, and microcoil NMR acquisition were performed on a mixture of four commercial drugs (cycloheximide, indapamide, digitoxin, and taxol).

Finally, a bioactive cyanobacterial extract was analyzed to demonstrate the system's applicability in natural product discovery. The LC-MS-NMR platform recognized four known natural products, ambiguine A, I, and E and hapalindole H, from a single 30 µg

LC injection of cyanobacterial crude extract LC and, most impressively, identified one LC-MS peak as a novel bioactive compound. This illustrates the system's significant potential in natural product discovery as well as its potential in metabolomics and other fields requiring trace analysis of components of complex mixtures.

#### 4.6 Materials and Methods

All work done for this chapter was done in collaboration with Dr. Yiqing Lin who was a post-doctoral fellow in the Vouros laboratory from December 2006-December 2007 as well as with Dr. Roger Kautz of the Barnett Institute at Northeastern University.

##### **Chemicals**

Deuterated solvents were obtained from Cambridge Isotope Laboratories (Andover, MA). HPLC-grade acetonitrile (99.9%) and methanol were from Fisher Scientific (Pittsburgh, PA). Water was purified by using a Milli-Q Plus system (Millipore, MA). Fluorocarbon FC-43 was from 3M Corp (St. Paul, MN). Cycloheximide, indapamide, digitoxin, paclitaxel (taxol), and all other chemicals were purchased from Sigma-Aldrich (St. Louis, MO).

##### **Materials**

Teflon capillaries and tubing were obtained from Cole-Parmer (Vernon Hills, IL). PEEK capillaries, unions, in-line filters, and adapters were from Upchurch (Oak Harbor, WA). The 96-well low retention PCR plates were obtained from Nunc (part #: 240600, Rochester, NY).



## **HPLC and Fraction Collector**

Chromatographic separations and fraction collection were performed on an HPLC system consisting of a binary pump, an autosampler, a UV-VIS diode-array detector (Agilent 1100 series), a fraction collector (Agilent 1200 series) controlled by Agilent ChemStation (version B.02.01) software. The HPLC column used for standards was a 4.6 x 150 mm HPLC column (Agilent Zorbax C-18SB 3.5  $\mu\text{m}$ ) and for cyanobacterial extracts a 4.6 x 250 mm HPLC column (Waters Atlantis C18 5  $\mu\text{m}$ ) was used. A restriction valve was used to split the flow from the LC column with ~98% of the flow to the UV-VIS diode-array detector and eventually to the fraction collector, and the other ~2% of the flow to the nanoSplitter. The delay volume between the UV detector and the fraction collector was determined to be 71  $\mu\text{L}$ . The chromatographic methods are described below.

## **The nanoSplitter Interface and Mass Spectrometer**

The nanoSplitter consists of a splitter (FSMUAS1.5, Valco Instruments Co. Inc, Houston, TX), a micro flow-thru connector (Valco Instruments Co. Inc, Houston, TX), a needle valve (86041, Alltech, Deerfield, IL) and a XYZ positioner (FP-2 Newport, Irvine, CA). These components are fastened to a rail-and-mount system (9742 (M), New Focus, Inc., Sunnyvale, CA). The fused silica picotip emitters, obtained from New Objective (Woburn, MA), had an inner diameter of 20  $\mu\text{m}$  with a tip (distal coated) of 10  $\mu\text{m}$  inner diameter. The high-voltage connection was made by attaching a clip to the emitter. The split ratio was adjusted using the needle valve to obtain optimal electrospray. The flow into the MS was ~ 200 nL/min and was measured by collecting the flow from the emitter

tip with the electrospray voltage off. More details regarding the design and construction of the nanoSplitter can be found in the previous publications<sup>22, 24, 25</sup>.

Both MS and MS/MS spectra were acquired on a Finnigan LCQ classic quadrupole ion trap (San Jose, CA) controlled by Xcalibur software (version 1.3).

### **Microdroplet NMR (Zero Dispersion Segmented Flow Analysis NMR)**

The automated system for loading samples from 96-well plates into the microcoil NMR probe consists of a Gilson (Middleton, WI) model 215 sample handler and a sample loader, model HTSL-1100, from Protasis Corp. (Marlborough, MA). The Gilson sample handler drew sample plugs from the 96-well plate into the HTSL sample loop. The sample plugs were formed by alternately drawing the immiscible fluorocarbon FC 43, the sample, and then more FC. Additionally, wash plugs of clean solvent were drawn between samples. The HTSL sample loader consists of an LC injection valve with sample loop, a high-pressure pump, and a microprocessor controller. It was used to deliver sample plugs from the sample loop to the microcoil probe via a 3-meter long transfer line of 150  $\mu\text{m}$  i.d. Teflon tubing. Gilson and HTSL automation was controlled using Varian VAST automation programming on the spectrometer host computer (Sparc Ultra 5, Solaris 8, VNMR 6.1 C NMR software).

NMR acquisition setup macros were written to automatically detect and position an arriving sample and to set up a standard spectrum of a sample. In addition, four sample handler programs (Tcl scripts) were written to (1) form a train of 3 samples and hold it in the needle line, (2) draw a train from the needle line into the sample loop, and (3) change

samples by triggering the sample loader to run until stopped by the autodetection macro. The fourth script (4) was run once on the first train to initialize the sample queue by moving this sample train one-half of the distance from the sample loop to the NMR probe. Additional details on the design, construction, and characterization of the automated segmented flow analysis NMR system can be found in our previous publication<sup>15</sup>.

The microcoil probe used in this study was an ICG capLC microflow probe manufactured by Magnetic Resonance Microsensors (MRM, Savoy, IL) and distributed by its parent company, Protasis Corp. This probe has an observed volume ( $V_{\text{obs}}$ ) of 1.5  $\mu\text{L}$  as determined by SFA of small plugs, in a fill volume of 6  $\mu\text{L}$ , through 75  $\mu\text{m}$  inlet and outlet capillaries. The probe was internally coated with fluoro-octyl silane for its use in microdroplet NMR studies.

NMR spectra were acquired on a Varian (Palo Alto, CA) Inova spectrometer with an 11.7-T (500 MHz) actively shielded magnet; the data were processed and analyzed with VNMR version 6.1C software.

### **System Reproducibility and Sample Recovery**

A test mixture comprising equimolar quantities (0.65 mM) of cycloheximide, indapamide, digitoxin, and taxol dissolved in 30% acetonitrile /70% water (v/v) was used for testing system reproducibility and compound recovery. A 100  $\mu\text{L}$  volume of this mixture (containing 24.1  $\mu\text{g}$  indapamide) was injected onto a 150  $\times$  4.6 mm i.d., Agilent Zorbax SB-C18 column (3.5  $\mu\text{m}$ ) (Wilmington, DE). The HPLC was operated at a flow

rate of 1 mL/min and in gradient elution mode. Mobile phase A was water with 0.1% (v/v) formic acid and mobile phase B was acetonitrile with 0.085% (v/v) formic acid. Mobile phase B was held at 30% for the first minute and then increased linearly to 95% over 15 min. Subsequently, mobile phase B was held at 95% for 4 min giving a total run time of 20 min. The eluents were monitored by the UV-DAD at 210 nm with DAD spectra acquired every 0.5 s.

The LCQ-classic ion trap was operated in positive ion mode, scanning between 100 and 2000 daltons. The ESI spray voltage was set to 2.5 kV and no sheath or drying gas was used to facilitate desolvation due to the low flow rate.

The fraction collector was operated in either a time-based or the peak-based mode as indicated, and the fractions were collected into a 96-well plate with a maximum collection volume of 250  $\mu$ L/well. After evaporating the solvents in the wells, all the wells containing indapamide were washed with acetonitrile (with 5% DMSO) and the solutions were then pooled and transferred into a well in another plate. The solvent in the well was evaporated again and the material in the well was dissolved in 5  $\mu$ L of deuterated DMSO containing 15.5 mM caffeine, used as internal standard for quantitation. The solution of the mixture in the well (3.5  $\mu$ L out of 5  $\mu$ L) was then loaded by the automated microdroplet NMR system into the microcoil NMR probe for NMR analysis.

The quantitative NMR spectra were acquired at ambient temperature (22.5<sup>o</sup> C) with 500 transients, 8000-Hz spectrum width, auto gain, water presaturation and, for this

quantitative analysis, a  $90^\circ$  pulse and an additional 30-s relaxation delay beyond the 2-s acquisition time. The above process was repeated six times to test the reproducibility of the LC-MS-NMR system.

Additionally, to determine indapamide recovered from the LC, 24.1  $\mu\text{g}$  of indapamide was dissolved in 5  $\mu\text{L}$  of deuterated DMSO containing 15.5 mM caffeine and the resulting mixture was added into a well of a 96-well plate. The solution in the well (3.5  $\mu\text{L}$  out of 5  $\mu\text{L}$ ) was also loaded by the automated sample loading system into the microcoil NMR probe for NMR analysis. The NMR spectrum was then acquired under the same conditions as described previously and the entire process was again repeated six times.

### **Detection limit and linearity**

A solution of 250 ng indapamide in 50  $\mu\text{L}$  of 30% acetonitrile / 70% water (v/v) was injected onto the Zorbax column. The LC, UV, MS, and fraction collection methods were the same as described for the reproducibility studies. The indapamide fraction was collected, dried, and resuspended in 5  $\mu\text{L}$  of deuterated DMSO and 3.5  $\mu\text{L}$  of the solution was loaded by the automated sample loading system into the microcoil probe for NMR analysis. The NMR spectra were acquired at ambient temperature with 1200 transients (1 hour), 8000-Hz width,  $30^\circ$  tip angle, fixed gain (max = 60), and 1 sec water presaturation after the 2-s acquisition time. The indapamide resonance was integrated as in the recovery determination described. The procedure was applied for the recovery of 250

ng, 500 ng, 750 ng, 1  $\mu$ g, 1.5  $\mu$ g, 15  $\mu$ g indapamide in 50  $\mu$ L of 30% acetonitrile / 70% water (v/v) to test the linearity of the system's performance.

### **Natural Products Characterization**

Through collaboration with Dr. Jimmy Orjala's research group at the University of Illinois at Chicago, a crude extract of cyanobacteria, strain *Fischerella ambigua*, was prefractionated by silica gel chromatography into 6 fractions (eluted with a step gradient of  $\text{CH}_2\text{Cl}_2$  and MeOH solvent mixtures). Fraction 6 (eluted from the silica gel with 100%  $\text{CH}_2\text{Cl}_2$ ) showed activity in a proteasome inhibition assay performed in Dr. Orjala's laboratory and was used to demonstrate the LC-MS-NMR system's applicability to drug discovery from natural products.

A solution of 30  $\mu$ g of the bioactive fraction in 30  $\mu$ L methanol, spiked with 300 ng of taxol, was loaded onto a 250  $\times$  4.6 mm i.d., Waters Atlantis<sup>®</sup> C18 column (5  $\mu$ m) (Milford, MA). The HPLC was operated in gradient elution mode at a flow rate of 1 mL/min. Mobile phase A was water and mobile phase B was methanol. Mobile phase B was held at 80% for the first minute and then was increased linearly to 90% in 50 min. After that, mobile phase B was increased linearly to 100% in 4 min and then decreased to 80% in 1 min and held at 80% for another 4 min, which gave a total run time of 60 min. The effluents were monitored by the UV-DAD at 254 nm with DAD spectra acquired every 0.5 s and by the LCQ-classic ion trap operating in positive ion mode, under the same conditions are previously discussed with additional MS/MS acquisition executed in data-dependent mode.

In addition, the fraction collector was operated in peak-based mode and the fractions were collected into a 96-well plate with a maximum collection volume of 250  $\mu\text{L}$ /well. After evaporating the solvents in the wells, all the wells containing same fraction (overall 13 fractions) were resuspended and washed with methanol (with 5% DMSO to facilitate efficient concentration to the bottom of the well) and transferred into another plate, pooling fractions of the same peak. The solvent in each well was evaporated again and the dried material was dissolved in 5  $\mu\text{L}$  of deuterated DMSO.

Subsequently, the solution in each well (3.5  $\mu\text{L}$  out of 5  $\mu\text{L}$ ) was transferred by the automated sample loading system into the microcoil NMR probe for NMR analysis. The NMR spectra were acquired at ambient temperature with 2000 transients (2 hr), 8000-Hz width, auto gain and 1 sec water presaturation after a 2 sec acquisition time.

In addition, two more LC runs (same LC, fraction collection and MS methods as the above run) were performed with a total loading of 80  $\mu\text{g}$  of the bioactive fraction onto the Atlantis column. Fractions containing the same chromatographic peaks from separate runs were pooled together for microcoil NMR analysis as described above.

#### 4.7 Results and Discussion

The goal of this work was to implement a high-throughput LC-MS-NMR platform which would provide the highest possible sensitivity for the structural identification of unknowns in complex sample matrices. A schematic of the microscale LC-MS-NMR platform is shown in Figure 4.3. As discussed previously, two innovative established techniques, the nanoSplitter for nanoESI-LC-MS<sup>22-24</sup> and the microplug automated sample loading method for offline microcoil LC-NMR<sup>15</sup>, were combined offline in tandem to best complement each detector's optimal working conditions. Successful integration of these techniques requires the preservation of the optimal performance of each individual system's components, and can be shown by overall system reproducibility, quantitative transfer of collected fractions for NMR analysis, and satisfactory limits of detection and dynamic range. Subsequently, the system will be demonstrated in the recognition of components in a natural product extract and prioritizing the unknowns identified for subsequent structural determination.



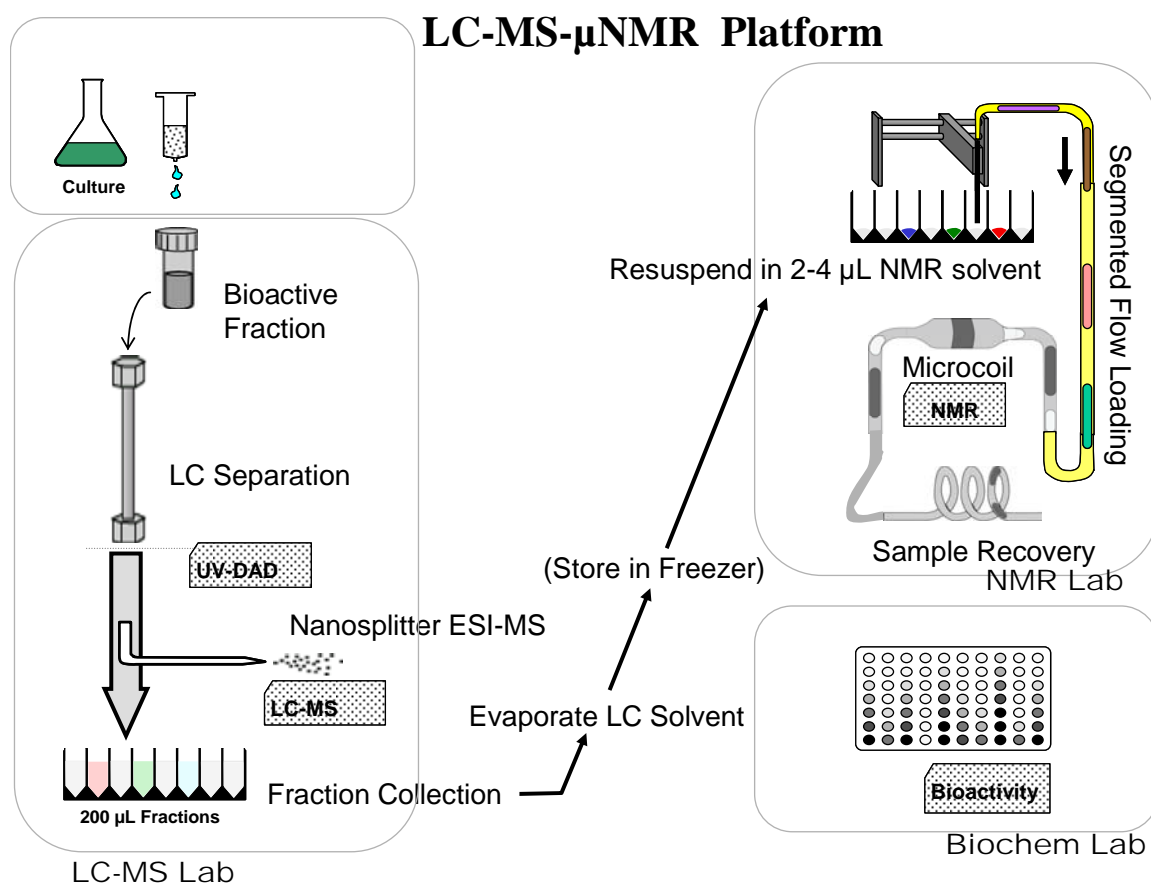


**Figure 4.3** Schematic diagram of the microscale LC-MS-NMR platform, as applied to natural product discovery. The complex sample (bioactive fraction) is separated using high resolution LC with UV and MS data acquired on-line. 98% of the eluent is directed to a UV-guided fraction collection. Fractions are concentrated by drying and may be stored. For NMR, fractions are resuspended in a small volume (2-5  $\mu$ L) of deuterated solvent and loaded into a microcoil NMR probe, with and observed volume of 1-2  $\mu$ L using microplate automation. Samples are recovered after NMR for additional analyses, archival or bioassays.

#### Correlation of UV, MS and NMR Data

An implicit requirement of any LC-MS-NMR system is that the NMR spectra can be correlated with features in the UV and MS chromatograms. This is very important in analysis of uncharacterized complex samples, so the system can reliably correlate the NMR spectra to specific time points in the chromatographic separation with enough confidence to confirm when signals are not seen on the other detectors, for example if

sample components lack UV chromophores and/or have poor MS ionization, such as glycans and lipids. Since the UV detector guides the fraction collection in this current implementation, in order to correlate the NMR data acquired for each fraction with its MS data, any variation in retention time between UV and MS chromatographic peaks must be negligible, relative to peak width.

The system's performance was tested with the analysis of a mixture of the commercially available drugs cycloheximide, digitoxin, indapamide and taxol. Figure 4.4 shows a comparison of the MS total ion chromatogram (TIC) and the HPLC UV chromatogram monitored at 210 nm. Minor peaks seen are either degradants from the analytes being dissolved in methanol or impurities. The red tic marks on the UV chromatogram indicate the time-based fractions collected. The NMR section of Figure 4.4 shows a stacked plot of a representative region of the NMR spectra (0.2 – 2.2 ppm) for the indicated fractions. The point where each compound is eluted is indicated, as is its corresponding MS. Time-based collection, as shown, provides data similar to on-line LC-NMR. In LC-MS-NMR, the NMR acquisition time is optimized by targeting specific features of interest, and peak-based fraction collection is generally preferred.

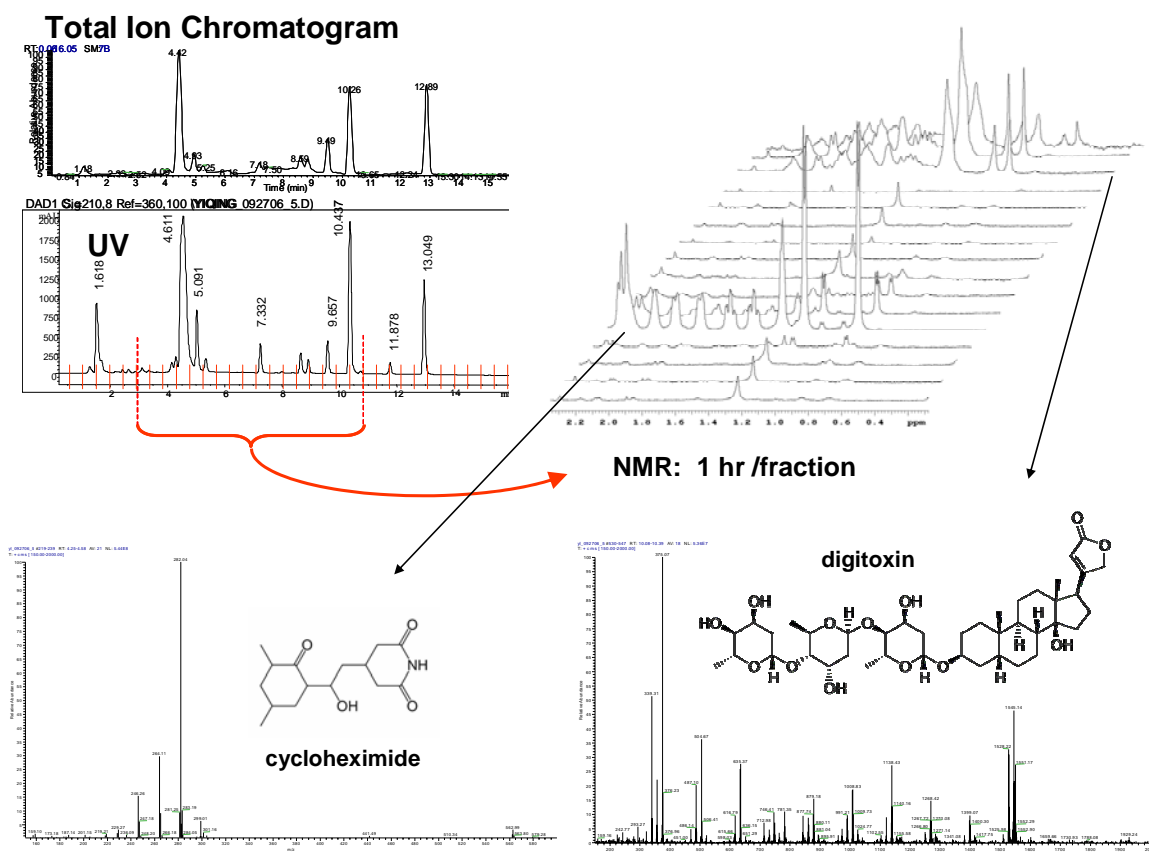


**Figure 4.4** LC-MS-NMR data is shown for a standard mixture of cycloheximide, digitoxin, and taxol. At left an MS total ion chromatogram (TIC) is compared with a UV chromatogram to show preservation of chromatographic integrity and peak retention times. The red tic marks on the UV trace indicate the time-based fractions collected, with the indicated fractions shown as stacked NMR spectra in the center. At bottom are MS spectra corresponding to the UV and NMR data shown.

Retention times between the UV and MS chromatograms were, compared and, in 6 repetitions of the analysis, MS and UV peaks aligned to within less than 0.1 minutes. Systematic differences were minimized by timing the MS acquisition start with that of the LC injection. Variations in retention times were minimal over the entire chromatogram, and were significantly less than the widths of the LC and MS peaks being compared. Also, reference standards could be used to compare retention times and give specific correlation between the two detectors if necessary. It should also be noted that each NMR spectrum corresponded accurately to both the UV and MS fraction with which

it was correlated, demonstrating the ability of all three detectors in the system to simultaneously and reproducibly detect all compounds in the entire chromatogram.

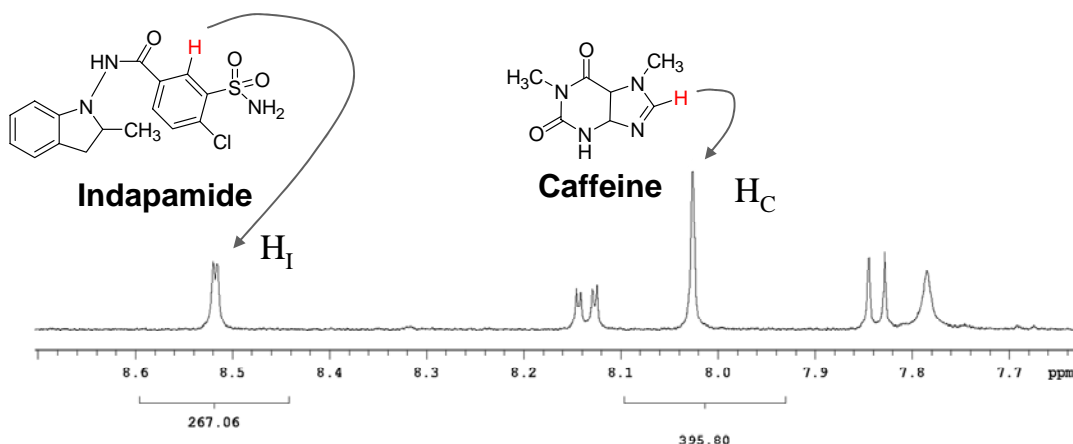
### Sample Recovery

An additional requirement for integration of LC-MS and NMR is near-quantitative recovery of compounds from LC-MS fraction collection and transfer to NMR. Because NMR sensitivity and data quality depend primarily on the amount of compound, the steps of fraction collection, concentration, transfer and reconstitution are critical, especially when low-level compounds are of interest. Experiments were thus performed to compare the amount of a standard injected onto the column with the amount collected and recovered for NMR. The comparison was made using quantitative NMR<sup>26</sup>, which is a precise method for comparing the concentrations of two analytes based on the property that the area of each NMR peak, under appropriate experimental conditions, is directly proportional (within 2%) to the number of the corresponding nuclei. Indapamide, added to the standard mixture used in the previous studies, was used as the standard for injection and recovery; the amounts injected and recovered were each compared to a quantitative addition of caffeine used as the reference standard for quantitative NMR.

To determine recovery, an aliquot of 24.1  $\mu\text{g}$  of indapamide was dissolved and injected into the HPLC. Its peak fraction was collected and resuspended in 5  $\mu\text{L}$  of DMSO- $d_6$  with quantitative addition of 15.5 mM caffeine as an internal standard. This mixture was then transferred by the automated segmented flow sample loading system into the microcoil probe, and quantitative spectra were acquired. In the  $^1\text{H}$  NMR spectra, a 1-

proton peak from caffeine (8.02 ppm) and a 1-proton peak from indapamide (8.52 ppm) were integrated and compared. The longitudinal relaxation times,  $T_1$ , of these caffeine and indapamide resonances were 6 sec and 1.5 s respectively, and the NMR relaxation delay was 30 seconds. The ratio of the caffeine and indapamide integrals was 1.47 with an RSD of 1.2 % over 6 repetitions. This low RSD shows consistency and reproducibility in the HPLC recovery and NMR sample handling process.

To compare this with the amount of indapamide loaded onto the LC column, an identical 24.1  $\mu\text{g}$  aliquot of indapamide was dissolved in the same caffeine-spiked DMSO- $d_6$  standard as the dried fraction-collected sample, and loaded to NMR using the same automated protocol, to normalize any NMR system losses. In those measurements the ratio between the integrals of the caffeine and indapamide resonances was 1.33, with an RSD of 1.1% over 6 repetitions. Therefore, as shown in Figure 4.5, based on the two integral ratios obtained (1.33 and 1.47) and the split ratio of LC flow (97.5% of the LC flow goes to fraction collector), the recovery from LC loading, separation, fraction collection, drying, and resuspension was 92.8%.



Run #	1	2	3	4	5	6	Average	RSD
Integral $H_C / H_I$ (after LC)	1.48	1.45	1.46	1.49	1.48	1.45	1.47	1.17%
Integral $H_C / H_I$ (injected)	1.30	1.33	1.34	1.33	1.34	1.32	1.33	1.13%

**Figure 4.5** A quantitative NMR spectrum of indapamide and caffeine indicating the NMR peaks integrated to determine recovery and reproducibility of the LC-MS-NMR platform. The values of integrals from 6 repetitions are tabulated.

This experiment clearly demonstrates the recovery and reproducibility of the nanoSplitter MS / microdroplet NMR approach. Results with other LC methods may of course vary the method used for the analyte of interest.

#### Limit of Detection and Dynamic Range

For hyphenated methods, the Limit of Detection is generally defined by the performance of the less-sensitive detector. Various interpretations of the “Limit of Detection” in NMR may span several orders of magnitude, depending on the sample (natural line width and multiplicity), the instrument (magnetic field strength and probe type), and the information sought from NMR. There can be as much as a 1000-fold difference in the amount of

sample required for a simple confirmation of a proposed structure (1D NMR), or a challenging *de novo* structure determination (heteronuclear 2D NMR).

For the LC-MS-NMR system in natural product applications, the limit of detection would appropriately be the amount of a minor component necessary to obtain an interpretable NMR spectrum, suitable for dereplication against a library of NMR spectra, under typical acquisition conditions. We thus performed experiments to determine the minimum amount of indapamide that, when spiked into the standard mixture, would generate a  $^1\text{H}$  NMR spectrum with a S/N of 3 for the smallest peak (10.6 ppm) in a 1-hour NMR acquisition. This definition would apply to a high throughput LC-NMR analysis of 12-48 fractions in an overnight or weekend, on our 500 MHz NMR spectrometer.

LC separations were performed by loading 250 ng, 500 ng, 750 ng, 1  $\mu\text{g}$ , 1.5  $\mu\text{g}$ , or 15  $\mu\text{g}$  of indapamide onto the LC column. After fraction collection, LC solvent evaporation, deuterated solvent resuspension, and NMR acquisition, the 250 ng (0.68 nmol) sample provided an S/N of 3 for the 10.6 ppm peak in one hour, as indicated in Figure 4.6. Therefore, 0.68 nmol is a reasonable expectation of the platform's limit of detection for the high-throughput characterization of unknowns.

If a specific LC peak were of interest but observed at a low amount, a similar S/N could be expected from a 16 hr overnight acquisition from  $\frac{1}{4}$  the amount of material, 0.17 nmol and so on. In targeted overnight analyses, NMR acquisition of a single well obtained interpretable 1D spectra from 50 ng of taxol (58 pmol), and HMBC spectra from 35  $\mu\text{g}$ .

This shows further how the offline LC-MS-NMR platform is useful for both targeted and screening analyses.

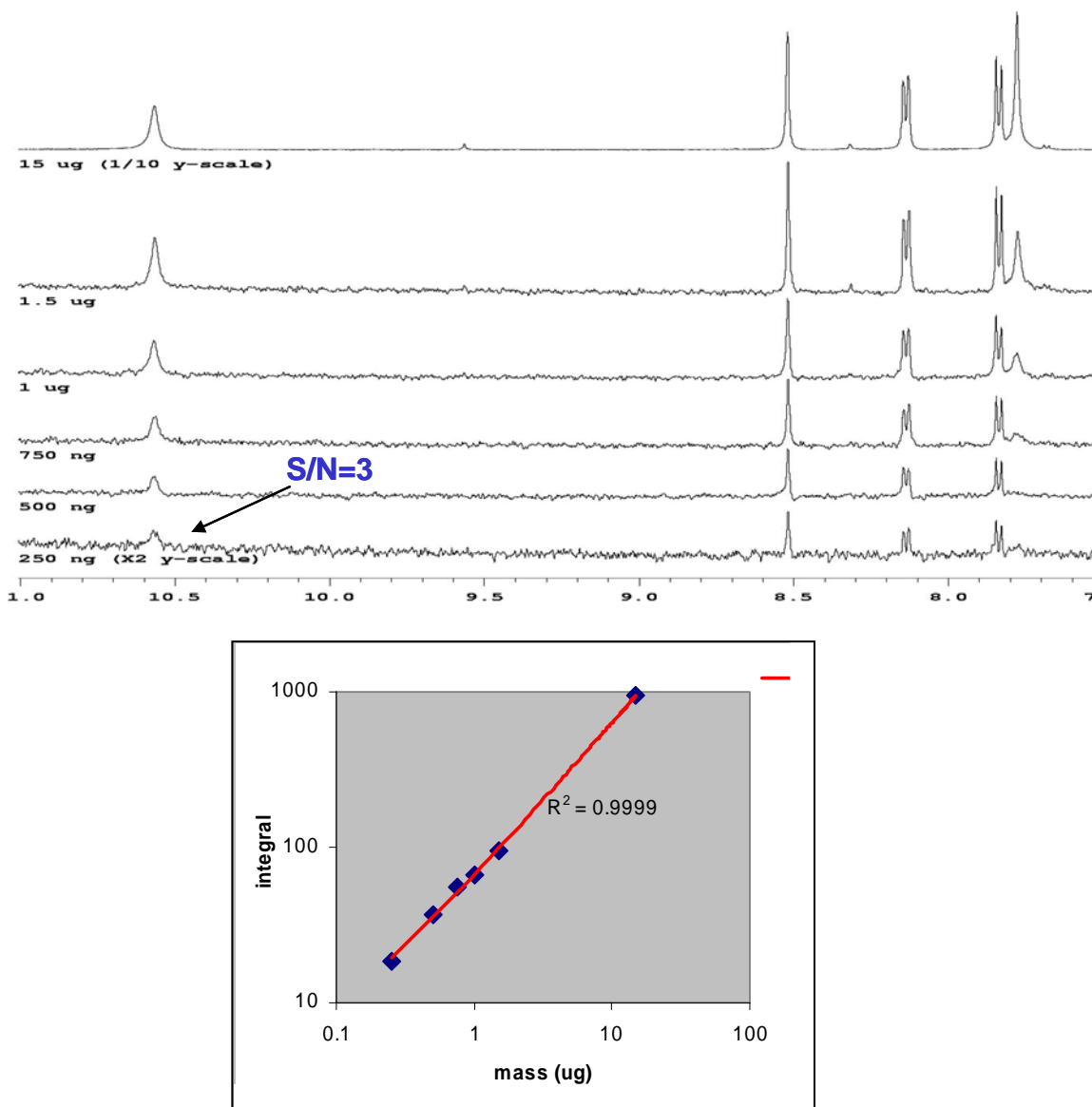


**Figure 4.6** Limit of detection (LOD) following the linearity of 8.5 ppm indapamide peak over 6 concentrations and resulting concentration curve. (Top) Regions of the NMR spectra of indapamide indicating the smallest peak, used to determine LOD. (Bottom) The plot of NMR integrals of indapamide (as in Figure 4.5) versus amount loaded onto the LC column, showing linear dynamic range over the six concentrations analyzed.



A second critical property of an analytical system is dynamic range. The complexity of a natural product extract requires analysis of many unknown compounds present in concentrations ranging over many orders of magnitude, and NMR provides an estimate of concentration to evaluate potency. To assess linear dynamic range, a representative resonance (8.5 ppm) was integrated for each of the above 6 loadings and is plotted in Figure 4.6. The  $R^2$  value of the series is 0.9999, which primarily indicates that sample recovery is constant over this loading mass range, given the established quantitative linearity of NMR.

The results displayed in Figure 4.6 show that a routine one hour NMR acquisition with the automated microdroplet NMR system can detect and quantitate analytes from over 10  $\mu\text{g}$  down to less than 300 ng with confidence. With the demonstration of reproducibility, recovery, sensitivity, and dynamic range above, the applicability of the system to the characterization of natural products and identification of components will be described next.

### **Identification of Metabolites in Extracts of Cyanobacteria**

Following confirmation of the reproducibility, recovery and dynamic range of the LC-MS-NMR system, its practical utility toward the identification and characterization of natural product unknowns in cyanobacteria was examined. A particularly compelling need for trace-level chemical analysis is seen in the field of drug discovery from natural products. Natural products and their derivatives have long played an important role in drug discovery; 61% of the 877 small molecule drug candidates developed during the

period of 1981-2002 can be traced to or were inspired by natural products<sup>27, 28</sup>. These compounds are traditionally discovered by “activity-guided fractionation”<sup>5</sup> where, when an active extract is found, it is separated chromatographically and fractions are tested again for activity in the bioassay. The active fraction is then separated again using an orthogonal separation method, and the fractions are re-assayed, until a pure compound is obtained. This series of separations is then scaled up and repeated to purify enough of the active component, typically several milligrams, for its structural identification and potency determination in a quantitative activity assay. However, because many active components involve the rediscovery of known compounds, this approach to the discovery of lead candidates from natural products can be time-consuming and costly. The combination of LC-MS and NMR data has been shown to be valuable in “dereplication”<sup>5, 29</sup> – elimination of known compounds from further investigation and prioritization of likely unknowns for the expensive steps of scale-up and structure determination.

The ability to obtain LC-MS-NMR data of submicrogram-level compounds in a complex sample can streamline the traditional bioactivity-guided fractionation approach to natural products discovery, obviating the need to perform scale-up purification of milligrams of the active component after it is isolated if it is already known<sup>5</sup>. A convenient LC-MS-NMR system could thus reduce this high overhead of purifying large amounts of redundant compounds, and thereby accelerate drug discovery from promising natural sources.

Therefore we went on to apply the LC-MS-NMR system to cyanobacteria, which are unique phyla which grow in competitive niches, and as a result are promising sources of

bioactive compounds<sup>30</sup>. However, their slow growth rate in culture and low biomass yield have made them prohibitively expensive and time-consuming to search for natural products by traditional methods, which require milligram amounts of material for identification. Successful characterization of active metabolites from cyanobacteria would thus establish significant practical advantages of the microgram-sensitivity LC-MS-NMR platform described herein.

An extract of the cyanobacterium *Fisherella ambigua* (Utex 1903) showed antibacterial activity against *Mycobacterium tuberculosis*. The most-active fraction of an initial silica-gel solid phase extraction, eluted with 100 % dichloromethane (“fraction 6”), was collected and 30 µg of this bioactive extract was subjected to LC-MS-NMR analysis. In the spectra shown in Figures 4.5, 4.6 and 4.7 the fraction was spiked with 300 ng of taxol as an internal standard. Based on the UV chromatogram of the separation shown in Figure 4.7, 12 peak fractions were collected, in addition to the taxol standard, and prepared for µNMR analysis. Each fraction then underwent a two hour <sup>1</sup>H NMR acquisition in an overnight autosampler run. The four largest LC peaks were readily recognized as four known isonitrile-containing indole alkaloids (isonitriles of ambiguines A, E, and I, and hapalindole H) by comparing the experimental MS and <sup>1</sup>H NMR spectra with published data<sup>31-36</sup>.

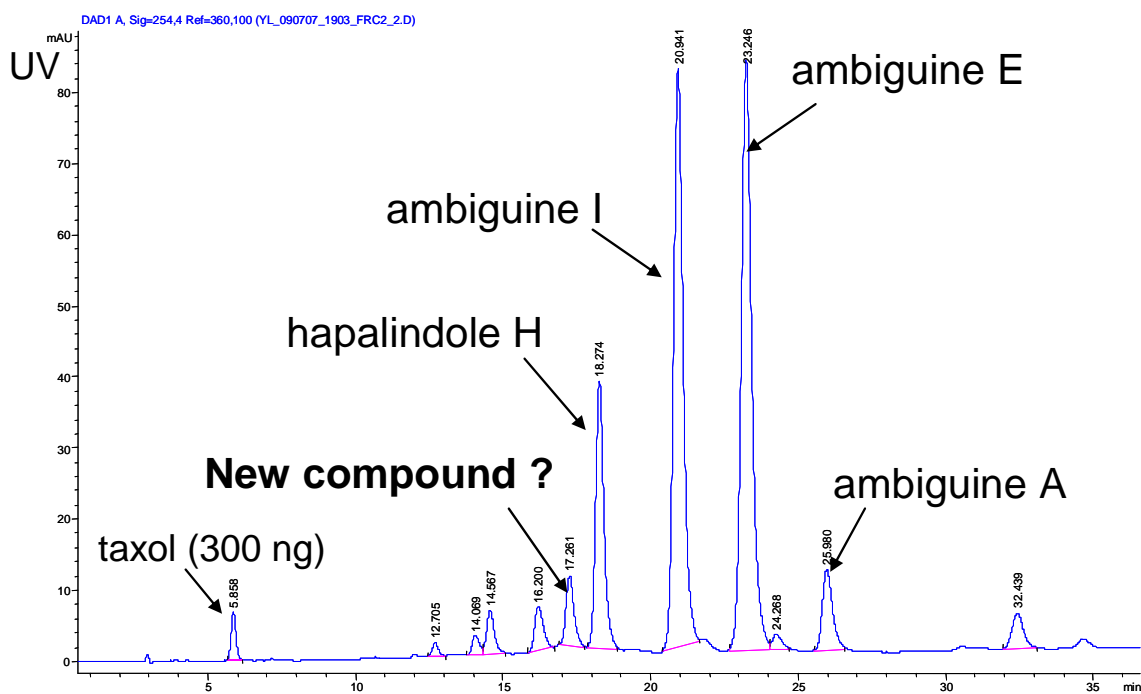


**Figure 4.7** UV chromatogram of the separation of a bioactive cyanobacteria extract analyzed with the LC-MS-NMR system, indicating known and unknown compounds found.

From the LC-MS and  $^1\text{H}$  NMR data shown above, the value of having sufficient data to recognize and eliminate known compounds from further consideration can be illustrated. In addition to the four known compounds identified (Table 4.1), the MS and NMR data for one peak, indicated as an unknown compound in Figure 4.7, had some similarities to the known ambiguines, as seen from the NMR and MS/MS spectra in Figure 4.8 but was not found in the literature or natural product databases. It was therefore prioritized for further study. A scaled-up growth (3 L, 32 days) yielded 0.85 mg of this product for rigorous *de novo* structure determination, including x-ray crystallography and conventional NMR on a 900 MHz cryoprobe, to establish the novel ambiguine K isonitrile (seen in Figure 4.1 and manuscript in preparation). A related compound, ambiguine L isonitrile, was also found in the scaled-up growth. This successful example illustrates how the microanalytical capabilities of the LC-MS-NMR system can prioritize

samples for scale-up, avoiding the four known compounds and streamlining the natural products drug discovery effort.

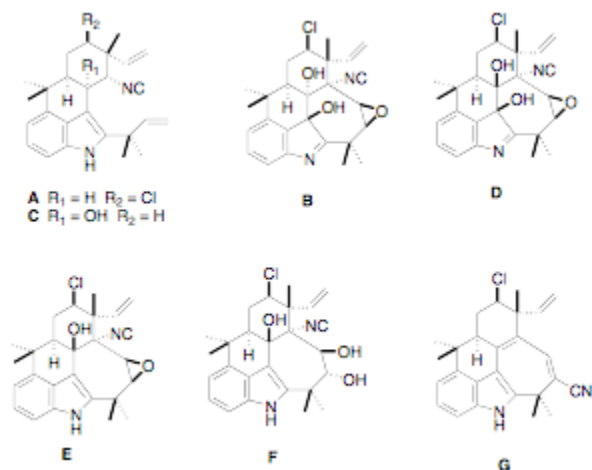


**Table 1** Table of Ambiguine compounds. A, and E were characterized in the cyanobacteria extract.

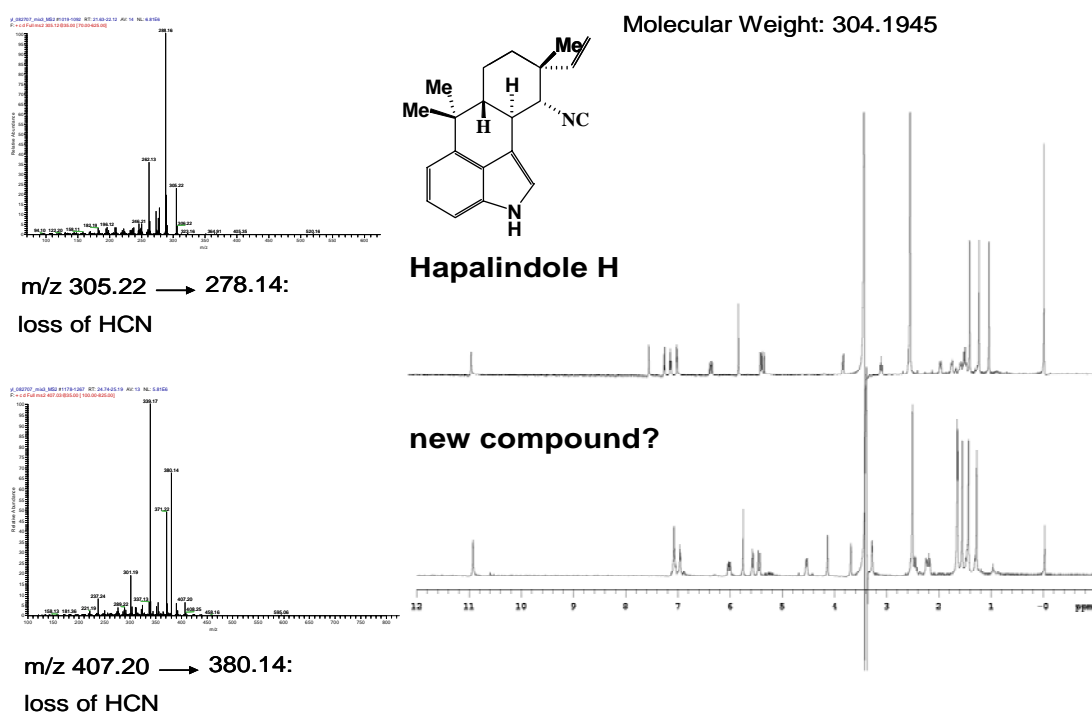


**Figure 4.8 (Top)** MS and NMR spectra of the 18.3 minute LC peak of Figure 4.7, identified from the literature as Hapalindole H. **(Bottom)** MS and NMR spectra of the 17.3 minute LC peak of Figure 4.7 (titled unknown compound) not found in the literature or natural product databases. It was therefore prioritized for detailed structure studies by scale-up purification.

The internal standard spiked into the extract confirms the limit of detection in complex matrices. The 2-hour  $^1\text{H}$  NMR acquisition of the collected taxol (0.35 nmol) shows a clear 1-to-1 correspondence of peaks with a reference spectrum, as shown in Figure 4.9. Some minor peaks attributed to its known degradation in methanol can be seen. From this result, it can be reasonably assumed that any fraction which cannot generate an interpretable  $^1\text{H}$  NMR spectrum in 2 hours using this system contains significantly less than 0.35 nmol of a pure compound. These data suggest that by loading only 30  $\mu\text{g}$  onto the column, the system can report components down to 1% of the total column loading. Alternatively, for 4 mm packed columns loaded at their 200  $\mu\text{g}$  capacity this number goes down to 0.2%, to below 0.01% for 4 mm monolithic columns with capacities of up to 3 mg or more.

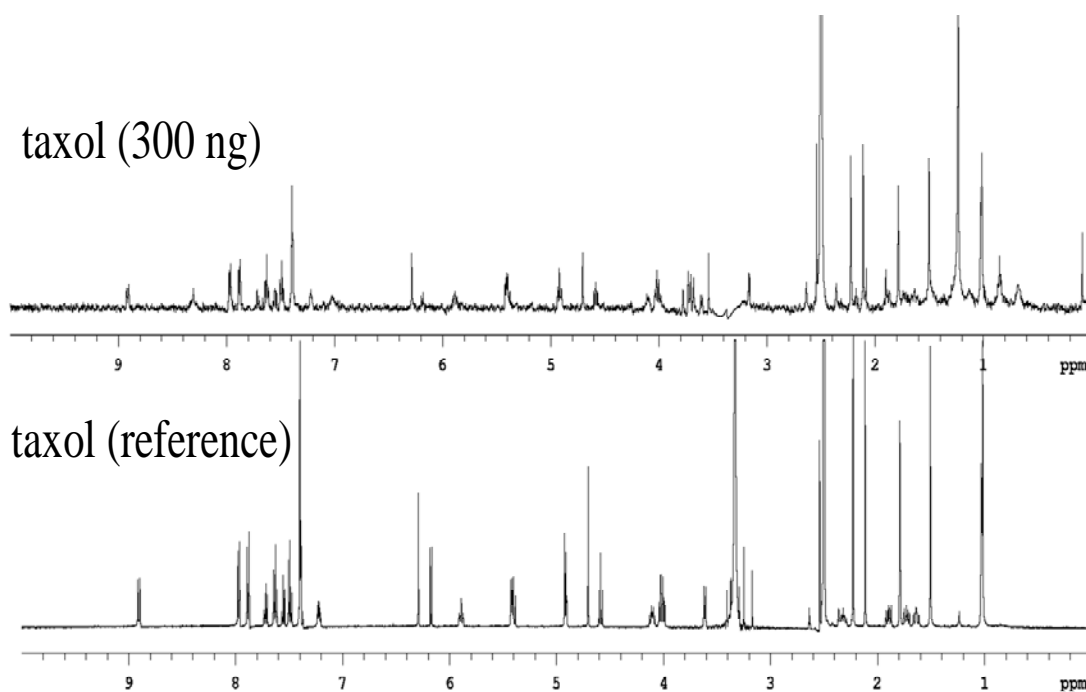


**Figure 4.9** Top: 1 hr NMR spectrum of LC fraction recovering 300 ng of taxol spiked into cyanobacterial extract shown in Figure 4.7 (5.9 minute peak). (Water, 3.3 ppm, suppressed by presaturation and solvent subtraction.) Bottom: the reference <sup>1</sup>H NMR spectrum, of 700  $\mu$ L of 1 mg/ml taxol in DMSO-d<sub>6</sub> acquired using an inverse probe, 16 total transients.

Significantly lower limits of detection can be obtained by pooling LC runs. Noting that the LC separation time of about 1 hour is considerably less than the NMR analysis time (e.g. 1 hr/fraction for multiple fractions), it is practical and time-efficient to perform multiple LC separations, pooling the fraction of interest. Off-line LC-NMR lends itself to this approach, which has been described in LC-SPE-NMR<sup>37, 38</sup>. Tripling the amount of material subsequently triples the S/N, or reduces the time required to obtain comparable S/N values by nearly 10-fold. If a specific peak is of interest, column loadings may be frequently increased significantly without broadening or contaminating the peaks of interest. From just two injections of the active cyanobacterial extract (total 80  $\mu$ g), the

S/N of similar NMR spectra for all fractions previously collected were doubled (data not shown).

#### 4.8 Conclusions

An LC-MS-NMR platform has been demonstrated, using an approach which accommodates the large disparities in the sample mass and time requirements of MS and NMR. The nanoSplitter LC-MS method can collect an analyte for NMR, while improving MS sensitivity and maintaining chromatographic resolution. An offline approach to NMR permits all of the analyte available in each LC peak to be concentrated into the most sensitive NMR probe readily available, and to allocate NMR analysis time intelligently among the most relevant LC peaks. The collection of LC fractions into 96-well plates is readily available in many laboratories, inexpensive enough to use routinely, and enables LC-NMR to be obtained retrospectively. Microdroplet NMR samples can be recovered for re-analysis, archival, or bioassay.

The combined MS and NMR system performed well in routine performance tests of recovery and reproducibility. Any validated LC method used with the microplate automation can be expected to perform equally as well. When applied to natural products, this new microanalytical platform could record LC-MS and NMR data during the discovery phase of bioactivity-guided fractionation. The recorded data was sufficient for dereplication where four LC peaks were recognized as known compounds, focusing time and effort on a drug-like compound not found in databases or literature. This capability streamlines the process of natural product discovery, and has the potential to



reinvigorate the field by making feasible sources that were too limited or slow-growing for traditional discovery methods.

Beyond natural products, this LC-MS-NMR platform promises to be similarly applicable in a variety of fields which rely on identification of trace components of complex mixtures, ranging from environmental remediation to metabolite identification in metabolomics as well as pharmaceutical DMPK, toxicology and ADME studies.

## 4.9 References

- (1) Silva Elipe, M. V. *Analytica Chimica Acta* **2003**, *497*, 1-25.
- (2) Murakami, T.; Fukutsu, N.; Kondo, J.; Kawasaki, T.; Kusu, F. *Journal of Chromatography, A* **2008**, *1181*, 67-76.
- (3) Norwood, D. L.; Mullis, J. O.; Feinberg, T. N. *Separation Science and Technology (San Diego, CA, United States)* **2007**, *8*, 189-235.
- (4) Weber, B.; Hartmann, B.; Stoeckigt, D.; Schreiber, K.; Roloff, M.; Bertram, H.-J.; Schmidt, C. O. *Journal of Agricultural and Food Chemistry* **2006**, *54*, 274-278.
- (5) Bobzin, S. C.; Yang, S.; Kasten, T. P. *J Chromatogr B Biomed Sci Appl* **2000**, *748*, 259-267.
- (6) Olson, D. L.; Norcross, J. A.; O'Neil-Johnson, M.; Molitor, P. F.; Detlefsen, D. J.; Wilson, A. G.; Peck, T. L. *Anal Chem* **2004**, *76*, 2966-2974.
- (7) Schroeder, F. C.; Gronquist, M. *Angew Chem Int Ed Engl* **2006**, *45*, 7122-7131.
- (8) Hoult, D. I.; Richards, R. E. *J.Magn.Reson.* **1976**, *24*, 71-85.
- (9) Jansma, A.; Chuan, T.; Albrecht, R. W.; Olson, D. L.; Peck, T. L.; Geierstanger, B. H. *Anal Chem* **2005**, *77*, 6509-6515.
- (10) Jayawickrama, D. A.; Sweedler, J. V. *J Chromatogr A* **2003**, *1000*, 819-840.
- (11) Brey, W. W.; Edison, A. S.; Nast, R. E.; Rocca, J. R.; Saha, S.; Withers, R. S. *Journal of Magnetic Resonance* **2006**, *179*, 290-293.
- (12) Keifer, P. A. *Annual Reports on NMR Spectroscopy* **2007**, *62*, 1-47.
- (13) Keifer, P. A. *Curr Opin Chem Biol* **2003**, *7*, 388-394.
- (14) Keifer, P. A. *Progress in Drug Research* **2000**, *55*, 137-211.
- (15) Kautz, R. A.; Goetzinger, W. K.; Karger, B. L. *J Comb Chem* **2005**, *7*, 14-20.
- (16) Lacey, M. E.; Sweedler, J. V.; Larive, C. K.; Pipe, A. J.; Farrant, R. D. *Journal of Magnetic Resonance* **2001**, *153*, 215-222.
- (17) Teh, S.-Y.; Lin, R.; Hung, L.-H.; Lee, A. P. *Lab on a Chip* **2008**, *8*, 198-220.
- (18) Nord, L. K., *B Anal . Chim. Acta* **1984**, 233-249.

- (19) Patton, C. J. W., A. P. *Analytical Instrumentation Handbook* **1997**, 153-155.
- (20) Curcio, M.; Roeraade, J. *Anal Chem* **2003**, *75*, 1-7.
- (21) Wilm, M.; Mann, M. *Anal Chem* **1996**, *68*, 1-8.
- (22) Gangl, E. T.; Annan, M. M.; Spooner, N.; Vouros, P. *Anal Chem* **2001**, *73*, 5635-5644.
- (23) Schiavo, S.; Ebbel, E.; Sharma, S.; Matson, W.; Kristal, B. S.; Hersch, S.; Vouros, P. *Anal Chem* **2008**, *80*, 5912-5923.
- (24) Andrews, C. L.; Yu, C. P.; Yang, E.; Vouros, P. *J Chromatogr A* **2004**, *1053*, 151-159.
- (25) Schiavo, S.; Ebbel, E.; Sharma, S.; Matson, W.; Kristal, B. S.; Hersch, S.; Vouros, P. *Anal Chem* **2008**, Accepted.
- (26) Shao, G.; Kaut, R.; Peng, S.; Cui, G.; Giese, R. W. *Journal of Chromatography, A* **2007**, *1138*, 305-308.
- (27) Newman, D.; Cragg, G.; Snader, K. *J Nat Prod* **2003**, *7*, 1022-1037.
- (28) Newman, D. J.; Cragg, G. M. *J Nat Prod* **2007**, *70*, 461-477.
- (29) Cordell, G. A.; Shin, Y. G. *Pure Appl. Chem.* **1999**, *71*, 1089-1094.
- (30) Clardy, J.; Walsh, C. *Nature* **2004**, *432*, 829-837.
- (31) Raveh, A.; Carmeli, S. *J Nat Prod* **2007**, *70*, 196-201.
- (32) Smitka, T. A. B., R.; Doolin, L.; Jones, N.D.; Deeter, J.B.; Yoshida, W.Y.; Prinsep, M.R.; Moore, R. E.; Patterson, G. M. L. *J.Org.Chem.* **1992**, *57*, 857-861.
- (33) Klein, D. D., D.; Braekman, J.C.; Hoffmann, L.; Demoulin, V. *Journal of Natural Products* **1995**, *58*, 1781-1785.
- (34) Moore, R. E. C., C.; Patterson, G.M.L. *J.Am.Chem.Soc.* **1984**, *106*, 6456-6457.
- (35) Park, A. M., R.E.; Patterson, G.M.L. *Tetrahedron Lett.* **1992**, *33*, 3257-3260.
- (36) Stratmann, K. M., R.E.; Bonjouklian, R.; Deeter, J.B.; Patterson, G.M.L.; Shaffer, S.; Smith, C.D.; Smitka, T. A. *J.Am.Chem.Soc.* **1994**, *116*, 9935-9942.
- (37) Xu, F.; Alexander, A. J. *Magnetic Resonance in Chemistry* **2005**, *43*, 776-782.

- (38) Exarchou, V.; Krucker, M.; van Beek, T. A.; Vervoort, J.; Gerothanassis, I. P.; Albert, K. *Magnetic Resonance in Chemistry* **2005**, *43*, 681-687.

Chapter 5:

Identification of Minor DNA Adduct Isomers using a Microscale LC-MS-NMR

Platform

## 5.1 Introduction to DNA Adducts and Metabolism

Exposure to toxic agents, through both endogenous and exogenous means, occurs daily to all living organisms. The electrophilic metabolites of these agents can bind covalently to DNA, forming DNA adducts<sup>1</sup>, which are of particular importance. While some are substrates for repair enzymes and polymerases, having little to no adverse effect on the organism, in contrast others block these repair agents, triggering biological responses such as cell death and mutation<sup>1,2</sup>. Over the last 30 years, the relationship between DNA adduct formation and biological endpoints such as apoptosis, mutagenesis and cancer has been studied<sup>3-5</sup>. It has been found that exposure to DNA-damaging agents both causes cells to increase the transcription of DNA repair genes<sup>6</sup> and also produces DNA adducts, which have emerged as biomarkers of disease or overexposure<sup>7,8</sup>.

The metabolism of exogenous genotoxins, many in the broad carcinogen classes of aromatic amines (AAs) and heterocyclic aromatic amines (HAAs), is generally activated through cytochrome P450-mediated *N*-hydroxylation in extrahepatic tissues<sup>9-13</sup>. Unless excreted, these activated *N*-hydroxy intermediates may then undergo a Phase II conjugation in which enzymes such as *O*-acetyltransferases catalyze the formation of highly reactive electrophiles such as *N*-acetoxy-arylamines<sup>14</sup>. These compounds then undergo a heterolytic cleavage to produce a reactive nitrenium ion/acetate anion pair, which can readily react with proteins or DNA in the body<sup>15</sup>. This scheme is illustrated in Figure 5.1 for the HAA 2-Amino-1-methyl-6-phenylimidazo[4,5-*b*]pyridine (PhIP).

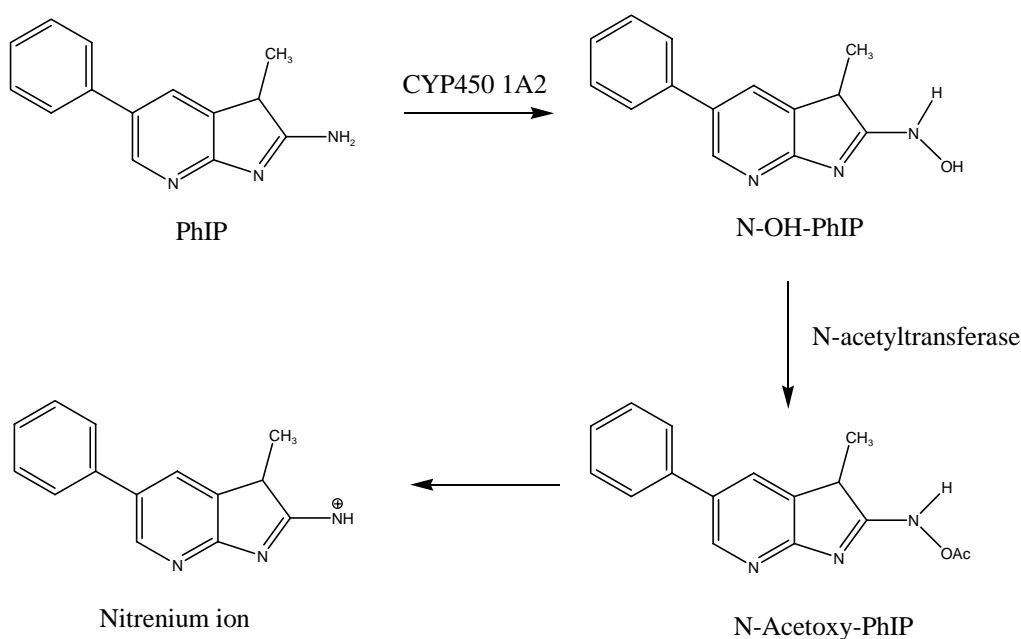


**Figure 5.1** Metabolism of PhIP, showing the conversion of its exocyclic amino group to its N-OH derivative with subsequent acetylation and ultimate nitrenium ion formation. (Reproduced with permission from the thesis of Dr. Jim Glick)

Nitrenium ion formation is a determining step in the formation of DNA adducts, especially when establishing the carcinogen adduction regiochemistry. Arylnitrenium ions can delocalize their positive charge to be reactive at any of several stable sites of addition, as illustrated for the aromatic amine carcinogen 2-aminonaphthalene in Figure 5.2. These positions are located at the nitrenium ion center as well as the ortho and para ring carbon, ultimately yielding different isomeric DNA adducts.

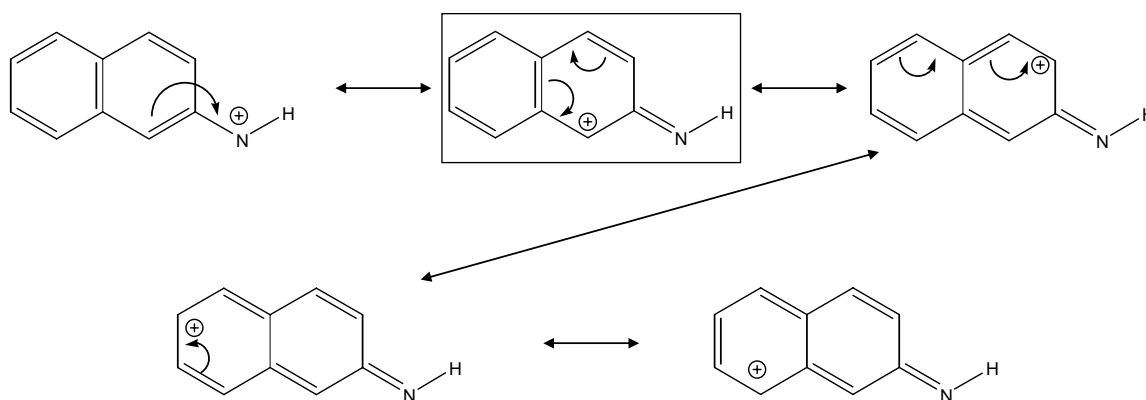


**Figure 5.2 Shows the 2-Aminonaphthalene nitrenium ion and subsequent isomers from charge delocalization. The box indicates the resonance structure predicted by AM1 calculations to be electronically stable.**

Additionally, DNA has numerous sites where these ions can attack, on the bases deoxyguanosine (dG), deoxyadenosine (dA) and deoxycytosine (dC); dG alone contains 4 possible positions of adduction. Some insights into the adduction process have been gained by using computational methods to predict the relative stability or reactivity of different adduction pathways and compare it to observed structures and product ratios. AM1 calculations, which are semiempirical methods used in computational chemistry to establish the best molecular electronic structure<sup>16</sup>, can be used to predict the most stable adduct, and in cases where the experimental data is available, correlate this calculation to the found values and structures<sup>17</sup>. Ford and Thompson applied this model to several AA compounds, including 2-aminonaphthalene. They went on to positively correlate this predicted resonance structure, with a box around it in Figure 5.2, to experimental research by Kadlubar and colleagues<sup>18</sup>. Thus, in order to better understand these important processes of DNA adduct formation and carcinogenesis, this example shows how it is necessary to synthesize and characterize all possible adducts not only to understand the



biological pathway *via* which they are formed but also to weight each isomer's potential biochemical risk.

## 5.2 DNA Adduct Synthesis *in vitro* and Isomer Persistence

To produce DNA-adducts, synthetic pathways have been established which mimic the biological process. For example, the *N*-hydroxy derivatives of common exogenous toxins, such as the AAs aminobiphenyl (ABP) and aminonaphthalene (AN), can be prepared by reduction of each compound's nitro species<sup>19</sup>. The *N*-acetoxy derivative can then be derived by reaction with acetic anhydride<sup>15</sup> or pyruvonnitrile<sup>20</sup>, and subsequently be allowed to form adducts by incubation with either polymeric DNA or individual deoxynucleosides. It has been shown that through this synthetic route, multiple isomeric DNA adducts are formed<sup>15, 21, 22</sup>. In most cases, the predominant isomer is the *N*-(deoxyguanosin-8-yl)-product (adduction of the nitrenium ion at the C-8 position of the deoxyguanosine (dG) ring) with minor isomers adducting at the N-2 position of dG. For deoxyadenosine (dA) both the C-8 and N-6 isomers have been characterized<sup>21, 23</sup>. For either nucleoside, the predominant isomer is generally 5-10 times more abundant than the others<sup>21, 24</sup>.

These synthetic routes give the range of isomers produced from each exogenous carcinogen metabolized; however, the correlation between each specific isomer produced and subsequent biological damage needs to be investigated. There are indications that some minor nucleoside adducts may have a more significant biological impact than their

more abundant isomers<sup>2, 25-27</sup>. For example, the high-abundance C-8 isomers have been found to be only moderately mutagenic<sup>28-30</sup>, which has led researchers to believe the N-2 adduct to be more biologically important. In one study, a cynomolgus monkey was administered the food carcinogen 2-amino-3-methylimidazo[4,5-f]quinoline (IQ) for a period of 3.6 years at a dose of 20 mg/kg of body weight 5 days per week for a cumulative dose of 37.5 g of IQ at the time of sacrifice. The pancreas tissue was assayed for the dG adduct of IQ, and both the N-2 and C-8 adducts were detected, with the N-2 four fold higher than the C-8<sup>31, 32</sup>. This isomer ratio is not in correlation with the authors' synthetic determination of the dG-IQ adduct, where the C-8 isomer was in a much greater abundance than the N-2, implying the C-8 was repaired *in vivo*. Further evidence of this was found with an acute single *in vivo* dose of IQ as opposed to the chronic dose study just described. When the monkey pancreas was examined after a single dose of IQ, the dG-C8-IQ adduct was predominate. This interpretation suggests that enzymes are repairing the adducted DNA during the longer course of carcinogen dosing.

Further in an extensive review covering the biological impact of small molecule-DNA adducts<sup>2</sup>, Sturla postulates that if a high-abundance adduct is a preferred substrate for an efficient repair enzyme, then the minor adducts may persist and consequently be more mutagenic. In view of this, it has become more and more necessary to not only quantify high abundance adducts but also consider the lower abundance isomers when assessing disease state and exposure levels.

This difference underscores the important need to be able to identify the lower abundance adducts when assessing *in vivo* biological carcinogen mutagenicity as well as evaluating the persistence of metabolically-activated isomer compounds. Identification at trace levels *in vivo* requires thorough characterization of the larger amounts of minor products which are available synthetically.

### 5.3 Low Abundance Isomer Characterization

This assessment of low abundance, minor adducts requires authentic standards for all adduct isomers but preparation of minor products is cumbersome. The synthetic method described previously, when applied to HAAs, produces < 10 % yield of the activated HAA intermediate<sup>24</sup>. Also, the final product pool has 8-10 times more C-8 adduct than the N-2 adduct isomers<sup>15</sup>. Common analytical techniques for characterizing DNA adduct standards require large amounts of material, such as microgram to milligram amounts for NMR, or, as in the case of mass spectrometry, destroy the product in the process of characterization. Consequently, it has then been necessary to implement a larger scale synthesis, which can be cumbersome or perform multiple normal-scale syntheses, pooling the reaction products to have enough material for characterization of minor products<sup>21</sup>. Groups have also tried to specifically synthesize the lower abundance adducts by altering the starting materials to force primarily N-2 adduction<sup>25</sup>, however, this also adds more time and synthesis steps in order to accurately represent the *in vivo* pathway of DNA adduction. It is therefore valuable; because authentic standards of low abundance adduct isomers are only going to be available in very low microgram to upper nanogram

levels, to have an analytical method that can characterize nanogram levels of analyte nondestructively, preserving most of the reaction product for post-characterization use.

Recently, our laboratory's efforts have developed an LC-MS-microcoilNMR platform, including fraction collection, for streamlined natural products identification and characterization<sup>33</sup>. As described in Chapter 4, this system combines normal-bore HPLC with nanoelectrospray mass spectrometry in such a way that >90% of the HPLC eluent is directed to a fraction collector, consuming 10% or less for MS and MS/MS characterization. The MS-directed flow is then split again from <100  $\mu\text{L}/\text{min}$  to  $\sim 300$  nL/min using a concentric splitting device, dubbed the nanoSplitter<sup>34, 35</sup>. The nanoSplitter has been shown previously to maintain chromatographic integrity of the separation between the two detectors which is quite significant when using an aggressive split, such as a ratio of 1:1000<sup>36, 37</sup>. This configuration allows precious samples to be analyzed and collected without fear of using up the material merely for MS characterization.

The analysis of complex samples such as crude reaction mixtures can be challenging and generally requires multiple separation steps, such as HPLC or prep-TLC isolation, all directed toward isolating and characterizing a single product of interest. Sample losses can be incurred at each fractionation step, as well as when these purified fractions are subsequently prepared for MS or NMR characterization. The system described herein attempts to streamline this process into a parallel, hyphenated technique, where the HPLC isolation and nanoelectrospray-MS identification are performed simultaneously with

fractionation for microcoil NMR. The NMR, because of its higher sample mass and time requirements is then performed offline, with all of the available sample concentrated into the most sensitive NMR detection available, ultimately providing NMR sensitivity comparable to MS. Overall, the platform was developed to exploit the most sensitive techniques of nanoSplitter nESI-MS<sup>34, 38, 39</sup> and microNMR<sup>40, 41</sup> under the optimal conditions for each. As applied to the characterization of DNA adducts, the platform can more readily characterize the low abundance isomers as well as preserve more for additional analyses.

#### 5.4 Project Goals

In this chapter we describe the synthesis, isolation and analytical characterization of two AA DNA-adducts by both MS and NMR. The two adducts are N-(deoxyguanosin-8-yl)-aminobiphenyl (dG-ABP) and N-(deoxyguanosin-8-yl)-aminobiphenyl-*d*<sub>9</sub> (dG-ABP-*d*<sub>9</sub>), as well as the identification of various isomers associated with both AA DNA-adduct compounds. This characterization was achieved using the LC-MS-NMR platform described in Chapter 4 of this dissertation, except using manual microdroplet injections of single samples into the microcoil NMR, instead of the automated sample handler. This single sample approach allowed faster set-up and injection into the NMR, interactive analysis, more efficient recovery of the analytes for post-NMR use, as well as provided more efficient sample injections for these trace analysis compounds. Both the LC-MS fraction collection and manual injection microdroplet NMR analyses will be discussed in terms of sample recovery and injection efficiency, using a dG standard, prior to adduct analysis. Each adduct was analyzed using LC-MS-microcoilNMR and subsequently

recovered for future use in *in vitro* and *in vivo* studies for correlating DNA adduct isomer persistence to biological endpoints such as apoptosis, gene transcription, mutagenesis and cancer.

## 5.5 Materials and Methods

The work in this chapter was done in collaboration with the following colleagues; Dr. Wennan Xiong, a post-doctoral fellow in the Vouros laboratory from spring 2003 until January 2008; Rose Gathungu, a current graduate student in the Vouros laboratory, and Dr. Roger Kautz from the Barnett Institute at Northeastern University.

### Chemicals

**Caution:** *4-Aminobiphenyl and its derivatives are carcinogenic to humans and should be handled carefully.* Deuterated solvents were obtained from Cambridge Isotope Laboratories (Andover, MA). HPLC-grade acetonitrile (99.9%) and water were purchased from Fisher Scientific (Pittsburgh, PA). Fluorocarbon FC-43 was from 3M Corp (St. Paul, MN). Pd/C catalyst, hydrazine, pyruvonnitrile, tiethylamine, diethyl ether, tetrahydrofuran (THF), 1-butanol, and 4-nitrobiphenyl were all purchased from Sigma-Aldrich (St. Louis, MO). 4-Nitrobiphenyl-*d*<sub>9</sub> (98%+) was obtained from Cambridge Isotope Laboratories (Andover, MA).

## **Materials**

Teflon capillaries and tubing were obtained from Cole-Parmer (Vernon Hills, IL). PEEK capillaries, unions, in-line filters, and adapters were from Upchurch (Oak Harbor, WA). The 96-well low retention PCR plates, used for fraction collection, were obtained from Nunc (part #: 240600, Rochester, NY).

## **HPLC and Fraction Collection System**

Chromatographic separations and fraction collection were performed on an HPLC system consisting of a binary pump, an autosampler, a UV-VIS diode-array detector (Agilent 1100 series), a fraction collector (Agilent 1200 series) controlled by Agilent ChemStation (version B.02.01) software. The HPLC column used was a 4.6 x 150 mm HPLC column (Agilent Zorbax C-18SB 3.5  $\mu\text{m}$ ). A restriction valve was used to split the flow from the LC column with ~90% of the flow to the UV-VIS diode-array detector and eventually to the fraction collector, and the other ~10% of the flow to the nanoSplitter. The delay volume between the UV detector and the fraction collector was determined to be 71  $\mu\text{L}$ . The chromatographic methods are described below.

## **The nanoSplitter Interface and Mass Spectrometer**

The nanoSplitter consists of a splitter (FSMUAS1.5, Valco Instruments Co. Inc, Houston, TX), a micro flow-thru connector (Valco Instruments Co. Inc, Houston, TX), a needle valve (86041, Alltech, Deerfield, IL) and a XYZ positioner (FP-2 Newport, Irvine, CA). These components are fastened to a rail-and-mount system (9742 (M), New Focus, Inc., Sunnyvale, CA). The fused silica emitter tips, obtained from New Objective

(Woburn, MA), had an inner diameter of 20  $\mu\text{m}$  with a tip (distal coated) of 10  $\mu\text{m}$  inner diameter. The high-voltage connection was made by attaching a clip to the emitter. The split ratio was adjusted using the needle valve to obtain optimal flow rate and electrospray performance. The flow into the MS was  $\sim 300$  nL/min, it was measured by collecting flow out of the picotip emitter, using a scored glass capillary, with the electrospray voltage off. More details regarding the design and construction of the nanoSplitter can be found in the previous publications<sup>34,35</sup>.

Both MS and MS/MS spectra were acquired on a Finnigan LCQ classic quadrupole ion trap (San Jose, CA) controlled by Xcalibur software (version 1.3).

### **Microcoil NMR**

The microcoil probe used in this study was an ICG (Inverse Carbon with Gradients) capLC microflow probe manufactured by Magnetic Resonance Microsensors (MRM, Savoy, IL) and distributed by its parent company, Protasis Corp. This probe has an observed volume ( $V_{\text{obs}}$ ) of 1.5  $\mu\text{L}$  (as determined by SFA of small plugs), in a fill volume of 6  $\mu\text{L}$ , through 75  $\mu\text{m}$  i.d. silica inlet and outlet capillaries. The probe was internally coated with fluoro-octyl silane for use with microdroplet NMR.

NMR spectra were acquired on a Varian (Palo Alto, CA) Inova spectrometer with an 11.7-T (500 MHz) actively shielded magnet; the data were processed and analyzed with VNMR version 6.1C software.



### Adduct Synthesis and HPLC Isolation

The DNA adduct standards were synthesized by converting the nitro compound, 4-nitrobiphenyl, to its *N*-acetoxy derivative as follows. 1 mmol of the nitro compound was dissolved in THF (5 mL) containing Pd/C catalyst (50 mg) and reduced to its *N*-hydroxyamine derivative by adding hydrazine (6.4 mmol) while maintaining the temperature of the reaction at 0°C for 20 min with gentle stirring<sup>19</sup>. The solution was filtered to remove the Pd/C catalyst and the solvent was removed by vacuum. The dried reaction mixture was dissolved in 5mL of anhydrous THF before adding triethylamine (1.1 molar equiv) and allowing the reaction mixture to cool to -30 °C. The *N*-hydroxy intermediate was subsequently converted to its *O*-acetyl derivative by adding pyruvonnitrile (1.5 mmol) to the reaction mixture and allowing the reaction to proceed for 1 hour while maintaining the temperature at -30 °C. The *N*-acetoxyamine product was reacted with 2'-deoxyguanosine (2'-dG) in a 10 molar excess of nucleoside dissolved in water to produce the adduct standard. The mixture was held at 0 °C for 2 hours before warming to room temperature where it then remained for 24 hours. The solvent was then removed under vacuum and the residue re-suspended in water. The product mixture was extracted 4 times with water saturated diethyl ether, discarding the ether layer each time. The aqueous phase was extracted further with 1-butanol 4 times, retaining and pooling the butanol from each extraction. The 1-butanol solvent was then removed under vacuum to yield the reaction product mixture.

The deuterated internal standard, deoxyguanosine-4-aminobiphenyl-d<sub>9</sub> (dG- ABP-d<sub>9</sub>), was prepared using 4-nitrobiphenyl-d<sub>9</sub> in the same manner, except on a smaller scale due to the limited availability of 4-nitrobiphenyl-d<sub>9</sub>.

After reconstitution in 70:30 methanol/water (v/v), purification and isolation of standards were performed by reverse phase HPLC with UV and MS detection. The HPLC was operated at a flow rate of 1mL/min with a 20 min linear gradient from 5-100% acetonitrile containing 0.1% formic acid (Mobile phase B). Mobile phase A consisted of water with 0.1% formic acid. The eluents were monitored by DAD-UV at 260nm and simultaneous MS detection. The MS was operated under a two segment method consisting of full scan positive ion detection mode with additional data dependent fragmentation of ions with intensity greater than  $4 \times 10^6$  abundance. Retention times between UV and MS peaks correlated within 0.1 minutes of each other, assuring that each of the UV peaks collected contained a unique DNA-adduct standard, as indicated by the MS and MS/MS spectra obtained.

The fraction collector was operated in time-dependent fraction collection mode, at 5 fractions/min. After review of MS data, fractions containing the sought after  $m/z$  value or MS/MS transition were collected, in relation to its UV retention time. The maximum fill volume was set to 200  $\mu$ L per well, and wells containing the same fractions of interest were pooled when necessary.

The entire separation of the reaction mixture for each adduct standard was collected in fractions; fractions of each adduct isomer were pooled by its unique UV retention time. Pools were then dried under vacuum in 200  $\mu\text{L}$  microcentrifuge tubes, adding 15  $\mu\text{L}$  of  $d_6$ -DMSO to facilitate sample concentration in the bottom of the vial. Samples were then reconstituted in 4  $\mu\text{L}$  of  $d_6$ -DMSO before manual injection, microdroplet microcoil-NMR analysis.

### **Manual Injection Microdroplet-NMR (Zero Dispersion Segmented Flow Analysis)**

Reconstituted DNA-adduct samples were loaded into a 25  $\mu\text{L}$  Hamilton syringe fitted with 10 cm of 200  $\mu\text{m}$  i.d. Teflon tubing terminated with a 4 cm 75  $\mu\text{m}$  capillary stub on the free end. The immiscible microdroplet carrier fluid, FC43, filled the syringe, to the 15 $\mu\text{L}$  mark. 3  $\mu\text{L}$  of the sample was drawn into the syringe through the capillary stub, followed by 2  $\mu\text{L}$  of FC43 and finally 3  $\mu\text{L}$  of  $d_6$ -DMSO. Working under a stereomicroscope, to confirm no air bubbles were drawn between. This sample sequence injects the DMSO wash plug through the NMR probe before the sample, facilitating positioning. The syringe is then placed into a syringe pump and the capillary stub on the end is connected into the inlet capillary of the  $\mu\text{coil}$  probe. The pump is activated to 2.5  $\mu\text{L}/\text{min}$  and the flow volume is monitored via  $\sim 60$  cm of 30 ga Teflon tubing attached to the outlet of the probe with a 1  $\mu\text{L}$  sample plug of dye in it (1 cm = 1  $\mu\text{L}$ ). This outlet line accurately monitors (to 0.1  $\mu\text{L}$ ) the amount of liquid entering and leaving the probe to aid in centering the injected sample, together with the deuterated solvent lock signal of the NMR spectrometer. The syringe pump is turned off when the sample is positioned in

the probe. Because the volume from the tip of the syringe stub to the NMR observed volume of the probe is known (6  $\mu\text{L}$ ), the sample can be positioned in the center of the probe by either injection time, outlet mark on the Teflon tubing, or lock signal maximum as the sample passes through the observed volume (1.5  $\mu\text{L}$ ). The maximum lock level is generally the most sensitive means to assure the sample plug is positioned correctly. Because the sample can be pushed forward and back through the flow cell without dilution, the plug could be repositioned if necessary. Once positioned, NMR spectra were acquired at ambient temperature with at least 100 to 8000 transients, depending on the concentration of the sample and observed signal. NMR spectra were acquired with a 8000-Hz scan width,  $60^\circ$  tip angle, fixed gain (max = 60), and, when necessary, a 1 sec water presaturation after the 2-s acquisition time.

### **Sample Recovery and LC-MS analysis**

Samples were recovered from the microcoil NMR probe by removing the syringe from the inlet capillary and directing the inlet into a 200  $\mu\text{L}$  microcentrifuge tube. The probe was then back-flushed with the inlet-to-outlet dead volume of FC43 and all material was collected out of the inlet. The DMSO plug injected before the sample washes the flow cell and inlet capillary. It is possible to dry samples down in the presence of FC43; however, because it is immiscible in the DMSO sample solvent, samples were extracted off of the FC and then dried down. Samples were then reconstituted to 100  $\mu\text{L}$  in 70:30 water/methanol (v/v), and the recovered material was re-injected into the LC-MS system, operated in the same manner as described previously.

The fraction collector was set to time-dependent fraction collection over a five minute time frame flanking the elution time of the DNA-adduct during the initial sample isolation/ with a maximum fraction volume of 200  $\mu$ L. Again, all like fractions were pooled together.

## 5.6 Results and Discussion

The microscale LC-MS-NMR system used here and described in detail in Chapter 4 of this thesis was optimized for automated microdroplet NMR analyses. In that set-up, samples were directed into and out of the NMR as a queue of plugs in Teflon tubing; plugs could be saved (inside the outlet tubing) for future use. For the characterization studies of the isomeric DNA adducts, we chose manual microdroplet NMR over the automated system because it was faster, gave more flexibility for which sample was repeated in available instrument time periods with interactive NMR data acquisition, and facilitated the recollection of samples post-NMR. Additionally, with the manual loading into the NMR, we were able to more clearly monitor the sample plugs moving through the probe to assure accurate positioning (the best line shape) with smaller volume samples, ultimately yielding the sharpest spectra from trace level NMR analyte characterization.

### Evaluation of LC-MS-NMR System

In order to evaluate this system of sample loading and overall LC-MS-NMR recovery, we performed a series of experiments using dG as a standard. The results of each experiment

and statistics are presented in Tables 5.1 and 5.2. Initially, we decided to establish the efficiency of the LC fraction collection, by injecting 5  $\mu\text{g}$  of dG on column through only the LC-UV system with the pump operated at 1 mL/min and the entire effluent directed to the UV detector and the fraction collector. The dG peak was collected using time-dependent fractionation, and subsequently evaporated down to 100  $\mu\text{L}$  or less which was re-injected to determine recovery based on peak area comparisons. As shown in Table 5.1, we were able to recover 95% of the injected dG sample through the LC system alone.

The complete LC-MS fraction collection system was then evaluated by splitting the injected 5 $\mu\text{g}$  dG sample, post column, 90:10 between the UV and MS detectors respectively. Time-dependent UV fractionation was similarly used to collect the dG peak which was pooled, evaporated, and then re-injected into the LC system as previously, directing the entire flow to the UV for recovery analysis. When utilizing both detectors, 87% of the injected dG was recovered, establishing with confidence that the majority of any injected sample, precious or not, will be collected and preserved for post LC-MS characterization.

Finally, the complete LC-MS-NMR system was evaluated in its entirety, as follows. After 5 $\mu\text{g}$  of dG was separated, analyzed by LC-MS and fraction collected, it was then prepared for microcoil NMR analysis by evaporating off the LC-MS analysis buffers and re-dissolving the sample in 4  $\mu\text{L}$  of DMSO-*d*<sub>6</sub>. After NMR analysis and recovery, the DMSO was evaporated and the samples were reconstituted into 100  $\mu\text{L}$  of HPLC grade water before being injected back onto the LC system, where the entire flow was directed to UV to compare peak areas.

LC Fraction Collection					LC-MS Fraction Collection			
Sample	Retention Time	Area			Sample	Retention Time	Area	
dG 1	3.93	6108.8			dG 1	4.1	6250	
	3.96	5775.4				3.96	5393.2	
	<b>% recovery</b>	94.54		<b>LC Only</b>		<b>% recovery</b>	86.29	<b>LC-MS</b>
dG 2	3.94	6069.9	<b>average</b>	95.51	dG 2	3.97	6235.8	<b>average</b>
	3.83	6153.4	<b>st. dev</b>	5.45		3.94	5459.5	<b>st. dev</b>
			<b>%CV</b>	5.70				<b>%CV</b>
	<b>% recovery</b>	101.38				<b>% recovery</b>	87.55	
dG 3	3.95	6076.3			dG 3	3.97	6231.3	
	3.95	5505.8				3.93	5550.4	
	<b>% recovery</b>	90.61				<b>% recovery</b>	89.07	

**Table 5.1** Statistical data from the LC and LC-MS fraction collection recovery experiments.

The experiments conducted showed the LC fraction collection procedure, utilized here, to yield 95% recovery, with a %CV of less than 6%. It should be possible to optimize this number in the future by more efficient washing of the fraction collection plates to more efficiently transfer the collection products to the evaporation vials. Small losses can also be attributed to the sample injection process and any sample transfer steps where pipetting was involved. These losses could also be ascribed to the LC-MS and LC-MS-NMR analyses recoveries to explain the less-than-ideal values obtained.

Additionally, in the microdroplet NMR analyses sample losses can be caused by the manual loading of the capillaries and the sample re-collection process. It was observed that when re-collecting samples from the NMR, small amounts of the immiscible carrier fluid, FC43, would often also be collected. When the FC43 would evaporate, the sample would no longer concentrate to the bottom of the vials and this phenomenon may also have caused sample losses. The recovery of 70% for the entire procedure, as seen in Figure 5.2, may appear inefficient, however, as stated above, by paying closer attention to

the fraction collection and recovery procedures, it should be possible to improve this value to approach 80% or more in future experiments.

<b>LC-MS Fraction Collection NMR Analysis</b>				
<u>Sample</u>	<u>Retention Time</u>	<u>Area</u>		
dG 1	3.82	6222.6		
	3.42	4396.2		
	% recovery	70.65		
dG 2	3.8	6186.5		
	3.42	4507.1		
	% recovery	72.85		
			<b>average</b>	<b><u>LC Only</u></b>
			<b>st. dev</b>	<b>Percent Recovery</b>
			<b>%CV</b>	70.43
				1.85
				2.62
dG 3	3.75	6021.6		
	3.44	4122.8		
	% recovery	68.47		
dG 4	3.76	6067.6		
	3.4	4231.7		
	% recovery	69.74		

**Table 5.2** Statistical results of the entire LC-MS-NMR fraction collection system including post-NMR recovery.

#### Evaluation of Manual Microdroplet microcoil-NMR Sample Loading

Because the previous system was optimized for automated sample injection and microdroplet NMR analysis, the use of manual injection microdroplet NMR needed to be assessed for its sample loading efficiency, prior to characterization of any DNA adduct sample. To do so, several injections of known amounts (5  $\mu\text{g}$ ) of dG were made on the LC-MS system and subsequently prepared for NMR analyses. The samples were loaded



into the NMR using the same microdroplet method outlined in the materials and methods section and each sample was analyzed for 100 scans. The single proton peak at 7.94 ppm, representing the proton located at the C-8 position of the guanine ring (indicated in red and circled in Figure 5.3), was then integrated in each resulting spectrum, and those integrals compared. Additionally, a 5  $\mu$ g sample of dG was pipetted into a sample vial, evaporated just as an LC-MS dG sample and prepared for NMR analysis, to evaluate the recovery of the LC-MS fraction collection process.

Figure 5.3 shows a representative NMR spectrum of the previously described dG analyses and Table 5.3 outlines statistics on the results of those experiments. In the data represented in Table 5.3, because the NMR settings were consistent between experiments, we integrated the peak at 7.94 ppm in each subsequent NMR experiment without the use of an internal standard<sup>42</sup>. Each spectrum was carefully phased after the Fourier transform to ensure a pure absorption mode frequency domain spectrum and we consistently used the same ppm range in all integrations. It should be noted that an interpretable 1D proton spectrum was obtained from a single scan of 5  $\mu$ g in the microcoil probe, which is 20 times lower than with a standard 5mm probe LOD (generally 100  $\mu$ g); however, 100 scans were acquired in order to optimize the signal-to-noise.

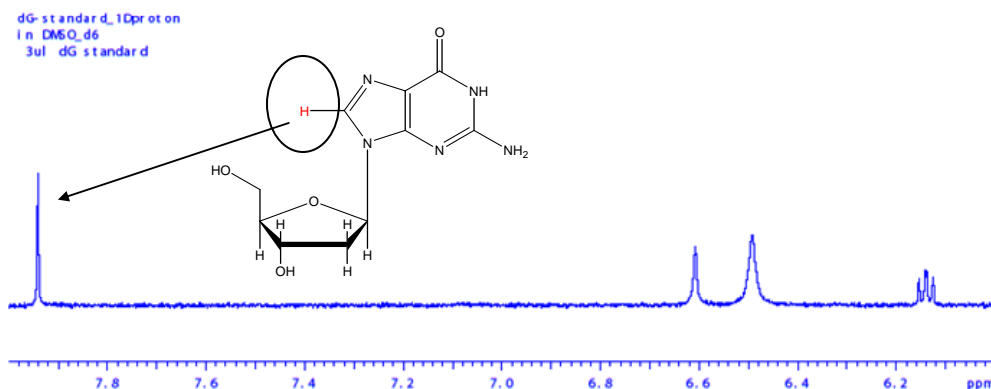


**Figure 5.3** Representative NMR spectrum (100 scans) of 5  $\mu\text{g}$  of dG loaded manually into the microcoil NMR. The single proton used to determine loading efficiency, is indicated in red at the C-8 position on the guanine ring.

The results in Table 5.3 show that LC-MS/fraction collection recovery was 93%, assessed from a comparison of an LC-MS fraction collected 5  $\mu\text{g}$  sample of dG to a 5  $\mu\text{g}$  sample that was simply pipetted. This number is slightly higher than the previously determined value of 87% recovery from the LC-UV experiments outlined in Table 5.1, but these two experiments monitor different aspects of sample loss throughout the sample handling process. The previous experiment was also subject to losses in the LC liquid handling system and post-fraction-collection isolation of each sample. The present experiment could more accurately establish any losses from the LC liquid handling system, post-fraction-collection isolation of the samples and the manual NMR loading of each sample. Repeated integration of the LCMS collected dG (Table 5.3) shows our loading was consistently within 1% variance across four samples, suggesting this method for microcoil NMR analysis of trace samples is relatively robust. Additionally, with only a 7% difference in signal between an LC-collected dG sample and a manually loaded

sample, the sample analysis and recovery from the entire microscale LC-MS-NMR platform is suitably efficient.

<b>NMR Assessment of Recovery</b>			
<u>Sample</u>	<u>Chemical Shift</u>	<u>Integral</u>	<u>LC/MS collection, NMR Analysis</u>
5ug dG	7.94	832.45	
5ug dG LCMS	7.94	793.94	
	<b>% recovery</b>	95.3739	
5ug dG	7.94	832.45	
5ug dG LCMS	7.94	776.25	
	<b>% recovery</b>	93.24884	
			<b>NMR assesed</b>
			<b>Percent Recovery</b>
			<b>average</b>
			93.61
			<b>st. dev</b>
			1.69
			<b>%CV</b>
			1.80
5ug dG	7.94	832.45	
5ug dG LCMS	7.94	785.61	
	<b>% recovery</b>	94.37324	
5ug dG	7.94	832.45	
5ug dG LCMS	7.94	761.19	
	<b>% recovery</b>	91.43973	

<b>NMR Loading Efficiency for manual injections</b>		
	<u>Chemical Shift</u>	<u>Integral</u>
5ug dG LCMS	7.94	793.94
5ug dG LCMS	7.94	776.25
5ug dG LCMS	7.94	785.61
5ug dG LCMS	7.94	761.19
	<b>Loading Efficiency</b>	
<b>average</b>	779.25	
<b>st. dev</b>	14.04	
<b>%CV</b>	1.80	

**Table 5.3 Statistical data from the NMR assesment of LC-MS fraction collection, and NMR loading efficiency experiments indicating 93% recovery from the LC-MS experiment and less than 1% variance in the NMR manual microdroplet loading method.**

## DNA Adduct Isolation and Characterization

### *i Non-deuterated dG-ABP*

Following the system evaluation, the DNA adduct reaction mixtures, prepared as described in the materials and methods section, were directly injected onto the LC-MS fraction collection system as a crude reaction mixture without initial clean-up, for both isolation and characterization purposes. To find dG-ABP adduct isomers, each MS spectrum was searched for the mass of the protonated intact compound ( $m/z$  435), and for the major fragmentation ion of dG-ABP ( $m/z$  319) arising from loss of the sugar moiety off of the dG portion. Three compounds were found having those characteristics and are highlighted in the the LC-MS and UV chromatograms in Figure 5.4. The MS/MS spectra of the  $m/z$  319 ion (MS<sup>3</sup> of the protonated intact molecule [M + H-116]<sup>+</sup>) from each of the 3 compounds yielded major fragmentations of  $m/z$  302 and  $m/z$  277 respectively, and the probable fragmentations yielding those ions are indicated in Figure 5.4.

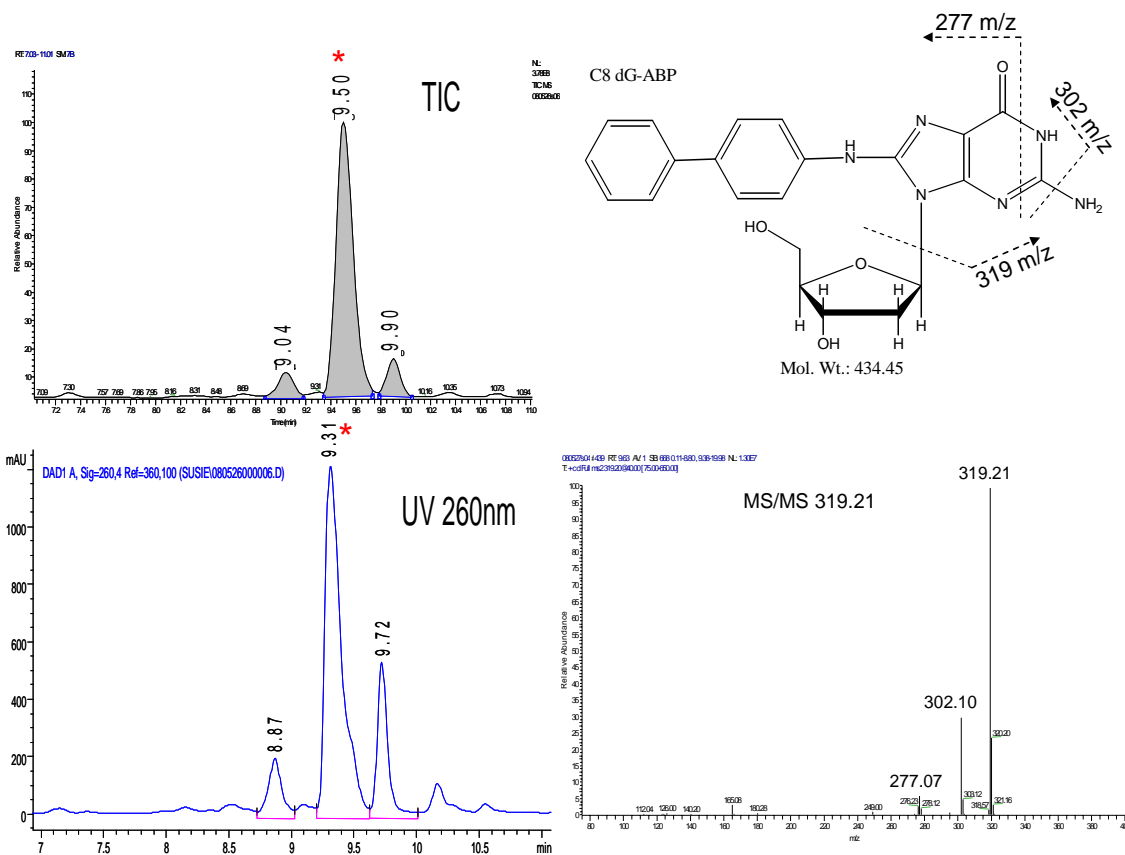


**Figure 5.4.** The left side shows comparison of the MS TIC and UV chromatograms for the 3 dG-ABP isomers identified. The top right shows the C-8 dG-ABP isomer and possible fragmentations as indicated in the MS/MS spectra for the  $m/z$  319 ion as seen in the bottom right.

The isolation of these 3 chromatographically distinct compounds, with the same MS and MS/MS fragmentations, suggests they are isomeric dG-ABP compounds. As discussed previously several isomers of the dG-ABP compound are expected, due to metabolic activation of the nitro compound to the nitrenium ion and subsequent charge delocalization as shown in Figure 5.2. As a means to discern between the 3 isomers, because the MS/MS fragmentation spectra were too similar to yield conclusive results, the fraction-collected compounds were analyzed using the microdroplet microcoil-NMR system for 1000 scans each and the resulting spectra are shown in Figure 5.5.

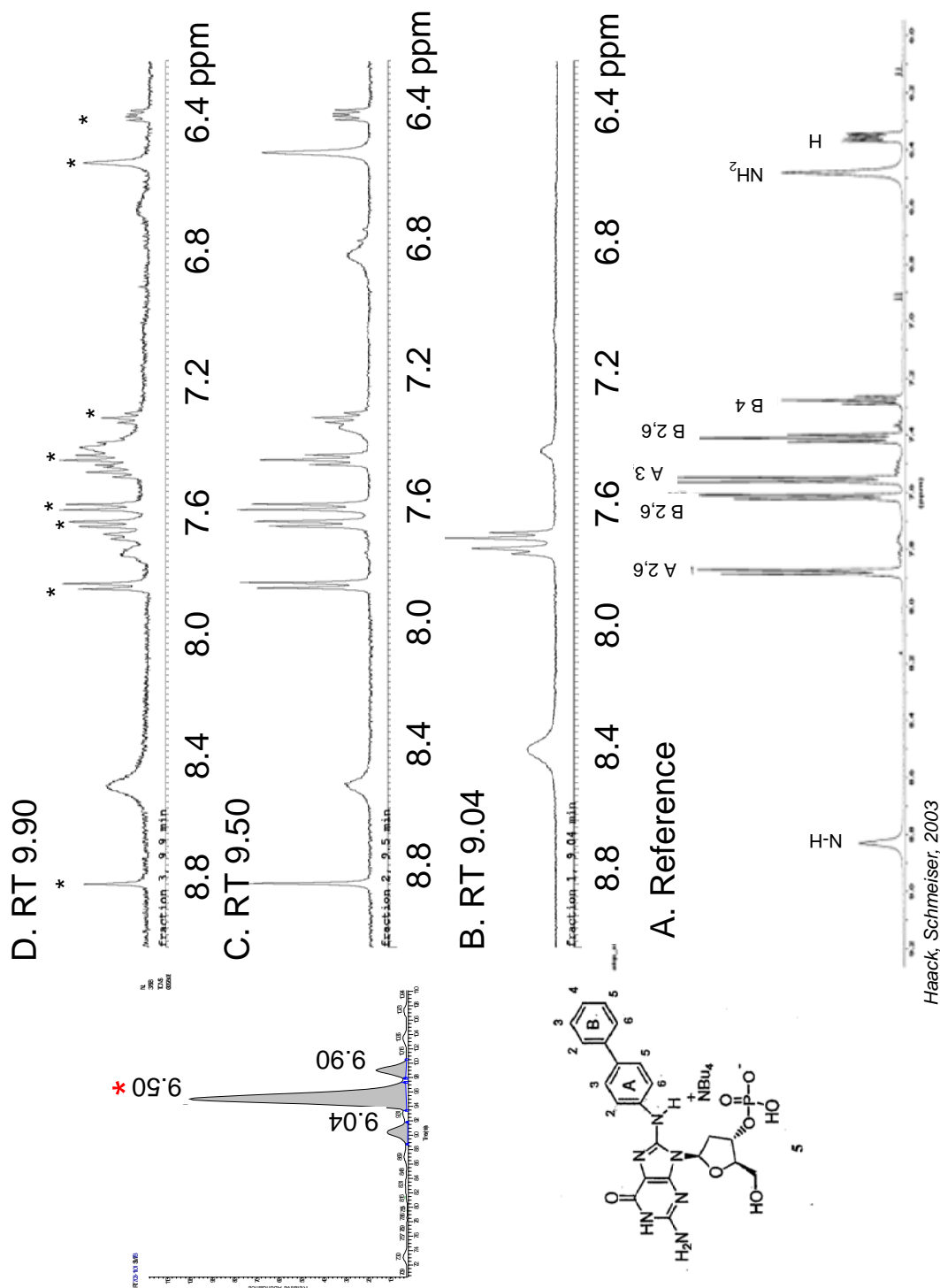
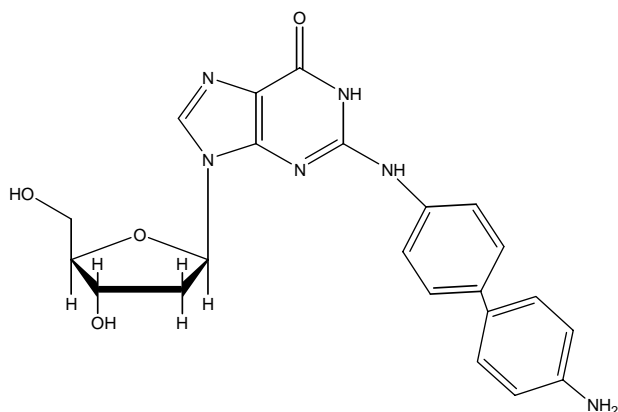


Figure 5.5. NMR spectra of the three dG-ABP isomers, the previously published reference spectrum (A), and LC peaks at 9.04 min (B), 9.50 min (C), and 9.90 min (D) from the bottom to top. Asterisks on panel D represent peaks also seen in panel C.

From the NMR spectra, we were able to correctly identify the 9.5 min LC peak as the C-8 dG-ABP isomer with reference to a previously published NMR spectrum and the chemical shifts provided by Haack and Schmeiser in 2003 from their characterization of the dG-ABP monophosphate<sup>43</sup>.

Characterization of the other two isomers, RT's 9.04 and 9.90 minutes, however, was not as straightforward. The compound isolated at RT 9.04 minutes, yielding the bottom NMR spectrum shown in panel B of Figure 5.5 is enigmatic. From initial inspection of the spectrum, because only the doublet of doublets between 7.6-7.8 ppm is seen it suggests that the ABP aromatic protons are now chemically equivalent, that the ABP is now symmetrical, yielding merely two NMR peaks as opposed to the six seen in the non-symmetrical C-8 compound. A possible structure of such a compound is drawn in Figure 5.6, with the N-2 nitrogen on the guanine ring and the 4-para position on the ABP ring forming the dG adduct. However, on further consideration this structure appears unlikely due to the lack of dG protons at both 6.4 ppm and 7.9 ppm, suggesting we may not have a dG-ABP compound as previously thought.



**Figure 5.6.** Shows the possible dG-ABP isomer at RT 9.04 minutes in the dG-ABP reaction mixture.

Noting, efficient recovery from the microdroplet microcoil-NMR platform was established in evaluation, the compound at 9.04 minutes was recovered post-NMR, the deuterated solvent evaporated, and the entire collection was then re-suspended in 100  $\mu$ L of water and re-injected into the LC-MS fraction collection system. Figure 5.7 compares two MS full scan mass spectra from this compound before and after NMR. The spectra are similar, indicating the NMR and MS are of the same compound. LC retention times were identical for both analyses and the MS spectra show not only the dG-ABP fragmentation ion of  $m/z$  319 but additionally the same MS/MS spectra of that ion, as the other two isomers at RT 9.50 and 9.90 minutes.



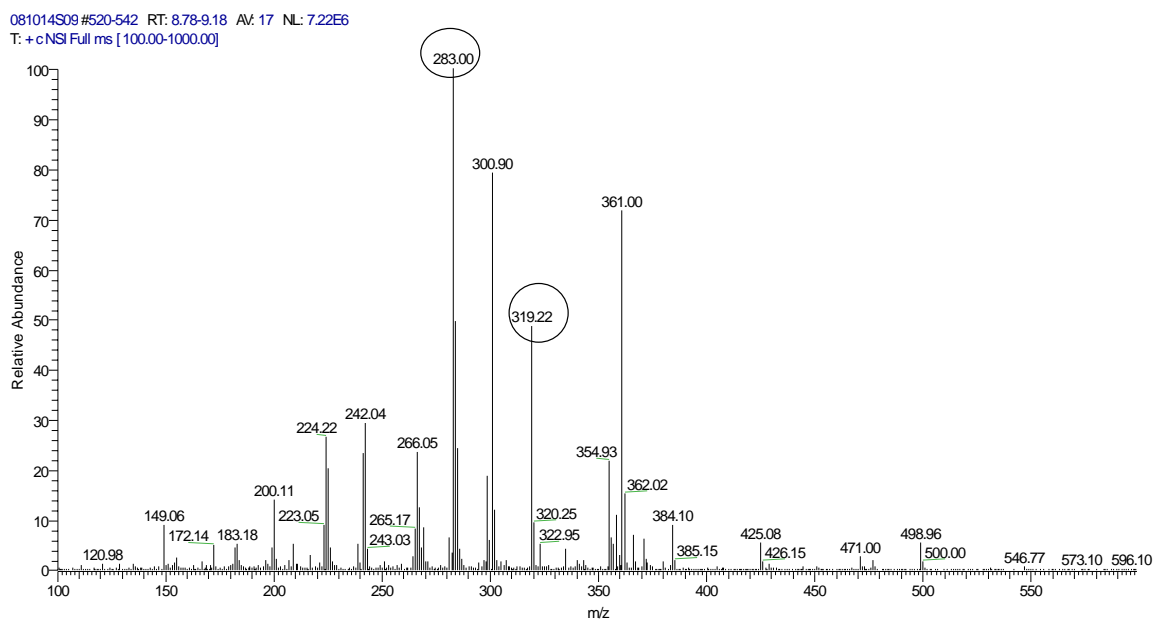
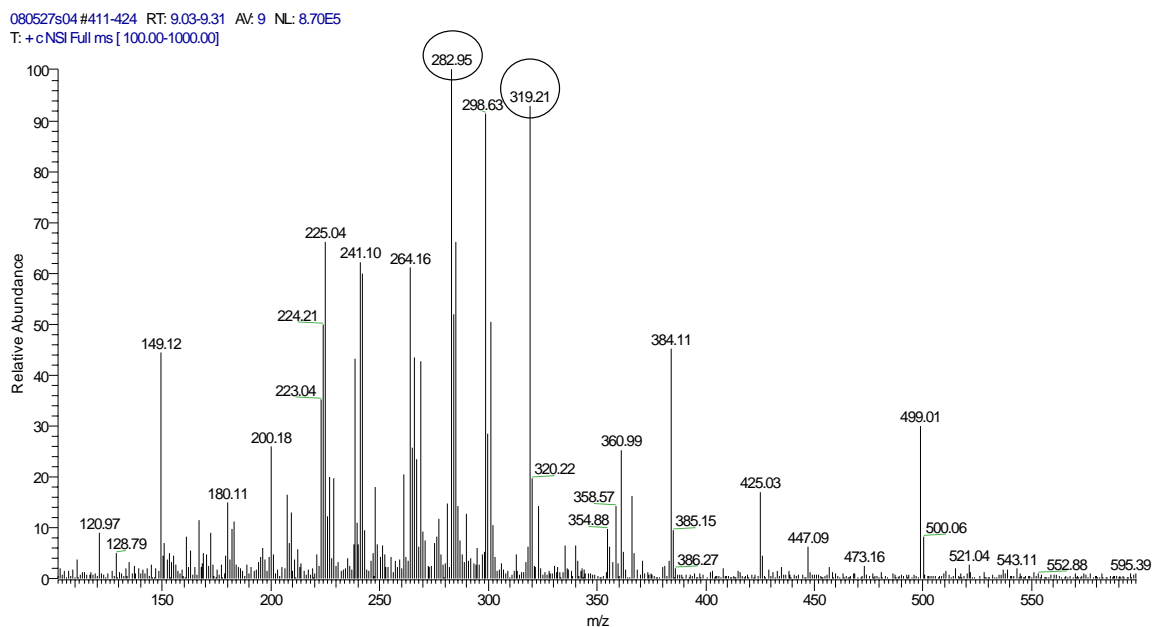


**Figure 5.7. Top Full scan MS spectrum from RT 9.04 minutes LC peak during LC-MS fractionation prior to NMR. Bottom Full scan MS spectrum after NMR-analysis.**

From this example, the significance of the streamlined microscale LC-MS-NMR platform becomes quite evident. Without NMR analysis, (including recovery and subsequent post-NMR LC-MS re-analysis) this minor adduct isomer would have been misidentified as the

N-2-dG-ABP adduct. Additional studies need to be done to reconcile enigmatic differences between the MS and NMR.

The third identified possible dG-ABP isomer, LC-MS RT 9.90 minutes, was also problematic in NMR characterization. As seen in panel D of Figure 5.5, there is an obvious overlap in peaks from the characterized C-8 isomer (indicated with an asterisk) in addition to several new peaks. This overlap caused us to question whether they are the same resonances which are observed from a different isomer or spillover from the LC major peak. Upon NMR recovery and subsequent LC-MS re-injection it became clear that there was chromatographic overlap with the C-8 isomer from the fraction collection and in order to completely characterize its structure, further fractionation and NMR analysis is necessary.

#### *ii Deuterated dG-ABP*

In view of the possible isomers associated with the dG-ABP adduct and the uncertainty of the results just presented, the deuterated dG-ABP-*d*<sub>9</sub> compound was synthesized and assessed for isomer persistence and characterization. In this case, the aromatic protons on the ABP rings are exchanged for deuterium and can therefore provide useful information to distinguish between amino-linked dG-ABP isomers and isomers linked via the aromatic rings due to the one Dalton mass difference that would be observed between them

In the same manner and due to the same reason as the non-deuterated compound (nitrenium ion charge delocalization), the dG-ABP-  $d_9$  reaction mixture yielded several chromatographically different compounds that appeared to be isomeric. The reaction produced five possible compounds with the characteristic MS and MS/MS fragmentations of  $m/z$  444 and 328, as expected 9 Daltons higher than the dG-ABP compounds, and 1 compound with the transition of  $m/z$  443  $\rightarrow$  327, one Dalton less than the fully deuterated species. Figure 5.8 shows the UV and LC-MS chromatograms along with representative MS and MS/MS spectra, as just defined, for the most predominant dG-ABP- $d_9$  adduct, whose peak is indicated with an asterisk.

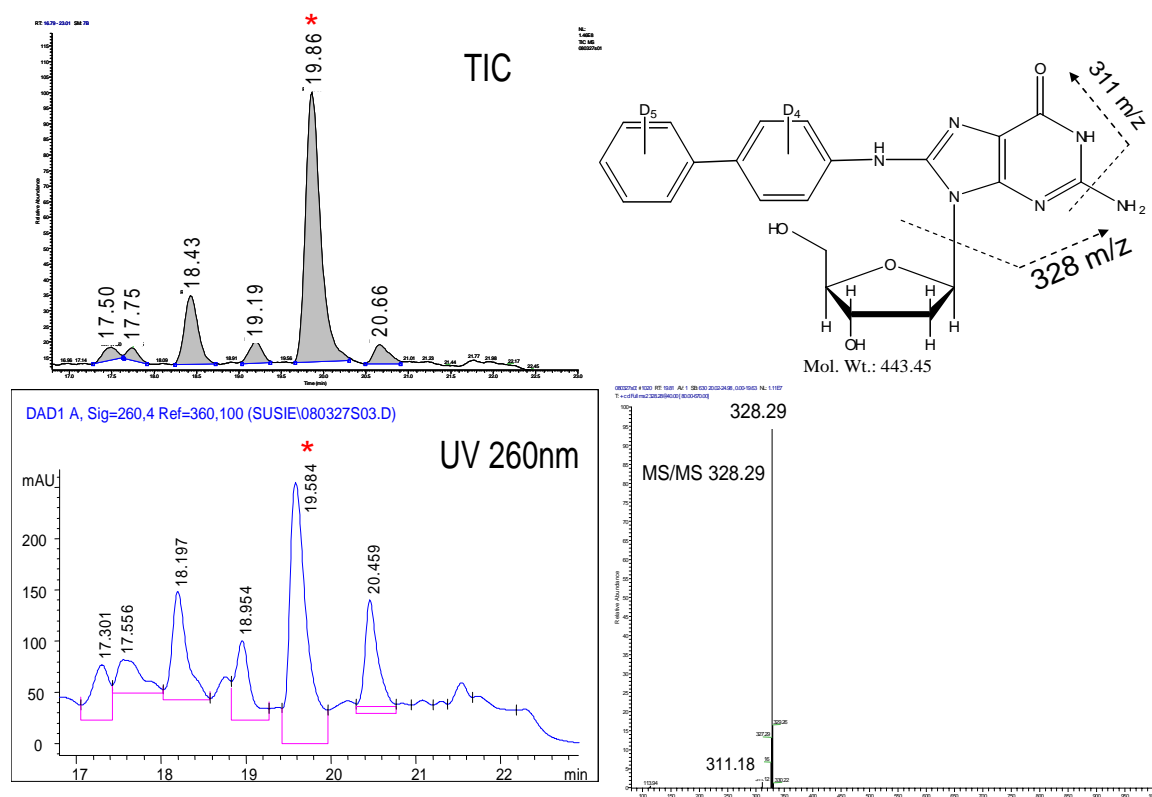


**Figure 5.8.** The left side shows the MS and UV chromatograms for the 6 dG-ABP- $d_9$  isomers identified. The top right shows the C-8 dG-ABP- $d_9$  isomer and likely fragmentations which would produce the MS/MS spectra for the 328  $m/z$  ion as seen in the bottom right.

The MS/MS fragmentations and NMR spectrum of this adduct were strikingly similar to the LC-MS-NMR characterization of the dG-ABP-C8 isomer, suggesting that it is the deuterated analog of the C-8 isomer. This hypothesis was further confirmed by mixing the two compounds together and showing LC-MS UV co-elution of the two species, as seen in Figure 5.9.

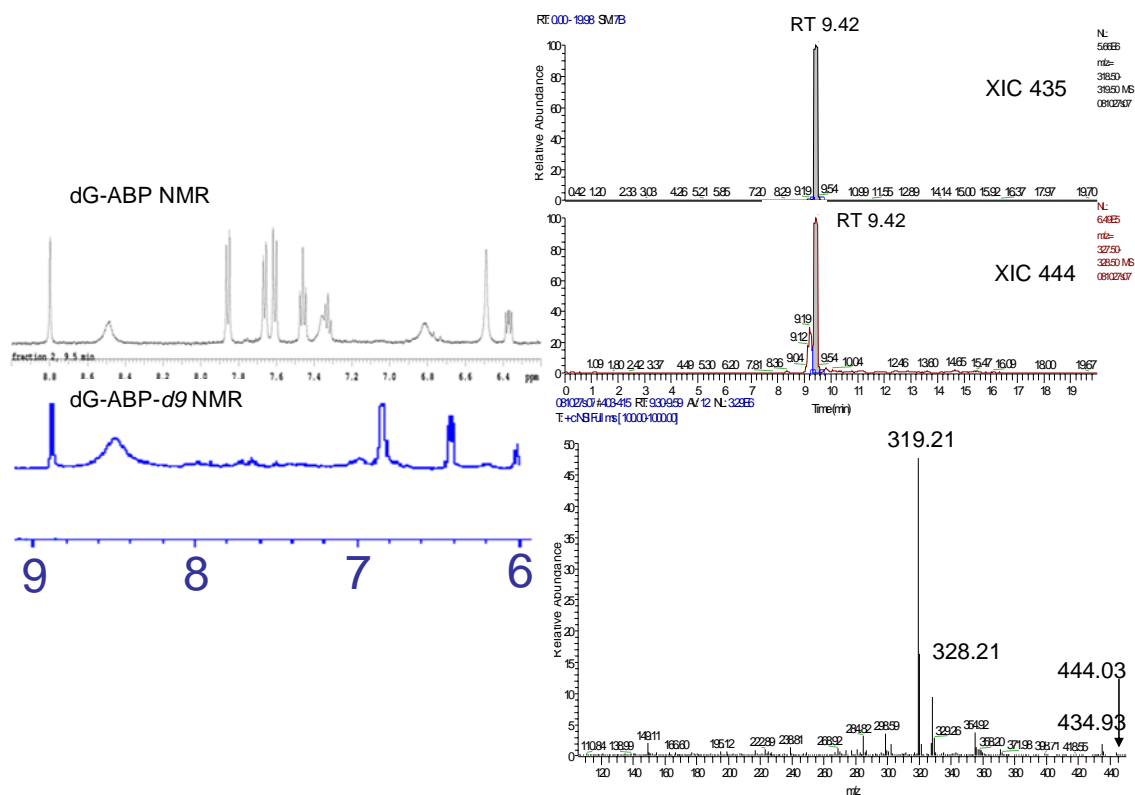


**Figure 5.9.** The left portion shows a comparison of the non-deuterated and deuterated dG-ABP NMR spectra. The right portion shows the co-elution of the two compounds, by comparing the two extracted ion chromatograms (XIC) of  $m/z$  435 and 444 respectively, as well as the resulting MS full scan spectrum, indicating the MS and MS/MS fragmentations of both species.

NMR was not expected to be useful in identification of the additional dG-ABP- $d_9$  isomer, because the deuteration eliminates the distinct ABP aromatic proton signals. It was then very important to use the MS/MS fragmentations from the LC-MS analyses of the

reaction mixture as well as using any representative dG proton signals in the NMR that may suggest either C-8 or N-2 dG adduction of the ABP molecule.

In the initial set of the NMR spectra, as shown in Figure 5.10, three regions of the spectra show differences possibly indicative of isomer structure. The peaks at 8.8 ppm, circled in Figure 5.5, assigned as the N-H proton when the amino group of the ABP molecule adducts to dG. Next, the peaks circled at 7.9 ppm are consistent with a C-8 proton on the dG portion of the adduct, as seen in Figures 5.3 and 5.5, meaning the dG-ABP-*d<sub>9</sub>* compound is probably adducted at the N-2 position on the guanine ring. The last set of resonances circled at 6.8 ppm, the chemical shift for the NH<sub>2</sub> protons on the guanine ring (Figure 5.5), could indicate adduction of the ABP to the C-8 of dG.

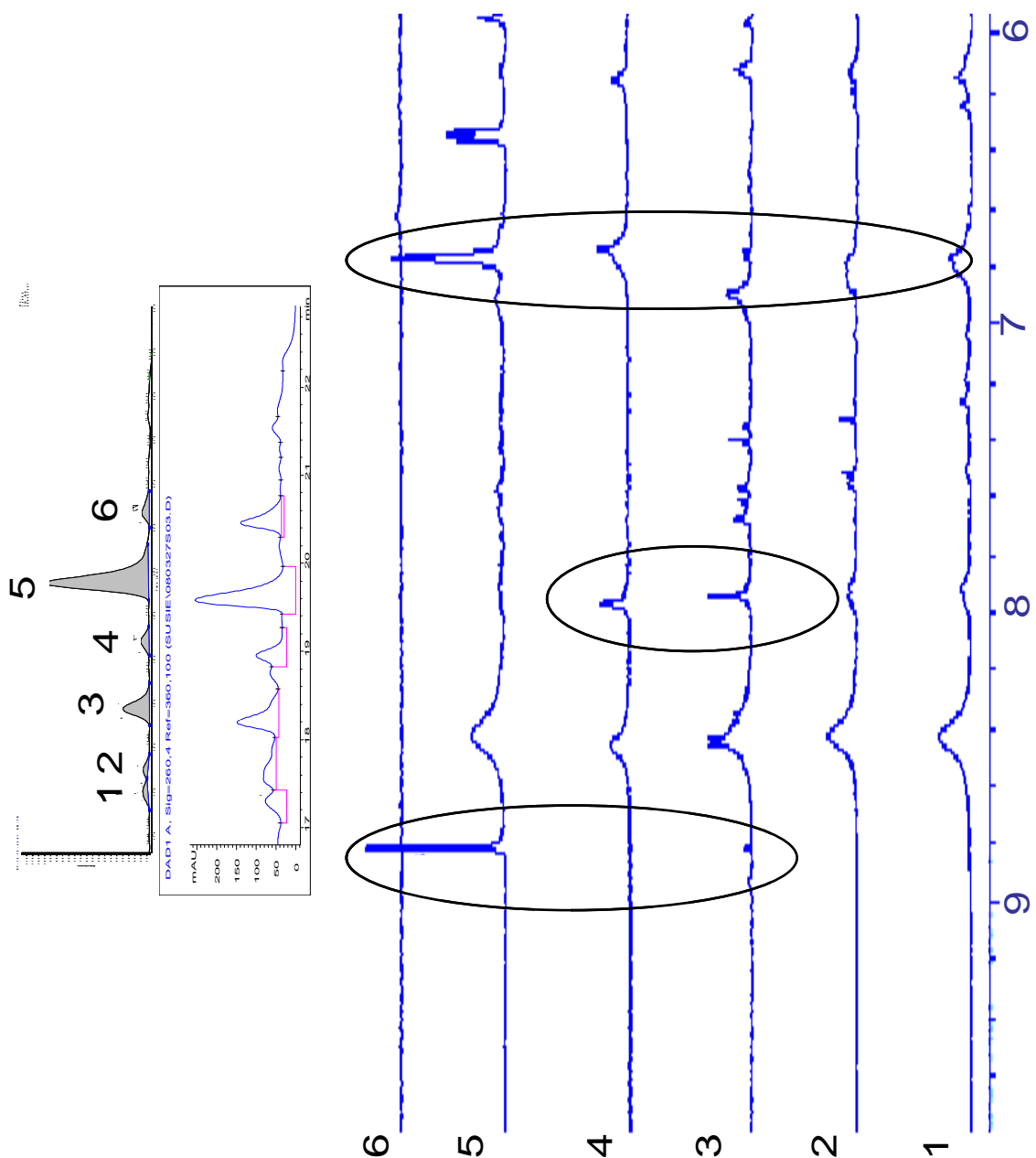


Figure 5.10 Top portion shows a comparison of the dG-ABP- $d_9$  reaction mixture and the 6 subsequent isomers numbered on the MS chromatogram. The bottom portion indicates the NMR spectra of each isomer, as indicated to the bottom left of each spectrum. The circles indicate portions of the spectrum indicative of the N-H from the amino-linked ABP adduction to the dG (8.8 ppm), C-8 dG protons (7.9 ppm) and N-2 NH<sub>2</sub> protons (6.8 ppm).

Chromatographically<sup>22, 31</sup> it is known that the N-2 adducts generally elute prior to the C-8 isomers, suggesting any of the first 4 molecules to be presumed to be N-2 dG adduction, because isomer 5 was characterized as the C-8 molecule. From this fundamental property and from the NMR spectra of isomers 3 and 4, which show a signal at 7.9 ppm, it is reasonable to suggest adduction at the N<sup>2</sup> exocyclic nitrogen.

Isomer labeled 4 yielded an  $[M+H]^+$  of  $m/z$  443 as opposed to  $m/z$  444 as well as a major fragment of  $m/z$  327 instead of  $m/z$  328, indicating ABP adduction at the ring rather than the amino group of the molecule. Figure 5.11 shows a proposed structure together with the full scan MS spectrum of isomer 4 and indicated molecular fragmentations. The proposed structure shows adduction at the ortho position of the ABP rings because the NMR spectrum of isomer 4 showed a peak at 6.7 ppm possibly suggestive of an  $-NH_2$  group adducted to the compound; shifting upfield slightly from the 6.8 ppm peak indicating the  $-NH_2$  protons on the dG ring.

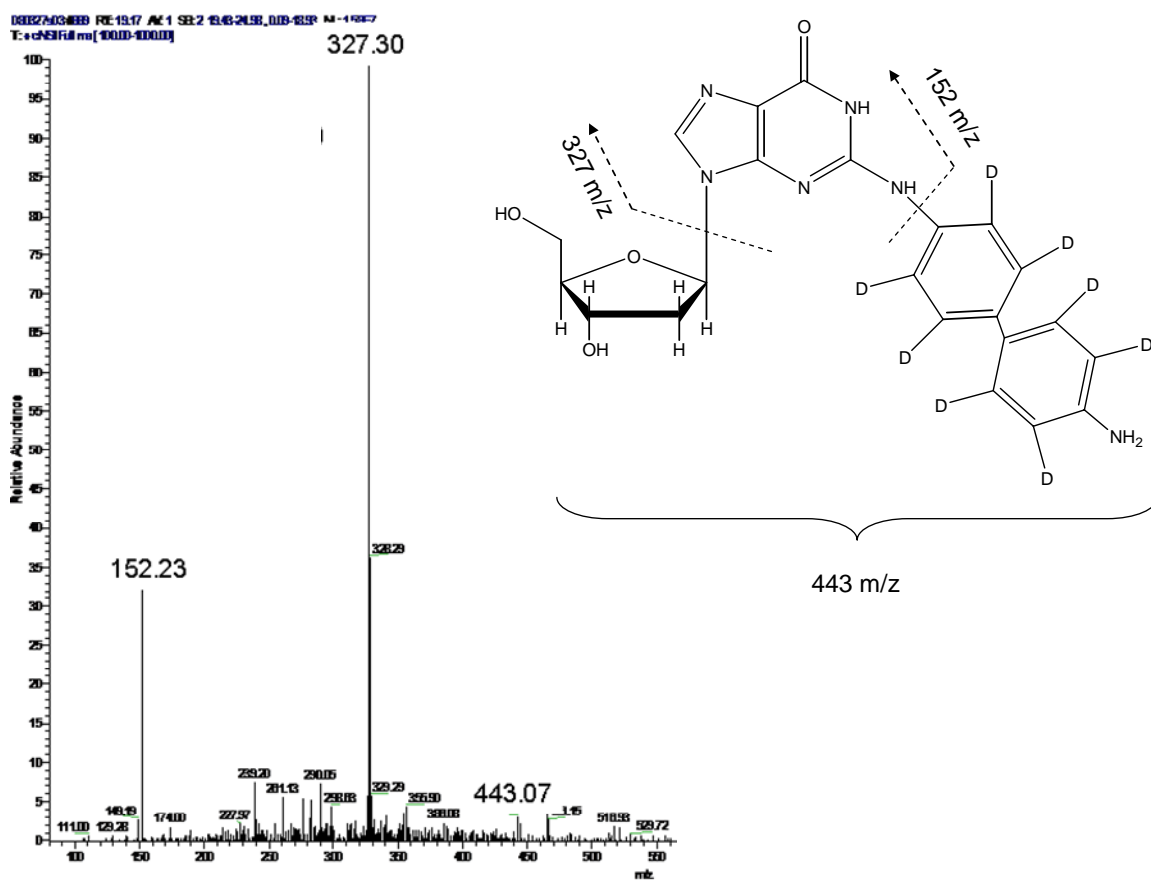
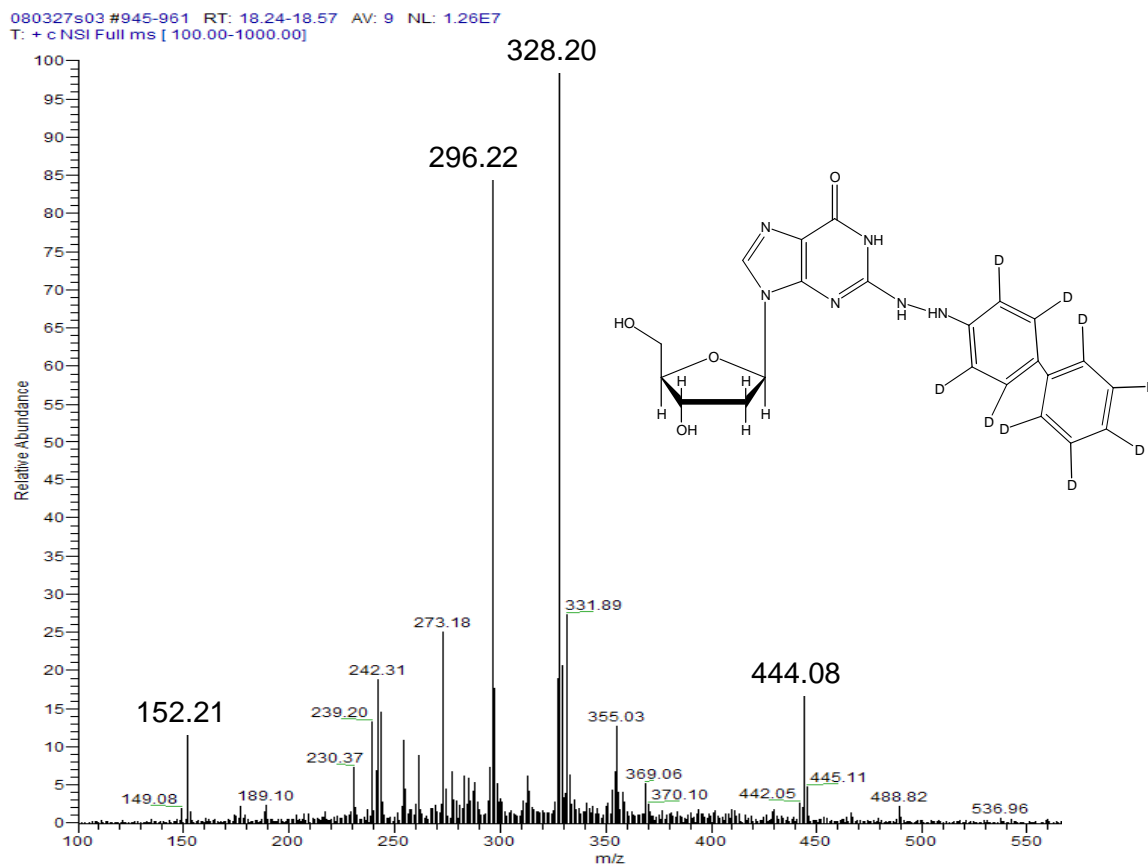


Figure 5.11. The figure shows on the left, a full scan MS spectrum of isomer 4 indicating a 1 Dalton loss from the C-8 amino-linked dG-ABP-d<sub>9</sub> molecule and to the right a representative structure and possible fragmentation sites on the molecule.



In the same manner as isomer 4, the NMR spectrum for isomer 3 suggests N-2 adduction with a peak at 7.9 ppm; however, the small N-H peak at 8.8 ppm suggests ABP adduction through the amino group. To further support this adduction site, the isomer shows the indicative dG-ABP- $d_9$  MS and MS/MS ions of  $m/z$  444 and 328 respectively. Analysis of all the LC-MS-NMR data acquired support a structure consistent with N-2 adduction at the amino group of the ABP molecule, allowing all 9 deuteriums to be intact, as shown in Figure 5.12.



**Figure 5.12.** Full MS spectrum of isomer 3 showing the MS/MS transition of 444  $\rightarrow$  328  $m/z$  as well as possible structure of isomer 3, indicating N-2 dG adduction to the amino group on the ABP molecule.

Again, as with the non-deuterated dG-ABP isomers it seems that we have been able to extract as much information as we could from the MS/MS fragmentations and the NMR spectra obtained, however, without further 2-D NMR analyses it appears that definitive characterization of the isomeric species can not be achieved. This is apart from isomer 5 which co-eluted with its non-deuterated analog and could be assigned the structure of the C-8 dG-ABP-*d*<sub>9</sub> isomer. It is obvious that the structures proposed for isomers 3 and 4 tentative, however, the inclusion of 1D proton NMR data narrowed the plausible possibilities than would be possible from MS or UV data alone.

The limited information that can be discerned about isomers 1 and 2 is not very straightforward. From their respective NMR spectra, there is no clear evidence of dG adduction, due to the lack of peaks at the C-8 proton position of 7.9 ppm as well as 6.8 ppm where the NH<sub>2</sub> protons at the N-2 position occur. However, their full MS spectrum showed several characteristic ions of dG-ABP-*d*<sub>9</sub> such as the *m/z* 444 ion for the intact molecule, the *m/z* 328 ion indicating loss of the dG sugar moiety, as well as the *m/z* 152 ion of the purine base of guanine. Additionally, the major MS<sup>3</sup> fragmentation for both compounds is the *m/z* 242/243 ion pair. The difference between the spectra, for the two isomers is merely that isomer 1 shows a large MS<sup>3</sup> fragment ion at *m/z* 271. The MS and MS/MS spectra for isomer 1 and 2 can be seen in Figures 5.13 and 5.14 respectively.

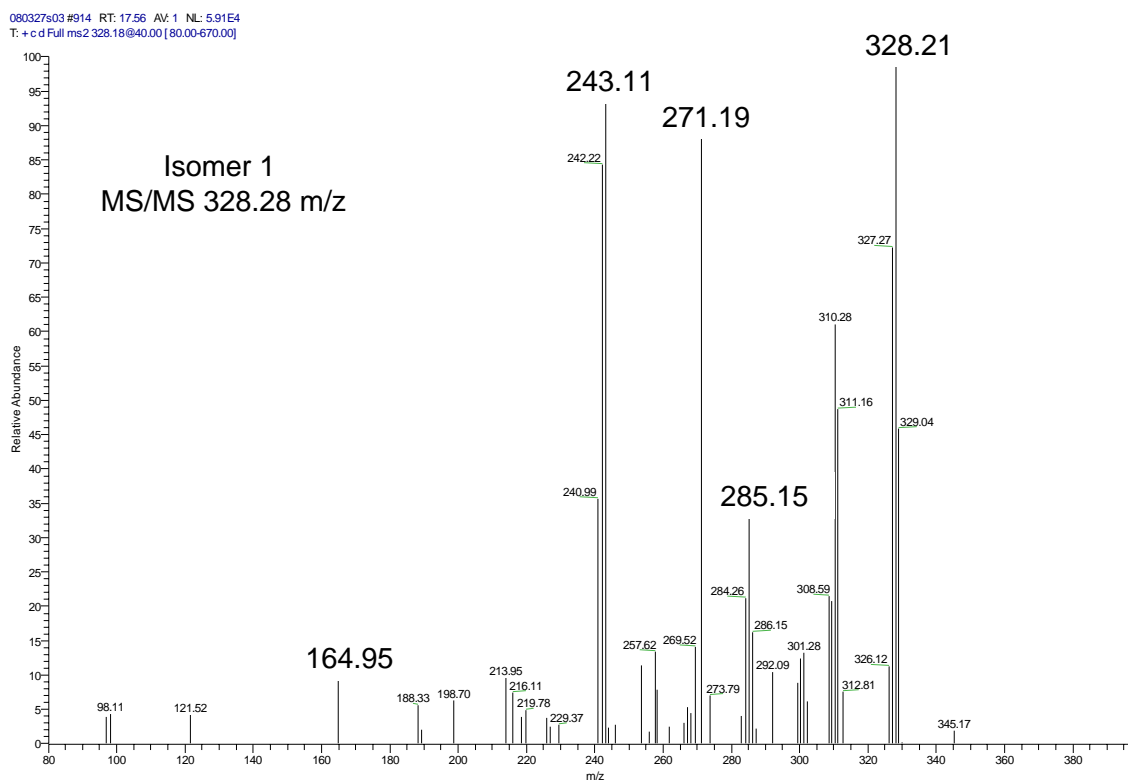
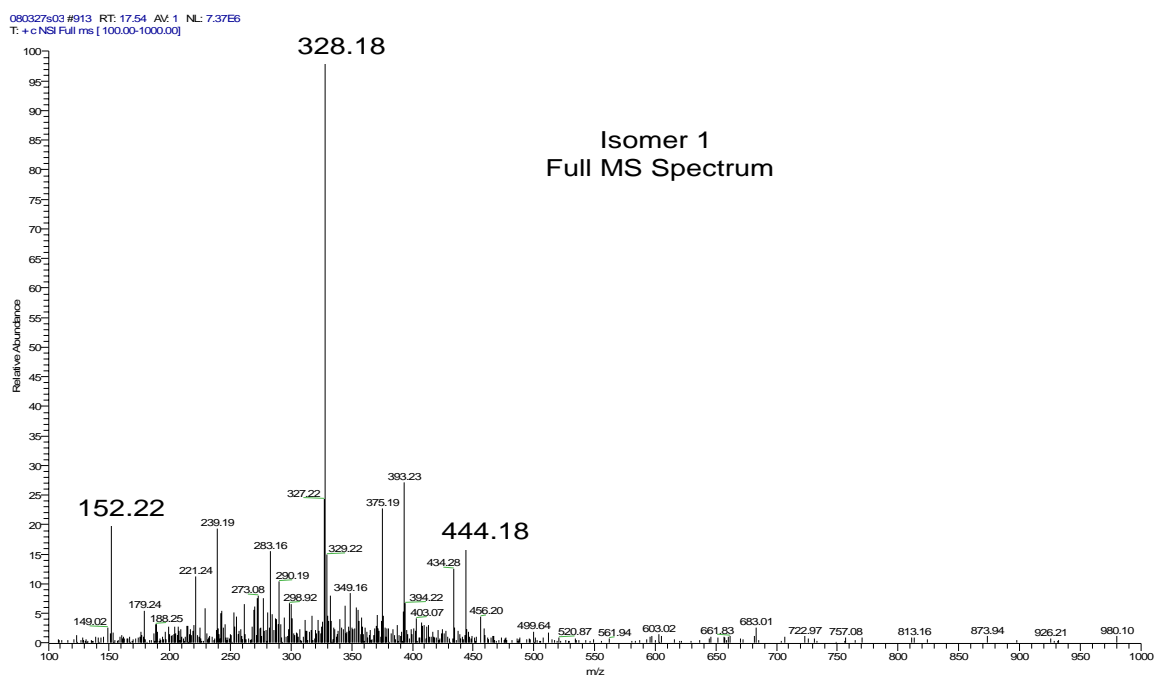


**Figure 5.13.** The top spectrum represents the full scan MS spectrum for isomer 1 while the bottom spectrum is the MS/MS fragmentation of the  $[M+H-116]^+$  ion of  $m/z$  328.

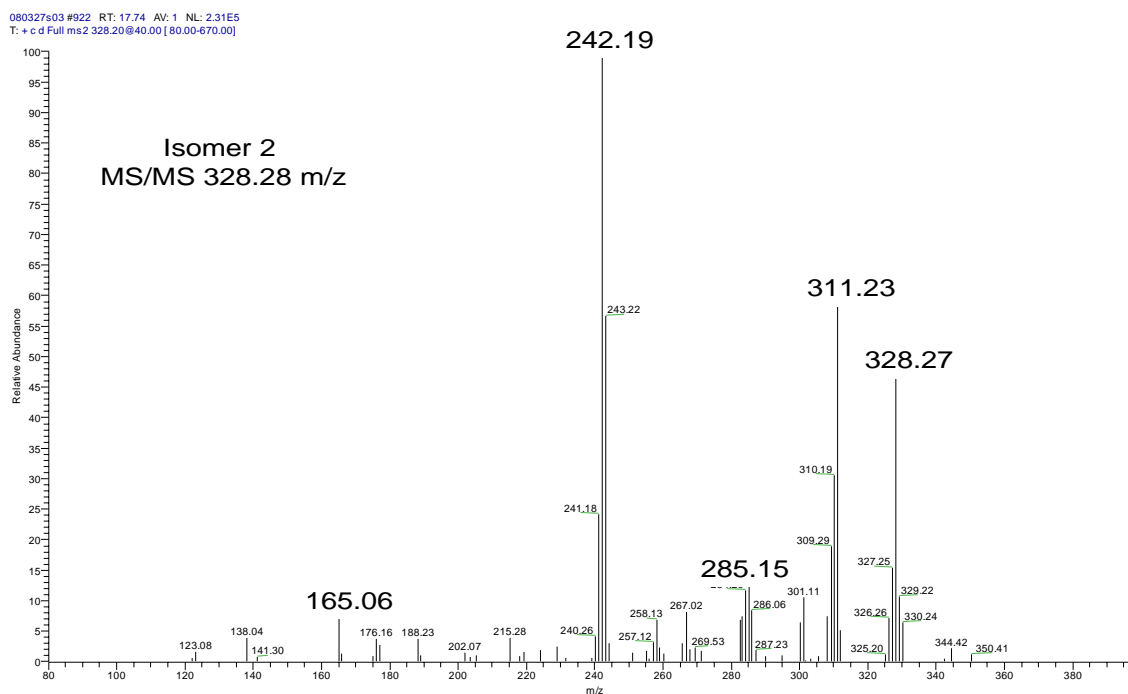
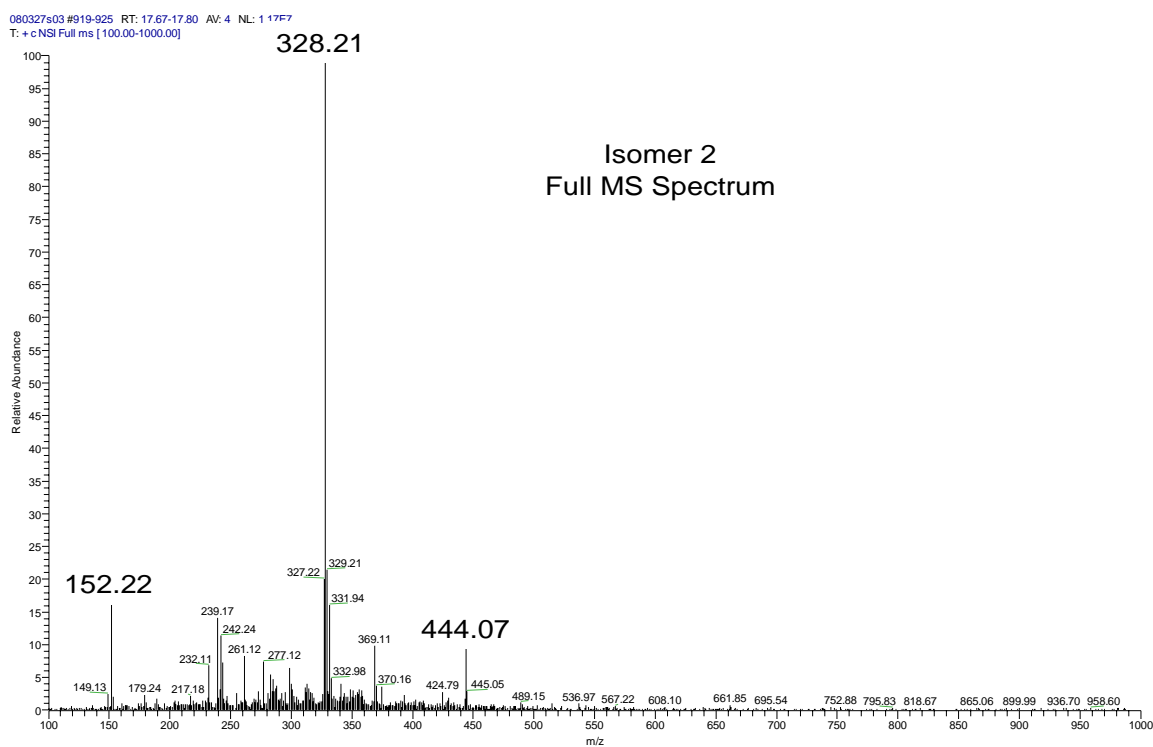


**Figure 5.14.** The top spectrum represents the full scan MS spectrum for isomer 2 while the bottom spectrum is the MS/MS fragmentation of the  $[M+H-116]^+$  ion of  $m/z$  328.

It is difficult to propose structures for isomers 1 and 2 with the limited information at hand. However, it is clear they are different compounds and yield MS ions and fragmentations very characteristic of a dG-ABP-*d*<sub>9</sub> molecule as expected.

Isomer 6, because it elutes closely after the characterized C-8 isomer, appears to be an additional C-8 adduct. Although its NMR spectrum does not show any peaks in the indicated aromatic region, however its MS spectra showed clear dG-ABP-*d*<sub>9</sub> ion peaks, ( $m/z$  328 for the  $[M+H-116]^+$  ion and  $m/z$  152 for the guanine base, as seen in Figure 5.15). Additionally, the MS<sup>3</sup> spectrum of the  $m/z$  328.29 ion shows fragmentation consistent with the characterized C-8 dG-ABP-*d*<sub>9</sub> isomer (Figure 5.7).

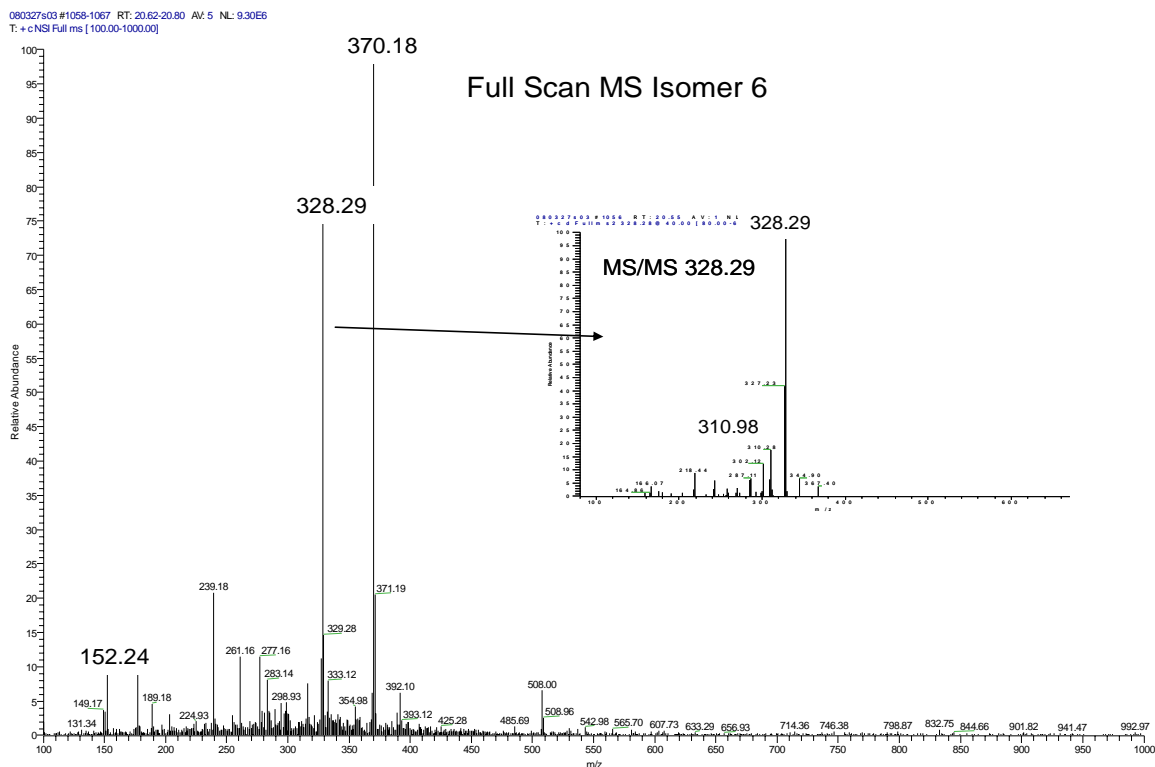


**Figure 5.15.** The large spectrum represents the full scan MS spectrum for isomer 6 while the inset spectrum is the MS/MS fragmentation of the  $[M+H-116]$  ion of 328  $m/z$ .

As with the RT 9.07 minute isomer from the non-deuterated dG-ABP sample, when isomer 6 recovered from the NMR was re-injected into the LC-MS system, the original retention time and MS spectrum were observed (Figure 5.16). In these cases, the ability to obtain microscale NMR data has possibly eliminated any misidentifications that could have occurred and focused questions for additional studies that will hopefully lead to their characterization.

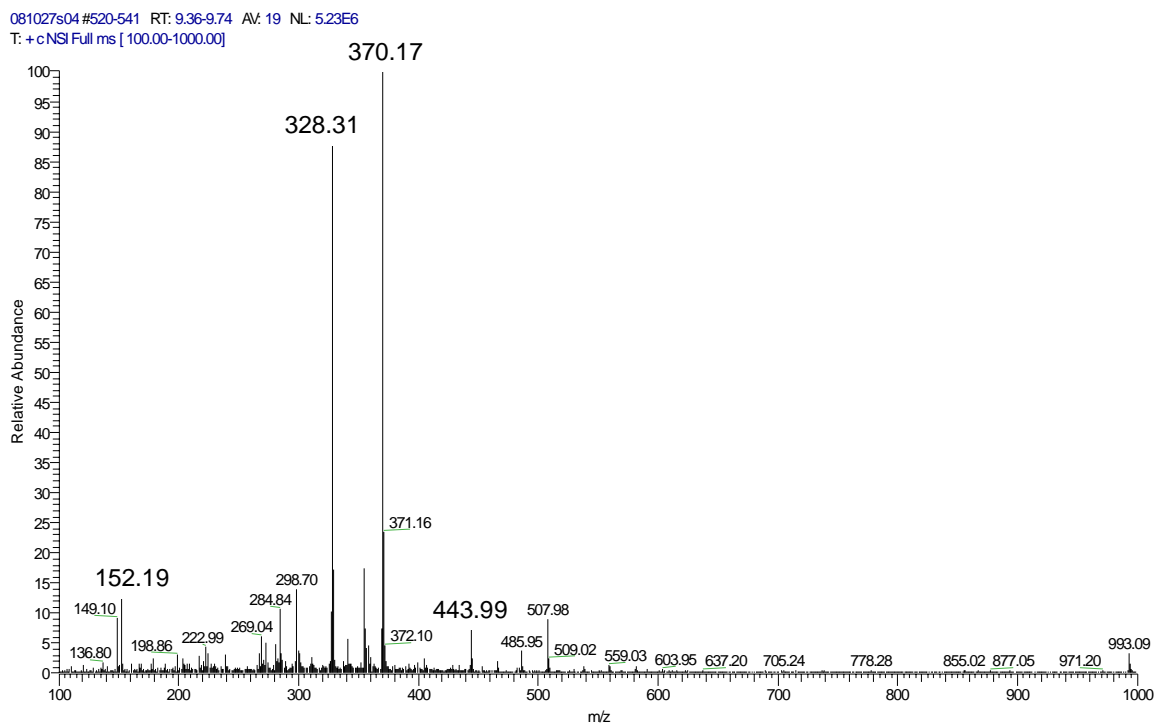


**Figure 5.16.** The full MS spectrum of the post-NMR collected LC-MS analyzed isomer 6, showing several indicative dG-ABP- $d_9$  ions as also seen in its pre-NMR analyzed LC-MS spectrum in Figure 5.14.

## 5.7 Conclusions

Following the development of the automated microdroplet LC-MS-NMR platform, described in Chapter 4, it was very straightforward to apply the platform to DNA adduct analyses. Also, because the platform could achieve excellent NMR sensitivity down to the ng level, it was obvious to apply it to characterization of minor adduct isomers. First, in order to establish its utility for manual injections, the loading efficiency and full LC-MS-NMR recovery was assessed to be efficient within 1% variation with greater than 70% recovery. For characterization of reaction mixtures, these values were adequate in terms of precious sample preservation. In practice, the platform was quite streamlined,

however, although the system could acquire 1D NMR at the ng level, the limit of detection for more advanced 2D and heteronuclear NMR remained a limitation to fully characterize the subtly different DNA adduct isomers. The microdroplet platform can acquire homonuclear 2-D NMR (COSY) at the low microgram level and possibly lower if overnight analyses are possible. The heteronuclear 2D (HSQC, HMBC) needed for *de novo* identification require 10 or 50  $\mu\text{g}$  even in overnight acquisition. Therefore, full characterization is possible with more in depth NMR experiments using the microdroplet LC-MS-NMR platform described here.

## 5.8 References

- (1) Sancar, A. *Annu Rev Biochem* **1996**, *65*, 43-81.
- (2) Sturla, S. J. *Curr Opin Chem Biol* **2007**, *11*, 293-299.
- (3) Guo, Y.; Breeden, L. L.; Fan, W.; Zhao, L. P.; Eaton, D. L.; Zarbl, H. *Mutat Res* **2006**, *593*, 121-142.
- (4) Guo, Y.; Breeden, L. L.; Zarbl, H.; Preston, B. D.; Eaton, D. L. *Mol Cell Biol* **2005**, *25*, 5823-5833.
- (5) Luo, W.; Fan, W.; Xie, H.; Jing, L.; Ricicki, E.; Vouros, P.; Zhao, L. P.; Zarbl, H. *Chem Res Toxicol* **2005**, *18*, 619-629.
- (6) Ricicki, E. M.; Luo, W.; Fan, W.; Zhao, L. P.; Zarbl, H.; Vouros, P. *Anal Chem* **2006**, *78*, 6422-6432.
- (7) Farmer, P. B.; Sepai, O.; Lawrence, R.; Autrup, H.; Sabro Nielsen, P.; Vestergard, A. B.; Waters, R.; Leuratti, C.; Jones, N. J.; Stone, J.; Baan, R. A.; van Delft, J. H.; Steenwinkel, M. J.; Kyrtopoulos, S. A.; Souliotis, V. L.; Theodorakopoulos, N.; Bacalis, N. C.; Natarajan, A. T.; Tate, A. D.; Haugen, A.; Andreassen, A.; Ovrebo, S.; Shuker, D. E.; Amaning, K. S.; Castelain, P.; et al. *Mutagenesis* **1996**, *11*, 363-381.
- (8) Farmer, P. B.; Singh, R. *Mutat Res* **2008**, *659*, 68-76.



- (9) Butler, M. A.; Iwasaki, M.; Guengerich, F. P.; Kadlubar, F. F. *Proc Natl Acad Sci U S A* **1989**, *86*, 7696-7700.
- (10) Crofts, F. G.; Sutter, T. R.; Strickland, P. T. *Carcinogenesis* **1998**, *19*, 1969-1973.
- (11) Shimada, T.; Hayes, C. L.; Yamazaki, H.; Amin, S.; Hecht, S. S.; Guengerich, F. P.; Sutter, T. R. *Cancer Res* **1996**, *56*, 2979-2984.
- (12) Shimada, T.; Iwasaki, M.; Martin, M. V.; Guengerich, F. P. *Cancer Res* **1989**, *49*, 3218-3228.
- (13) Turesky, R. J.; Constable, A.; Richoz, J.; Varga, N.; Markovic, J.; Martin, M. V.; Guengerich, F. P. *Chem Res Toxicol* **1998**, *11*, 925-936.
- (14) Turesky, R. J.; Lang, N. P.; Butler, M. A.; Teitel, C. H.; Kadlubar, F. F. *Carcinogenesis* **1991**, *12*, 1839-1845.
- (15) Turesky, R. J.; Rossi, S. C.; Welti, D. H.; Lay, J. O., Jr.; Kadlubar, F. F. *Chem Res Toxicol* **1992**, *5*, 479-490.
- (16) Dewar, M. J. S.; Zoebisch, E. G.; Healy, E. F.; Stewart, J. J. P. *Journal of the American Chemical Society* **1985**, *107*, 3902-3909.
- (17) Ford, G. P.; Thompson, J. W. *Chem Res Toxicol* **1999**, *12*, 53-59.
- (18) Kadlubar, F. F.; Anson, J. F.; Dooley, K. L.; Beland, F. A. *Carcinogenesis* **1981**, *2*, 467-470.
- (19) Westra, J. G. *Carcinogenesis* **1981**, *2*, 355-357.
- (20) Marques, M. M.; Mourato, L. L.; Santos, M. A.; Beland, F. A. *Chem Res Toxicol* **1996**, *9*, 99-108.
- (21) Cui, L.; Sun, H. L.; Wishnok, J. S.; Tannenbaum, S. R.; Skipper, P. L. *Chem Res Toxicol* **2007**, *20*, 1730-1736.
- (22) Wolf, S. M.; Vouros, P. *Chem Res Toxicol* **1994**, *7*, 82-88.
- (23) Jacobsen, M. I.; Meier, C. *Nucleic Acids Symp Ser (Oxf)* **2008**, *52*, 439-440.
- (24) Turesky, R. J.; Vouros, P. *J Chromatogr B Analyt Technol Biomed Life Sci* **2004**, *802*, 155-166.
- (25) De Riccardis, F.; Bonala, R. R.; Johnson, F. *Journal of the American Chemical Society* **1999**, *121*, 10453-10460.

- (26) Yasui, M.; Dong, H.; Bonala, R. R.; Suzuki, N.; Ohmori, H.; Hanaoka, F.; Johnson, F.; Grollman, A. P.; Shibutani, S. *Biochemistry* **2004**, *43*, 15005-15013.
- (27) Tan, X.; Bonala, R. R.; Suzuki, N.; Johnson, F.; Grollman, A. P.; Shibutani, S. *Chem Biol Interact* **2005**, *152*, 131-138.
- (28) Mitchell, N.; Stohrer, G. *J Mol Biol* **1986**, *191*, 177-180.
- (29) Michaels, M. L.; Johnson, D. L.; Reid, T. M.; King, C. M.; Romano, L. J. *J Biol Chem* **1987**, *262*, 14648-14654.
- (30) Shibutani, S.; Fernandes, A.; Suzuki, N.; Zhou, L.; Johnson, F.; Grollman, A. P. *J Biol Chem* **1999**, *274*, 27433-27438.
- (31) Gangl, E. T.; Turesky, R. J.; Vouros, P. *Chem Res Toxicol* **1999**, *12*, 1019-1027.
- (32) Gangl, E. T.; Turesky, R. J.; Vouros, P. *Anal Chem* **2001**, *73*, 2397-2404.
- (33) Lin, Y.; Schiavo, S.; Orjala, J.; Vouros, P.; Kautz, R. *Anal Chem* **2008**, *80*, 8045-8054.
- (34) Gangl, E. T.; Annan, M. M.; Spooner, N.; Vouros, P. *Anal Chem* **2001**, *73*, 5635-5644.
- (35) Gangl, E. T.; Vouros, P.: US, 2004.
- (36) Schiavo, S.; Ebbel, E.; Sharma, S.; Matson, W.; Kristal, B. S.; Hersch, S.; Vouros, P. *Anal Chem* **2008**, *80*, 5912-5923.
- (37) Andrews, C. L.; Li, F.; Yang, E.; Yu, C.-P.; Vouros, P. *J Mass Spectrom* **2006**, *41*, 43-49.
- (38) Andrews, C. L.; Yu, C. P.; Yang, E.; Vouros, P. *J Chromatogr A* **2004**, *1053*, 151-159.
- (39) Wilm, M.; Mann, M. *Anal Chem* **1996**, *68*, 1-8.
- (40) Olson, D. L.; Norcross, J. A.; O'Neil-Johnson, M.; Molitor, P. F.; Detlefsen, D. J.; Wilson, A. G.; Peck, T. L. *Anal Chem* **2004**, *76*, 2966-2974.
- (41) Schroeder, F. C.; Gronquist, M. *Angew Chem Int Ed Engl* **2006**, *45*, 7122-7131.
- (42) Shao, G.; Kautz, R.; Peng, S.; Cui, G.; Giese, R. W. *J. Chromatogr., A FIELD Full Journal Title:Journal of Chromatography, A* **2007**, *1138*, 305-308.

- (43) Haack, T.; Boche, G.; Kliem, C.; Wiessler, M.; Albert, D.; Schmeiser, H. H. *Chem. Res. Toxicol. FIELD Full Journal Title:Chemical Research in Toxicology* **2004**, *17*, 776-784.

Chapter 6:  
Future Directions

The research products presented in this dissertation exploited the use of hyphenated analytical technologies as a means to gain more information from a single analysis.

### 6.1 LC-EC-array-MS Platform

Chapters 2 and 3 utilized the hyphenation of LC-MS and LC-EC-array in parallel for the identification of novel SPB metabolites from treated HD patients. The novel parallel system was developed in our laboratory and utilized a high-loading HPLC column with nESI-MS and EC-array detection. This set-up allowed for each detector to be used under its optimum conditions, with higher flow rates being delivered to the EC-array and less to the MS. The HPLC chromatographic integrity was maintained between both instruments, allowing confident correlation between the two detectors. Additionally, the use of nESI and a large bore HPLC column precluded the need for tiresome sample preparation which can often cause sample losses. Ultimately, the parallel system proved to be a unique method for unknown metabolite profiling and identification.

Future work concerning this system will be applied toward other metabolomic profiling or metabolite identification studies. For example, collaborators of ours at the Bedford, VA have developed a robust system using a 16 electrode LC-EC-array detection system for profiling studies where they diagnosed Parkinson's disease from control<sup>1</sup> by using sophisticated statistical analysis methods such as principle component analyses. However, the strongest discriminating compounds, creating the important statistical difference between the groups, are often structurally unknown. The parallel LC-EC-

array-MS system could then be used for identification and characterization of these compounds.

### 6.3 Microscale LC-MS-NMR Platform

Chapters 4 and 5 utilized LC-MS and microdroplet-NMR analyses in a streamlined platform for natural product research and low abundance isomeric DNA adduct characterization. In a similar manner to the just described LC-EC-array-MS hyphenated system, the ability to use large bore HPLC columns with large loading capacities in addition to sensitive nESI-MS proved very useful for fraction collecting large amounts of material to be used in subsequent NMR analyses. The microdroplet-NMR studies were performed as both automated and manual runs showing the advantages and disadvantages of each technique. This offers two detection method options to the analyst concerning which best suits their needs. The automated system was successfully used to identify known natural product compounds from bioactive cyanobacteria samples as well as to characterize one compound as unknown and prioritize it for further studies. The manual system was used to characterize isomeric DNA adduct species at low microgram levels while also easily preserving the samples for further studies.

Future work on this hyphenated system will be directed at further natural product studies for streamlined compound identification as well as being directed toward further optimizing the manual microdroplet-NMR analysis method. Also, future DNA adduct work should be done to better characterize the minor isomeric species. It is possible that

more efficient syntheses and LC separation would lead to better fraction collection of the different compounds effectively helping yield sharper more definitive NMR spectra. These studies are currently being done with the aromatic amine 2-aminonaphthalene adducted to dG as well as ABP adducted to dA. Deoxyadenosine adducts have been found prominently in human studies with ABP<sup>2</sup>.

#### 6.4 References

- (1) Bogdanov, M.; Matson Wayne, R.; Wang, L.; Matson, T.; Saunders-Pullman, R.; Bressman Susan, S.; Flint Beal, M. *Brain FIELD Full Journal Title:Brain : a journal of neurology* **2008**, *131*, 389-396.
- (2) Bessette, E. E.; Goodenough, A. K.; Langouet, S.; Yasa, I.; Kozekov, I. D.; Spivack, S. D.; Turesky, R. J. *Anal. Chem. (Washington, DC, U. S.) FIELD Full Journal Title:Analytical Chemistry (Washington, DC, United States)* **2009**, *81*, 809-819.

**BIOGRAPHICAL DATA**

NAME	Susan Schiavo
PLACE OF BIRTH	Scranton, PA
EDUCATION	Doctorate of Philosophy in Analytical Chemistry, 2009 Barnett Institute / Dept. of Chemistry and Biological Chemistry, Northeastern University, Boston MA  Bachelor of Science (Honors), 2002 Moravian College, Bethlehem PA
PROFESSIONAL EXPERIENCE	Postdoctoral Research Fellow, March 2009 - Present Department of Neurosurgery, Harvard Medical School / Brigham and Women's Hospital, Boston, MA  Graduate Research Assistant, Sept. 2004– Present Barnett Institute / Dept. of Chemistry and Biological Chemistry, Northeastern University, Boston MA  Graduate Teaching Assistant, Sept 2002-May 2004 Dept. of Chemistry and Biological Chemistry, Northeastern University  Undergraduate Research Assistant, September 2001-May 2002 Department of Chemistry, Moravian College, Bethlehem PA  Undergraduate Summer Research, June 2000 – September 2000 Department of Chemistry, Moravian College, Bethlehem PA
PROFESSIONAL AFFILIATIONS	American Chemical Society, Student Affiliate (1998-Present) American Society of Mass Spectrometry, Student Member (200-Present) Greater Boston Mass Spectrometry Discussion Group (2003-Present) Massep.org (2003-Present)
HONORS	Barnett Institute Alumni Fellowship 2008 Douglas and Irene DeVivo Award for Continued Excellence 2007 Department of Chemistry and Chemical Biology Citizenship Award 2006



## LIST OF PUBLICATIONS

Schiavo, S.; Gathungu, R.; Muentner, M.; Kautz, R.A.; Vouros, P.: Identification of Minor DNA Adduct Isomers using an LC-MS- $\mu$ NMR platform (*In preparation*).

Ebbel, E; Schiavo, S; Sharma; Gevorkain, S.; Hersch, S.; Bogdanov, M.; Wang, L.; Costello, C.E. and Matson, W.R.; Identification of Unknown Phenyl Butyrate-Generated Metabolites in Huntington 's Disease Patients using Parallel LC-EC-array-MS Detection (*Submitted to Analytical Biochemistry*).

Lin, Y., Schiavo, S; Orjala, J.; Vouros, P., Kautz, R.A.; A Microscale LC-MS-NMR Platform Applied to the Identification of Active Cyanobacterial Metabolites *Analytical Chemistry* **2008**, 80, 8045-8054.

Schiavo, S; Ebbel, E; Sharma, S; Matson, WR; Kristal, B.S.; Hersch, S.; Vouros, P.; Metabolite Identification Using a Nanoelectrospray LC-EC-array-MS Integrated System *Analytical Chemistry* **2008**, 80, 5912-5923.

Ricicki, E.R.; Andrews, C.L.; Schiavo, S.; Vouros, P.; "Mass spectrometric methods for the analysis of DNA adducts: A perspective" *Encyclopedia of Mass Spectrometry*, R. Caprioli and M.L. Gross, Eds. Elsevier, New York, NY, **2006**, Vol. 3, 61-85.

Schiavo, S.; Yang, W; Chiu, N.H.L.; Krull, I.S.; Comparison of Fluorometric Detection Methods for Quantitative Polymerase Chain Reaction (PCR) *Journal of Immunoassay & Immunochemistry* **2005**, 26(1), 1-12.

Schiavo, S.; El-Shafey, A.; Jordan, N.; Orazine, C.; Wang, Y.; Zhou, X., Chiu, N.H.; Krull, I.S; Pushing the Limits of Detection with Immuno-PCR. *Pharmagenomics* **2004**, 4(1), 36-45.

**LIST OF PRESENTATIONS**

(Presenter in bold)

Poster: *Metabolite Identification Using a Novel Nanoelectrospray LC-EC-array-MS Integrated System* **Susan Schiavo**, Erika Ebbel, Swati Sharma, Wayne Matson, Bruce S. Kristal, and Paul Vouros: 56<sup>th</sup> American Society for Mass Spectrometry and Allied Topics Conference, June 2008, Denver, CO

Poster: *Natural Product Discovery Using An Integrated Nanoelectrospray LC-MS-microcoil NMR System*

Paul Vouros, Jimmy Orjala, Yiqing Lin, **Susan Schiavo**, Roger Kautz: 56<sup>th</sup> American Society for Mass Spectrometry and Allied Topics Conference, June 2008, Denver, CO.

Poster: *Simultaneous Measurement of Serum Metabolites using Nanoelectrospray LC-MS and Coulometric Detection* **Schiavo, S.**, Matson, W.R., Kristal, B.S., Vouros, P.; 3<sup>rd</sup> Annual Advances in Metabolic Profiling Conference and Exhibition, October 2007, Boston, MA.

Poster: *Simultaneous Measurement of Rat Serum Metabolites using Nanoelectrospray LC-MS and Coulometric Detection* **Schiavo, S.**, Matson, W.R., Kristal, B.S., Vouros, P.; 55<sup>th</sup> American Society for Mass Spectrometry and Allied Topics Conference, June 2007, Indianapolis, IN.

Oral: *Approaches for Improved Assays of Prion Proteins in Simple Biofluids.*; **Krull, I.S.**; Chiu, N.H., El-Shafey, A.; Jordan, N., Wang, Y.; Schiavo, S.; Orazine, C.; Zhou, X.; Li, G.; 226<sup>th</sup> ACS National Meeting; American Chemical Society: New York, NY, 2003.

Poster: *The Effects of Substrate Structure on the Reaction Pathways of Chloroperoxidase Catalyzed Oxidation of Phenols and Analines*; **Schiavo, S.**; Horn, S.; Williams, L.; 221<sup>th</sup> ACS National Meeting; American Chemical Society: San Diego, CA, 2001